Single-Cell Transcriptional Analysis of Malaria-Specific T Lymphocytes Following Vaccination and Protection in Humans

Thesis submitted for the degree of Doctor of Philosophy

Trinity Term 2016

Kailan Sierra-Davidson

Merton College

Word Count ~42,000 (excl. Bibliography, Appendices, Diagrams and Tables)

Single-Cell Transcriptional Analysis of Malaria-Specific T Lymphocytes Following Vaccination and Protection in Humans

Kailan Sierra-Davidson, Merton College, University of Oxford

Thesis submitted for the degree of Doctor of Philosophy, Trinity Term 2016

Abstract

Vaccine approaches that confer durable and high-level protection against malaria infection are urgently needed. Development of next-generation vaccines is partially hindered by a limited understanding of the mechanisms underlying protective immunity. In-depth characterization of such responses will be critical in identifying immune correlates and ultimately guiding the development of next-generation vaccine strategies. The aim of this thesis was to dramatically enhance the breadth and depth of phenotypic analysis from cellular immune responses induced by two malaria vaccine candidates that have demonstrated high-level protection against CHMI: the PfSPZ Vaccine and ChAd63/MVA ME-TRAP. Single cell gene expression analysis of antigen-specific $CD4^+$ and $CD8^+$ T lymphocytes following vaccination and/or CHMI revealed a number of important findings. First, PfSPZ-specific $CD4^+$ T cells from vaccinated and protected subjects in a small cohort were enriched in *IL21* gene expression compared to unprotected subjects prior to challenge. Average *IL21* expression per-subject correlated with antibody responses against the immunodominant CS protein. Analysis of a larger independent cohort confirmed both of these findings and provided greater power to dissect this population of $IL21^+$ $CD4^+$ T cells. Interestingly, these data provided evidence for a class of Th1/TFH-like cells that could potentially provide help for both $CD8^+$ T cells and humoral responses elicited by PfSPZ vaccination. Second, analysis of $CD8^+$ T cells from subjects vaccinated with ChAd63/MVA ME-TRAP provided the opportunity to investigate cellular immune responses that are critical for clearance of infected hepatocytes. There was evidence for multifunctional use of effector molecules in TRAP-specific $CD107a^+CD8^+$ T cells and a broad transcriptional signature of monofunctional $IFNG^+$ $CD8^+$ T cells, which have been previously correlated with protection induced by viral vectors. Overall, data presented in this thesis demonstrate that single-cell transcriptional analysis is a powerful tool to expand the characterization of cellular immune responses and elucidate potential correlates of protection in Phase II clinical trials.

Acknowledgements

First and foremost, I would like to than my NIH supervisor Bob Seder, not only for the opportunity of this DPhil but also for the endless support throughout the process. You have inspired me and encouraged me to take part in all aspects of the projects. My time at the VRC has been an invaluable experience, and for that, I am extremely grateful. Everyone in the Seder lab has helped me with an experiment, talked through an idea, and chatted with me through the late nights in lab. Geoffrey Lynn, Andrew Ishizuka, Barbara Flynn, and Kylie Quinn have all been extremely helpful. However, this thesis would not have been possible without the constant scientific and emotional support from Tricia Darrah.

Secondly, I would like to thank Katie Ewer and Helen McShane for providing constant support through my DPhil, and in particular for reviewing my thesis. Furthermore, I would like to thank the Jenner Institute Director Adrian Hill for giving me the opportunity to work on clinical trials from malaria to Ebola and allowing me gain a broad knowledge of cellular immunology. Georgie Bowyer, Carly Bliss, Danny Wright, Anita Gola, and Jonathan Pawlson were all extremely kind in helping me learn the ins and outs of the Jenner. Tess Lambe, Eneida Parizotto, Adai Ramasamny, and Julius Muller also provided ideas and solutions during my DPhil.

Next, I would like to thank Steve Hoffman, Kim Lee Sim, Sumana Chakravarty, Adam Ruben and everyone else at Sanaria for providing all of the PfSPZ reagents.

My research would not have been possible without the supplies, the clinical samples, and a great team to help me understand everything known PfSPZ Vaccines.

Greg Finak and Raphael Gottardo at the University of Washington in Seattle provided invaluable assistance with the statistical analysis. None of it would have been possible without Greg and Raphael helping me to understanding how to use powerful software programs to dissect these large data sets.

Furthermore, I would like to thank Mario Roederer and Pratip Chattopadhyay for providing invaluable insight into understanding the Fluidigm results and bouncing off ideas for potential avenues of analysis. In addition, Madhu Prabhakaran, Steven Ma, and Adam Wheatley all were crucial during my first year in learning the nuts and blots of the assay.

None of this research would have been possible without the due attention from the sorting facility at the VRC, particularly David Ambrozak, Steve Perfetto and Richard Ngyuen. From my early days in optimizing the assay to more batch analysis of a large number of samples, everyone has taken the time to walk me through the process and ensure that the sorts were of the highest quality.

Outside of the lab, I would like thank the Howard Hughes Medical Institute (HHMI) and the NIH-Oxford-Cambridge Program for providing financial support and mentorship. In particular, HHMI has provided research support for me since I was a freshman in college. Even though I had never stepped foot in a lab, the leadership encouraged me to pursue a career in science, for which I am eternally grateful.

Last but not least, I would like to thank my parents, siblings and fiancé. Without each and everyone's support, I would not have made it to where I am now.

Table of Contents

Abstract **2**

Acknowledgements **3**

Table of Contents **6**

Table of Figures **10**

Table of Tables **12**

List of Abbreviations **13**

1. Introduction **17**

1.1 Malaria **17**

1.1.1 A global health threat 17

1.1.2 Life cycle of *Plasmodium falciparum* 19

1.1.3 Pathogenesis 21

1.1.4 Current control measures 24

1.2 Human immune system **28**

1.2.1 Innate immunity 28

1.2.2 Adaptive immunity 29

1.2.3 Acquisition of naturally acquired immunity 31

1.3 Vaccine development **35**

1.3.1 Aim of malaria vaccines 35

1.3.2 Identifying protective mechanisms and targets in pre-erythrocytic immunity 38

1.3.3 Experimental human model 46

1.4 Current status of pre-erythrocytic vaccine development **48**

1.4.1 RTS,S/AS01 48

1.4.2 Whole sporozoite vaccines 49

1.4.3 Viral vectored vaccines 53

1.5 Advances in single cell transcriptional analysis **57**

1.6 Thesis aims and outline **60**

1.6.1 Aims 61

1.6.2 Outline 62

2. Material and Methods 64

2.1 Materials 64

2.1.1 Reagents 64

2.1.2 Buffers and solutions 66

2.1.3 Flow cytometric antibodies 66

2.1.4 Primers 67

2.1.5 Electronic equipment 69

2.2 Clinical Trials 70

2.2.1 VRC312 70

2.2.2 VRC314 71

2.2.3 MAL34 72

2.2.4 VAC45 73

2.2.5 VAC52 74

2.3 Clinical immunology 75

2.3.1 Blood separation 75

2.3.2 PfCSP ELISA 75

2.4 Flow cytometry 77

2.4.1 Intracellular staining of PfSPZ-specific T cells 77

2.4.2 TRAP peptide pools 78

2.4.3 Isolation of PfSPZ-specific $CD4^+$ T cells 78

2.4.4 Isolation of TRAP-specific $CD8^+$ T cells 78

2.4.5 Single cell sorting 79

2.5 Acquisition of single cell gene expression 80

2.5.1 Fluidigm 80

2.6 Data analysis 82

3. Optimization of Single Cell Gene Expression Acquisition 84

3.1 Introduction 84

3.2 Results 86

3.2.1 Detection of antigen-specific T cell responses following intravenous administration of PfSPZ Vaccine 86

3.2.2 Optimization of PfSPZ-specific $CD4^+$ T cell isolation 88

3.2.3 Simultaneous detection of CD154 and CD69 for capture of broad PfSPZ-specific $CD4^+$ T cell response 91

3.2.4 High-resolution transcriptional analysis of virus- vs. PfSPZ-specific $CD4^+$ T cells 94

3.2.5 Validation of single cell gene expression from PfSPZ-specific $CD4^+$ T lymphocytes 99

3.3 Discussion 108

4. VRC 312- PfSPZ Vaccine Trial #1 112

4.1 Introduction 112

4.2 Results 114

4.2.1 Isolation of individual PfSPZ-specific $CD4^+$ T cells from vaccinated subjects prior to challenge 114

4.2.2 Global transcriptomic profiles of PfSPZ-specific $CD4^+$ T cells from vaccinated subjects and infection controls 121

4.2.3 Differential gene expression signatures of PfSPZ-specific $CD4^+$ T cells following vaccination versus infection 125

4.2.4 Modular analysis for examination of cooperation of gene expression at the single-cell level 129

4.2.5 Plasticity and heterogeneity of $CD4^+$ T cell gene expression 133

4.2.6 Gene signatures associated with protection following vaccination 136

4.3 Discussion 140

5. VRC 314- PfSPZ Vaccine Trial #2 145

5.1 Introduction 145

5.2 Results 149

5.2.1 Isolation of PfSPZ-specific $CD4^+$ T cells from subjects vaccinated with varying doses under clinical study VRC314 149

5.2.2 Global transcriptomic profiles of PfSPZ-specific $CD4^+$ T cells from vaccinated subjects across different vaccination regimens 153

5.2.3 Gene signatures associated with short-term protection following vaccination 157

5.2.4 Further investigation of IL21-expressing $CD4^+$ T cells 164

5.2.5 Expanded modular analysis of protected vs. unprotected subjects 168

5.2.6 Coexpression analysis of cytokines associated with canonical Th subsets as function of protection outcome 171

5.3 Discussion 177

6. ChAd63/MVA ME-TRAP Vaccination 182

6.1 Introduction 182

6.2 Results 184

6.2.1 Isolation of live TRAP-specific $CD8^+$ T cells from vaccinated subjects 184

6.2.2 Global characterization of TRAP-specific $CD8^+$ T cells 191

6.2.3 Multifunctional use of effector molecules 194
6.2.4 Characterization of monofunctional IFNG$^+$ CD8$^+$ T cells 198
6.2.5 Global gene signatures from protected vs. unprotected cohorts 201
6.2.6 Gene set enrichment analysis of sterilely protected subjects 211
6.3 Discussion 215
7. Concluding Remarks 220
7.1 Overview 220
7.2 Conclusion and Future Directions 223
7.2.1 Single-cell transcriptomics as a powerful technology for analysis of large clinical trials 223
7.2.2 Role of CD4$^+$ T cells in PfSPZ-mediated protection 226
7.2.3 CD107a$^+$CD8$^+$ T cells in ChAd63/MVA ME-TRAP induced immunity 228
7.3 Final Remarks 231
References 232
Appendix 251

Table of Figures

Figure 1.1 Life cycle of the malaria parasite *P. falciparum* 20

Figure 1.2 The effect of control measures on malaria clinical cases between 2000 and 2015. 25

Figure 1.3 Distribution of naturally acquired immunity (NAI) 33

Figure 1.4 Hypothesized mechanisms of cell-mediated immunity in liver-stage infection 39

Figure 1.5 Relative structure of data from single-cell analyses 58

Figure 3.1 Detection of antigen-specific $CD4^+$ T cells following PfSPZ Vaccine... 87

Figure 3.2 Optimization of PfSPZ-specific $CD4^+$ T cell capture. 90

Figure 3.3 Coordinate expression of CD154 with commonly measured cytokines. 93

Figure 3.4 High-resolution transcriptional analysis of HA- vs. PfSPZ-specific $CD4^+$ T cells 98

Figure 3.5 Single-cell gene expression from PfSPZ-specific $CD4^+$ T cells 102

Figure 3.6 Benefits of gene expression from single cells vs. bulk populations. 103

Figure 3.7 Hypothesized contribution of "background" $CD154^+$ $CD4^+$ T cells. 107

Figure 4.1 VRC312 clinical study. 116

Figure 4.2 PfSPZ-specific $CD4^+$ T cell responses. 117

Figure 4.3 Sensitivity of single cell gene expression from vaccinated subjects in VRC312 120

Figure 4.4 Global gene expression of vaccinated subjects and unvaccinated infection controls 124

Figure 4.5 Differential gene expression of PfSPZ-specific $CD4^+$ T cells following vaccination vs. CHMI. 128

Figure 4.6 GSEA of vaccinated subjects vs. infection controls using BTM 131

Figure 4.7 GSEA of vaccinated subjects vs. infection controls using curated modules for T helper subsets 132

Figure 4.8 Heterogeneity of PfSPZ-specific $CD4^+$ T cells 135

Figure 4.9 Gene signatures of vaccinated and protected vs. unprotected subjects . 138

Figure 4.10 *IL21* expression and humoral immunity 139

Figure 5.1 VRC314 clinical study 146

Figure 5.2 PfSPZ-specific $CD4^+$ T cell responses 151

Figure 5.3 Controls for gene expression analysis 152

Figure 5.4 Fluidigm analysis of vaccine immunogenecity 156

Figure 5.5 Fluidigm analysis of short-term protection 162

Figure 5.6 Accuracy of protective model by vaccination group 163

Figure 5.7 *IL21* gene expression and PfCSP antibodies 166

Figure 5.8 Canonical Th transcriptional factors 167

Figure 5.9 Modular analysis by vaccination group 170

Figure 5.10 Coexpression of canonical Th cytokines 173

Figure 5.11 Combinations of canonical Th cytokines 176

Figure 6.1 Gating strategy for isolation of live TRAP-specific $CD8^+$ T cells. 187

Figure 6.2 $CD107^+$ $CD8^+$ T cell responses. 188

Figure 6.3 Gene expression controls. 190

Figure 6.4 Global characterization of all TRAP-specific $CD107a^+$ $CD8^+$ T cells. . 193

Figure 6.5 Coordinate expression of effector molecules among all TRAP-specific $CD107a^+$ $CD8^+$ T cells. 197

Figure 6.6 Characterization of monofunctional *IFNG*$^+$ $CD8^+$ T cell subset. 200

Figure 6.7 Assessment of $CD8^+$ T cell functionality based on previous studies. ... 203

Figure 6.8 Global differences among protected vs. nonprotected cohorts. 206

Figure 6.9 Differential gene expression between sterilely protected and nonprotected vaccinated subjects 210

Figure 6.10 Modular analysis of sterilely protected subjects. 213

Table of Tables

Table 2.1 MAL34 study design 72

Table 2.2 VAC45 study design 73

Table 2.3 VAC52 study design 74

Table 2.4 Fluidigm premix for sorting 80

Table 2.5 Fluidigm pre-amplification 81

Table 4.1 VRC312 subjects initially selected for Fluidigm analysis. 116

Table 4.2 List of genes in curated modules for GSEA of T helper subsets 132

Table 5.1 VRC314 subjects analyzed by Fluidigm 152

Table 5.2 Analysis of Th transcription factors for *IL21*$^{+}$ CD4^{+} T cells 167

Table 6.1 ChAd63/MVA ME-TRAP vaccinated subjects assessed by Fluidigm... 185

Table 6.2 Vaccination regimen for selected subjects from each trial. 185

Table 6.3 Modules enriched in sterilely protected vs. nonprotected subjects. 214

Table 6.4 Modules enriched in sterilely protected vs. delayed subjects. 214

List of Abbreviations

ACT	Artemisinin-based combination therapy
ADCC	Antibody-dependent cell-mediated cytotoxicity
AIDS	Acquired immune deficiency syndrome
AMA1	Apical membrane antigen 1
APC	Antigen presenting cell
AUC	Area under curve
BAFF-R	B-cell activating factor receptor
BCR	B cell receptor
BSA	Bovine Serum Albumin
CDR	Complementarity Determining Region
CDR	Cellular detection rate
CH-1	One day before day of challenge
ChAd	Chimpanzee-derived simian adenovirus
CHMI	Controlled human malaria infection
CMV	Cytomegalovirus
CSP	Circumsporozoite protein
CVac	Chloroquine prophylaxis
CXCL	C-X-C Chemokine Ligand
CXCR	C-X-C Chemokine Receptor
CyTOF	Cytometry by time of flight technology
DC	Dendritic cells
DDT	Dichloro-diphenyl-trichlorethane
DMSO	Dimethyl sulfoxide
DVI	Direct venous inoculation
EDTA	Ethylenediaminetetraacetic acid
ELISA	Enzyme-linked immunosorbent assay
ELISPOT	Enzyme-linked immunosorbent spot assay
EMP	Erythrocyte membrane protein
EPCR	Endothelial protein receptor C
EPI	Expanded Program on Immunization
Exp	Exported protein

FACS	Fluorescence-activated cell sorting
FCS	Fetal calf serum
FP	Fowlpox
GAP	Genetically attenuated parasites
HIV	Human immunodeficiency virus
HLA	Human leukocyte antigen
HRP	Histidine rich protein
HSA	Human serum albumin
HSPGs	Heparin sulfate proteoglycans
HuAd	Human adenovirus
ICAM	Intracellular adhesion molecule
ICS	Intracellular cytokine staining
ID	Intradermal
IFN-γ	Interferon-gamma
Ig	Immunoglobulins
IL	Interleukin
IM	Intramuscular
IPT	Intermittent preventative therapy
IQR	Interquartile range
IRS	Indoor residual spraying
ITN	Insecticide-treated bed net
IV	Intravenous
KC	Kupffer cell
LDA	Linear discriminant analysis
LSA	Liver-stage antigen
MAST	Model-based Analysis of Single-cell Transcriptomics
MDG	Millennium Development Goal
ME	Multi-epitope string
MHC	Major histocompatibility complex
MSP	Merozoite surface protein
MVA	Modified Vaccinia Ankara
NAI	Naturally acquired immunity
NK	Natural killer cell

NO	Nitric oxide
NOD	Nod-like receptor
PAMP	Pathogen associated molecular patterns
Pb	*P. berghei*
PBMCs	Peripheral blood mononuclear cells
PBS	Phosphate-buffered saline
PCA	Principal components analysis
Pf	*P. falciparum*
Pfu	Particle forming units
PRR	Pattern recognition receptors
Pv	*P. vivax*
PV	Parasitophorous vacuole
RAS	Radiation attenuated sporozoites
RBC	Red blood cell
Rh	Reticulocyte-binding homologue
ROC	Receiver Operating Characteristic
ROS	Reactive oxygen species
RT-qPCR	Real-time quantitative PCR
SC	Subcutaneous
scRNA-Seq	Single cell RNA-sequencing
SEM	Standard error of the mean
SPICE	Simplified Presentation of Incredibly Complex Evaluations
SPZ	Sporozoite
STARP	Sporozoite threonine-asparagine-rich protein
TCR	T cell receptors
TFH	T follicular helper cell
Th	T-helper
TLR	Toll-like receptors
TNF	Tumor necrosis factor
TRAP	Thrombospondin-related adhesion protein
Treg	T regulatory
TSR	Thrombospondin repeat
VLP	Virus like particle

Vp	Viral particle
VSA	Variant specific antigens
WHO	World Health Organization
γδ	Gamma-delta T cells

1. Introduction

1.1 Malaria

1.1.1 A global health threat

At the turn of the 20th century, leaders from around the world declared malaria as one of the greatest public health threats to be tackled in the next 15 years *(1)*. As the deadline for the Millennium Development Goals passes, malaria remains a significant killer of young children in Africa. The scientific community must take care to evaluate the progress and challenges ahead.

In 2015, the World Health Organization estimated 214 million cases of malaria infection, resulting in over 400,000 deaths (*2*). Young children under the age of five and pregnant women shoulder the greatest burden of morbidity and mortality, constituting 90% of all malaria deaths (*2*). For countries that bear the brunt of disease, the economic and social costs of malaria are incalculable. Malaria infection prevents children from going to school, discourages international investment, and increases healthcare costs, draining over $10 billion dollars from Africa each year (*3-5*). Many organizations have put sustained pressure on world leaders for increased efforts to halt the spread of the disease. Notably, Bill and Melinda Gates renewed the call for eradication (6), invigorating countries to double global funding for malaria control within a decade *(2, 7)*.While treatment expansion and transmission control have averted one million deaths over the past decade (*8*), a deficit of $5 billion dollars per year funding threatens sustainable results (*7*). Furthermore, the Ebola outbreak in West Africa highlighted the precarious nature of

malaria elimination in regions with inadequate health infrastructure (*9*). As transmission continues in 99 countries, placing 3.2 billion people at risk of infection (*2*), new tools for disease control are required.

Malaria infection in humans is caused by five different species of the Apicomplexan parasite of the genus *Plasmodium (10).* Four of these pathogens- *P. falciparum, P. vivax, P. malariae,* and *P. ovale*- can all be spread from human to human, while *P. knowlesi* is limited to zoonotic transmission from forest macaque monkeys in Southeast Asia (*11, 12*). *P. vivax* has the widest geographical distribution, accounting for half of all malaria infections outside of Africa *(2).* As *P. falciparum* causes 80% of clinical infections and 90% of deaths (*2*), this pathogen constitutes the greatest public health challenge. Nonetheless, the global distribution of *P. vivax* coupled with need for adequate surveillance of emerging zoonotic *P. knowlesi* infections *(13)* should not be understated.

1.1.2 Life cycle of **Plasmodium falciparum**

Multiple stages in human and mosquito hosts contribute to different antigenic targets and immunological responses **(Figure 1.1)** *(10).*

Malaria infection in humans is transmitted via the bite of the female Anopheline mosquito. There are 400 different species of *Anopheles*, of which *A. gambiae* is the principal vector in heavily endemic regions (*14*). During a blood meal, tens to hundreds highly motile, haploid sporozoites are deposited into the skin of the host. While a fraction of sporozoites remain local in the dermis or are drained into the lymphatic system, the majority invade blood vessels and migrate to the liver within minutes *(15).* Within the liver sinusoids, these parasites transverse endothelial cells and liver-resident macrophages called Kupffer cells before hepatocyte invasion *(16-18).* Asexual replication and maturation of the parasite occurs over 7-10 days, during which one sporozoite can expand into 40,000 merozoites per hepatocyte (*10*). Parasite-filled vesicles called merosomes then bud from host cells, before bursting and releasing thousands of merozoites into the peripheral circulation *(19).* It is important to note that the life cycle of *P. falciparum* diverges from *P. vivax* and *P. ovale* at the pre-erythrocytic stage. In the liver, *P. vivax* sporozoites can revert to dormant hypnozoites prior to maturation, accounting for relapses months after infection (*20*). The only drug family that can kill hypnozoites, 8-aminoquinolines, is toxic in humans deficient in glucose-6-phosphate dehydrogenase (G6PD), a common genetic mutation in malaria-endemic regions (*21*).

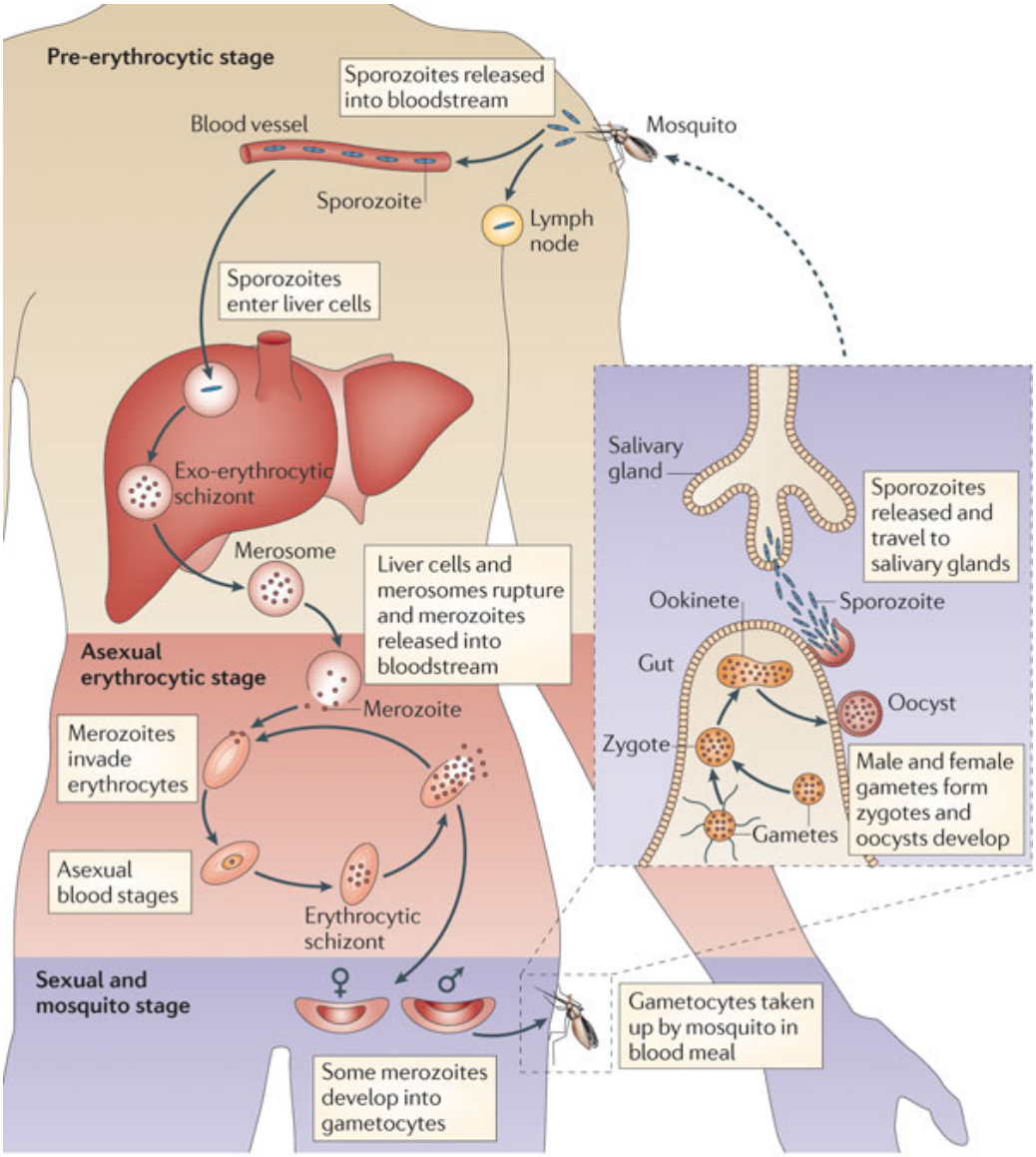

Figure 1.1 Life cycle of the malaria parasite *P. falciparum*

Image taken from ***(22)*** that illustrates that life cycle of *P. falciparum.* Briefly, an infected female *Anopheles* mosquito injects sporozoites into the blood where they migrate to liver within minutes. Over 7-10 days in humans, sporozoites develop as exo-erythrocytic schizonts inside parasitophorous vacuoles within infected hepatocytes. Fully matured merozoites are then packaged as merosomes, which then erupt in the bloodstream and invade erythrocytes. During the asexual erythrocytic stages, symptoms of clinical malaria appear. The development of sexual forms called gametocytes and subsequent differentiation within the mosquito gut ensures transmission of *P. falciparum*.

Clinical presentation of malaria manifests during the erythrocytic stage. Merozoite invasion of erythrocytes drives remodeling of host intracellular structure to facilitate transport of *P. falciparum* erythrocyte membrane protein 1 (PfEMP1) to the cell surface (*23*), a key mechanism of immune evasion (further discussed in section 1.1.3). Over 48 hours, merozoites mature through ring, trophozoites and schizont stages, before replicated parasites ultimately burst from the erythrocyte *(24)*. Synchronized invasion and rupture of erythrocytes coincide with the cyclical fevers and chills, a classical symptom of malaria *(25, 26)*. After an unknown number of cycles, concurrent gametocytogenesis leads to the development of male and female pre-sexual stages (*27*). Cell-to-cell communication and/or stochastic activation of transcriptional switch may play a role in triggering differentiation of male and female gametocytes *(28, 29)*.

Upon ingestion of gametocytes during a blood meal, mature gametes fertilize in the midgut lumen, undergo sexual development into ookinetes, and transform into hundreds of sporozoites in the salivary gland, thus perpetuating the cycle of human disease (*30*).

1.1.3 Pathogenesis

Maturation of sporozoites during the pre-erythrocytic stages is clinically silent. The hallmark of malaria infection occurs during the blood-stage, classically characterized by cyclical fevers and chills that coincide with rupture of parasitized erythrocytes. Initial symptoms are very nonspecific: headache, fever, and myalgia, often leading to misdiagnosis of other common infections. Disease severity in areas

of high-transmission is highly-dependent on age, such that risk of death increases during the first six months of life and then gradually declines *(31).* The notable exception is primagrade women, as infection during the second and third trimesters is associated with an increased risk of low birth weight, stillbirth and maternal death (*32*). Severe malaria in children typically manifests as a combination of three overlapping symptoms: impaired consciousness (cerebral malaria), severe anemia and respiratory distress (acidosis). While the underlying mechanisms are still unclear, pathogenesis is hypothesized to be driven by host-parasite interactions and a dysregulated inflammatory immune response *(33).*

Sequestration of parasitized erythrocytes is a key tactic of *P. falciparum* for evasion of the host immune system and plays an important role in disease severity. First shown in the autopsied brains of patients who died from cerebral malaria (*34*), adherence of parasitized erythrocytes to endothelial receptors has been demonstrated to the microvasculature bed of a wide range of organs. Sequestration prevents destruction of infected erythrocytes in the spleen, ultimately blocking blood vessels and impairing oxygen delivery to critical organs (acidosis) *(33).* The best-characterized adhesion ligand is the highly polymorphic *P. falciparum* erythrocyte membrane protein 1 (PfEMP1), which is encoded by 60 antigenically distinct *var* genes (*35-37*). Antigenic variation allows the parasite to bind to a wide range of host receptors such as endothelial protein receptor C (EPCR) *(38)* with expression of certain *var* genes strongly associated with binding in the brain and placenta *(39, 40).* Furthermore, *var* gene silencing in response to immune pressure alters surface expression of antigenically distinct PfEMP1 variants, enabling evasion of the specific host immune responses *(35, 41).* While sequestration is clearly a risk factor

for severe malaria, many studies question a direct link between the two phenomena *(33, 42-44).* Recent studies have suggested that detection of *P. falciparum* histidine rich protein 2 (PfHRP2) approximates the total parasite biomass, accounting for circulating and sequestered parasites. Soluble PfHRP2 is higher in patients with severe vs. uncomplicated malaria and may serve as a better predictor of severe malaria *(43, 44).*

While inflammatory responses may be protective during blood-stage malaria, excessive inflammation is hypothesized to contribute to severe malaria (*45*). Cytokines such as tumor necrosis factor (TNF-α), interleukin-6 (IL-6), and interferon-gamma (IFN-γ) and free oxygen radicals are greater in children with cerebral malaria and respiratory distress vs. uncomplicated malaria *(46).* Murine models of experimental cerebral malaria demonstrate a critical role of immunopathology (*47*), but the mechanism is likely more complicated in humans involving timing and a balanced regulatory response. Vascular endothelium dysfunction may form the link between sequestration and excessive inflammation in the pathogenesis of severe malaria. Inflammatory mediators combined with mechanical disruption of the blood flow caused by sequestered erythrocytes may cause vascular endothelium activation and impair barrier function, potentially leading to signal amplification of metabolic derangement and organ dysfunction *(33).* However, more studies are necessary to fully unravel this mechanism for the development of adjunctive treatments tailored to specific severe malaria syndromes.

1.1.4 Current control measures

Almost as old as malaria are interventions that aim to prevent death. Ancient civilizations around the world developed tools to ward off disease with varying degrees of success (*48*). While ancient Roman amulets inscribed with "Abracadabra" likely did little to stop death, ancient medicines from China form the basis of essential modern tools. Current control measures funded by Roll Back Malaria, the Global Fund to AIDS, Tuberculosis and Malaria, and the Bill and Melinda Gates Foundation are targeted at treating the disease in humans and limiting vector transmission *(2, 49)*. In particular, three interventions have played a key role in averting 663 (542-735) million clinical cases over the past fifteen years: insecticide-treated bed nets (ITNs), indoor residual spraying (IRS), and antimalarial chemotherapy **(Figure 1.2)** (*8*).

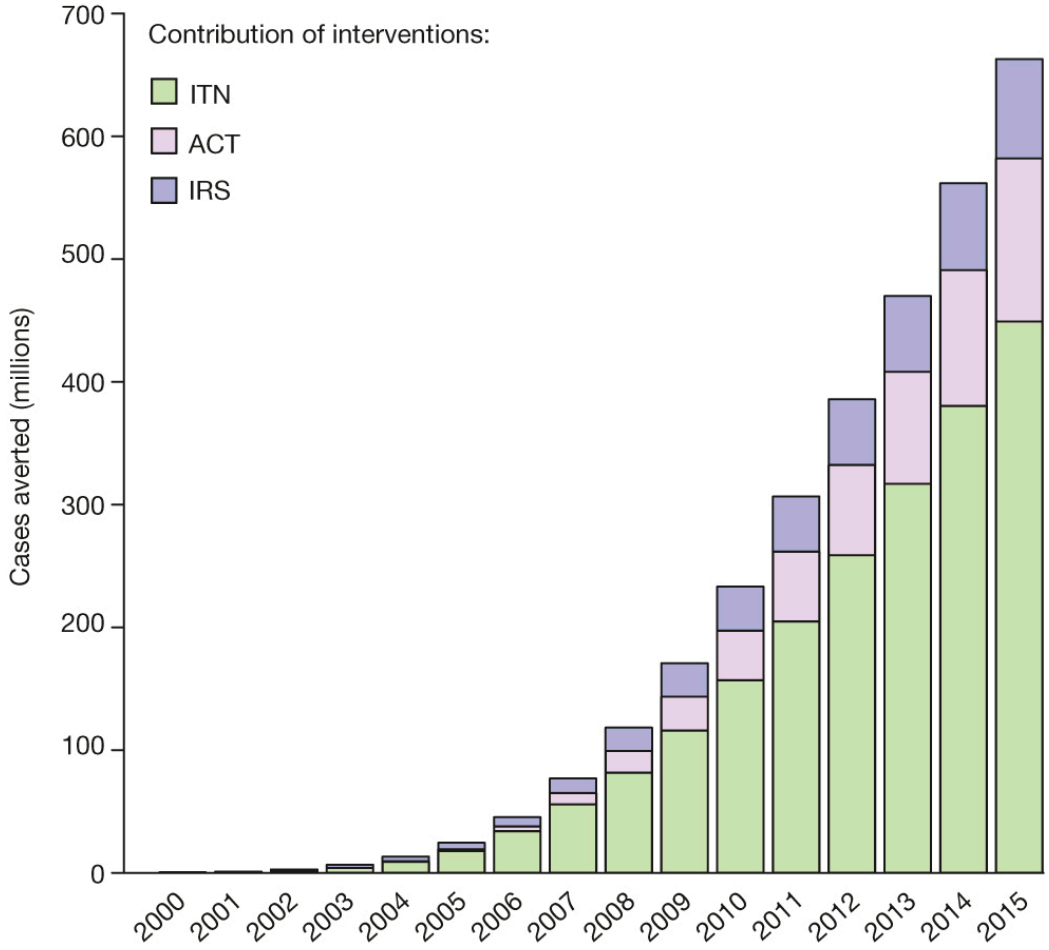

Figure 1.2 The effect of control measures on malaria clinical cases between 2000 and 2015.

Image taken from ***(8)***. This graph depicts the estimated number of malaria clinical cases averted over fifteen years by three key interventions: insecticide-treated bed nets (ITN), artemisinin-based combination therapy (ACT), and indoor residual spraying (IRS). Note that ACT is intended to primarily prevent severe disease, rather than halt the spread of new infections.

One of the most cost-effective public health interventions against childhood deaths, ITNs were responsible for a 68% decrease in clinical cases between 2000 and 2015 (*8*). The use of nets to prevent disease has been described since the 5th century BCE, when historian Herodotus documented how Egyptian fishermen slept under their nets at night to ward off insects *(50)*. Modern widespread use swung into full force in the mid-1990s, following discovery of insecticide treatment of nets with pyrethroids to increase effectiveness. ITNs provide a two-hit punch by directly preventing infection of the person sleeping under the net and indirectly protecting others by suppressing community-wide transmission. Regional variations in transmission intensity and usage impact effectiveness *(51, 52),* but in some areas introduction of ITN reduced overall child mortality by 60% *(53)*. Despite such promise, operational difficulties in achieving widespread appropriate use (*2, 54*) has contributed to the emergence of insecticide-resistant mosquitoes (*55*) and evolutionary shift of daytime biting (*56*). Furthermore, some studies have warned that decreased acquisition of naturally acquired immunity may shift burden of mortality to older children *(57, 58)*.

IRS provides an alternative strategy in tackling vector control, particularly in regions with unstable transmission *(59)*. Spraying with dichloro-diphenyl-trichlorethane (DDT) critically contributed to malaria elimination in Europe and North America in the 20th century (*60*). However, IRS currently face similar problems as ITNs with growing insecticide resistance coupled with low implementation (2).

Prompt treatment of clinical malaria cases is critical in the prevention of severe disease and deaths. Other uses of malaria chemotherapy include intermittent preventative therapy (IPT) for routine treatment of pregnant women and children regardless of infection status (*61-63*) and continuous prophylaxis for non-immune travelers (*64*). Quinine, first extracted from the bark of the cinchona tree in 1820 *(48),* served as the foundation for the synthetically derivative compound, chloroquine. Once heavily deployed around the word, chloroquine soon became obsolete following the spread of drug-resistant parasites (*65*). Consequently, the WHO recommends artemisinin-based combination therapies (ACT) as the front-line therapy against malaria *(2, 66, 67).* Unfortunately, the distribution of counterfeit drugs (*68*) and widespread availability of artemisinin monotherapies (*69*) has likely contributed to the emergence of artemisinin resistance characterized by reduced susceptibility of ring-stage parasites (*70-72*). No new antimalarial drug classes will be available for clinical use in the near future.

1.2 Human immune system

1.2.1 Innate immunity

The innate immune system provides a first-line defense against a wide range of pathogens (*73*). While innate immunity is limited to only acting in a non-specific manner, rapid and broad responses halt the initial spread of infection and ultimately shape the adaptive immune system to best target the pathogen (*74*). The epithelium provides the first physical barrier against invading pathogens by trapping microbes in mucus and secreting antimicrobial peptides to include defensins, cathelicidins, and histatins (*75*). The complement system encompasses serum and membrane proteins that form three closely interlinked activation pathways: the classical, lectin, and alternative pathways. Pathogen recognition occurs via antigen-antibody complexes, surface carbohydrates and direct pathogen surface, respectively and ultimately results in phagocytosis by opsonization, cell lysis, and inflammation (*76*). Innate immune cells such as macrophages, neutrophils, and monocytes play a critical role in the removal of invading pathogens (*77*). Recognition of pathogen associated molecular patterns (PAMP) occurs via pattern recognition receptors (PRR) such toll-like receptors (TLRs) and nod-like receptors (NODs). Activated macrophages internalize and kill pathogens via phagocytosis-mediated oxidative burst, while also secreting chemoattractants to recruit other leukocytes. The innate immune system also includes NK and γδ T cells that kill infected cells via perforin and granzymes (*78, 79*), in addition to basophils, eosinophils, and mast cells that amplify the inflammatory response via the release of histidine (*80*).

1.2.2 Adaptive immunity

Innate immunity activates the adaptive immune system to generate long-term specific responses that respond more rapidly and in greater magnitude upon reinfection. The adaptive immune system is fundamentally based on the clonal expansion of somatically mutated, antigen-specific T and B lymphocytes that compose cellular and humoral immunity, respectively. Specialized antigen-presenting cells (APCs) called dendritic cells (DCs) link innate and adaptive immunity. While B cells and macrophages can also function as professional APCs, DCs are necessary to prime naïve T cells *(81, 82).*

1.2.2.1 Cellular immunity

Cellular immunity is composed of T lymphocytes expressing T cell receptors (TCRs) that recognize peptide fragments bound to major histocompatibility complex (MHC) molecules on the surface of APCs. T cells are broadly divided into two classes based on surface expression of co-receptors that broadly reflect ontogeny, phenotype and function: $CD4^+$ and $CD8^+$ T cells. $CD4^+$ T cells recognize endogenous antigen presented on MHC class II molecules of the surface of APCs in the presence of costimulatory molecules including CD40 and CD80/CD86 (*83*). Antigens are engulfed by professional APCs in phagosomes, degraded into smaller peptide fragments and then loaded onto MHC class II molecules in endosomal compartments before trafficking to the cell surface *(84).* Upon antigen recognition, naïve $CD4^+$ T cells expand and differentiate into different effectors with specialized functions tailored to combat a specific type of pathogen. $CD4^+$ T cell subsets are

often categorized based on the differential expression of cytokines, transcription factors, and surface molecules (*85*). Effector $CD4^+$ T cells are classically divided into Th1 and Th2 cells that recognize intracellular and extracellular pathogens, respectively (*86*). However, recent studies have defined many more subsets to include Th17, T regulatory cells (Tregs), and T follicular helper cells (TFH) (*87*). Often analogized as the arm of the adaptive immune system, $CD4^+$ T cells control the proliferation of $CD8^+$ T cells and maturation of antibodies.

By contrast, cytolytic $CD8^+$ T cells recognize peptides from endogenous peptides presented on MHC class I molecules, which are expressed on all nucleated cells (*73*). Following cross presentation of antigen from endosomes or the direct infection of an APC, peptide fragments are translocated to the endoplasmic reticulum via chaperone proteins and loaded onto MHC class I molecules prior to transportation to the cell surface (*84*). IL-2 produced autologously or from $CD4^+$ T cells as well as proinflamatory cytokines such as IL-12 drive clonal expansion and differentiation of $CD8^+$ T cells (*88*). The main function of effector $CD8^+$ T cells is to induce apoptosis in infected cells via cytotoxic proteins such perforin and granzymes stored in lytic granules or Fas-Fas ligand interactions that activate downstream caspases. Secretion of IFN-γ and TNF-α can mediate killing and also play an important indirect role by increasing expression of MHC class I molecules on the surface of infected cells, recruiting macrophages to the site of infection, and amplifying further cytokine production. Following acute infection, a subset of $CD4^+$ and $CD8^+$ T cells differentiate into long-term memory cells that reside in secondary lymph nodes and peripheral tissues. Central, effector and resident memory T cells facilitate immunosurveliance of the body and respond faster upon reinfection (*89*).

1.2.2.2 Humoral immunity

Humoral immunity is composed of B cells whose main function is to produce antibodies against soluble antigens (*73*). Membrane-bound BCR and secreted antibodies are composed of paired heavy and light chains, the latter of which form either lambda or kappa chains. B cells initially recognize soluble antigen via membrane-bound BCR. Exogenous antigen is then internalized, processed and presented on the surface as a peptide-MHC class II molecule complex. Upon binding with the complementary antigen-specific $CD4^+$ T cell, B cells proliferate and secrete soluble immunoglobulins (Ig). Mature B cells initially secrete IgM and IgD, weakly binding antigen based on germ-line sequences. Upon activation, B-$CD4^+$ T cell interactions in histological structures called germinal centers drive affinity maturation and somatic hypermutation (*90*). Class switching promotes secretion of IgG, IgA, or IgE, isotypes with specialized functions and tissue-homing properties. A subset of mature B cells differentiates into long-lived plasma cells that migrate to the bone marrow and maintain humoral immunity (*91, 92*). Antibodies also mediate non-neutralizing functions via the Fc receptor to enhance phagocytosis by neutrophils and macrophages through opsonization, promote antibody-dependent cellular cytotoxicity by NK cells, and activate the complement system.

1.2.3 Acquisition of naturally acquired immunity

While the mechanisms underlying the immune response to malaria have not been fully elucidated, individuals living in endemic-regions develop naturally acquired

immunity (NAI), largely in an age-dependent manner **(Figure 1.3)** (*31*). Infants younger than six months rarely exhibit clinical disease, likely due to maternal IgG antibodies acquired in utero and/or IgA found in breast milk *(93, 94).* Afterwards, children under the age of five are at the greatest risk of severe disease and death. Following repeated exposure, children develop partial immunity against mortality and severe disease, ultimately acquiring the ability to control high-density parasitemia. Sterilizing immunity is never fully achieved. Continuous parasitemia is ubiquitous among asymptomatic adults in endemic regions, with the notable exception of women during their first and second pregnancies. The distribution of severe disease and death is directly affected by transmission intensity, such that the greater the number of infectious mosquito bites received per person per unit of time (entomological inoculation rate) is, the earlier acquisition of NAI (*31, 95*). The risk of severe disease is also shaped by the evolution of certain populations to select for genetic mutations that protect against mortality, such as those that cause sickle cell disease, thalassemia and Duffy-negative phenotype *(96).*

Sero-epidemiologcal studies consistently suggest acquired immunity is primarily directed against blood stage *(97).* Although sporozoite-specific antibodies against immunodominant circumsporozoite protein (CSP) are detected in the sera of individuals from endemic regions, passive transfer fails to protect against malaria *(98, 99).* Furthermore, T cell responses against pre-erythrocytic antigens thrombospondin -related adhesion protein (TRAP) and liver-stage antigen (LSA) are very low and greatly vary among populations *(100).*

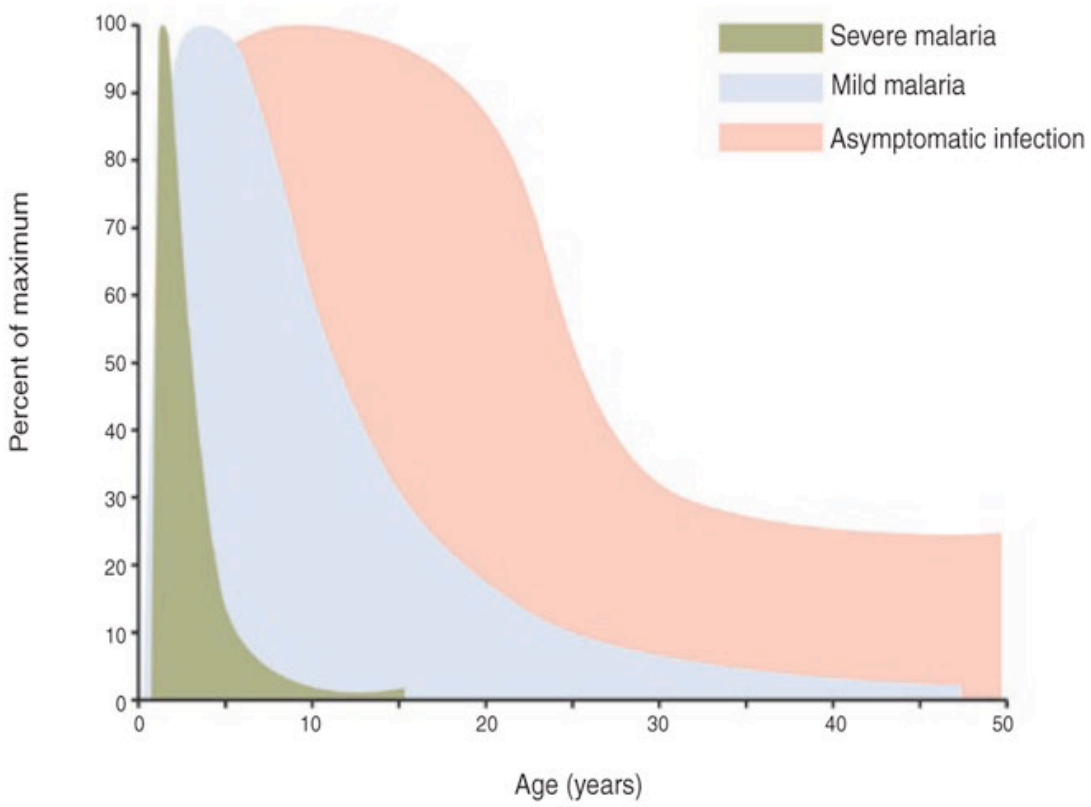

Figure 1.3 Distribution of naturally acquired immunity (NAI)

Image taken from **(*101*)**. In malaria-endemic regions, individuals gradually develop NAI against severe disease, clinical disease, and high-density parasitemia. Severe malaria is restricted to children under five years of age, whereas asymptomatic infection is nearly ubiquitous among adults.

Passive transfer of purified IgG from malaria-immune adults to children with severe disease led to dramatic reduction in parasitemia and resolution of fever *(102, 103),* suggesting a critical role for humoral immunity against blood-stage parasites. The gradual acquisition of a repertoire of specific antibodies against polymorphic variant specific antigens (VSAs) on the surface of infected erythrocytes is hypothesized to play a critical role in NAI. Protective antibodies could block invasion of merozoites into erythrocytes, aid ADCC-mediated killing by T cells or enhance phagocytosis by macrophages. The most extensively studied VSA is PfEMP1. Of the 60 clonal variants, a restricted subset of PfEMP1 variants is hypothesized to be the critical target of NAI against severe disease and death (*104*). Furthermore, increased susceptibility of severe disease among primagrade women is associated with PfEMP1 variants that bind to unique host receptors in the placenta, exploiting a gap in malaria immunity (*40*). Other merozoites surface antigens such as apical membrane antigen 1 (AMA1) and merozoite surface protein 1 (MSP1) may also serve as key immune targets of humoral immunity. More recently, high levels of antibodies against *P. falciparum* reticulocyte-binding homologue 5 (PfRh5) have been associated with protection. PfRh5 is particularly unique because it is highly conserved and necessary for parasite invasion of erythrocytes (*105*). Unfortunately, acquisition of protective humoral immunity may be hampered by disturbances in peripheral B cell homeostasis *(97).* Dysregulation of BAFF-R expression on B cells may contribute to short-lived antibody responses in children and the slow onset of NAI *(97, 106, 107).*

1.3 Vaccine development

1.3.1 Aim of malaria vaccines

Despite remarkable progress achieved with vector control and prompt treatment, recent hurdles suggest that eradication of malaria will ultimately require a highly effective vaccine. Over the 20th century, vaccines have been critical in control of deadly diseases such as smallpox, polio, and measles (*108*). Arguably the most cost-effective public health intervention, immunizations are estimated to save 2.5 million lives each year (*109*). Traditional vaccines often confer immunity through administration of attenuated whole pathogens or purified toxins. They predominantly function by inducing neutralizing antibodies against highly conserved antigens to mimic immunity acquired following natural infection (*110*). However, repeated exposure in the setting of malaria does not induce sterilizing immunity, suggesting that alternative approaches to vaccine development are necessary.

The Malaria Vaccine Technology Roadmap lays out key goals and strategies for the development of a product that would substantially reduce malaria-related morbidity and mortality and enable eradication of *P. falciparum (111)*. An ideal vaccine would prevent clinical disease in children under five and pregnant women, as well interrupt transmission. Short-term travelers and military personal would also benefit from vaccine-elicited immunity. Ideally, a vaccine regimen would fit within the schedule set up by the World Health Organization Expanded Program on Immunization (WHO EPI). By 2030, the public health community aims to develop a malaria

vaccine for at-risk group in endemic region that reduces risk of clinical disease by 75%. There is currently no licensed vaccine that is widely deployed.

Malaria vaccine strategies are traditionally classified based on the stage of the parasite's lifecycle that it targets (*112*).

Pre-erythrocytic vaccines aim to induce antibodies that block sporozoite invasion of the liver and/or cellular immunity that kill infected hepatocytes (*113*). Intervening at this stage would eliminate or dramatically reduce the load of infectious merozoites that erupt from hepatocytes, decreasing the risk of clinical or severe disease. The most clinically advanced malaria candidate, RTS,S/AS01, along with many other platforms in Phase I/II trials target the pre-erythrocytic stage *(114-117).*

Blood-stage vaccines target antigens that coat free merozoites or are expressed on the surface of parasitized erythrocytes (*118*). These strategies typically aim to induce antibodies that could block invasion of erythrocytes or enhance clearance of infected erythrocytes, thereby reducing the density of parasitemia and risk of severe disease. Unfortunately, development with polymorphic antigens AMA1 and MSP1 has been generally slow with successful induction of durable antibodies and strain-specific protection, but limited evidence of efficacy against clinical disease *(119, 120).* However, recent preclinical studies demonstrate that the highly conserved PfRh5 antigen can induce cross-strain neutralizing antibodies (*105, 121*) and protect non-human primates *(122).* This platform is currently being evaluated in humans.

Transmission blocking vaccines would not prevent disease in the vaccinated individual but aim to protect the community as a whole, by interrupting the development of sexual stages (*123*). Potential targets include gametocytes in the bloodstream or gametes, zygotes and ookinetes within the gut of the mosquito host. Currents efforts focused on the Pfs25 antigen aim to demonstrate that vaccine-elicited antibodies in humans can reduce mosquito infections *(124, 125).*

There are a number of obstacles that have impeded development of a malaria vaccine. First, the size and plasticity of the *P. falciparum* genome coupled with mitotic replication in humans ensures that the parasite can mutate quickly under selective pressure, creating multiple antigenic targets (*126, 127*). Second, differential expression of antigens throughout the complex parasitic lifecycle means that different components of the immune system are required to recognize intracellular and extracellular targets (*128*). Third, a complete understanding of protective immunity against malaria is hampered by the fact that NAI is not sterilizing (*31*), indicating the vaccine-elicited immunity will have to surpass that induced by nature. For these reasons, a multi-stage, multi-antigen vaccine that induces humoral and cellular immunity will be likely to be required for eradication.

1.3.2 Identifying protective mechanisms and targets in pre-erythrocytic immunity

The pre-erythrocytic stage is an attractive vaccine target. Interruption of parasite maturation at this stage can prevent clinical disease in the vaccinated individual, as well as transmission. Furthermore, the number of sporozoites and infected hepatocytes is substantially lower than the number of blood-stage merozoites, reducing the number of targets that must be cleared by vaccine-elicited immunity in order to prevent disease. However, the mechanisms underlying pre-erythrocytic immunity are not completely understood, as NAI fails to protect at this stage. The scientific rationale of a pre-erythrocytic vaccine is based on observations that the administration of irradiated *Anopheles* mosquitoes carrying sporozoites confers sterile protection in mice and humans (*129-131*). Radiation-attenuated sporozoites (RAS) are infectious and arrest during development in the liver before the on-set of blood-stage infection. These groundbreaking papers spearheaded decades of research aimed at dissecting the mechanism of protection induced by pre-erythrocytic immunity **(Figure 1.4)**.

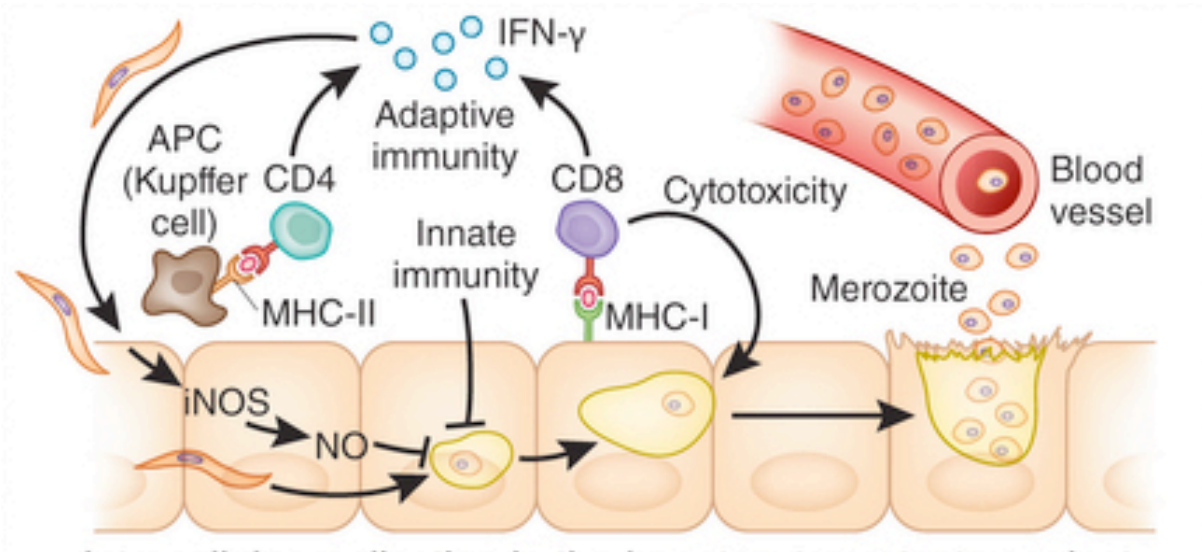

Figure 1.4 Hypothesized mechanisms of cell-mediated immunity in liver-stage infection

Image adapted from **(*132*)**. Hepatocyte invasion of sporozoite triggers many functions of adaptive immunity. Recognition of parasite peptide-MHC class I complex on infected hepatocytes triggers cytokine secretion of antigen-specific $CD8^+$ T cells. IFN-γ can induce the nitric oxide (NO) pathway inside hepatocytes and inhibit parasite development into merozoites. MHC class II recognition of antigen-presenting Kupffer cells can also activate IFN-γ production from $CD4^+$ T cells, as well as mediate $CD8^+$ T cell expansion, antibody maturation, regulatory activity, and direct cytolytic functions.

1.3.2.1 Antibodies

Sporozoite-specific antibodies can function via three broad mechanisms: (1) block invasion of liver, (2) enhance opsonization of free sporozoites or infected hepatocytes, and (3) interfere with intrahepatic development of exoerythrocytic forms. Antibodies from RAS-immunized mice inhibit parasite replication *in vitro* (*133*) and passive transfer of immune sera confers partial protection against murine malaria (*134, 135*). RAS-elicited humoral immunity is predominantly directed against CSP, the immunodominant surface antigen that densely coats the sporozoite surface. CSP mediates several critical steps in the *Plasmodium* lifecycle, including motility to the mosquito salivary glands, migration to the liver in humans, and hepatocyte invasion (*136*). The highly conserved structure is composed of a central repeat domain that is flanked by a N-terminal region with a proteolytic cleavage site and C-terminal region containing a thrombospondin repeat (TSR) motif. The observation that monoclonal antibodies targeting the NANP repeat region directly correlated with protection in mice paved the way for vaccine platforms based on synthetic peptide and DNA recombination, *(137),* most notably RTS,S/AS01 (discussed in further detail in section 1.4.1).

How CSP-specific antibodies mediate sterile protection is unclear, but evidence exists for a number of mechanisms. First, intravital imaging in mice suggests that antibodies can block migration to the liver, by specifically halting sporozoite invasion of the dermal blood vessels (*138*). This could be potentially mediated by cross-linking essential actin-myosin motor machinery, causing paralysis of the

parasite. Second, antibody binding to the CSP N-terminal region blocks *P. falciparum* infection *in vivo* by inhibiting proteolytic cleavage *(139),* a necessary step for invasion. Third, opsonization and phagocytosis of *P. berghei* sporozoites by Kupffer cells are enhanced by CSP polyclonal antibodies *(140, 141).* Fourth, antibodies could inhibit traversal within the liver, specifically by inhibiting critical interactions between CSP and heparin sulfate proteoglycans (HSPGs) on the surface of hepatocytes (*142*). Finally, CSP antibodies can interfere with the intra-hepatic development even when sporozoite invasion is complete, as evidenced by the presence of abnormal trophozoites and schizonts in long-term culture *(143).* The contribution of all of these mechanisms is unknown. Antibodies to other targets such as TRAP and AMA1 have been shown to inhibit sporozoite invasion of hepatocytes *in vitro*, but these are less well studied (*144-146*).

Overall, a pre-erythrocytic vaccine that elicits humoral immunity alone must overcome significant hurdles. CSP-specific antibodies in adults from malaria-endemic regions do not predict resistance to infection (*98*), suggesting that vaccine-elicited antibodies must be qualitatively and quantitatively distinct. Sporozoites remain in the bloodstream for less than an hour, and only one parasite is needed to reach the liver for the maturation of thousands of merozoites and the development of clinical disease.

1.3.2.2 $CD8^+$ T cells

The protracted maturation of sporozoites over 7-10 days in the human liver provides an attractive vaccine target, requiring cellular immunity to recognize intrahepatic

parasites. Preclinical studies have demonstrated that $CD8^+$ T cells that recognize parasite peptide-MHC class I complex molecules on hepatocytes are critical for sterile protection against malaria-liver-stage infection (*147, 148*). $CD8^+$ T cell responses are necessary for RAS-mediated protection in multiple murine models and non-human primates (*135, 149-152*). Furthermore, $CD8^+$ T cells directly correlate with protection elicited by subunit-based platforms in humans *(153).* However, whether they are sufficient is still debatable, and often varies based on the preclinical model and immunization strategy (*149, 154, 155*). Notably, RAS can elicit sterile immunity against *P. berghei* and *P. yoelii* in CD8-deficient BALB/C mice, where antibodies and $CD4^+$ T cells mediate protection (*155*).

Studies using CSP-specific transgenic sporozoites suggest that protective $CD8^+$ T cell responses are primed in skin-draining lymph nodes associated with the site of infection *(156).* $CD8^+$ T cells are hypothesized to migrate and potentially reside long-term in the liver. Further development of intrahepatic $CD8^+$ effector T cells may be initiated by liver sinusoidal cells such as Kupffer cells that are able to cross-present liver-stage antigens (*157, 158*). The phenotype of protective $CD8^+$ T cells is unknown, but recent studies highlight an important role for effector memory cells *(116, 152, 159)* expressing liver-trafficking protein CXCR6 *(160, 161).*

Following recognition of parasite peptide-MHC class I molecules, $CD8^+$ T cell activation triggers a wealth of effector functions. It is hypothesized that IFN-γ secretion is critical for killing infected hepatocytes, as loss of IFN-γ via blocking antibodies or genetic manipulation ablates sterile immunity in mice (*135, 149*). Furthermore, sterile protection in humans elicited by subunit vaccines correlates

with $CD8^+$ T cells producing IFN-γ, but not TNF-α or IL-2 (*153*). Such immunity could be driven by induction of nitric oxide (NO) that kills exoerythrocytic forms *(162, 163),* though IFN-γ derived from innate cells such as γδ or NK cells may also trigger this pathway (*151, 154*). $CD8^+$ T cells with cytolytic activity have been isolated from RAS-immunized mice *(164),* however, the contribution of this mechanism in protection is unknown. Killing activity appears to require direct recognition of infected hepatocytes, as bystander activity does not demonstratively reduce liver burden *(165).*

Multiple different liver-stage proteins have been identified as targets of cell-mediated pre-erythrocytic immunity; however, no single antigen has been demonstrated to be associated with high-level sterile protection. While CSP is the immunodominant antigen for humoral immunity, CSP-specific responses constitute a minority of the $CD8^+$ T cells population elicited by RAS in mice (*166*) and humans (*116, 167*). Furthermore, transgenic *P. berghei* sporozoites that do not express homologous CSP can induce sterile protection *(168),* suggesting an important role for non-CSP antigens. Identification of novel pre-erythrocytic antigen targets remains an area of active investigation *(169-171).* One hypothesis is that a repertoire of different antigenic determinants are involved in protection, instead of a single protective antigen (*114, 167*). For this reason, one vaccine approach is to target multiple epitopes, such as the recombinant immunogen composed of a multiple epitope (ME) string that contains $CD4^+$ and $CD8^+$ T cell epitopes from six antigens (LSA1, LSA3, CSP, STARP, Exp1 and TRAP) (*172*) fused to TRAP (ME-TRAP; further discussed in section 1.4.3). An additional consideration is not the identity of the antigen but the duration of expression over the infection. Prolonged

antigen presentation appears to be critical in sterile immunity, as clearance of sporozoites with antimalarial drugs abrogated protection in mice (*173*). Parasite molecules are retained by the liver for months following infection, enhancing memory formation and expansion of $CD8^+$ T cells (*174*).

1.3.2.3 $CD4^+$ T cells

Less attention has been focused on the protective role of $CD4^+$ T cells, despite the ability to enhance both humoral- and $CD8^+$ T cell-mediated protection (*175*). Murine studies suggest that $CD4^+$ T cells are required for RAS-elicited protection. Depletion of such cells during (but not following) immunization fails to protect against murine malaria infection (*176-178*), suggesting that such cells predominantly orchestrate the induction of effector functions. Preclinical findings are complicated by the fact that the requirement for $CD4^+$ T cells depends on the pathogen species, murine model and immunization strategy *(149)*. In a few human studies, $CD4^+$ T cells specific for pre-erythrocytic antigens correlate with vaccine-elicited protection *(179)* and natural infection *(180)*. However, the mechanism of such protection is unclear.

The inherent heterogeneity of $CD4^+$ T cells allows for functional diversity in pre-erythrocytic immunity. First, $CD4^+$ T cells can mediate an indirect role by augmenting the expansion and survival of cytotoxic $CD8^+$ T cells, likely through the induction of IL-2 or IL4 (*177, 178*). Indeed, effector memory $CD8^+$ T cells immunized in the absence of $CD4^+$ T cells were fully functional but greatly reduced, consistent with a high threshold for cell-mediated protection (*152*).

Second, secretion of IFN-γ by Th1 cells can have a direct effector role by enhancing killing of sporozoites by infected hepatocytes and macrophages via the NO pathway (*155*). Class II restricted immunity is largely dependent on production of IFN-γ *(155).* This is consistent with the observation that the addition of IL-2 or antibodies does not afford protection in mice depleted of $CD4^+$ T cells prior to immunization *(176).*

Third, $CD4^+$ T cells with cytolytic activity may directly kill sporozoites phagocytized by liver-resident Kupffer cells. Passive transfer of $CD4^+$ T cell clones producing perforin and granzymes confer a high degree of protective immunity (*181*) and eliminate hepatocytes in a MHC class II restricted manner *in vitro (164, 182).* Moreover, $CD4^+$ T cells expressing CD107a, a marker of degranulation, are associated with sterile immunity in human immunized with infectious mosquitoes under chloroquine chemoprophylaxis (*179*).

Fourth, regulatory $CD4^+$ T cells (Tregs) could potentially downregulate damaging host inflammatory responses in blood-stage malaria infection (*183*). Less information is known about the role of Tregs during pre-erythrocytic immunity, but depletion of Tregs appears to augment vaccine-induced responses against liver-stage malaria *(184).* At that same time, blood-stage infection may dampen naturally acquired pre-erythrocytic immunity *(185)* and facilitate parasite escape through the production of IL-10 (*186*).

Finally, $CD4^+$ TFH cells in germinal centers mediate production of high-affinity antibodies that reduce the liver burden by modulating the somatic hypermutation

and class switching *(135).* Very little information is known about the role of TFH in pre-erythrocytic immunity (*175*). However, passive transfer of sera from RAS-immunized mice fails to confer reconstitute sterile protection in CD4-depleted mice *(176),* suggesting that other CD4-mediated humoral factors may be necessary.

Overall*,* the contribution of all of these mechanisms in humans is unclear. It is likely that $CD4^+$ T cells are critical for optimal $CD8^+$ T cell and/or humoral immunity, such that the dose of sporozoite challenge and host genetics will dictate requirements for sterile immunity.

1.3.3 Experimental human model

Identification of the mechanism of protection against liver-stage immunity is a critical step in the development of a highly effective pre-erythrocytic vaccine. Studies of natural infection in humans are confounded by ongoing asymptomatic malaria infection, pre-existing immunity and co-infection. Furthermore, most studies are limited to the leukocytes from peripheral circulation, which do not account for tissue-resident T cells that likely play a critical role in liver (*152, 167, 187*). For these reasons, mechanistic studies have taken advantage of murine malaria infection models, including *P. berghei*, *P. yoelii*, and *P. chabaudi (188-190).* Non-human primates models such as *P. falciparum* infection in *Aotus* and *P. knowlesi* infection in *Rhesus* also allow for closer comparisons to the human immune system (*189*). While these models have provided insights into protective immunity, there are notable differences from humans, including the length of liver-stage infection and progression to blood-stage infection (*189*).

Exposure of human volunteers to the bites of infectious mosquitoes or administration of cryopreserved sporozoites has greatly accelerated the development of pre-erythrocytic malaria vaccines (*22, 191, 192*). Standardized as controlled human malaria infection (CHMI), these protocols are safe and have been used in individuals with varying degrees of previous malaria exposure (*22, 193-195*). While profiling of liver-resident cells is still difficult on a large scale, CHMI provides critical information about vaccine efficacy prior to large clinical trials.

1.4 Current status of pre-erythrocytic vaccine development

1.4.1 RTS,S/AS01

The RTS,S/AS01 is composed of the CSP C-terminal region plus 19 NANP central repeats fused to hepatitis B virus surface antigen to form a virus-like particle formulated with the liposome-like AS01 adjuvant. After receiving a positive scientific opinion from the European Medicines Agency in 2015, RTS,S/AS01 will likely become the first malaria vaccine deployed in endemic regions. However, efficacy against clinical and severe malaria in children is partial and wanes dramatically over time, even with boosting (*117, 196-198*). In a large phase 3 trial including 11 sites across seven sub-Saharan African countries, vaccine efficacy against clinical malaria in children 5-17 months old was 50.4% (95% CI 45.8-54.6%), one year after administration of the third dose. Overall efficacy in children who received the fourth "booster" dose declined to 36.3% (95% CI 31.8-40.5%) over four years. Furthermore, a long-term study demonstrated an increased incidence of malaria cases in children who were administered three doses of RTS,S/AS01 compared to the control group five years following vaccination *(199)*. Long-term efficacy of children who received a fourth "booster" shot is unknown. More modest protection against clinical malaria is observed in infants 6 to 12 weeks of age approximately three years following administration of the first vaccine dose, even in those who received a fourth "booster" shot (vaccine efficacy = 25.9%, 95% CI 19.9–31.5) (*200*).

Immunization induces antibodies and $CD4^+$ T cells that target the repeat region of CSP. Time to onset of parasitemia in unprotected children directly correlates with

anti-CS titers (*117, 197*), and IFN-γ-producing $CD4^+$ T cells are associated with reduced risk of infection (*201*). If deployed, surveillance of efficacy in settings of high-intensity transmission *(117)* and genetic diversity of escape parasites *(202)* will be critical.

1.4.2 Whole sporozoite vaccines

The induction of sterile protection via the bites of irradiated mosquitoes carrying sporozoites has provided critical insights into the mechanisms of pre-erythrocytic immunity, but has not provided an immediate vaccination strategy. Clear logistic and regulatory hurdles have prevented deployment. Maintenance of large numbers of irradiated infectious mosquitoes in malaria-endemic regions would likely be insurmountable. Remarkably, Sanaria™ developed the ability to generate aseptic, metabolically active, highly purified, radiation-attenuated sporozoites (PfSPZ Vaccine) that met regulatory standards in 2009 (*203*).

Intravenous (IV) administration of the PfSPZ Vaccine is safe, strongly immunogenic and confers high-level protection against CHMI (*116, 204, 205*). Six out of nine subjects who received four doses of 1.35×10^5 PfSPZ, and six out of six subjects who received five doses were protected against homologous challenge 3 weeks after the final vaccination. One out of six nonvaccinated controls did not exhibit blood-stage parasitemia. Interestingly, intramuscular (IM) or intradermal (ID) administration of the same dose ablates protection (*167*).

Immunization generated both anti-SPZ antibodies that block invasion of hepatocytes *in vitro* and robust cellular immunity (*116*). PfSPZ-specific $CD4^+$ T cells are largely polyfunctional (IFN-γ^+IL-2^+TNF-α^+) with a dose-dependent increase in frequency. Of note, fold-expansion of γδ T cells distinguished protected vs. unprotected vaccinees, consistent with long-term observations of individuals following infection and treatment *(206)*. As discussed above, preclinical studies suggest that IFN-γ secretion mediated by intrahepatic $CD8^+$ T cells is critical in SPZ-elicited protection (*135, 207*). While the PfSPZ Vaccine elicited $CD8^+$ T cell-derived IFN-γ in blood and liver of NHPs (*167*), five out of twelve PfSPZ-vaccinated and protected humans had low to undetectable $CD8^+$ T cell responses in the peripheral blood (*116*). One hypothesis for the observation of protection in the absence of antigen-specific $CD8^+$ T cells is that these cells are sequestered in the liver without circulating. Liver-resident $CD8^+$ T cells are associated with administration of the PfSPZ Vaccine IV, but not ID or IM in NHPs (*167*). However, the inability to challenge *Rhesus macaques* with *P. falciparum* or phenotype liver cells from PfSPZ vaccinated individuals makes this a difficult hypothesis to test. Ongoing clinical trials across three different continents are addressing a number of essential questions: the safety, immunogenicity, and protective efficacy in a wide range of cohorts including semi-immune adults, HIV-infected individuals, and infants; overall optimal dosage; the benefit of multiple immunizations vs. a truncated regimen; the duration of protection; breadth of protection against heterologous strains; and immunologic correlates of protection *(204)*.

Exposure of infectious non-irradiated mosquitoes under chloroquine prophylaxis (CPS) also induces a high-level of sterile protection in mice (*208*) and humans (*179,*

206, 209). This approach exposes the immune system to a broad array of pre-erythrocytic as well as erythrocytic antigens to the immune system, as parasites fully mature to blood-stage merozoites to be cleared by chloroquine in bloodstream (*210*). In an early clinical trial, all ten subjects in the vaccine group were protected against CHMI, while all subjects in the control group exhibited blood-stage parasitemia (*209*). Two later years, four out of six re-challenged subjects were completely protected, suggesting durable PfSPZ-specific cellular immunity (*206*). CPS appears to elicit more efficient longer lasting protection than RAS and requires significantly fewer sporozoites (~45 vs. 1000 infectious mosquito bites), possibly because the PfSPZ Vaccine does not replicate in liver. In parallel experience to the PfSPZ Vaccine, IV (but not ID) administration of infectious nonirradiated cryopreserved PfSPZ under chloroquine prophylaxis (PfSPZ-CVac) induced high-level immunogenicity and protection (*204, 211*).

Despite recent success in early clinical trials, deployability of the PfSPZ Vaccine or PfSPZ-CVac remains a critical challenge. First, sporozoites must be cryopreserved to remain viable and immunogenic, as heat killed sporozoites do not induce protective $CD8^+$ T cell responses (*135, 212*). Deployment of a vaccine that requires long-term liquid nitrogen storage in sub-Saharan Africa is unprecedented, but there is some evidence to suggest that this approach would be as effective as standard cold chains *(213).* Furthermore, it is unclear whether IV administration or direct venous inoculation (DVI) is practical for mass deployment of a vaccine targeted towards children. Development of genetically attenuated parasites (GAP) designed to arrest at the late liver-stage is in early stages (*214-216*) and could address concerns about route. Intradermal administration of sporozoites lacking an essential gene encoding a

protein for fatty acid biosynthesis, but not RAS, provides sterilizing immunity against *P.berghei (217).* However, liquid nitrogen storage of a GAP-based vaccine would likely still be required.

1.4.3 ***Viral vectored vaccines***

Given the critical nature of $CD8^+$ T cells in protection against liver-stage malaria, induction of high-level responses will likely be a crucial component of an effective vaccine. Preclinical studies in mice and NHPs demonstrate that subunit platforms based on highly potent adenoviruses elicit $CD8^+$ T cell responses of high magnitude (*218, 219*). Simian-based vectors such as chimpanzee-derived simian adenovirus 63 (ChAd63) not only induce higher responses, but also address concerns that naturally acquired anti-vector immunity from human-derived viral vectors could diminish induced T cell responses (*220*). The recombinant vaccine insert ME-TRAP targeting liver-stage antigens elicits protective $CD8^+$ T cell responses in mice (*159, 221*) and durable memory T cell responses in NHPs (*222*).

Heterologous prime-boost immunization with ChAd63/MVA ME-TRAP is safe, immunogenic, and elicits protection in malaria-naïve individuals (*153, 223*). This immunization regimen induced a high proportion of cytokine-producing $CD4^+$ and $CD8^+$ T cells, predominantly directed towards TRAP rather than ME. While no protection was induced with ChAd63 alone, the MVA boost clearly improved protective efficacy: 3/14 volunteers were sterilely protected and 5/14 showed a two-day delay in time to patent parasitemia, the latter representing a 95% reduction in liver parasite burden. Overall, ChAd63-MVA provided a total efficacy (delay plus sterile protection) of 58% (8/14), marking the first study to show statistically significant high-level protection induced by a prime-boost regimen. Analysis of immune responses revealed that $CD8^+$ T cells secreting IFN-γ, but not IL-2 or TNF-α, at time of challenge significantly correlated with protection, consistent with

previous studies assessing a similar construct in mice (*221*). Notably, antibodies targeting TRAP did not appear to play a role. Duration of protection is unclear. Three sterilely protected volunteers were rechallenged: one was sterilely protected again and two showed significant delay to patency. While inconclusive, these results encourage larger studies to appropriately assess durability of protective immunity.

ChAd63/MVA vaccination induced greater immunogenicity and efficacy compared to DNA or fowlpox (FP9) priming with the same antigenic insert (*224, 225*). Only 9/38 volunteers were protected with either regimen, the overwhelming majority of whom manifested as delay to patency. This study also demonstrated a substantial improvement over DNA/HuAd5 CSP/AMA1 vaccination, the first regimen to induce predominantly malaria-specific $CD8^+$ vs. $CD4^+$ T cell responses (*226*). The differential results of immunogenicity and efficacy may be caused by a number of reasons. First, pre-existing neutralizing antibody titers against the vector were low. Furthermore, they did not correlate with induced T cell responses, reducing earlier concerns of anti-vector immunity in human adenovirus vaccination. Second, simian adenoviruses induce predominantly $CD8^+$ T cell responses that directly kill infected hepatocytes *in vitro* (*227*) compared to FP9 and DNA priming which induces primarily $CD4^+$ T cell responses (*224, 225*). Third, differential innate immunity elicited by viral vectors may play a critical role in shaping vaccine-induced T cells (*228, 229*).

Promising strategies tested in malaria-naïve individuals often fail to recapitulate high-level immunogenicity and efficacy when deployed in endemic regions (*224, 225, 230, 231*). The role of immunosuppression caused by high parasitemia or

interference of naturally acquired T cells and/or antibodies in vector-induced immunity is unknown. Accordingly, a Phase IIb field study was designed to assess the protective efficacy of this regimen in adults with previous exposure (*115*). Kenyan male volunteers were given either ChAd63/MVA ME-TRAP or the rabies vaccine and monitored for eight weeks for malaria infection. All volunteers were given antimalarials after vaccination and prior to the PCR monitoring period in order to clear any residual parasites (*232*).

Immunogenicity was very promising. Immune responses were biased toward IFN-γ^+ $CD8^+$ T cells and detected up to six months post vaccination, albeit a quarter of the peak. Similarities in the quantity and quality of T cell responses between exposed adults vs. malaria-naïve suggest that vaccination did not boost naturally acquired immunity (*233*). Interestingly, T cell responses were biased to a single TRAP peptide pool. Whether this reflects an enrichment of certain HLA alleles in the region or a mechanism of protection is unclear. Protective efficacy was more difficult to assess. An unexpected spike in rainfall curtailed transmission rates and decreased the overall number of infections, making it difficult to assess efficacy after the 2^{nd} week. Cox-regression analysis suggests that the vaccination regimen reduced the risk of infection by 67% (95% CI 33%-88%), p=0.002 during the 8 weeks of monitoring. Furthermore, risk of high parasitemia (>10 parasites/ml) was reduced by 82% (95% CI 46-94%), p=0.002. Once again a T cell correlate of vaccine efficacy was identified with this approach, in this case the *ex vivo* IFN-γ ELISPOT response to the immunodominant pool of TRAP peptides. Interestingly, efficacy here was higher than previously observed in malaria-naïve adults (*153*). It is unclear whether this reflects a lower challenge inoculum in the field, the extended

effect of atovaquone administered prior to the PCR monitoring period, or a synergistic effect of naturally acquired- and vaccine-elicited immunity. Future field studies will be necessary to answer these questions.

Recombinant viral vectors offer a number of advantages over whole sporozoite-based vaccines. First, the greater ease and cost of manufacture and storage compared to cryopreserved PfSPZ-based vaccines limits hurdles in deployment. Second, ChAd63/MVA ME-TRAP is administrated IM, instead of IV, likely requiring less infrastructure and easing delivery. Finally, there is a good safety profile among adults, children and infants, permitting incorporation into the EPI schedule. However, vaccine efficacy and durability of protection will likely need to be increased in order to demonstrate substantial reductions in clinical malaria among children in areas of high-intensity transmission. One approach could be administering ChAd63/MVA ME-TRAP in combination with RTS,S/AS01. Results from early phase I/IIa trials of this approach have been encouraging (*234*). Furthermore, addition of antigenic inserts such as PfRh5 could enhance humoral immunity against breakthrough merozoites, limiting blood-stage parasitemia.

1.5 Advances in single cell transcriptional analysis

A number of immunological assays are standard in clinical trials for the assessment of vaccine immunogenicity and identification of immunological correlates of protection. In many clinical trials, analysis of cellular immunity is limited to detection of IFN-γ production alone by *ex vivo* ELISPOT (*235, 236*) or IFN-γ, IL-2, and TNF-α by multiparameter flow cytometry in response to restimulation with antigen of interest (*237-240*). Elucidation of protective cellular immunity against a multistage parasite composed of 5000 antigens may likely require technologies that allow assessment of number of parameters at the single-cell level.

Highly multiplexed, single-cell transcriptomics technologies have the potential to unveil functional heterogeneity that may be masked by bulk analyses of seemingly homogenous populations **(Figure 1.5)** (*241-243*). Microfluidic chips from Fluidigm enable thousands of parallel real-time quantitative PCR (RT-qPCR) reactions of up to 96 samples or individual cells at a time (*244*). This technique has been used across a wide range of fields including neurology, developmental biology and cancer *(245-249).* Within immunology, dendritic cells *(250, 251),* $CD4^+$ T cells *(252-254),* and $CD8^+$ T cells *(255, 256)* in mice have been assessed. Recent analysis has described intra-population variance (*256*) and early fate determination (*255*) among vaccine-induced $CD8^+$ T cells. However, these studies are often limited to transgenic or manipulated leukocytes in mice, which may not be predictive of higher animals. In humans, single-cell transcriptional analysis of HIV-specific $CD4^+$ T cells from individuals on antiretroviral treatment has revealed the importance of TFH *(252)* and cytolytic phenotypes *(253).* In the context of human malaria infection, Fluidigm analysis of whole blood following *P.vivax* infection revealed subtle

changes between naïve and malaria-immune volunteers *(257)*. However, single-cell gene expression analysis of malaria-specific T cells in the context of a protective vaccine in humans is lacking (*258*).

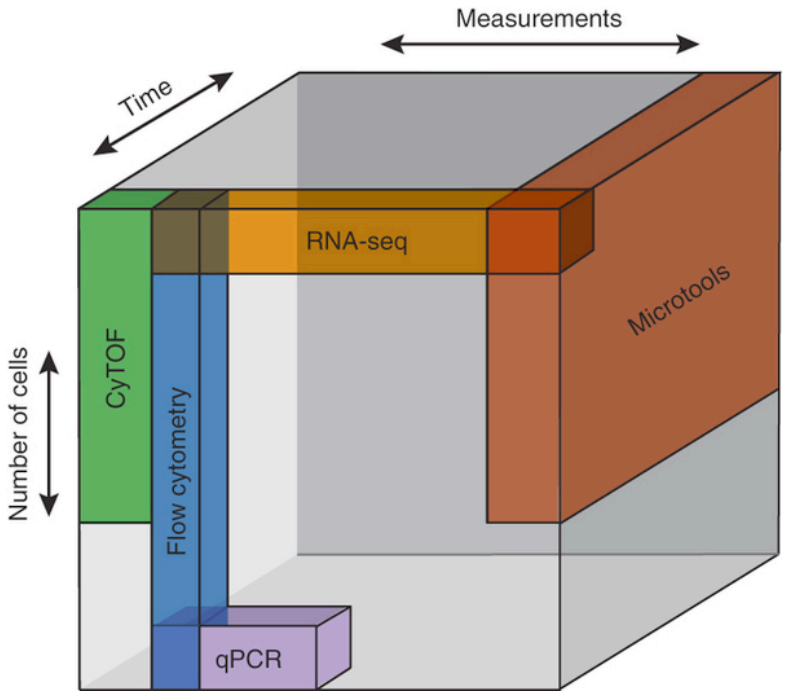

Figure 1.5 Relative structure of data from single-cell analyses

Image taken from **(*241*)**. Major classes of single-cell technologies are plotted schematically in a three-dimensional data cube, reflecting the numbers of parameters assessed (x axis), the numbers of cells measured (y axis), and breadth of temporal resolution afforded (z axis). Overlapping regions highlight complementary technologies that could be used simultaneously.

Single cell RNA-sequencing (scRNA-Seq) is an important extension of transcriptomic technologies (*259-261*). In principle, scRNA-Seq allows unbiased profiling of mRNA without relying on previously described cellular markers and increasing the likelihood of discovery of novel phenotypes compared to RT-qPCR. This technology has already revealed heterogeneity among tumor cells (*262*) and pluripotent stem cells (*263*) that were masked by bulk measurements. However, methodologies are still immature for immunology (*241, 264*). First, lymphocytes inherently contain very little mRNA, such that many important transcripts with low expression do not meet the threshold for scRNA-seq. Second, it is still unclear how many cells are necessary to assess in order to account for variability within antigen-specific T cells. Finally, data analysis tools are relatively underdeveloped, and typical computational approaches such as hierarchical clustering do not necessarily reveal biologically meaningful groups.

Incorporation of additional single-cell technologies such as cytometry by time of flight technology (CyTOF, or mass cytometry) (*265, 266*) and multiplexed secretomes (*267*) will help corroborate transcriptomics findings with proteomic and functional data. Commercial development of the necessary reagents will help guide standardization of these emerging techniques.

1.6 Thesis aims and outline

Vaccine approaches that confer durable and high-level protection are urgently needed, but development is partially hindered by a limited understanding of the mechanisms underlying protective immunity. An effective pre-erythrocytic vaccine will likely required cellular immunity with a broad range of effector functions. Remarkable progress in pre-erythrocytic vaccine development has depended upon strategies that exploit the plasticity of $CD4^+$ T cells and induce potent $CD8^+$ T cells that target liver-stage antigens. The relative contribution of known T cell functions as well as the identification of novel functions is unknown. In-depth characterization of immune responses that may play a role in protection is critical in evaluating next-generation vaccine strategies. Elucidation of effector functions elicited by protective regimens could be used to optimize immunization schedules, design novel adjuvants that promote specific responses or predict protection outcome prior to malaria exposure.

1.6.1 Aims

In this thesis, single-cell transcriptional analysis of malaria-specific T cells from a number of protective Phase I/IIa clinical trials was performed with the following goals:

1. Optimize capture of live malaria-specific T cells and downstream gene expression analysis
2. Evaluate the heterogeneity of the PfSPZ-specific $CD4^+$ T cell response following immunization at the single cell level
3. Assess the molecular signature of such responses induced by PfSPZ vaccination compared to CHMI alone in unvaccinated infection controls
4. Compare the quantitative gene expression profiles of PfSPZ-specific $CD4^+$ T cell responses from protected and non-protected subjects following vaccination
5. Investigate quantitative gene expression profiles of TRAP-specific $CD8^+$ T cells from subjects immunized with ChAd63/MVA ME-TRAP and who exhibited sterile protection, delayed to patent parasitemia or no protection following CHMI
6. Explore transcriptional signatures of $CD4^+$ vs. $CD8^+$ T cell responses induced by a whole parasite vaccine vs. a subunit vaccine, respectively

1.6.2 Outline

Chapter 2 describes the material and methods employed throughout this study.

Chapter 3 describes optimization of CD154 capture assay, single cell gene expression acquisition with the Fluidigm platform, and initial data analysis.

Chapter 4 describes Fluidigm results from VRC312, the first clinical trial to assess the efficacy of IV administration of PfSPZ Vaccine.

Chapter 5 describes Fluidigm results from VRC314, a follow up study to assess durable protective efficacy of the PfSPZ Vaccine.

Chapter 6 describes Fluidigm results from individuals immunized with ChAd63/MVA ME-TRAP over three clinical trials designed to assess immunogenecity and protection.

Chapter 7 summarizes and discusses the results of this study and explores future directions.

2. Material and Methods

2.1 Materials

2.1.1 Reagents

Reagent	Company	Cat. Number
1000uL Pre Sterilized tips	Rainin	RT-L1000F
10uL Pre Sterilized tips	Rainin	RT-L10F
200uL Pre Sterilized tips	Rainin	RT-L200F
20uL Pre Sterilized tips	Rainin	RT-L20F
20X GE Sample Loading Reagent	Fluidigm	100-7610
2x Assay Loading Reagent	Fluidigm	85000736
96-well U bottom plates	VWR International	734-0027
96-well V bottom plates	VWR International	734-0029
Anti-CD28	BD Biosciences	340975
Anti-CD49d	BD Biosciences	340976
BD CompBeads anti-mouse Ig, K	BD Biosciences	51-90-900-1229
Benzonase ® Nuclease	Novagen	70664-3
Bovine Serum Albumin (BSA)	PAA Laboratories	K41-001
Brefeldin A (GolgiPlug™)	BD Biosciences	555029
Cayston Counting Buffer	Sedna Scientific	3813
Control Line Fluid Kit- 96.96	Fluidigm	89000021
Cytofix/Cytoperm™ fixation/permabilization kit	BD Biosciences	555028
Dimethyl suplohoxide (DMSO)	Sigma-Aldrich	D2650
Easy-Peel Heat Sealing Foil, 85 mm x 135 mm	Thermo Scientific	AB-0745

Ethanol	Sigma-Aldrich	32221
Fetal Calf Serum (FCS)	Sigma-Aldrich	F2442
Fluidigm Dynamic Array 96.96 chips	Fluidigm	N/A
Gene Expression Sample Loading Reagent	Fluidigm	85000735
L-glutamine	Sigma-Aldrich	G7513
LIVE/DEAD ® Fixable AquaBlue Dead Cell Stain	Invitrogen	L34955
Luecosep tubes	VWR International	GRE122790UK
MicroAmp Optical 96-Well Reaction Plate with Barcode	Ambion/Applied Biosystems	4306737
Monensin (GolgiStop™)	BD Biosciences	554724
Penicillin/streptomycin (100U penn/100 ug strep)	Sigma-Aldrich	P0781
Percoll	Sigma-Aldrich	P1664
Phosphate Buffered Saline (PBS)	Sigma-Aldrich	D8537
RPMI-1640	Sigma-Aldrich	R0883
Sodium Azide (NaN3)	Fluka Analytical	08591
Staphylococcal enterotoxin B (SEB)	Sigma-Aldrich	S4881
Superasein	Life Tech	AM2696
Superscript III Platinum One-Step qRT-PCR kit	Life Tech	11732-088
TaqMan Universal PCR Master Mix	Life Tech	4364338
TempPlate semi-skirted 96-well PCR plate, natural	USA Scientific	1402-9700
UltraPureTM DEPC-Treated Water	ThermoScientific	750023
Virkon	Fisher	HYG-205-230B

2.1.2 Buffers and solutions

Buffer/Solution	**Components**
R10	RPMI Pen/Strep (0.1 mg/mL) L-glutamine (4mM) FCS (10%)
FACS Buffer	PBS 1% FCS 0.1 NaN_3

2.1.3 Flow cytometric antibodies

Marker	**Clone**	**Isotype**	**Company**	**Cat. Number**
CD3 Cy7APC	SP34-2	Mouse IgG1, λ	BD Biosciences	557757
CD4 Cy55PE	S3.5	Mouse IgG1, κ	Invitrogen	6629154
CD8 BV570	RPA-T8	Mouse IgG1, κ	Biolegend	301038
CD27 Cy5PE	1A4CD27	Mouse IgG1, κ	Beckman Coulter	6607107
CD45RO BV785	UCHL1	Mouse IgG2a, κ	Biolegend	304234
CD69 ECD	TP1.55.3	Mouse IgG1, κ	Beckman Coulter	6607110
CD154 PE	TRAP	Mouse IgG1, κ	BD Biosciences	555700
IFN-γ APC	B27	Mouse IgG1, κ	BD Biosciences	554702
IL2 PE	MQ1-17H12	Rat IgG2a, κ	Biolegend	500307
TNF PE	MAb11	Mouse IgG1, κ	Biolegend	502909
CD14 BV510	M5E2	Mouse IgG2a, κ	Biolegend	301842
CD19 BV510	HIB19	Mouse IgG1, κ	Biolegend	302242
CD107A BV421	H4A3	Mouse IgG1, κ	BD Biosciences	562623

2.1.4 Primers

		Assay Name	ABI Taqman assay ID
Common T Cell Markers	1	BAX	Hs00180269_m1
	2	BCL2	Hs99999018_m1
	3	BCL6	Hs00277037_m1
	4	BIRC3, CIAP2	Hs00154109_m1
	5	CCR1	Hs00174298_m1
	6	CCL3, MIP1a	Hs00234142_m1
	7	CCL5, RANTES	Hs00174575_m1
	8	CCR3	Hs00266213_s1
	9	CCR4	Hs99999919_m1
	10	CCR7	Hs99999080_m1
	11	CCR8	Hs00174764_m1
	12	CD27	Hs00154297_m1
	13	CD28	Hs00174796_m1
	14	CD40LG, CD154	Hs00163934_m1
	15	CD48, BLAST	Hs00152927_m1
	16	CD69	Hs00934033_m1
	17	CD84	Hs01547121_m1
	18	CSF1, MCSF	Hs00174164_m1
	19	CSF2, GMCSF	Hs00929873_m1
	20	CTLA4	Hs03044418_m1
	21	CXCL13, BLC	Hs00757930_m1
	22	CXCR3, MIGR	Hs01847760_s1
	23	CXCR4	Hs00237052_m1
	24	CXCR5	Hs00540548_s1
	25	DPP4, CD26	Hs00175210_m1
	26	EOMES, TBR2	Hs00172872_m1
	27	FAS	Hs00531110_m1
	28	FASLG, CD95LG	Hs00181225_m1
	29	FLIP	Hs01116280_m1
	30	FOXP1	Hs00212860_m1
	31	FOXP3	Hs00203958_m1
	32	GABPA	Hs01022023_m1
	33	GAPDH	Hs99999905_m1
	34	GATA3	Hs00231122_m1
	35	GZMA, CTLA3	Hs00989184_m1
	36	GZMB, CTLA1	Hs01554355_m1
	37	HLADRA	Hs00219575_m1
	38	ICOS	Hs00359999_m1
	39	IFNg	Hs00174143_m1
	40	IL13	Hs99999038_m1

	41	IL16	Hs00189606_m1
	42	IL2	Hs00174114_m1
	43	IL21R	Hs00222310_m1
	44	IL2Ra, CD25	Hs00907777_m1
	45	IL2RB	Hs01081697_m1
	46	IL3	Hs99999081_m1
	47	IL4R	Hs00166237_m1
	48	IL6R, CD126	Hs00169842_m1
	49	IL7R, CD127	Hs00233682_m1
	50	IRF4	Hs01056533_m1
	51	LEF1	Hs01547250_m1
	52	LIF	Hs00171455_m1
	53	MAF	Hs00193519_m1
	54	MKI67, Ki67	Hs01032443_m1
	55	MYC	Hs00905030_m1
	56	CXCR6	Hs00174843_m1
	57	PD1	Hs00169472_m1
	58	POU2AF1	Hs01573371_m1
	59	PRDM1, Blimp1	Hs00153357_m1
	60	PTPN6, SHP1	Hs00169359_m1
	61	RORA	Hs00536545_m1
	62	RORC	Rh02892670_m1
	63	RUNX1	Hs00231079_m1
	64	RUNX3	Hs00231709_m1
	66	SH2D1A, LYP	Hs00158978_m1
	67	SLAMF1, CD150	Hs00234149_m1
	68	CCR5	Hs00152917_m1
	69	SOCS1	Hs00705164_s1
	70	SOCS2	Hs00919620_m1
	71	SOX5	Hs00753050_s1
	72	STAT1	Hs01013996_m1
	73	STAT3	Hs01047580_m1
	74	STAT6	Hs00598625_m1
	75	TBX21, TBET	Hs00894392_m1
	76	TCL1A	Hs00951350_m1
	77	TGFB1	Hs00998133_m1
	78	TGFBR1	Hs00610318_m1
	79	TIMP1	Hs99999139_m1
	80	TIMP2	Hs00234278_m1
	81	TNF, TNFa	Hs00174128_m1
	82	TNFRSF11A, RANK	Hs00187192_m1
	83	TNFRSF4, OX40	Hs00533968_m1
	84	TNFSF10, TRAIL	Hs00921974_m1
	85	TNFSF13B, BAFF	Hs00198106_m1
	86	TNFSF14, LIGHT	Hs00542477_m1

	87	TRAF2	Hs00184192_m1
	88	TRAT1, TRIM	Hs00179626_m1
$CD4^+$ T Cell-Specific Markers			
	1	CCR6	Hs00171121_m1
	2	CD4	Hs00181217_m1
	3	IL10	Hs99999035_m1
	4	IL17α	Hs00174383_m1
	5	IL21	Hs00222327_m1
	6	IL4	Hs00174122_m1
	7	IL5	Hs99999031_m1
	8	TNFRSF9, CD137	Hs00155512_m1
$CD8^+$ T Cell-Specific Markers	1	CD8a	Hs00233520_m1
	2	GZMH	Hs00277212_m1
	3	GZMK	Rh02841007_m1
	4	GZMM	Hs00193417_m1
	5	KLRG1	Rh00929962_m1
	6	LAMP2	Rh02841752_m1
	7	NKG2D	Rh01095630_m1
	8	TNFSF8	Hs00174286_m1

2.1.5 Electronic equipment

Equipment	**Company**	**Applicable Software**
BD LSRII Flow Cytometer	BD Biosciences	BD FACSDIVA + FlowJo v.9.7.5
Biomark HD System	Fluidigm	Fluidigm Data Collection + Real-Time PCR Analysis Software
IFC Controller HD	Fluidigm	N/A
BD FACs ARIA III Flow Sorter	BD Biosciences	BD FACsDIVA + FlowJo v.9.7.5
CasyCounter	Scharfe System	N/A
G Storm PCR Machine	Lab Tech	N/A

2.2 Clinical Trials

2.2.1 VRC312

VRC 312 (ClinicalTrials.gov #NCT01441167) was approved by the Intramural Institutional Review Board (IRB) of the National Institute of Allergy and Infectious Diseases (NIAID). Immunized human specimens were collected under this protocol. Malaria-naïve human specimens (unexposed to *Plasmodium falciparum*) were obtained from fully anonymized donors and used under IRB (NIH, NIAID) exception.

The clinical design of VRC312 has been previously discussed (*116*). Briefly, VRC312 was a phase 1, open-label, dose escalation trial to assess safety, immunogenicity and efficacy of the PfSPZ Vaccine administered by intravenous (IV) injection. The analysis described in this thesis is based on data from malaria-naïve, healthy adults, 18-45 from the Greater Baltimore-Washington area who received 4 or 5 doses of the $1.35x10^5$ PfSPZ Vaccine and unvaccinated infection controls. These subjects underwent controlled human malaria infection (CHMI) with Pf3D7, a clone derived from NF54 strain. CHMI was achieved three weeks after the final vaccination, and a re-challenge was administered in a selected group of subjects approximately four months later. Subjects were considered protected if daily thick blood smears were negative 28 days post-CHMI. Further details on the clinical protocol rationale and vaccination schedule are provided in Chapter 4.

2.2.2 VRC314

VRC 314 (ClinicalTrials.gov #NCT02015091) was approved by the IRB of NIAID. Immunized human specimens were collected under this protocol.

The clinical design of VRC314 has been previously discussed (*205*). Briefly, VRC314 was a multi-institution phase 1, open-label, dose escalation trial to assess safety, immunogenicity and efficacy of the PfSPZ Vaccine administered by IV or IM injection. The analysis described in this thesis is based on data from malaria-naïve, healthy adults, 18-45 from the Greater Baltimore-Washington area who received three different vaccine regimens: four doses of $1.35x10^5$ PfSPZ followed by a fifth dose of $4.5\ x10^5$ PfSPZ (Group 3), three doses of $2.7\ x\ 10^5$ PfSPZ (Group 1) or four doses of $2.7\ x\ 10^5$ PfSPZ (Group 4 and 5). These subjects underwent CHMI with Pf3D7 at either 3 weeks (Groups 1,3,4) or 21-24 weeks (Group 5) following the final vaccination. Subjects were considered protected if daily thick blood smears were negative 28 days post-CHMI. Further details on the clinical protocol rationale and vaccination schedule are provided in Chapter 5.

2.2.3 MAL34

MAL34 (ClinicalTrials.gov #NCT00890760) has been previously described (*153*). Briefly, MAL34 was a phase I/IIa sporozoite challenge trial to assess protection against malaria in healthy adults, 18-50 recruited from the United Kingdom who were vaccinated with ChAd63 ME/TRAP alone, and as a heterologous boost with MVA ME/TRAP. Of note, the trial was conducted in two parts (A and B). As immunogenicity data from both studies were not significantly different, the groups were combined and analyzed together. All study groups assessed under this protocol are described in **Table 2.1**. However, only subjects who were vaccinated with ChAd63/MVA ME-TRAP and assessed for short-term protection (Groups 1 and 5) were analyzed in this thesis.

Group	Part	Vaccine regimen	Interval between vaccinations	Interval between vaccination and challenge (weeks)
1	A	ChAd63 – MVA	8 week	2-3
2	A	ChAd63		3-4
3	A	No vaccine control		
4	B	ChAd63 – MVA	8 week	12
5	B	ChAd63 – MVA	8 week	2-3
6	B	Re-challenge		
7	B	No vaccine control		
8	B	Ad+M – Ad+M – Ad+M	8 week	2-3
9	B	Ad+M – Ad+M	8 week	2-3
10	B	Ad+M – Ad+M – Ad+M	4 week	2-3

Table 2.1 MAL34 study design

Table obtained from MAL034 Study Protocol. ChAd63 = ChAd63 ME/TRAP, MVA= MVA ME/TRAP, Ad+M = both vaccines mixed prior to administration.

2.2.4 VAC45

VAC45 (ClinicalTrials.gov # NCT01623557) has been previously described (*268*). Briefly, VAC45 was a phase I/IIa sporozoite challenge trial to assess protection against malaria in healthy adults, 18-50 recruited from the United Kingdom who were vaccinated with ChAd63/MVA containing the ME-TRAP or CS insert.

All study groups assessed under this protocol are described in **Table 2.2**. However, only subjects who were vaccinated with ChAd63/MVA ME-TRAP and assessed for short-term protection (Group 2) were analyzed in this thesis.

Group Number	No of volunteers	Prime- Day 0	Boost- Day 56	CHMI
1	15	ChAd63 CS 5×10^{10} vp IM	MVA CS 2×10^{8} pfu IM	YES
2	15	ChAd63 ME-TRAP 5×10^{10} vp IM	MVA ME-TRAP 2×10^{8} pfu IM	YES
3	6	-	-	YES

Table 2.2 VAC45 study design

2.2.5 VAC52

VAC52 (ClinicalTrials.gov # NCT01623557) has been previously reviewed (*219*). Briefly, VAC52 was a phase I/IIa sporozoite challenge trial to assess protection against malaria in healthy adults, 18-50 recruited from the United Kingdom who were vaccinated with ChAd63/MVA ME-TRAP combined with ChAd63/MVA CS or with ChAd63/MVA CS plus ChAd63/MVA AMA1. All study groups assessed under this protocol are described in **Table 2.3**. However, only subjects who were vaccinated with ChAd63/MVA CS/ME-TRAP and assessed for short-term protection (Group 1) were analyzed in this thesis.

Group Number	No of volunteers	Prime- Day 0	Boost- Day 56	CHMI
1	13	Mixture of ChAd63 ME-TRAP/CS, each at $5x10^{10}$ vp IM	Mixture of MVA ME-TRAP/CS, each at $2x10^{8}$ pfu IM	YES
2	13	Mixture of ChAd63 ME-TRAP/CS/AMA-1, each at $5x10^{10}$ vp IM	Mixture of MVA ME-TRAP/CS/AMA-1, each at $1.33x10^{8}$ pfu IM	YES
3	6	-	-	YES

Table 2.3 VAC52 study design

2.3 Clinical immunology

2.3.1 Blood separation

PBMCs were isolated by density-gradient centrifugation from EDTA anti-coagulated whole blood as previously described (*116, 153*). All assessment of cellular immune responses using multi-parameter flow cytometry was done from PBMCs on cryopreserved samples at the completion of all studies. To thaw, PBMCs were immersed in a 37°C water bath for 90 seconds. Cells were then added drop-wise to 15ml warm R10 in a falcon tube. Cells were centrifuged at 750xg for 5 minutes and the pellet resuspended in complete RPMI (RPMI-1640 containing 2 mM L-glutamine, 10% v/v heat-inactivated FCS, 100 U/mL penicillin, 100 µg streptomycin, 25 mM HEPES buffer, 0.1% v/v 2-mercapto-ethanol) containing 25 U / mL Benzonase.

2.3.2 PfCSP ELISA

ELISA measurement of IgG against PfCSP has been previously described (*116, 205*). Briefly, a recombinant Pf circumsporozoite protein (rPfCSPv2, lot#122006) expressed in *Picha pastoris* encoding Pf3D7 minus the first 48 amino acids was used. 96-well plates were coated overnight at 4°C with 2.0 µg rPfCSP/mL in 50 µL per well in coating buffer. Plates were then washed three times with 1x imidazole-based wash solution containing 2 mM imidazole, 160 mM NaCl, 0.02% Tween-20, 0.5 mM EDTA and blocked with 1% Bovine Serum Albumin (BSA) blocking buffer (KPL) containing 1% non-fat dry milk for 1 hour at 37°C. Plates were washed three times and serially diluted samples (in triplicates) were added and incubated at 37°C for 1 hour. After washing three times, peroxidase-labeled goat anti-human IgG

(KPL) was added at a dilution of 0.1 μg/mL and incubated at 37°C for 1 hour. After washing three times, ABTS peroxidase substrate was added for plate development, and the plates were incubated for 75 minutes at 22°C. The plates were read with a Spectramax Plus384 microplate reader (Molecular Devices) at 405 nm. The data were collected using Softmax Pro GXP v5. Data were fit to a 4-parameter sigmoidal curve, and the reciprocal serum dilution at which the optical density was 1.0 (OD1.0) calculated.

2.4 Flow cytometry

2.4.1 Intracellular staining of PfSPZ-specific T cells

Thawed PBMCs were rested for 8 hours in complete RPMI, and plated in 200 μL of media at $1.5x10^6$ cells per well in a 96-well V-bottom plate and stimulated for 17 hours at 37°C with: (a) PfSPZ Vaccine diluent (1% Human Serum Albumin); (b) $1.5x10^5$ viable, irradiated, aseptic, purified, cryopreserved PfSPZ from a single production lot; (c) $2x10^5$ lysed, infected RBC consisting of >90% parasitemic late-stage schizonts (PfRBC) from a single production lot; or (d) a single lot of donor-matched uninfected erythrocytes (uRBC). For the last 5 hours of the stimulation, 10 μg/mL Brefeldin A (BD) was added to the culture. A positive control sample from a subject vaccinated with 5 doses of $1.35x10^5$ PfSPZ IV and negative malaria-naïve control were included for each day subjects were analyzed to determine the consistency of antigen stimulation.

Following *in vitro* stimulation, cells were stained as previously described (*116*). Dead cells were identified by Aqua Live-Dead dye (Invitrogen) per manufacturer's instructions. This was followed by 15 min surface staining at room temperature for CD3, CD4, CD8, CD27, and CD45RO. Cells were washed, fixed, and permeabilized using Cytofix/Cytoperm kit (BD) and stained intracellularly for IFN-γ, IL-2, TNFα. Cells were washed, fixed in 0.5% paraformaldehyde, and acquired on a modified LSR II (BD Biosciences). Flow cytometric data were analyzed using FlowJo. All antigen-specific cytokine frequencies are reported after background subtraction of identical gates from the same sample incubated with the control antigen stimulation (1% HSA).

2.4.2 TRAP peptide pools

Crude 20-mer peptides overlapping by 10 amino acids spanning the length of the *P. falciparum* T9/96 sequence contained in the ME.TRAP vaccine insert were synthesized by Thermo Fisher Scientific (See Appendix for details). Peptides were reconstituted in DMSO at a concentration of 50-100mg/ml depending on solubility and stored at -80°C until use. A pool containing all 56 peptides spanning the T9/96 strain of TRAP antigen (1μg/ml) was used for *in vitro* stimulation.

2.4.3 Isolation of PfSPZ-specific CD4$^+$ T cells

PBMCs were stimulated with PfSPZ or 1% HSA as described above for only 14 hours without BFA. CD154 PE (TRAP1) was added at the beginning of the stimulation. For optimization experiments only, 2μM monensin (BD Biosciences) were added for the last 5 hours. Surface staining was similar to described above, except without permeabilization and intracellular staining. This was followed by surface staining at room temperature for the remaining antibodies (including CD69) and AquaBlue.

2.4.4 Isolation of TRAP-specific CD8$^+$ T cells

Thawed PBMCs were rested for 8 hours in complete RPMI and plated in 200 μL of media at 2x10^6 cells per well in a 96-well V-bottom plate, and stimulated for 18 hours with either (1) TRAP peptide pools, anti-CD28 and anti-CD49d, all at 1 μg/ml or (2) anti-CD28 and anti-CD49d alone. CD107a BV421 (H4A3) was added at the beginning of the stimulation. Brefeldin A or monensin was not added. Surface staining was similar to described above. Briefly, cells were surface stained with

CCR7 for 20 min. This was followed by surface staining at room temperature for the remaining antibodies and AquaBlue.

2.4.5 Single cell sorting

After washes, 1-100 $CD69^{+}CD154^{+}$ $CD4^{+}$ T cells or $CD107a^{+}CD8^{+}$ T cells were sorted on a 20-parameter FACSARIA Sorter, running FACSDiVa software to allow indexed sorting.

2.5 Acquisition of single cell gene expression

2.5.1 Fluidigm

Inventoried TaqMan gene-expression assays (20×, Life Technologies) were pooled to a final concentration of 0.2× for each of the 96 assays. Single or bulk antigen-specific $CD4^+$ T cells were sorted directly into 96-well PCR plates containing Cells Direct Reaction Mix (Invitrogen) and pooled gene expression assays (PreMix; See **Table 2.4**). Reverse transcription, cDNA synthesis, and sequence-specific amplification were performed using the Invitrogen Cells Direct Kit™ (Life Technologies), as previously described (**Table 2.5**) (*244*). High-throughput quantitative PCR was done on 96.96 Dynamic Arrays with the BioMark system (Fluidigm). Cycling threshold values were calculated with BioMark system software.

PREMIX (1X)	Single Cell Sample, 1 well
Sample	0 ul
DEPC H_2O	1.4 ul
Cells Direct 2X Reaction Mix	5 ul
Superscript III + Taq	1 ul
0.2X Dilute TaqMan Assays (200nM)	2.5 ul
Superasein	0.1 ul
TOTAL (per well):	10 ul

Table 2.4 Fluidigm premix for sorting

Reverse Transcription	50°C for 15 min	
Inactivation of RT enzyme	95°C 2 min	
1st Cycle	95°C 15sec 60°C 4min	
Repeat 1st Cycle 17 additional times		**18 Pre-Amplification Cycles**

Table 2.5 Fluidigm pre-amplification

2.6 Data analysis

Flow cytometry data were analyzed using FlowJo v9.8.5 (Tree Star). Statistical analysis was performed with Pestle v1.7 and SPICE v5.3 (M. Roederer) (*269*) and Prism 6 (GraphPad). Graphs were rendered in FlowJo, SPICE, and Prism.

Single cell gene expression data were analyzed using JMP 11 (SAS) and R (R 3.2.2). Model-based Analysis of Single-cell Transcriptomics (MAST) was use for filtering of failed reactions and statistical outliers and is available as an R package (http://www.github.com/ RGLab/MAST) (*270*). Statistical significance for gene expression considered at $p<0.001$ and 2-fold change, unless noted otherwise.

3. Optimization of Single Cell Gene Expression Acquisition

3.1 Introduction

Immunization with irradiated SPZ is the gold standard for conferring high-level protection in mice and humans at the pre-erythrocytic stage of malaria infection (*129-131*). Protection in mice is multi-factorial and involves antibodies, $CD4^+$ and $CD8^+$ T cells. In humans immunized with irradiated PfSPZ, there has been limited characterization of PfSPZ-specific cell-mediated immunity. As such, there is an ongoing investigation of the magnitude, quality and phenotype of T cell responses elicited by PfSPZ Vaccine using a variety of technologies.

Preclinical studies suggest that cellular immunity is required for attenuated SPZ-induced protection against murine malaria (*271*). To date, multi-parameter flow cytometry has been used to characterize the phenotype, magnitude and quality of PfSPZ-specific T cell responses following vaccination or infection. To substantially expand the analysis of such responses, high-resolution, quantitative transcriptome analysis of PfSPZ-specific $CD4^+$ T cells was performed using Fluidigm 96.96 Dynamic Arrays. The aim of this chapter was to optimize the isolation of PfSPZ-specific $CD4^+$ T cells from vaccinated subjects and assess the Fluidigm platform for downstream bulk and single-cell gene expression analysis.

The VRC312 clinical trial was designed to assess the immunogenecity and efficacy of the PfSPZ Vaccine against malaria infection (*116*). Fifteen subjects were vaccinated with either four or five doses of $1.35x10^5$ PfSPZ by the intravenous (IV) route. Three weeks following the final vaccination, all subjects underwent controlled human malaria infection (CHMI). Six out of nine subjects who received four doses were sterilely protected, six out of six who received five doses were sterilely protected. As the aim of this thesis was to identify immune correlates of protection, T cell responses at one week prior to challenge in samples from this trial will be examined and reported in subsequent chapters (Chapters 4 and 5). In this chapter, in order to optimize the assay without wasting precious samples, PBMCs isolated post-challenge were analyzed.

3.2 Results

3.2.1 Detection of antigen-specific T cell responses following intravenous administration of PfSPZ Vaccine

Multi-parameter flow cytometry was first used to assess the frequency of antigen-specific IFN-γ-producing T cells from a representative subject immunized with five doses of $1.35x10^5$ PfSPZ Vaccine IV. Three weeks following the final vaccination, this subject was sterilely protected upon CHMI. One week prior to CHMI, this volunteer was bled, and PBMCs were subsequently isolated and cryopreserved. Antigen-specific T cells were assessed on thawed PBMCs by overnight restimulation with $1.5x10^5$ cyropreserved irradiated sporozoites (PfSPZ) or $2.0x10^5$ *P. falciparum*-infected red blood cells (PfRBCs). The PfSPZ diluent (1% human serum albumin [HSA]) and mock-cultured uninfected RBCs (uRBCs) served as the respective controls. The memory phenotype of malaria-specific T cells was determined based on the differential expression of CD27 and CD45RO. IFN-γ is postulated to be important for protection elicited by this vaccine and other pre-erythrocytic vaccines in humans (*129, 135, 272*), and thus served as an initial surrogate measure of immunogenecity in this study.

One week prior to CHMI, memory T cell responses were assessed **(Figure 3.1)**. $CD4^+$ T cells produced IFN-γ in response to PfSPZ and PfRBC stimulation *in vitro*. Antigen-specific memory $CD8^+$ T cells were not detected in response to either stimulation (data not shown), consistent with published data *(116)*.

Given the potential role of $CD4^+$ T cells in PfSPZ-elicited protective immunity and the significant increase in antigen-specific responses following vaccination, further phenotypic analysis of PfSPZ-specific $CD4^+$ T cells was pursued.

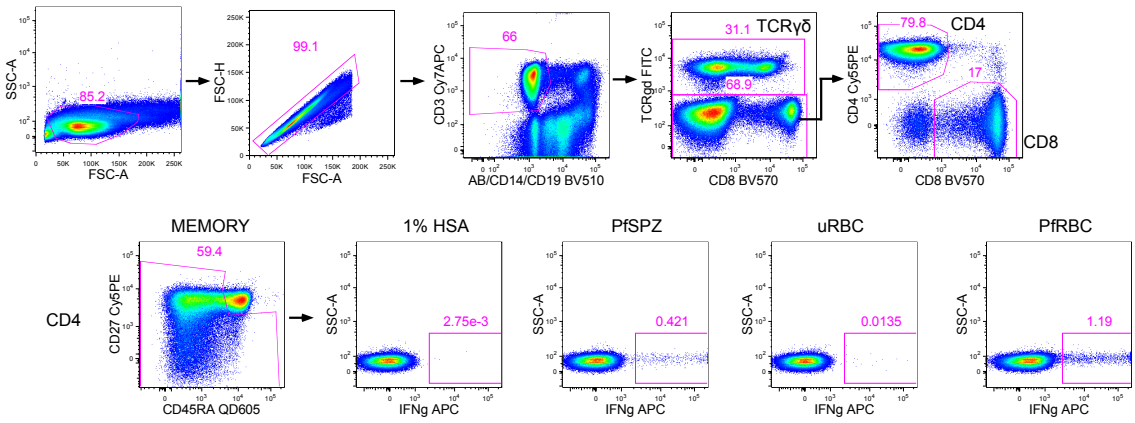

Figure 3.1 Detection of antigen-specific $CD4^+$ T cells following PfSPZ Vaccine.

PBMCs from an individual administered $1.35x10^5$ PfSPZ Vaccine IV, three weeks following the final vaccination. PBMCs were stimulated for 17 hours with $1.5x10^5$ PfSPZ or $2.0x10^5$ PfRBCs. The PfSPZ diluent (1% HSA) and uRBCs served as the respective controls.

3.2.2 Optimization of PfSPZ-specific CD4$^+$ T cell isolation

The first aim was to establish the capacity to detect the global malaria-specific CD4$^+$ T cell response without altering the viability of responding cells. As such, the cell surface expression of CD154, a costimulatory maker expressed on activated but not resting CD4$^+$ T cells following *in vitro* stimulation was assessed (*273-276*). Detection of CD154 on recently activated CD4$^+$ T cells is particularly difficult due to rapid internalization of the marker upon surface expression. In this setting, detection is further complicated by the unique stimulation of PBMCs with an entire parasite (PfSPZ), unlike traditional assays that are restricted to a single peptide or protein. Preliminary studies sought to confirm *de novo* detection of CD154 on memory CD4$^+$ T cells using a relatively simple protein stimulation.

To define optimal conditions for capturing CD154$^+$ CD4$^+$ T cells, antigen-specific responses to cytomegalovirus (CMV) pp65 protein were assessed in a seropositive individual **(Figure 3.2-A)**. Peak CD154 responses were detected 10 hours following *in vitro* stimulation in the presence of monensin, as described in previous studies (*273, 274*). Monensin likely inhibits acidification of endosomes containing the internalized CD154-antibody complex, preserving detection of the fluorochrome over a longer period of time. However, Golgi inhibitors can potentially affect detection of cellular mRNA via alterations in intracellular transport, precluding simultaneous use with downstream transcriptomic analysis. Thus, all experiments henceforth were performed in the absence of monensin. In this setting, the peak expression of CD154 on CMV-specific CD4$^+$ T cells was detected 10 hours after stimulation, decreasing with a longer incubation time.

It was hypothesized that optimal CD154 detection on PfSPZ-specific $CD4^+$ T cells may require a longer period of stimulation, due to the fact the whole parasite must be processed by antigen presenting cells. To resolve this issue, PBMCs isolated three months post CHMI from a subject vaccinated with $1.35x10^5$ PfSPZ IV and sterilely protected were stimulated with PfSPZ for various time periods. The peak expression of CD154 on PfSPZ-specific $CD4^+$ T cells was detected 14 hours after stimulation **(Figure 3.2-B)**.

In order to minimize noise in the downstream mRNA expression assays, it was necessary to increase the purity of the antigen-specific T cells. To reduce frequency of background events from matched control samples (1% HSA), a gate was applied to encompass only $CD69^+CD154^+$ CD4 T cells for the purpose of identifying PfSPZ-specific responses. Activation of T cells induced upregulation of CD69, which is then stably expressed on the cell surface for up to 48 hours (*277*). Dual expression of CD69 and CD154 clearly delineated a distinct population of PfSPZ-specific $CD4^+$ T cells compared to control samples. Furthermore, the background CD154 response in the presence of 1% HSA or cell media did not increase significantly over time **(Figure 3.2-C)**. CD154 responses did not increase in the presence of a CD40-blocking antibody **(Figure 3.2-D)**, as previously shown in murine studies (*278*). Therefore, PfSPZ-specific CD4 T cells were subsequently identified as $CD69^+CD154^+$ $CD4^+$ T cells detected 14 hours after *in vitro* stimulation.

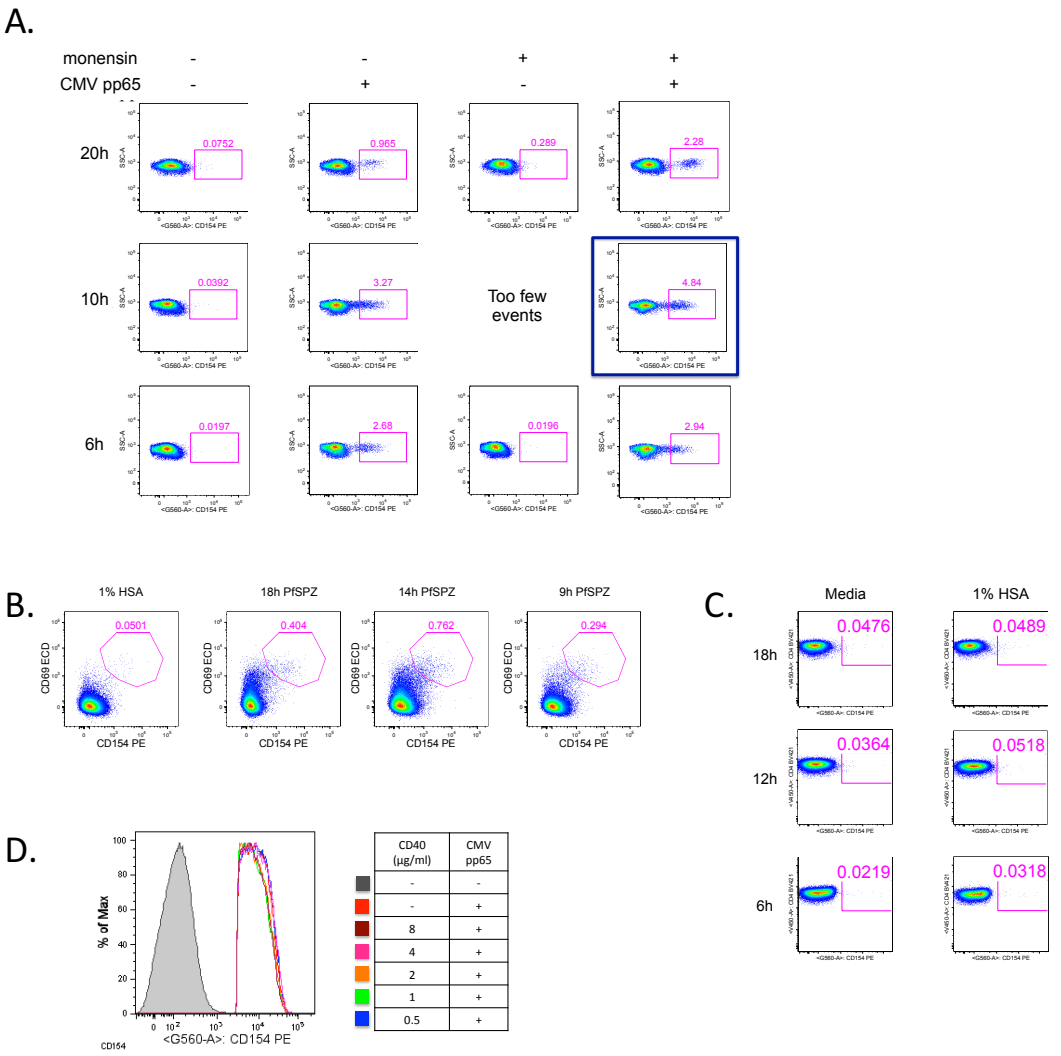

Figure 3.2 Optimization of PfSPZ-specific CD4$^+$ T cell capture.

(A) PBMCs from a malaria-naïve individual were stimulated with CMV pp65 protein for various time periods in the presence or absence of monensin. CD154 antibody was included in the beginning of the stimulation and monensin was added for the last 5 hours. **(B)** PBMCs from a malaria-naïve individual were incubated for various time periods with media alone or 1% HSA in the presence of CD154 antibody. **(C)** PBMCs from an individual administered 1.35x10^5 PfSPZ Vaccine IV were restimulated *in vitro* with 1.5x10^5 PfSPZ in the presence of CD154 antibody for various time periods. **(D)** Same individual and stimulation in part (C) except with varying concentrations of CD40 blocking antibody.

3.2.3 Simultaneous detection of CD154 and CD69 for capture of broad PfSPZ-specific CD4$^+$ T cell response

The second aim was to validate the ability of the assay to detect a predominant proportion of PfSPZ-specific, cytokine-producing CD4$^+$ T cells. In principle, all recently activated CD4$^+$ T cells express CD154 on the cell surface (*276*). The concordance of CD154 expression from activated CD4$^+$ T cells and the production of IFN-γ, IL-2 and TNFα was determined. These are the most common cytokines used to characterize effector functions of CD4$^+$ T cell responses to many vaccines based on their role in protection and the high sensitivity of detecting them.

First, the proportion of CD69$^+$CD154$^+$ CD4$^+$ T cells that produced any combination of IFN-γ, TNFα and IL-2 was estimated **(Figure 3.3-A)**. Approximately 84% of PfSPZ-specific CD4$^+$ T cells that produced any of the measured cytokines above background were CD69$^+$CD154$^+$. This confirmed that the assay detected a substantial proportion of the PfSPZ-specific CD4$^+$ T cell response heretofore characterized by intracellular staining.

Next, the limitations of the assay were determined. The coupled expression of CD69 and CD154 on cells produced any of the measured cytokines was assessed. Expression of antigen-specific CD154 in the absence of CD69 was marginal (1.25 vs. 11 fold-change of CD69$^+$CD154$^-$ vs. CD69$^+$CD154$^+$ upon restimulation), confirming specificity of CD154 to mark recent activation. A notable proportion (25%) of cytokine-producing CD69$^+$ CD4$^+$ T cells did not express CD154. However, a similar proportion was also detected on cells from control samples.

Despite the stated benefits, there was an initial concern that sorting $CD69^{+}CD154^{+}$ $CD4^{+}$ T cells would skew representation of the total PfSPZ-specific response. Comparison of $CD69^{+}$ cytokine-producing cells that did or did not express CD154 illustrated that the both groups were composed of a similar proportion of each possible phenotypic population measured in this assay **(Figure 3.3-B)**. This suggests that $CD69^{+}CD154^{+}$ detection selects a representative subset of the total PfSPZ-specific $CD4^{+}$ T cell response.

Finally, the benefits of this assay for enhanced detection of antigen-specific $CD4^{+}$ T cells were described. Among $CD69^{+}CD154^{+}$ PfSPZ-specific $CD4^{+}$ T cells, approximately 38% (range: 30-52%, n = 4 subjects) did not produce IFN-γ, IL-2 or TNFα **(Figure 3.3-C)**.

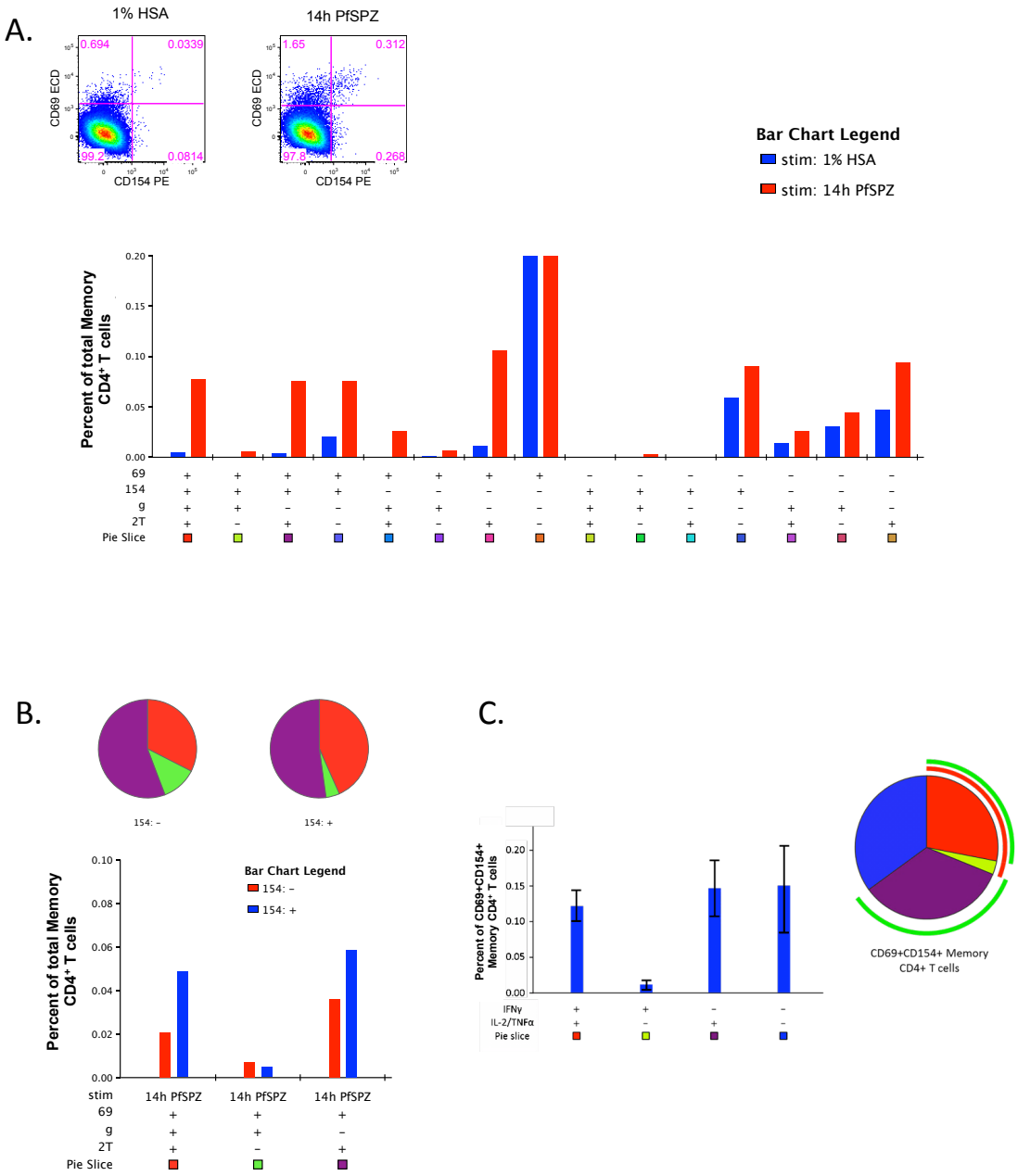

Figure 3.3 Coordinate expression of CD154 with commonly measured cytokines.

(A) PBMCs from a PfSPZ-vaccinated subject were stimulated with $1.5x10^5$ PfSPZ for 14 hours. Monensin was added for the last five hours in order to assess expression of IFN-γ, IL2, and TNFα. **(B)** $CD4^+$ T cell quality of $CD154^-$ vs. $CD154^+$ populations. **(C)** Characterization of the $CD69^+CD154^+$ $CD4^+$ T cell population as a function of IFN-γ, IL2, and TNFα expression.

3.2.4 High-resolution transcriptional analysis of virus- vs. PfSPZ-specific CD4$^+$ T cells

To further expand the analysis of CD69$^+$CD154$^+$ PfSPZ-specific CD4$^+$ T cells, a technology platform that would increase the number of parameters available for measurement beyond those available by flow cytometry was investigated. In this regard, microfluidic chips from Fluidigm enable quantitative gene expression analysis of ~100 markers (*246, 255, 256*). This approach dramatically increases the breadth of phenotypic and functional analysis, even down to single-cell resolution.

The sensitivity of the Fluidigm platform for small bulk mRNA measurements was evaluated. PBMCs were analyzed from sterilely protected subjects approximately six months following the final PfSPZ vaccination and CHMI **(Figure 3.4-A)**. Antigen-specific responses were analyzed from PBMCs following *in vitro* stimulation with PfSPZ or a pool of antigenically distinct hemagglutinin (HA) purified proteins from various influenza virus strains circulating between 2005 and 2011. This allowed a direct comparison of the gene expression profile of a parasite- and virus-specific CD4$^+$ T cells within the same individual. In each subject, gene expression was analyzed from isolated pools of 25 CD69$^+$CD154$^+$ HA- and PfSPZ-specific CD4$^+$ T cells. CD69$^-$CD154$^-$ memory CD4$^+$ T cells served as an internal control **(Figure 3.4-B)**.

Thousands of parallel RT-PCR reactions enabled the quantitative measurement of mRNA expression for 96 genes. Selected genes included those that have been previously reported to play a role in vaccine-induced protection and influence

differentiation of diverse $CD4^+$ T cell subsets such as Th1, Th2, TFH, Treg, and Th17 (*279*). This includes, but is not limited to cytokines, chemokines, and their receptors (*280*); canonical transcription factors (*281*); cytolytic enzymes (*282, 283*); and molecules associated with homing to the liver (*160, 161, 284*), a critical site for immune protection (*163*). All primers were previously qualified to ensure efficient linear amplification of input RNA, absence of primer competition for multiplexing capability, and low technical variation (i.e. high reproducibility of replicate samples) *(244)*. Of the 96 genes measured in this study, 93 were significantly expressed above the limit of detection in 10% of the samples and were examined in downstream analysis.

Principal-component analysis (PCA) was first used to visualize the expression data globally from total memory, influenza-specific and malaria-specific $CD4^+$ T cells. PCA illustrated that cells with similar antigen-specificities clustered together within each of the three respective phenotypes, forming three distinct transcriptome profiles **(Figure 3.4-C)**. Of note, unsupervised separation was driven by a common cellular phenotype across subjects, and not a subject-intrinsic transcriptional profile. Furthermore, unsupervised hierarchal two-way clustering revealed that the greatest separation among the samples was between the antigen-specific population (HA- and PfSPZ-specific combined) vs. the total memory population **(Figure 3.4-D)**.

Of 93 genes analyzed, 45 were differentially expressed between any of the three groups ($p < 0.0001$). Of these, 73% (33/45) were commonly upregulated in HA- and PfSPZ-specific samples vs. total memory. The genes most significantly upregulated

between the antigen-specific vs. total memory samples were *CD154*, *IFNG* and *IL2* **(Figure 3.4-E and F)**.

The malaria vs. flu-specific transcriptional profile was then assessed. Twelve markers were significantly expressed in HA- vs. PfSPZ-specific $CD4^+$ T cells or vice-versa (**Figure 3.4-E and F**; $p<0.0001$). The markers with the greatest order of fit for each cohort were assessed. Of interest, PfSPZ- but not HA-specific $CD4^+$ T cells displayed significant upregulation of a canonical Th2 cytokine *IL13* compared to total memory (*285*). *GZMB* and *FAS,* markers of cytolytic activity*,* were the genes most significantly upregulated in HA- vs. PfSPZ-specific $CD4^+$ T cells. Of note, *FAS* was also enriched in PfSPZ-specific responses compared to the total memory population but to a lesser extent ($p<0.01$; **Figure 3.4-E**).

A.

Patient ID	Immunization Dose	Challenge 1	Challenge 2
VRC 312-401	5 x 135k PfSPZ	Protected	n/a
VRC 312-402	5 x 135k PfSPZ	Protected	n/a
VRC 312-426	5 x 135k PfSPZ	Protected	n/a
VRC 312-450	4 x 135k PfSPZ	Protected	n/a

B.

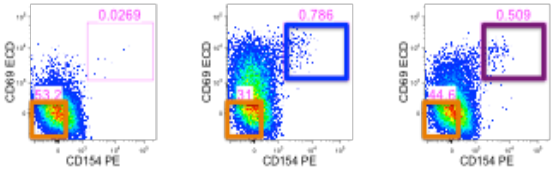

Stimulation	Phenotype	# of cells
1% HSA	CD69-CD154-	3 x 25
HA Protein	CD69-CD154-	3 x 25
HA Protein	CD69+CD154+	3 x 25
PfSPZ	CD69-CD154-	3 x 25
PfSPZ	CD69+CD154+	3 x 25

C.

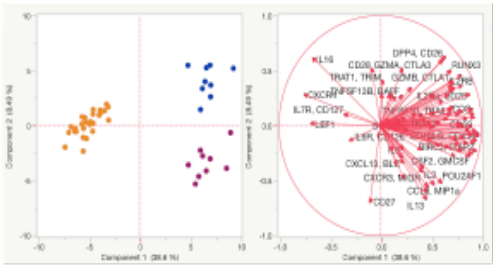

Total Memory CD4 T cells
Flu-specific CD4 T cells
PfSPZ-specific CD4 T cells

D.

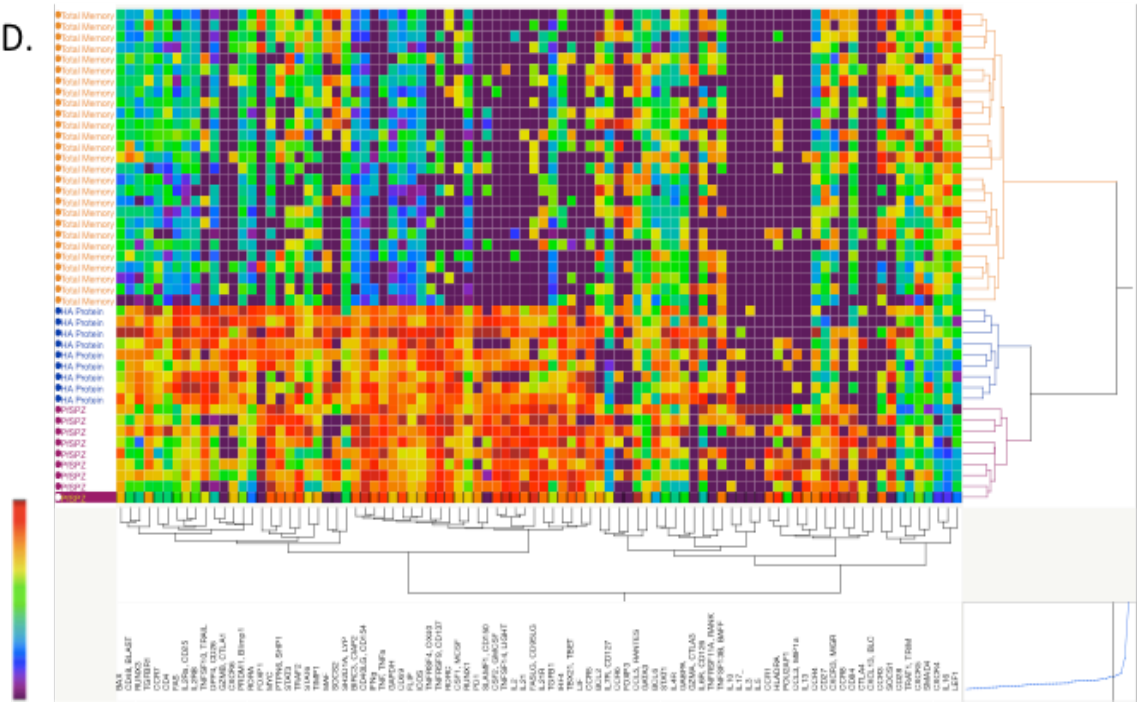

E.

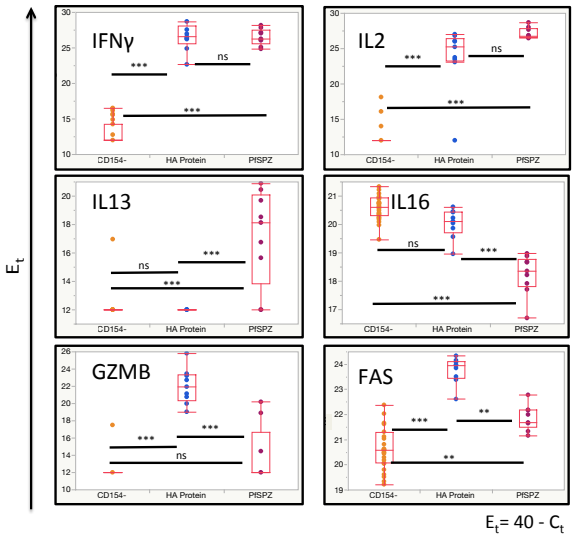

F.

Gene Groups	Common Antigen-specific		Flu	Malaria
	CD154	CXCR4*	GZMB	IL13
	IL2	LIF	FAS	IL16*
	IFNG	CSF1	DPP4	POUF2AF1
	BIRC3	TBET	RUNX3	FASLG
	IL21	TGFB1	PRDM1	CCR1
	GAPDH	IRF4	RORA	HLADRA
	ICOS	RUNX1		
	TNF	PD1		
	CSF2	IL21R		
	TNFSF14	CCR5		
	TNFRSF4	MYC		
	CD69	LEF1*		
	FLIP	BAX		
	RORC	CD48		
	IL2R	TIMP1		
	TNFRSF9	TNFSF10		
	IL2RB			

Figure 3.4 High-resolution transcriptional analysis of HA- vs. PfSPZ-specific CD4$^+$ T cells

(A) Subject immunization information. **(B)** CD154 sorting strategy for all subjects. **(C)** Principal components analysis, accounting for all gene components. **(D)** Unsupervised hierarchal clustering of all wells labeled by cohort. **(E)** Examples of "common" antigen-specific genes (top) and those enriched in HA-specific (bottom) or PfSPZ-specific CD4$^+$ T cells. **(F)** List of all genes differentially expressed for each group ($p<0.0001$). ***$p<0.0001$, **$p<0.001$, *$p<0.01$

3.2.5 Validation of single cell gene expression from PfSPZ-specific CD4$^+$ T lymphocytes

3.2.5.1 Data processing and quality control

The final aim was to assess the efficiency and limitations of single-cell gene expression from PfSPZ-specific CD4$^+$ T cells. Note that the analysis and quality control strategies examined in this section will form the foundation for the remaining analysis in this thesis.

For the pilot experiments, four subjects with varying vaccination regimens and protection outcomes were selected to test the assay against a variety of subject phenotypes (**Figure 3.5-A**). Subjects received either four or five doses of the 1.35x10^5 PfSPZ Vaccine. Three out of the four subjects were sterilely protected following CHMI three weeks after the final vaccination. Two subjects were then rechallenged three months later, of which one was sterilely protected. PfSPZ-specific CD154 responses were assessed approximately nine months following the final PfSPZ vaccination. For each subject, gene expression was analyzed from approximately 140 PfSPZ-specific CD69$^+$CD154$^+$ CD4$^+$ T cells, in addition to control wells described in the previous section **(Figure 3.5-B and C)**.

Fluidigm Biomark data were processed and filtered using the methods previously published to ensure retention of high quality PCR reactions (*244*). As this thesis employs a unique gene panel and cell isolation strategy, it was critical to ensure that these quality control measures were appropriate for this dataset. Based on previous data that suggests that expression of common housekeeping genes widely varies

among single cells and fails to correlate with each other, gene expression was not normalized in this study. Instead, statistical outliers were removed using a multistep data filtering process. Samples with discrete expression of less than 10% genes above the limit of detection (E_t >13, or approximately 1 RNA molecule) were removed. Furthermore, samples with gene expression greater than 7 standard deviations above the median based on the overall distribution were used to remove outliers. Genes were removed from analysis if discrete expression was not detected in at least 10% of samples. This eliminated 33 of 96 genes.

Following filtering, samples discretely expressed on average 54% of all genes (range: 30-81%; **Figure 3.5-D**). In samples with discrete expression of any given gene, median quantitative expression was E_t of 19 **(Figure 3.5-E)**. Overall, an average of 77% of individual RT-PCR reactions (range: 70-92% across six different Fluidigm chips) were of sufficient quality to be retained for downstream analysis **(Figure 3.5-F)**. Of the remaining cells, 98% expressed CD154 by gene expression.

The single-cell gene expression data were validated against pooled bulk wells of the same population. Consistent with previous studies, gene expression of the "average" single cells within a subject correlated with the signal in bulk populations (R^2 = 0.76, $p<0.0001$; **Figure 3.5-G)**. These data suggest that the single cell gene expression analyzed following filtering reflects biological variation.

A.

Patient ID	Immunization Dose	Challenge 1	Challenge 2
VRC 312-426	5 x 135k PfSPZ	Protected	n/a
VRC 312-444	5 x 135k PfSPZ	Unprotected	Unprotected
VRC 312-445	5 x 135k PfSPZ	Protected	Unprotected
VRC 312-450	4 x 135k PfSPZ	Protected	n/a

B.

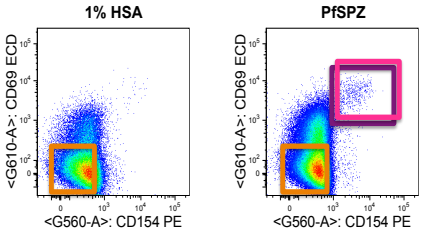

Stimulation	Phenotype	# replicates x # of cells
1% HSA	CD69-CD154-	3 x 25
PfSPZ	CD69-CD154-	3 x 25
PfSPZ	CD69+CD154+	3 x 25
PfSPZ	CD69+CD154+	~140 x 1

C.

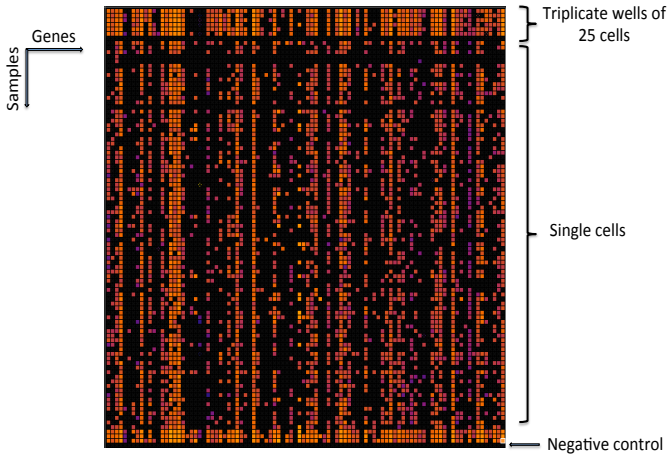

D.

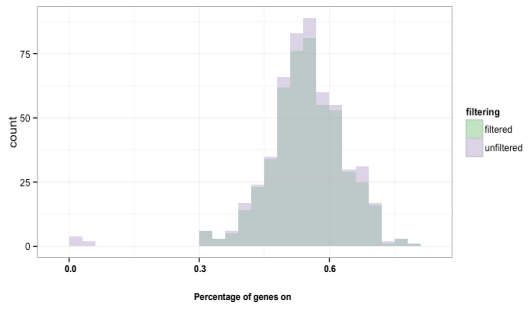

E.

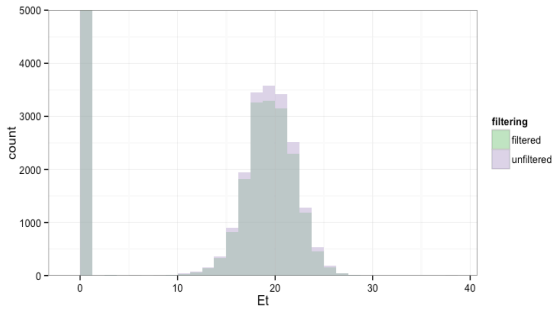

F.

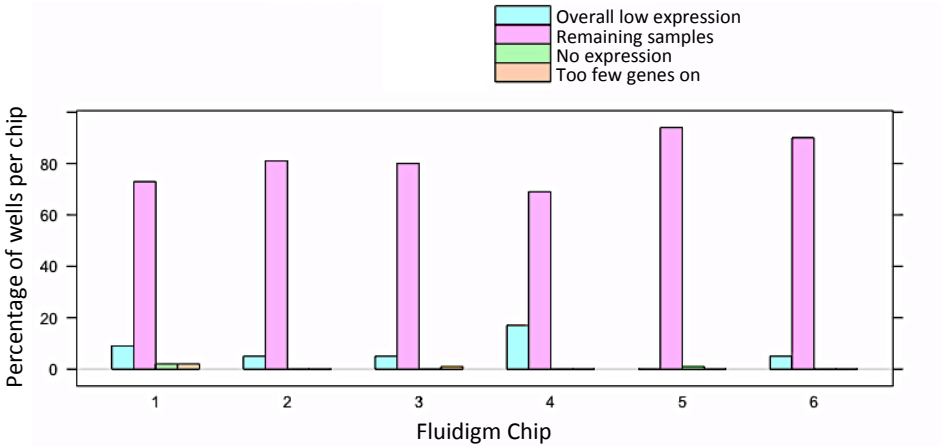

G.

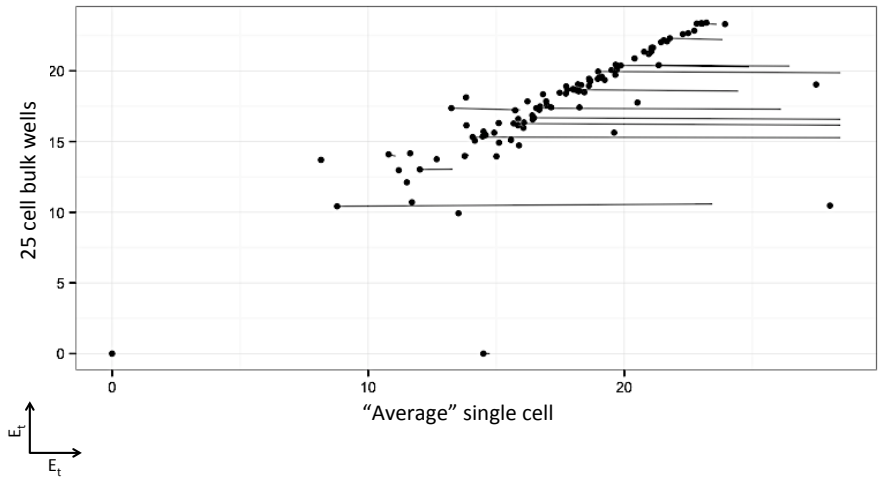

Figure 3.5 Single-cell gene expression from PfSPZ-specific CD4$^+$ T cells

(A) Subject immunization information. **(B)** CD154 sorting strategy for all subjects. **(C)** Representative Fluidigm 96.96 Array following data acquisition. **(D)** Discrete and **(E)** continuous gene expression before and after data filtering of all sorted cells. **(F)** Percentage of wells filtered from each chip due to overall low expression of all genes, absence of any gene expression, and low number of genes discretely expressed. **(G)** Expression of analyzed genes from bulk wells containing 25 cells per well or "average" single cell. Each dot represents the expression from one gene post filtering and the opposite end of the line represent expression prior to data filtering.

As there were only four subjects in this study, there was not enough power to assess correlations between gene expression profiles and protection outcome. However, the benefit of single cell transcriptomics in revealing true coexpression, semi coexpression and discordant expression was highlighted **(Figure 3.6)**.

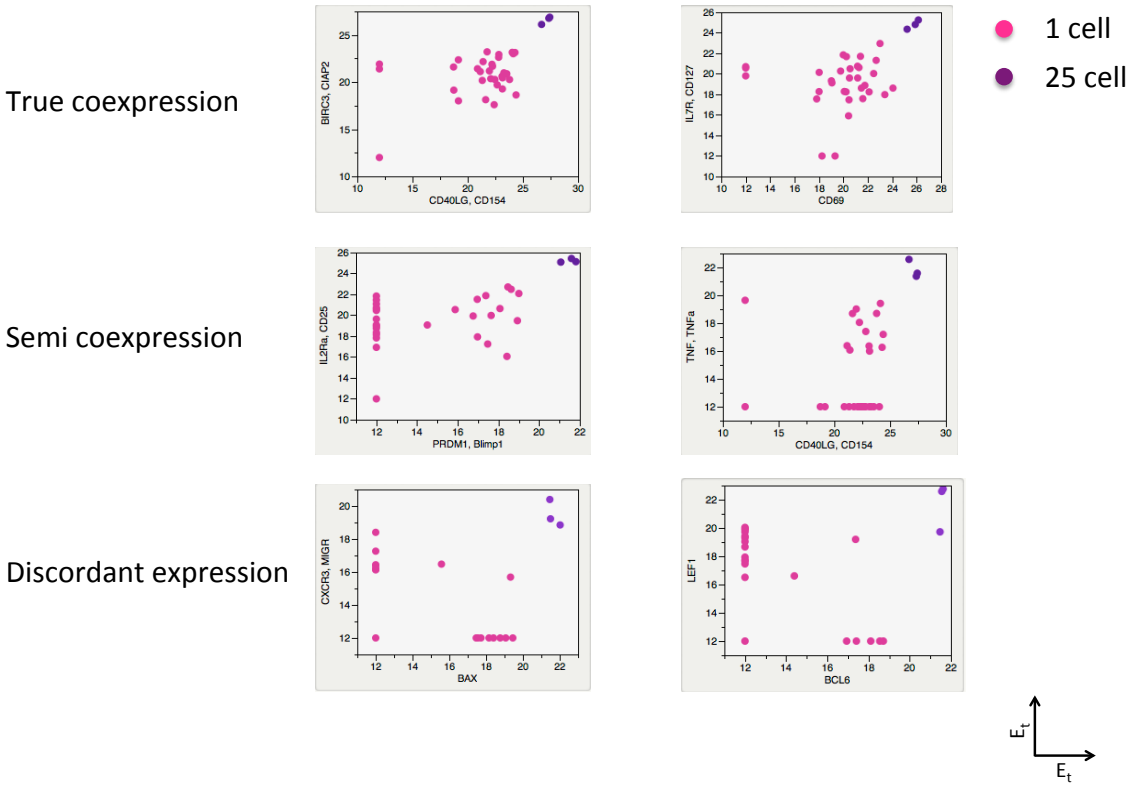

Figure 3.6 Benefits of gene expression from single cells vs. bulk populations.

Examples of gene pairs that display true coexpression (top), semi coexpression (middle) or discordant coexpression (bottom).

3.2.5.2 Hypothesized contribution of "background" CD154$^+$ cells

An important limitation of this assay is the presence of a limited number of CD69$^+$CD154$^+$ CD4$^+$ T cells in the control samples stimulated with the PfSPZ diluent (1% HSA). These "background" cells are not PfSPZ-specific, but likely contaminate the matched gate in the PfSPZ stimulated samples. In other words, there exist non-antigen-specific cells that are isolated and analyzed downstream in the Fluidigm assay as recently activated PfSPZ-specific cells. It was hypothesized that the greatest difference among isolated single cells would be those that are recently activated (i.e. antigen-specific) and the "background" CD4$^+$ T cells.

The PfSPZ-specific CD69$^+$CD154$^+$ response for each subject was calculated as the fold-change over the matched population in the sample incubated with 1% HSA **(Figure 3.7-A)**. The CD69$^-$CD154$^+$ and CD69$^+$CD154$^-$ populations served as internal controls, as these populations are expected to have limited change upon antigen stimulation. One subject with a significantly low antigen-specific response was identified as potentially having a large contribution of background cells.

Unsupervised two-way hierarchical clustering of all analyzed single cells revealed two phenotypically distinct cohorts, identified by red and blue **(Figure 3.7-B)**. It was hypothesized that the population highlighted in red consisted of background CD69$^+$CD154$^+$ cells that were not PfSPZ-specific. The percentage of the background response by flow cytometry and the percentage of cells in the red population as a proportion of the total number isolated samples by the downstream Fluidigm assay per subject were calculated. While there were only four subjects,

there was positive correlation between calculated percentages of background cells by flow cytometry vs. Fluidigm **(**R^2 = 0.93, p =0.31**; Figure 3.7-C).** PCA suggested that separation of these two groups was largely driven by increased expression of six markers: *IL2RB, DPP4, FAS, CCR1, RORA,* and *IL16 (***Figure 3.7-D)**. All of these genes were significantly enriched, but not exclusively expressed, in the hypothesized background vs. antigen-specific cells **(Figure 3.7-E)**.

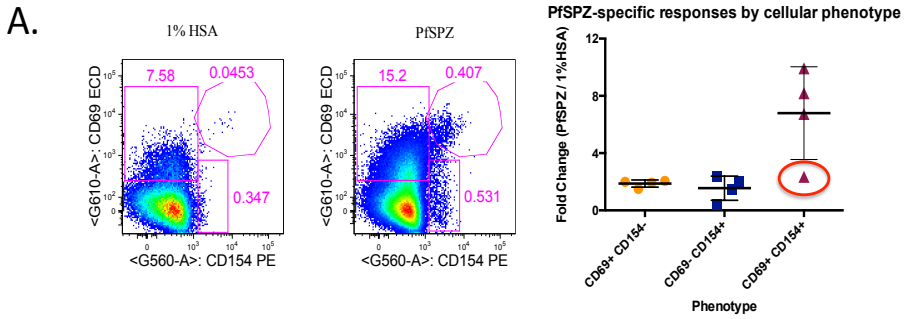
A.
1% HSA
PfSPZ
7.58
0.0453
0.347
15.2
0.407
0.531
<G610-A>: CD69 ECD
<G560-A>: CD154 PE
PfSPZ-specific responses by cellular phenotype
Fold Change (PfSPZ / 1%HSA)
CD69+ CD154-
CD69- CD154+
CD69+ CD154+
Phenotype

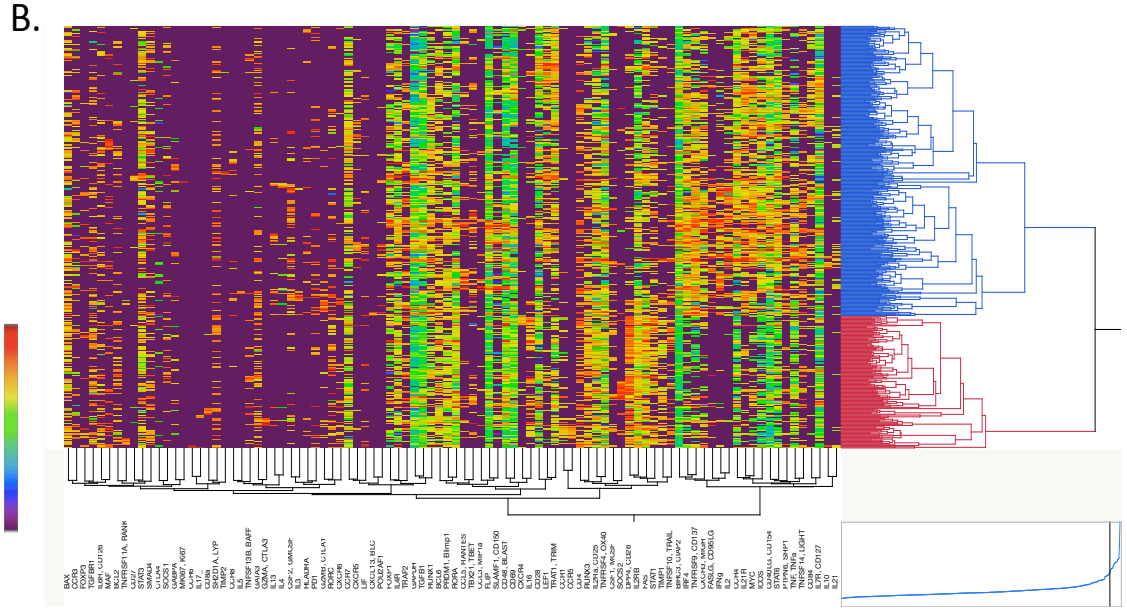
B.

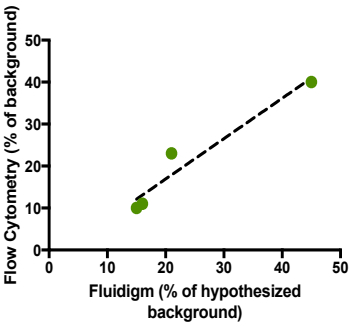
C.
Flow Cytometry (% of background)
Fluidigm (% of hypothesized background)

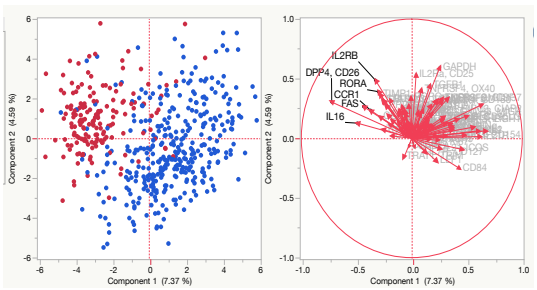
D.
Component 1 (7.37 %)
Component 2 (4.59 %)
IL2RB
DPP4, CD26
RORA
CCR1
FAS
IL16

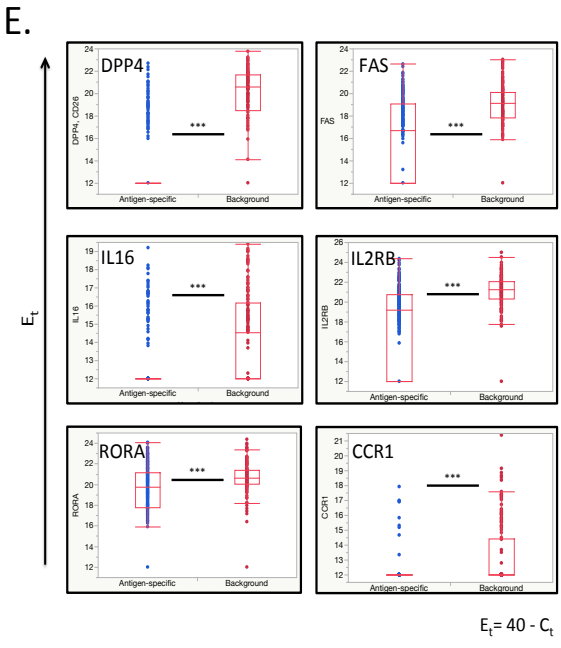
E.
DPP4
FAS
IL16
IL2RB
RORA
CCR1
Antigen-specific
Background
***
E_t
$E_t = 40 - C_t$

Figure 3.7 Hypothesized contribution of "background" CD154$^+$ CD4$^+$ T cells.

(A) Fold-change of three CD4$^+$ T cell populations following *in vitro* restimulation with PfSPZ: CD69$^+$CD154$^-$, CD69$^-$CD154$^+$, and CD69$^+$CD154$^+$. **(B)** Unsupervised single cell hierarchal clustering of all cells. Proposed "background" cells are highlighted in red. **(C)** Percentage of background responses as assessed by flow cytometry (% CD154$^+$CD69$^+$ from PfSPZ stimulated wells divided by matched control) or as estimated by Fluidigm analysis (% red/(red+blue)). Line of best fit calculated from four subjects. **(D)** Principal components analysis with proposed background cells labeled, as well as gene components that drive separation. **(E)** Quantitative gene expression of six markers enriched in proposed background population.

3.3 Discussion

The aim of this chapter was to optimize the isolation of PfSPZ-specific $CD4^+$ T cells from vaccinated subjects and assess the Fluidigm platform for downstream bulk and single-cell gene expression analysis. First, dual expression of CD69 and CD154 identified PfSPZ-specific $CD4^+$ T cells, of which 30-50% did not produce cytokines typically measured by multi-parameter flow cytometry. This finding highlights the increased sensitivity of our assay to identify PfSPZ-specific T cells that would not be detected by standard flow cytometry panels. Thus, the assay provides enhanced breadth of the antigen-specific response and the ability to detect additional mediators that may influence protection. Second, high-resolution microarray analysis revealed that malaria-specific $CD4^+$ T cells had a distinct gene expression profile compared to virus-specific $CD4^+$ T cells in protected subjects. Third, the quality control and validation measures to analyze single-cell gene expression data were described, in addition to a key limitation of the assay. Overall, this chapter laid the foundation for the in-depth transcriptional analysis of cellular immune responses from large clinical trials, which will constitute the remainder of this thesis.

In the following chapters regarding clinical assessment of the PfSPZ Vaccine, $CD4^+$ T cells will be examined. $CD8^+$ T cells are hypothesized to be critical for protection; however, PfSPZ- and PfRBC-specific responses are low to absent in vaccinated subjects *(286)*. One possibility may be that antigen-specific $CD8^+$ T cells are sequestered in the liver, and do not circulate in the peripheral blood. Murine studies suggest that PfSPZ antigens are retained in liver up to six months following vaccination (*174*). Preclinical studies suggest that $CD4^+$ T cells may be necessary

for SPZ-elicited protection. Furthermore, in-depth single cell analysis in this setting may provide insights into the heterogeneity elicited by a whole parasite vaccine.

While the *de novo* detection of CD154 to identify live antigen-specific $CD4^+$ T cells has been previously described (*273, 274*), its use to isolate responses in an *in vitro* restimulation assay using a whole parasite is unique. Individual PfSPZ antigens may be presented less efficiently than a single immunodominant protein or peptide used in conventional restimulation assays. Yet, responses against the immunodominant CSP antigen are low to undetectable in vaccinated subjects as assessed by ELISPOT, suggesting that CD154 responses target a wealth of antigens. This is impossible to know in absence of a tetramer or downstream T cell receptor (TCR) analysis. Furthermore, it is important to note that the total $CD4^+$ T cell responses detected by this live-cell assay may be lower the total immune responses detected by standard ICS assays due to the absence of Golgi inhibitors. However, these data demonstrate the breadth of phenotypic responses is dramatic, as the assay is not restricted to a set of three predefined cytokines.

Fluidigm analysis of PfSPZ- vs. HA-specific $CD4^+$ T cells revealed subtle differences on a bulk level between the different responses and common antigen-specific signature. Overall, these data suggest that there exists a common $CD69^+CD154^+$ "antigen-specific" transcriptional phenotype distinct from total memory T cells. Not surprisingly, the genes most significantly upregulated between $CD154^+$ vs. $CD154^-$ cells were *CD154*, *IFNG* and *IL2*. These genes are among the most sensitive and commonly measured markers in standard flow cytometry assays *(239, 240).* Critically, unsupervised analysis by two-way clustering and PCA was

driven by antigen-specificity, and not by individual. This suggests that subject-level variation in gene expression is smaller than pathogen-specific variation as assessed by this assay. This allows for comparison of transcriptomic profiles across subjects, critical for assessment of correlations of protection in a clinical trial.

Following a multi-step filtering process that removed statistical outliers and failed RT-PCR reactions, the majority of samples were retained for downstream analysis. Furthermore, validation methods comparing gene expression detected in the "average" single cell vs. the bulk wells suggest that the single-cell data analyzed downstream reflects biological variation masked by larger populations. While a number of genes were removed from downstream analysis in this chapter, many of these were markers of interest that may play a role in protective immunity against the pre-erythrocytic stage of malaria, such IL-4, IL-5 and IL-10. As it was impossible to exclude the possibility that expression would only be detected one week prior to challenge, all markers remained in the gene panel.

It is important to be aware of the limitations of a new assay, even if it is difficult to remove them. These data suggest that a phenotype consisting of six enriched genes may resemble the background $CD69^{+}CD154^{+}$ cells that are not specific for PfSPZ but are nonetheless analyzed in the downstream Fluidigm assay as "antigen-specific." Unfortunately, these data do not create a sufficient definition for background cells nor allow for a possibility to filter out these cells. All of these markers have also been documented to play a role in vaccine-induced immunity. For example, *RORA* is a critical transcription factor for Th17 cells, and *FAS* plays a critical role in cytolytic activity. However, it suggests that the presence of

background cells must be taken into account with downstream analysis to prevent skewed results that reflect the magnitude, and not the quality of T cell. As such for future analysis, only subjects with a total PfSPZ-specific $CD154^+$ T cell response three-fold above the background responses were utilized for downstream analysis. Furthermore, any samples with an antigen-specific response greater than five standards of deviation above the average were noted.

4. VRC 312- PfSPZ Vaccine Trial #1

4.1 Introduction

Intravenous administration of highly purified, irradiated sporozoites can provide high-level protection against CHMI in humans. However, the mechanism of protection is unclear. In terms of cellular immunity, pre-clinical studies in rodents and non-human primates demonstrate a critical role for $CD8^+$ T cells in mediating protection in the liver through production of IFN-γ (*135, 150, 152*). The protective role of $CD4^+$ T cells may be more complex as such cells are heterogeneous and can have diverse functions (*155, 175, 176, 181*) (See Chapter 1.3.2 regarding more in-depth discussion of the protective mechanisms in pre-erythrocytic immunity).

VRC312 was the first clinical trial to assess the safety and immunogenicity of the intravenous administration of cryopreserved irradiated sporozoites (PfSPZ Vaccine) (*116*). Fifteen subjects who received the highest administered dose of vaccine ($1.35x10^5$ PfSPZ) underwent CHMI. Of those subjects that received four doses, six out of nine were sterilely protected. Of those that received five doses, five out of five were protected.

Immunization induced a dose-dependent increase in PfSPZ-specific antibodies and T cell responses (*116*). Analysis examining the quality of cellular immune responses with multiparameter flow cytometry revealed largely polyfunctional ($IFN\text{-}\gamma^+IL\text{-}2^+TNF\text{-}\alpha^+$) $CD4^+$ T cells. Moreover, protected subjects who received four doses

showed a trend of higher monofunctional IFN-γ-producing $CD8^+$ T cell responses than unprotected subjects in the same group. Analysis of the $CD8^+$ T cell responses is limited, as five of the subjects had low to undetectable immune responses. Of note, the PfSPZ-induced antibodies in this study blocked invasion of hepatocytes *in vitro* and therefore may have contributed to protection.

Based on the multi-factorial role that $CD4^+$ T cells may have in vaccine-elicited protection and limited analysis possible for $CD8^+$ T cells, vaccine-induced $CD4^+$ T cells were characterized in greater depth than with current technologies. In this regard, detection of *de novo*-synthesized CD154 following *in vitro* restimulation is a powerful strategy to capture the global malaria-specific $CD4^+$ T response elicited by PfSPZ vaccine. Following isolation of $CD154^+CD4^+$ T cells, highly multiplexed, single-cell technologies were used for in-depth characterization of the PfSPZ-specific response and elucidation of mechanisms of immunity. The findings from the optimization studies described in Chapter 3 will be directly applied here.

The aims of this chapter are the following: (1) define the molecular signatures of PfSPZ-specific $CD4^+$ T cell responses induced by malaria infection versus vaccination with a whole live parasite; (2) evaluate the heterogeneity of the $CD4^+$ T cell response at the single cell level; and (3) compare the gene expression profiles of such responses from protected and unprotected subjects following vaccination and challenge in order to identify potential correlates of protection.

4.2 Results

4.2.1 Isolation of individual PfSPZ-specific CD4$^+$ T cells from vaccinated subjects prior to challenge

The first aim was to isolate individual PfSPZ-specific CD4$^+$ T cells from vaccinated subjects in the clinical trial VRC312 **(Figure 4.1** and **Table 4.1)**. Responses from vaccinated subjects were assessed from PBMCs isolated two weeks following the final immunization (approximately one week prior to CHMI). Due to low immune responses elicited using lower doses of the PfSPZ Vaccine, analysis was restricted to the fifteen subjects who received 4 or 5 doses of the 1.35×10^5 PfSPZ Vaccine, where high-level protection was observed (*116*).

In addition, PfSPZ-specific CD4$^+$ T cells from five unvaccinated infection control subjects were isolated two weeks following CHMI. As the magnitude of IFN-γ-producing T cells peaks at this timepoint over the 28-day monitoring period following CHMI as assessed by flow cytometry (*286*), it was hypothesized that these samples represent the primary immune response to *Pf* malaria infection.

Overall CD4$^+$ T cell responses defined by coexpression of CD154 and CD69 protein were assessed by flow cytometry for each cohort **(Figure 4.2)**. During each sort, a positive and negative control for the CD154 staining assay was run. The positive control was a PfSPZ-vaccinated subject six months post the final vaccination. The negative control was a subject who had not been infected with malaria or immunized with a malaria vaccine. The PfSPZ-specific CD4$^+$ T cell responses from three vaccinated subjects were equal to or below the threshold required for downstream

analysis as defined in Chapter 3. Furthermore, the CD154 responses from these three subjects were not significantly different from the negative controls. Of note, these three subjects had the lowest $CD4^+$ T cell responses as assessed by cytokine production of IFN-γ, IL-2 and TNF-α in a previous study *(116)*. When these three subjects were removed from the analysis, CD154 responses did not differ significantly across the three cohorts. Overall, twelve vaccinated subjects and five infection controls had PfSPZ-specific $CD4^+$ T cell responses of sufficient magnitude for downstream analysis.

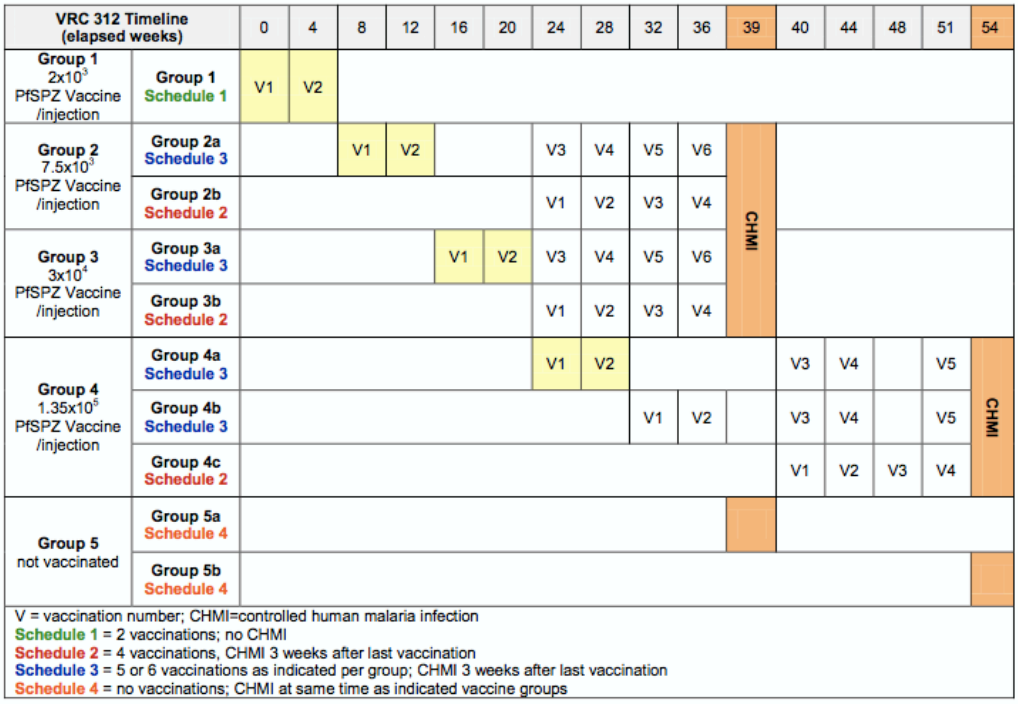

Figure 4.1 VRC312 clinical study.

The vaccination schedule, PfSPZ Vaccine dose and route for all subjects under the VRC312 clinical study. Note that only groups 4 and 5 are assessed in this thesis. This figure is taken from reference (*116*).

	Group	Vaccine Regimen	Timepoint	CHMI #1 Outcome	# of volunteers
Vaccinees	4a/4b/4c	4 or 5 doses of $1.35x10^5$ PfSPZ Vaccine	2 weeks post final vaccination	Protected	12
				Unprotected	3
Infection Controls	5a/5b	N/A	2 weeks post CHMI	Unprotected	5

Table 4.1 VRC312 subjects initially selected for Fluidigm analysis.

All subjects who were assessed following detection of $CD69^+CD154^+$ $CD4^+$ T cell responses for downstream transcriptional analysis.

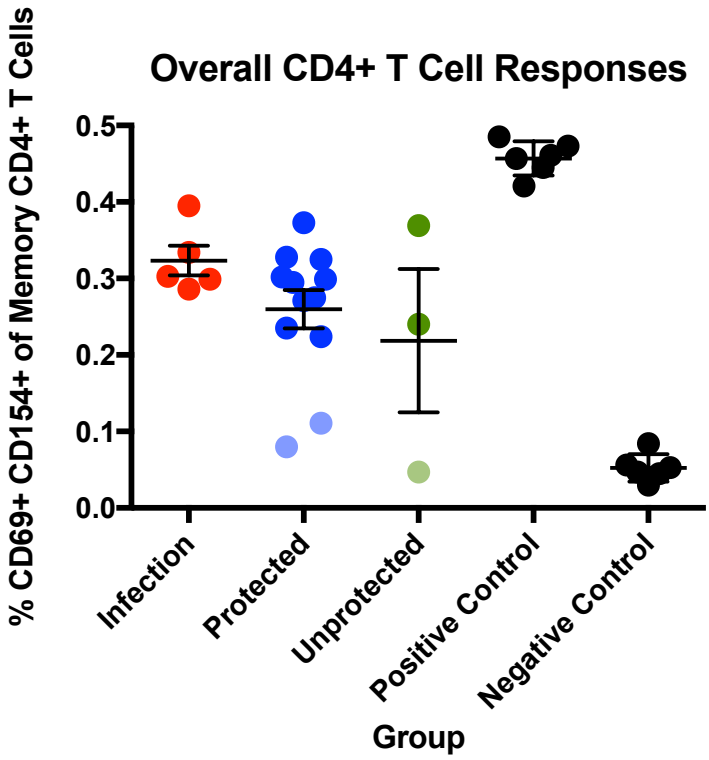

Figure 4.2 PfSPZ-specific $CD4^+$ T cell responses.

PBMCs isolated from samples at two weeks following the final vaccination were stimulated *in vitro* with 135,000 PfSPZ for 15 hours. The frequency of $CD69^+CD154^+$ cells is represented as a percentage of the memory CD4+ T cell population as assessed by flow cytometry. Subjects with responses below the limit for Fluidigm analysis are shaded. Mean +/ standard error of the mean (SEM).

Fluidigm 96.96 Dynamic Arrays were used for quantitative RT-PCR analysis, allowing for simultaneous measurement of 96 genes in 96 individual samples. For each subject, analysis was performed on approximately 100 individual PfSPZ-specific $CD4^+$ T cells, in addition to bulk wells of 25 cells in triplicate. The gene panel described in Chapter 3 for $CD4^+$ T cells was used. Failed reactions and statistical outliers were removed using the multistep data filtering process described in Chapter 3.3 to ensure analysis of only high quality RNA. The single-cell gene expression data were also validated against pooled microarrays, as described in Chapter 3.4 (data not shown). Expression of 82 genes from 1,475 single cells was retained for downstream analysis.

In order to assess the sensitivity of downstream quantitative RT-PCR, mRNA expression of key transcripts was examined. Although gene expression was not normalized, *CD69* and *CD154* mRNA levels did not differ significantly across the different cohorts **(Figure 4.3-A)**. There was evidence of considerable T cell heterogeneity in vaccinated subjects prior to challenge at the single-cell level. 91% of vaccine-induced cells that remained following data filtering expressed *CD154* mRNA, serving as an internal positive control **(Figure 4.3-B)**. Gene expression of markers associated with a wide spectrum of T-helper (Th) subsets, such as Th1, Th2, Th17, TFH, and T regulatory subsets was detected. In accordance with previous estimates by flow cytometry (See Chapter 3.2), 53% of sorted cells from vaccinated subjects did not express *IFNG, TNF* or *IL2.* These data highlight that this experimental approach dramatically increased the breadth of phenotypic and functional analysis, even down to single-cell resolution.

A.

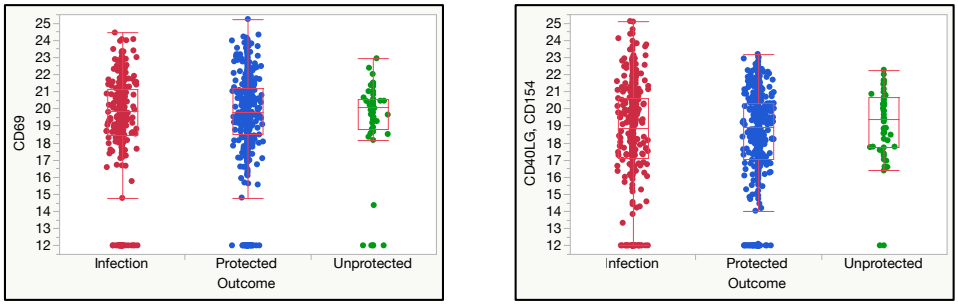
CD69
25
24
23
22
21
20
19
18
17
16
15
14
13
12
Infection
Protected
Unprotected
Outcome
CD40LG, CD154
25
24
23
22
21
20
19
18
17
16
15
14
13
12
Infection
Protected
Unprotected
Outcome

B.

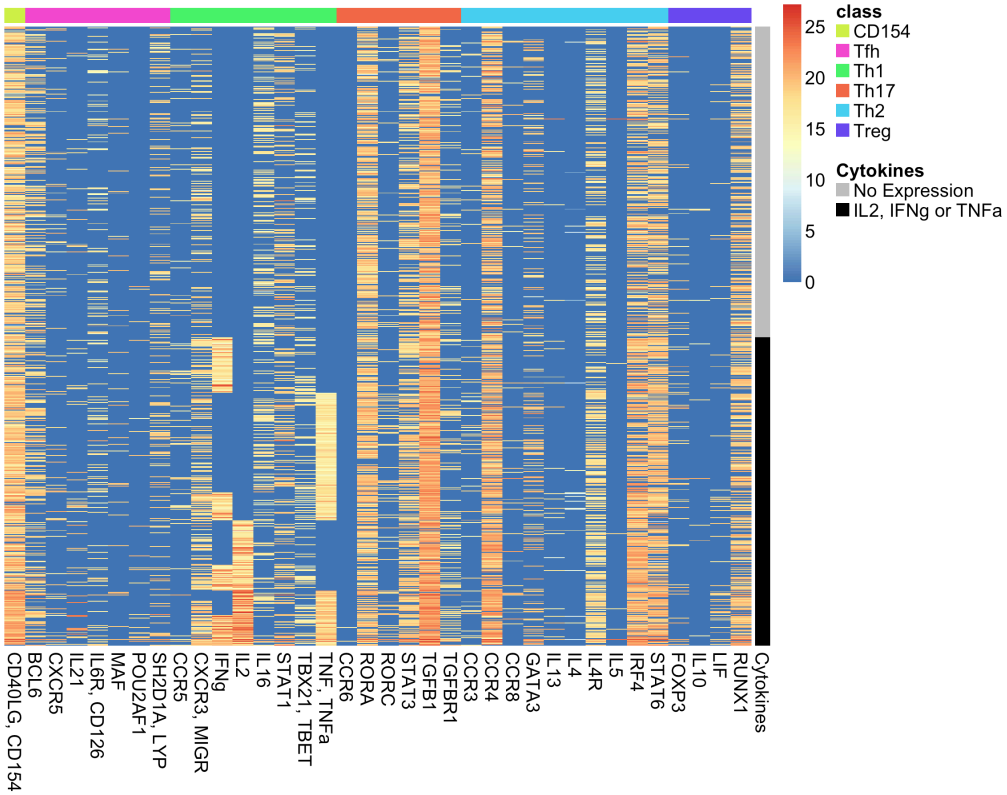
class
CD154
Tfh
Th1
Th17
Th2
Treg
Cytokines
No Expression
IL2, IFNg or TNFa
25
20
15
10
5
0
CD40LG, CD154
BCL6
CXCR5
IL21
IL6R, CD126
MAF
POU2AF1
SH2D1A, LYP
CCR5
CXCR3, MIGR
IFNg
IL2
IL16
STAT1
TBX21, TBET
TNF, TNFa
CCR6
RORA
RORC
STAT3
TGFB1
TGFBR1
CCR3
CCR4
CCR8
GATA3
IL13
IL4
IL4R
IL5
IRF4
STAT6
FOXP3
IL10
LIF
RUNX1
Cytokines

Figure 4.3 Sensitivity of single cell gene expression from vaccinated subjects in VRC312

(A) Single-cell gene expression from subjects across all three cohorts for *CD40L/CD154* and *CD69*. E_t values are shown on the y-axis. Median +/- quantiles (IQR). **(B)** Expression of key transcripts associated with canonical T helper subsets from all from vaccinated subjects. *CD154* expression is shown on the left axis. Cells which do not discretely express *IFNG*, *IL2* or *TNF* are highlighted in grey on the right axis. E_t values are displayed.

4.2.2 Global transcriptomic profiles of PfSPZ-specific CD4$^+$ T cells from vaccinated subjects and infection controls

The transcriptomic profile of CD4$^+$ T cells induced by a protective vaccine composed of a live parasite was compared to that induced by a primary malaria infection. Principal-component analysis (PCA) was first performed to visualize the global changes in expression from vaccinees prior to the first challenge versus the non-vaccinated infection controls. Analysis was restricted to the first principal component (PC1) in order to transform the data into one eigenvalue that would account for as much variation as possible, simplifying multivariate patterns within a complex dataset to a single variable. Note that principal components are determined in an unsupervised fashion without regard for class labels.

The cellular detection rate (CDR), which reflects the proportion of genes discretely expressed in a given sample, has been described as an important source of technical variation in single-cell expression studies (*270, 287-289*). In the original dataset, PC1 was strongly correlated to the cellular detection rate (CDR), accounting for 15% of the variance in the original dataset **(Figure 4.4-A and B)**. After removing the CDR effect, PC1 accounted for 7.97% of the variance in the dataset **(Figure 4.4-C)**.

Single cell analysis revealed that the three cohorts were composed of globally different transcriptomic profiles, as the median PC1 value among all three cohorts was statistically significant **(Figure 4.4-D)**. The fold-change in the median PC1

value between infection and all vaccinated subjects was 4.4 times greater than the fold-change between protected and unprotected vaccinees.

The first ten principals components retained only 22% of all of the original variance **(Figure 4.4-C)**. Traditional representation of PCs in a two-dimensional plot would fail to represent over 80% of the variance in the original data set. Instead, linear discriminant analysis (LDA) was performed in order to provide insight into the variables that would best maximize the separation of known classes.

LDA confirmed that there exist sets of genes that distinguish each of the three cohorts **(Figure 4.4-E)**. In line with the PCA, the first linear discriminant (LD1) best accounted for the variance between the infection and vaccinated cohort, and was characterized by upregulation of a set of genes following CHMI. Of note, the gene component that maximized the greatest separation within the dataset was *CCL5/RANTES*, which encodes a chemokine involved in recruitment of CCR1- and CCR5-expressing activated T cells to sites of inflammation *(290)*. LD2 provided some information about separation between protected and unprotected vaccinees; however, two-way analysis is required in order to control for the derivation of discriminants based on the infection cohort. 86.4% of cells were accurately characterized into the three classes.

Overall, these data suggest that there are global qualitative differences among these three cohorts that will be parsed into individual genes or groups of genes in the following sections. In order to accurately characterize the transcriptomic profiles of the three different cohorts, further analysis was restricted to two groups at a time.

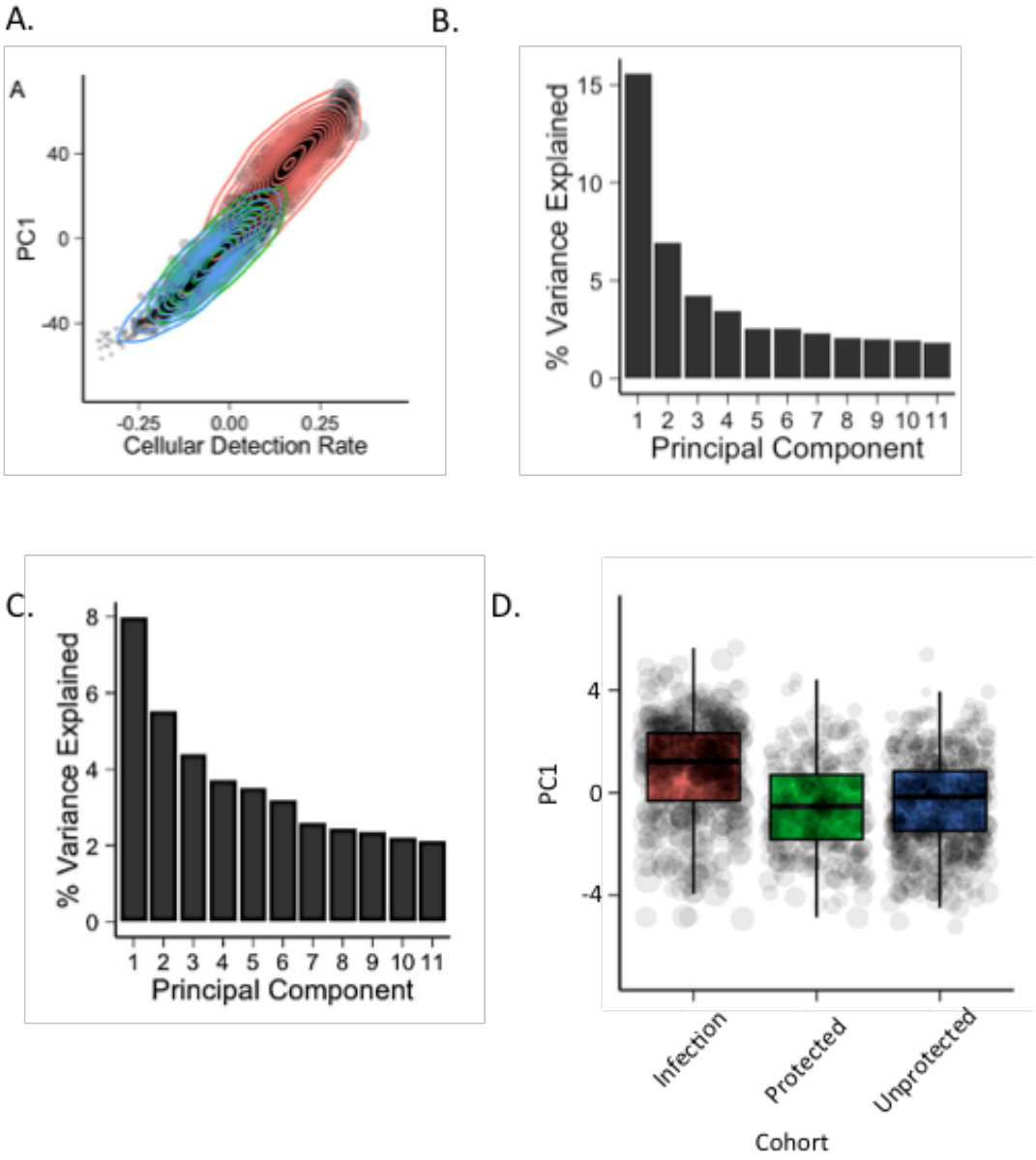
A.
B.
A
PC1
40
0
-40
-0.25
0.00
0.25
Cellular Detection Rate
% Variance Explained
15
10
5
0
1 2 3 4 5 6 7 8 9 10 11
Principal Component
C.
D.
% Variance Explained
8
6
4
2
0
1 2 3 4 5 6 7 8 9 10 11
Principal Component
PC1
4
0
-4
Infection
Protected
Unprotected
Cohort

E.

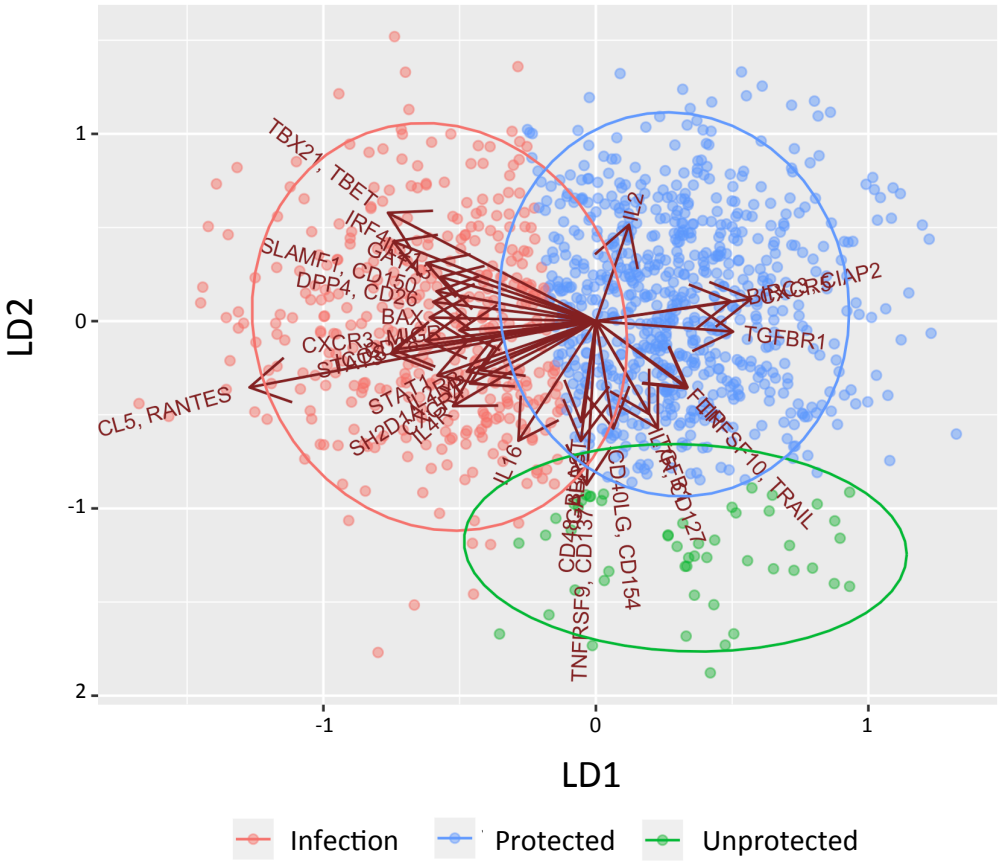

Figure 4.4 Global gene expression of vaccinated subjects and unvaccinated infection controls

(A) Cellular detection rate (or fraction of genes discretely expressed) as a function of the first principal component. Both values transformed. Variance explained by first three eigenvalues before **(B)** and after **(C)** correction for model-based correction for cellular detection rate. **(D)** Scaled values of first principal component and **(E)** linear discriminant analysis of all three cohorts. Circles display normal 50% contours. Median +/- IQR. Infection: unvaccinated infection controls two weeks post CHMI. Protected = vaccinated and protected subjects two weeks post final immunization. Unprotected = vaccinated and unprotected subjects two weeks post final immunization.

4.2.3 Differential gene expression signatures of PfSPZ-specific CD4$^+$ T cells following vaccination versus infection

As the global variance between the infection and vaccinated cohort was much greater than that within the vaccinated cohort, the effect of live malaria vaccination versus infection was assessed first without regard for protection outcome. Differentially expressed genes were those that exhibited a statistically significant effect due to vaccination ($p < 0.001$) based on a likelihood ratio test of the combined discrete and continuous model components, and which exhibited at least a two-fold change in expression associated with vaccination. Thirty-four genes were identified, of which 20 were enriched in infection controls **(Figure 4.5-A and B)**.

In line with the multivariate analysis in the previous section, the top five genes enriched in the infection controls in terms of median fold-change were *CCL5/RANTES*, *DPP4/CD26*, *GZMB/CTLA1*, *TBX21/TBET*, and *CD28,* in order of decreasing fold-change. In the vaccinated cohort, the top five genes with the same criteria were *BIRC3/CIAP2, CCR4, TNFSF14/LIGHT, IL21R* and *IL2* **(Figure 4.5-B)**.

It is important to note median expression of *GAPDH*, a commonly used housekeeping gene was significantly greater ($p<0.001$) in the infection cohort. However, the fold-change change was 2.4, barely over the threshold for significance. Moreover, the median expression of CD154 and CD69 was not significantly different across all cohorts.

In order to assess the molecular networks uniquely induced by infection vs. vaccination, the sets of genes that discriminated between these two cohorts at the single cell level were examined using unsupervised hierarchal clustering **(Figure 4.5-C)**. This analysis was restricted to genes that were differentially expressed between infection and vaccination. Only 2% of cells from the vaccinated cohort and 8.6% of cells from control subjects were misclassified by hierarchical clustering. Of note, the gene expression profiles from non-vaccinated infection control subjects appeared more transcriptionally homogeneous compared to vaccination. Furthermore, such subjects were marked by a group of genes that are distinctly upregulated, while the vaccinated subjects profiles were characterized by a combination of downregulated genes in a subset of cells.

In the infection cohort, expression of *TBX21/TBET*, *CCL5/RANTES* and *DPP4/CD26* (three of the top five significantly expressed genes) clustered together. 41% of cells that discretely expressed any one of these genes coordinately expressed all three. Furthermore, these markers were clustered with *IFNG* by single cell hierarchal clustering, consistent with previously reported cell-intrinsic coordination.

Discrimination between the two groups was also accurate when gene expression was represented as the per-subject median **(Figure 4.5-D)** or proportion of discrete expression **(Figure 4.5-E)**. *CD4* and *SLAMF150/CD150* were removed from further analysis, as expression in one subject was greater than three logs from the median level in the infected cohort. Overall, a coherent subject-level increase is evident in natural infection, demonstrating that differential expression is not driven by outlier

subjects and single-cell gene expression patterns were representative of subject-level effects.

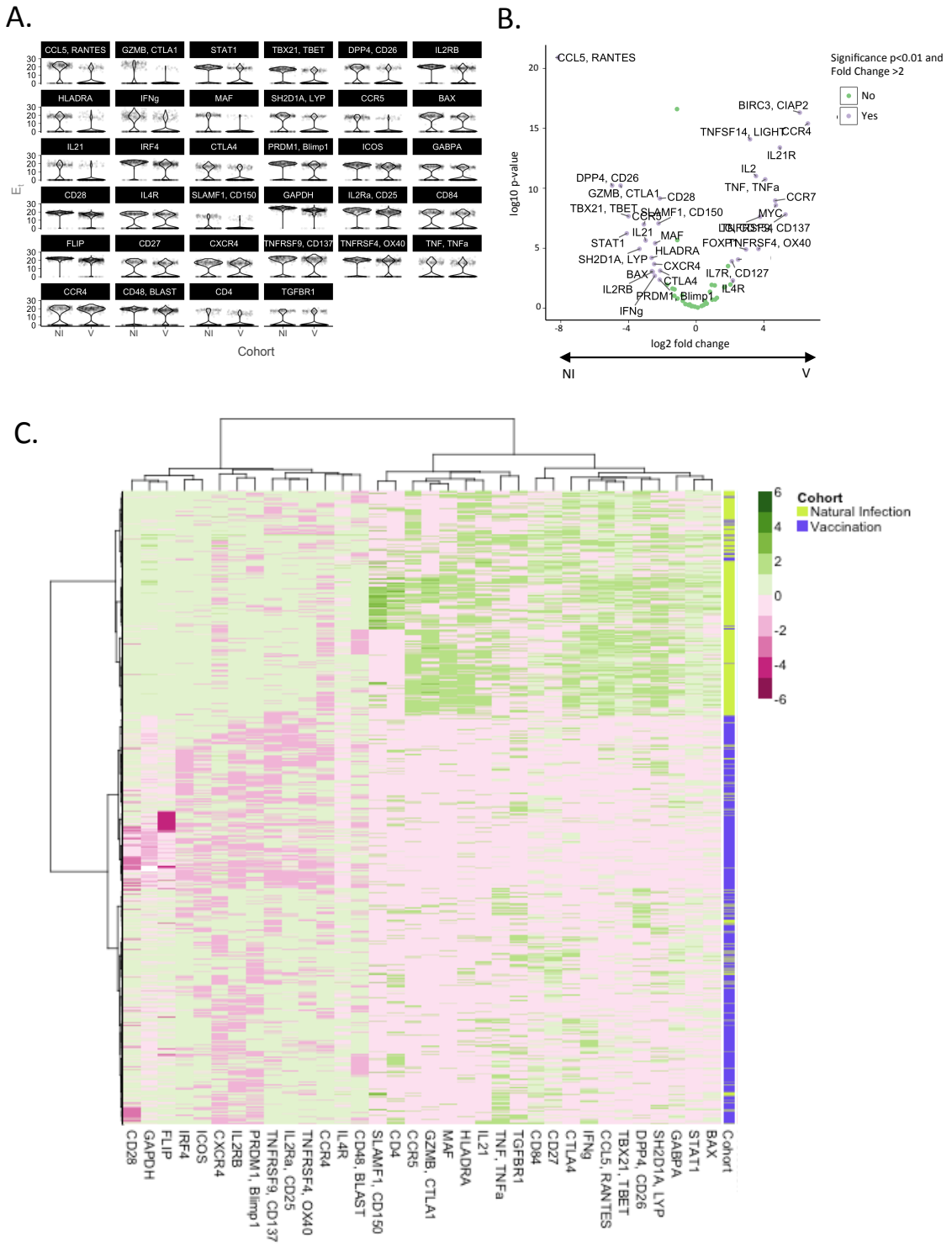

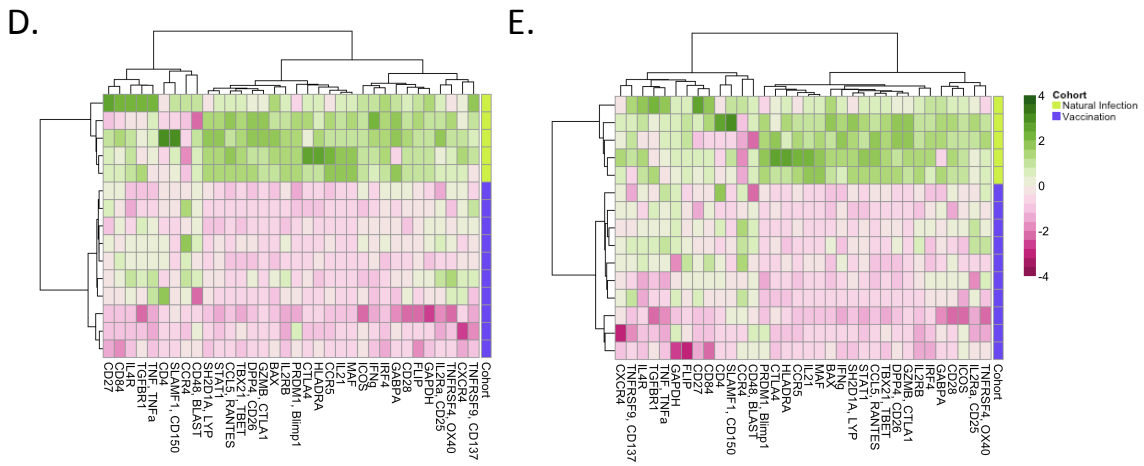

Figure 4.5 Differential gene expression of PfSPZ-specific CD4$^+$ T cells following vaccination vs. CHMI.

(A) All differentially expressed genes (DEGs) between the infection and vaccination cohort ($p<0.001$ and 2-fold change). **(B)** Volcano plots of all genes displaying significance and fold-change. **(C)** Unsupervised hierarchal clustering. Single cells labeled as vaccination (purple) or infection (yellow). Expression of all DEGs represented as the per-subject median **(D)** or proportion of discrete expression **(E).** In all heatmaps, expression is centered and standardized by column.

4.2.4 Modular analysis for examination of cooperation of gene expression at the single-cell level

Overall, the enriched expression of molecules involved in activation and chemotaxis in the infected cohort suggests a key role for $CD4^+$ T cell-mediated trafficking of leukocytes during the primary immune response to malaria. In order to gain greater insight into the molecular networks following CHMI versus vaccination, gene set enrichment analysis (GSEA) was performed (*270*) based on previously developed blood transcriptional modules (*270, 291*) **(Figure 4.6-A and B)**. Only modules containing at least four genes that were measured by Fluidigm were included for analysis (n=11 modules). The average effect of genes in a module was calculated while controlling for gene-gene correlation using Bootstrap replicates. A Z-score was generated, taking into account both the discrete and continuous components of mRNA expression.

Of the 11 modules tested, 8 exhibited a significant vaccine effect ($p<0.01$). Analysis identified six modules that were enriched in non-vaccinated controls, including T cell activation (I)(M7.2), T cell activation (II)(M7.3), and enriched in T cells (I)(M7.2). Two modules were enriched to a lesser extent in vaccinated subjects (|Z-score| <5), specifically cell adhesion (GO)(M117) and receptors and cell-migration (M109).

Although these modules have been previously used in a number of studies (*291-295*), this analysis has two important limitations. First, the modules were developed based on DNA microarray data from whole blood, which does not necessarily reflect

molecular networks intrinsic to $CD4^+$ T cells. Two, only a subset of the genes that comprise the modules are reflected in the Fluidigm analysis. New modules were developed based on genes associated with $CD4^+$ T cell differentiation pathways described in the literature **(Table 4.2)**. GSEA was performed as described above **(Figure 4.7)**.

Modules associated with Th17, Th2 and Treg differentiation did not differ significantly between vaccinees and infection controls **(Figure 4.7)**. Modules associated with homing to the liver and TFH differentiation were enriched in infection cohorts (|Z-score| = 4.95 and 5.70, respectively). Enrichment of the module "homing to the liver" in infection controls was characterized by increased expression in *CXCR3* and *CCR5*; and "TFH differentiation" by *ICOS*, *MAF* and *IL21*. There was no difference in expression of the remaining genes in these two modules.

Markers associated with a Th1 signature were significantly enriched in vaccinees (|Z-score| = 5.62; **Figure 4.7**). Of note, *TBX21/TBET*, *STAT1* and *IFNG* were enriched in infection controls. However, *IL2* and *TNF* were enriched in vaccinated subjects with a greater statistical significance and fold-change in expression **(Figure 4.5-B).**

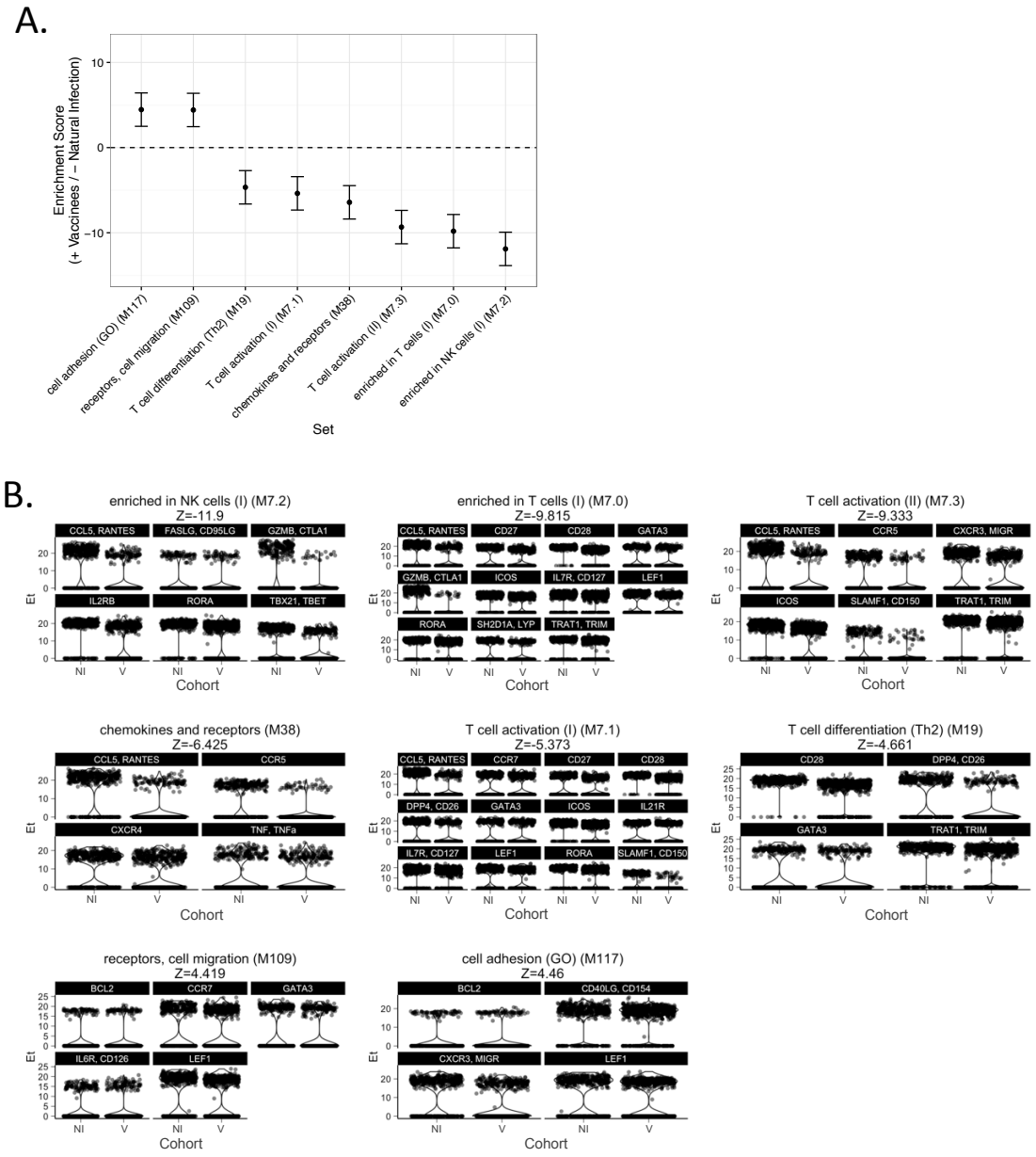

Figure 4.6 GSEA of vaccinated subjects vs. infection controls using BTM

(A) Gene set enrichment analysis showing blood transcriptional modules (BTM) enriched in vaccinated subjects or infections controls ($p<0.01$). Positive Z-scores indicate enrichment in protected vaccinated subjects. Negative Z-scores indicate enrichment in natural infection. Composite Z-score with 95% confidence intervals. (**B)** Violin plots of the individual genes within each module.

Liver Homing	TFH	Th1	Th17	Th2	Treg
CCR1 CCR5 CXCR3 CXCR6	BCL6 IL21 CXCR5 ICOS MAF	TBET IFNG IL2 TNF STAT1	RORC IL17 STAT3 RORA CCR6	GATA3 IL4 IL5 IL13 STAT6 IL4R	FOXP3 IL10 TGFB1

Table 4.2 List of genes in curated modules for GSEA of T helper subsets

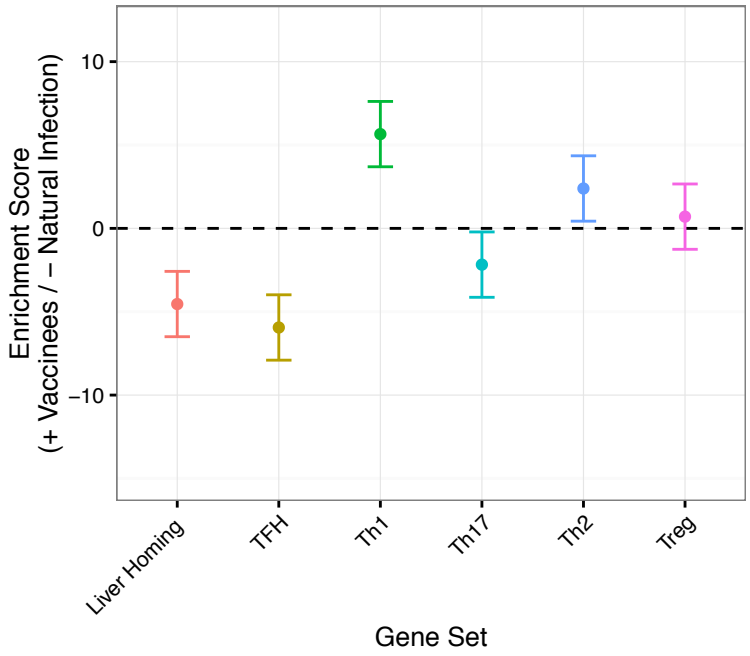

Figure 4.7 GSEA of vaccinated subjects vs. infection controls using curated modules for T helper subsets

Gene set enrichment analysis with Th modules described in **Table 4.2** showing enrichment in vaccinated subjects or infections controls ($p<0.01$). Positive Z-scores indicate enrichment in vaccinated subjects. Negative Z-scores indicate enrichment in natural infection. Composite Z-score with 95% confidence intervals.

4.2.5 Plasticity and heterogeneity of CD4$^+$ T cell gene expression

To determine CD4$^+$ T helper cell lineage fidelity at the single cell level, coexpression analysis was restricted to genes that regulate key Th differentiation pathways **(Figure 4.8-A)**. Coordinate discrete expression of three predominant Th subsets (Th1, Th2 and TFH) and their respective canonical cytokines (*IFNG*, *IL13*, and *IL21*) and master transcriptional regulators (*TBET*, *GATA3*, and *BCL6*) was examined. It was hypothesized that cells expressing any given canonical transcription factor would be more likely to express the cytokine associated with the Th subset. For example, *TBET*-positive cells would be more likely to express *IFNG* than *IL13* or *IL21*, conforming to a traditional Th1 signature.

The hypothesis was true for all three Th subsets. Among *GATA3*-positive cells, 97% expressed *IL13* compared to 43% *IFNG* and 31% *IL21* expression. (Note that the percentages do not add up to 100, as cells commonly express multiple cytokines at a time.) Among *TBET*-positive cells, 91% expressed *IFNG* compared to 43% *IL21* and 37% *IL13* expression. *IL21* expression in *BCL6*-positive cells was statistically greater than *IFNG* or *IL13,* but cooperation between TFH canonical genes appeared less stringent. Together, these data suggest that there exists cooperation among canonical genes associated with functional Th subsets at the single cell level.

In order to assess the polyfunctionality of PfSPZ-specific CD4$^+$ T cells as a function of vaccination, the coexpression of all genes (not just those differentially expressed) was assessed in both cohorts in a two-way hierarchal clustering analysis. Overall, there was evidence of greater co-expression and structure in CD4$^+$ T cells from

infection controls **(Figure 4.8-B)** compared to vaccinated subjects **(Figure 4.8-C)**. In both cohorts, the groups of genes with the greatest positive cooperation were *CCR5* and *CCL5/RANTES*; and *IL2RA* and *TNFRSF14/OX40*, and *TNFRSF9/CD137*. However, there is little evidence to suggest that overall patterns of gene cooperation distinguish the infection and vaccinated cohort.

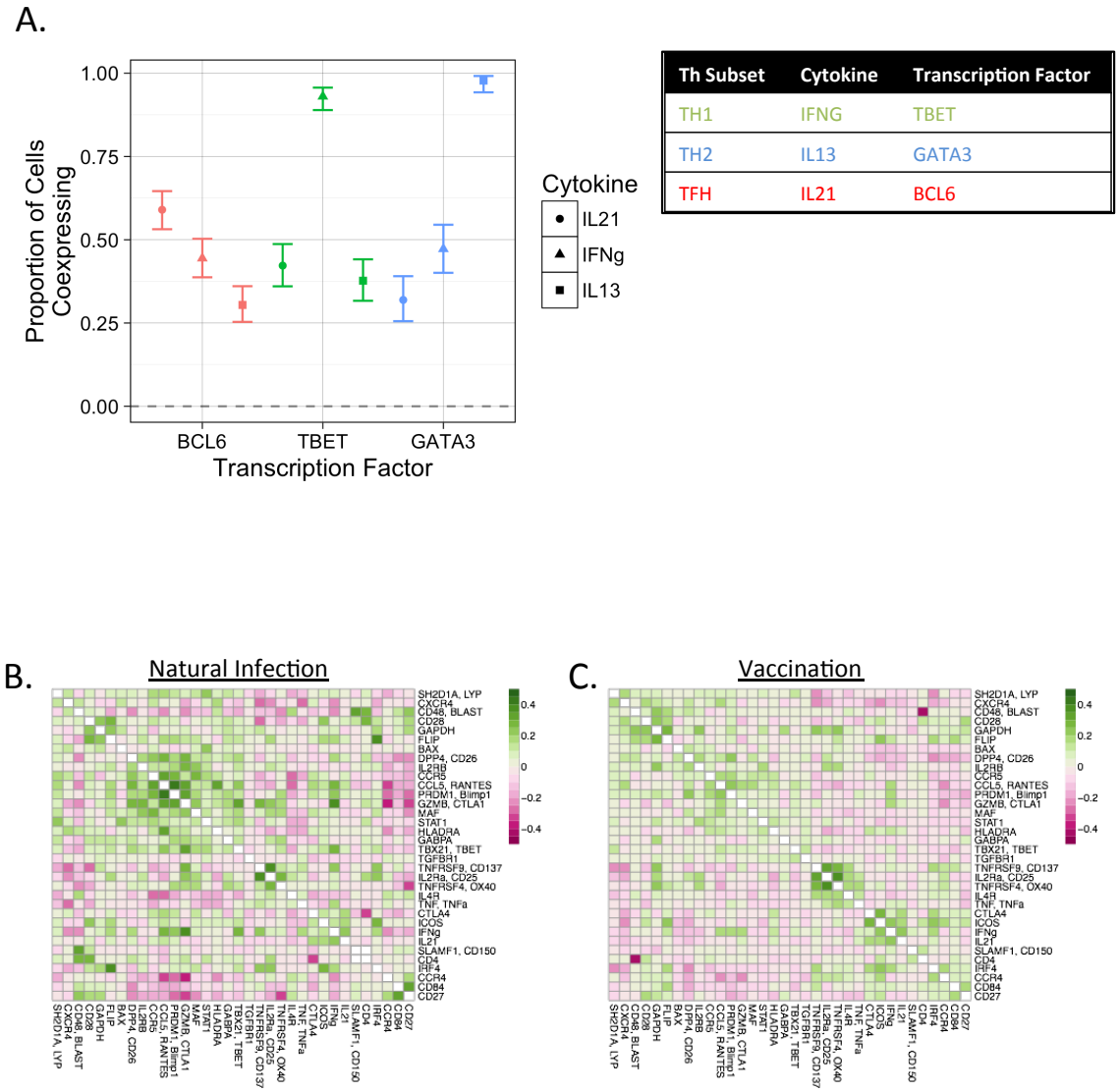

Figure 4.8 Heterogeneity of PfSPZ-specific CD4$^+$ T cells

(A) Coexpression of canonical Th cytokines (*IL21*, *IFNG*, *IL13*) and transcription factors (*BCL6*, *TBET*, *GATA3*) for all subjects. Y axis displays proportion of cells that discretely express any gene. 95% confidence intervals. **(B)** Correlation matrix for the infection control and **(C)** vaccinated cohort. Green indicates gene pairs where the difference between infection controls vs. vaccination is significantly greater than 0.05 and purple indicates gene pairs where the difference between infection controls vs. vaccination is significantly less than -0.05%.

4.2.6 Gene signatures associated with protection following vaccination

The transcriptomic profiles of $CD4^+$ T cells from vaccinated subjects were assessed in order to determine if T cell quality prior to challenge was associated with protection. Note that in this clinical study, there were only 10 protected versus 2 unprotected vaccinated subjects with CD154 responses above the threshold for Fluidigm analysis.

Twelve genes were differentially expressed ($p<0.001$ and fold-change >2) between protected and unprotected vaccinees prior to challenge **(Figure 4.9-A and B)**. 10/12 genes were enriched in nonprotected subjects, including *RORA*, a promoter of Th17 differentiation (*296*); *IL4R*, a receptor responsible for IL-4- and IL-13-mediated Th2 differentiation (*297, 298*), and a number of activation markers such as *TNFRSF9/CD137*, *IL2RA*, *CD48/BLAST*. Of note, *IL21* was exclusively expressed in protected subjects prior to challenge.

As there were only two unprotected subjects and twelve differentially expressed genes, there was not sufficient power to perform single-cell hierarchal clustering. Instead, coexpression analysis of all genes (not just those differentially expressed) at the subject level was performed in order to understand networks of genes that characterized the protected cohort. Coexpression of *HLADRA* and *TRAT1*, as well as coexpression of *IL21* with any marker best distinguished between the two cohorts **(Figure 4.9-C)**. Furthermore, *IL21* expression at the single-cell level in the protected cohort was not driven by any individual subject. Among all genes, IL21

expression was correlated at a statistically significant level (spearman rank correlation: $\rho > 0.25$ and $p<0.001$) with *ICOS*, *CTLA4*, and *CXCR3*.

In order to understand the relevance of key $CD4^+$ T cell differentiation pathways, GSEA was performed, using modules previously described in **Table 4.2**. The TFH gene set is enriched in the protected vs. unprotected cohort (|Z-score| = 10.0), while other modules were not significantly different between the two cohorts **(Figure 4.10-A)**. Among IL21-positive cells, a plurality discretely expressed either *BCL6* (41%) or *TBET* (34%), with marginal expression of the remaining canonical transcription factors (*GATA3* 15%, *FOXP3* 4%, and *RORC* 12%). There was not sufficient power for second-order correlations at the single cell level (i.e. coexpression of *BCL6* and *TBET* in a single cell).

IL21 is required for efficient development of TFH via the upregulation of BCL-6 (*299-301*) and subsequent affinity maturation of B cells in the germinal center (*300, 302, 303*). Therefore, increased *IL21* expression may reflect enhanced humoral responses. Accordingly, the subject-level median gene expression of *IL21* significantly correlated (spearman rank correlation: $\rho = 0.69$, $p < 0.001$) with antibodies titers against the circumsporozoite protein (CSP), the major surface protein on PfSPZ **(Figure 4.10-B)**.

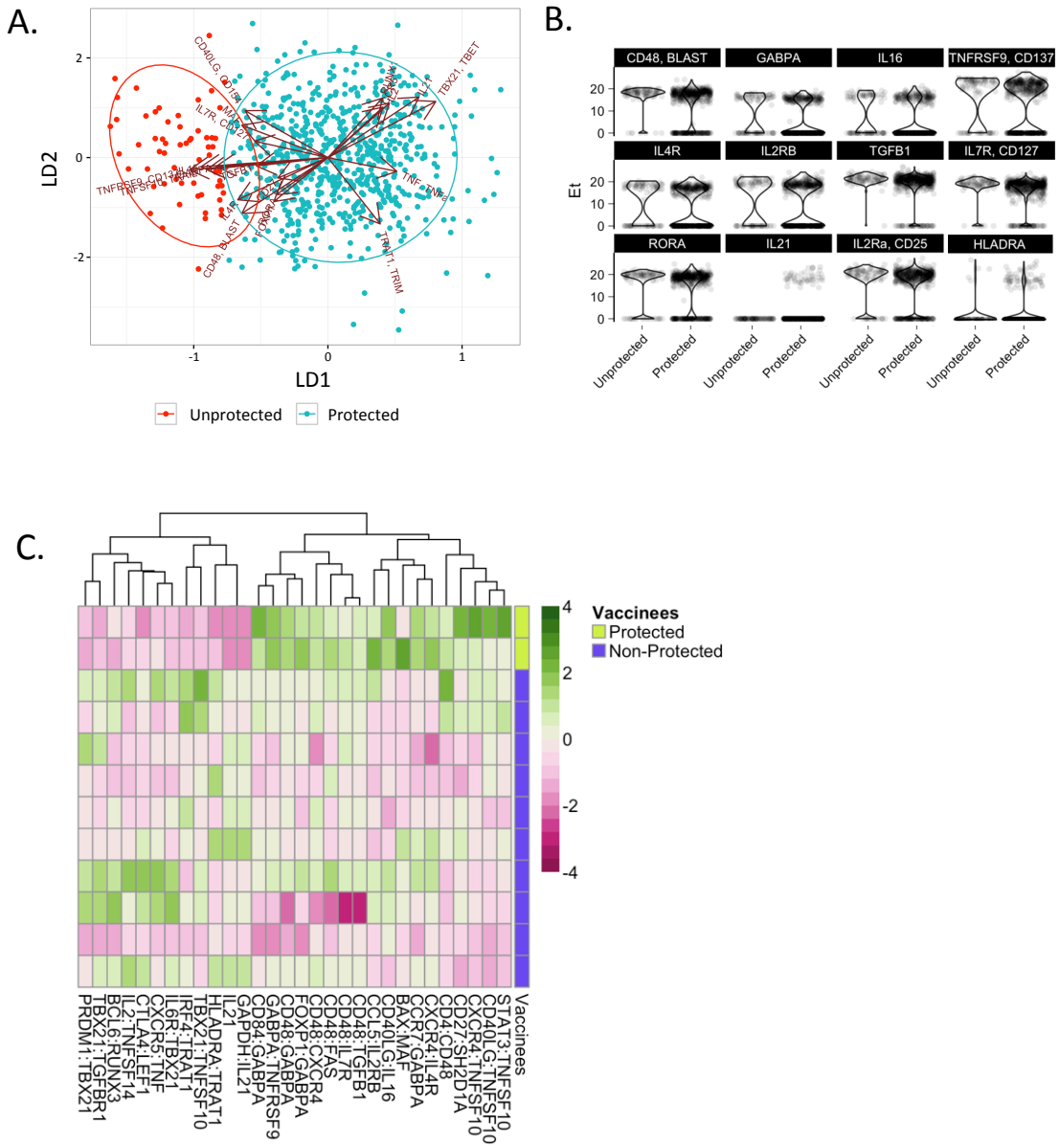

Figure 4.9 Gene signatures of vaccinated and protected vs. unprotected subjects

(A) Linear discriminant analysis and **(B)** violin plots of genes identified as differentially expressed between protected and non-protected subjects within the vaccinated cohort ($p<0.001$ and fold-change >2). **(C)** Subject-level average expression of pairs of genes discriminating between protection and non-protection in vaccinated subjects using penalized logistic regression.

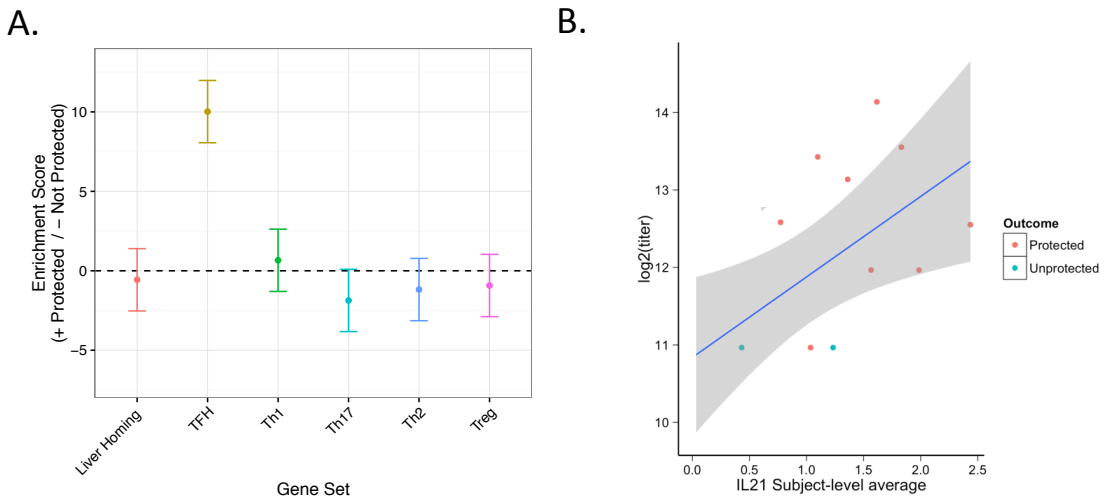

Figure 4.10 *IL21* expression and humoral immunity

(A) GSEA with Th modules described in **Table 4.2** showing enrichment in protected vs. unprotected subjects ($p<0.01$). Positive Z-scores indicate enrichment in protected vaccinated subjects. Negative Z-scores indicate enrichment in unprotected vaccinated subjects. Composite Z-score with 95% confidence intervals. **(B)** Correlation between *IL21* subject-level average gene expression detected by Fluidigm assay and PfCSP-specific antibody titers measured by ELISA.

4.3 Discussion

The main aims of this chapter were to assess the single-cell transcriptomic profiles of (1) vaccination with a live whole parasite vaccination versus malaria infection and (2) protected versus unprotected vaccinated subjects prior to challenge. First, single-cell gene expression profiles from the three analyzed cohorts (vaccinated/protected, vaccinated/unprotected and infection controls) are broadly distinct by unsupervised dimensionality reduction analysis. These data supported later studies that characterized this phenotype by differential expression of individual genes or sets of genes. Second, hierarchal clustering and modular analysis suggested the CHMI was predominately characterized by T cell activation, TFH differentiation, and homing to the liver compared to vaccination alone. Finally, while there was limited power for correlates of protection analysis, initial data demonstrated enriched *IL21* expression in protected subjects prior to challenge. Furthermore, *IL21* gene expression on per-subject basis correlated with antibodies against the immunodominant CS protein, suggesting an important role for circulating TFH $CD4^+$ T cells in protection.

It is important to note that downstream analysis was not possible for all vaccinated subjects, as three subjects had $CD4^+$ T cell responses that were not significantly different from the negative control. Note that these three subjects had the lowest $CD4^+$ T cell responses as previously assessed by multiparameter flow cytometry. However, by removing these three subjects, the magnitude of the remaining CD154 responses did not differ across the three cohorts. From optimization data in Chapter 3, there was an initial concern that the CD154 responses by flow cytometry would

vary dramatically and affect interpretation of downstream transcriptomics (see Section 3.5 for more details). Thus, while this filtering step removed 1/3 unprotected and 2/12 protected subjects, it ensured that transcriptional profiles reflected the quality of $CD4^+$ T cell responses, and not the proportion of background $CD154^+$ cells.

Not surprisingly, the global transcriptomic differences between the infection and vaccination cohorts was much greater than within the vaccination cohort when comparing protected and unprotected subjects prior to challenge. Overall, the infection controls had a more homogeneous gene expression profile by single-cell hierarchal clustering, in line with relatively consistent primary immune responses to malaria under control conditions *(22)*. Increased expression of activation markers coupled with enrichment of previously described modules associated with T cell activation and differentiation likely reflects an increased antigen load present in the liver following CHMI vs. PfSPZ immunization (*304*). Alternatively, PfSPZ vaccination alone and CHMI both induce multi-stage immune responses that target both liver and blood stage antigens. However, there is a likely a different repertoire of antigen specificities, potentially skewing a direct comparison of the two groups.

Curated modules based on literature describing the molecular mechanisms of $CD4^+$ T cell differentiation pathways provided a more nuanced interpretation of the data. The enrichment of modules reflecting homing to the liver and TFH differentiation were characterized by significant upregulation of the individual genes in the infection controls, or no difference between the two cohorts. This TFH phenotype may reflect the role of antibody-mediated protection in natural acquired immunity

(*31, 100, 305*). Furthermore, exposure to the sporozoites for the first time in infection controls compared to subjects vaccinated with the attenuated parasite may explain the enrichment of genes associated with homing to the liver. The Th1 module was overall enriched in the vaccinated cohort, but the signature was less significant. A Th1 phenotype in vaccinated subjects versus infection controls may reflect the importance of $CD4^+$ T cell help for $CD8^+$ T cells in PfSPZ-mediated immunity (*176, 306*), but again this finding is less clear.

Correlates of protection analysis was limited in this study, as there were only two unprotected subjects with sufficient CD154 responses for downstream single cell transcriptomics. Analysis was overall restricted to differential gene expression comparisons at the subject or cohort level, as well as first-order coexpression analysis. *IL21* was one of two genes enriched in the protected cohort, and discrete *IL21* expression was undetectable in the two unprotected subjects. While IL21 protein is produced by many different subsets of $CD4^+$ T cells (*303, 307-309*), a positive correlation with CSP antibodies suggests that the *IL21* gene expression reflects circulating TFH cells. Predominant expression of *BCL* and *TBET* in *IL21*-producing cells further suggests that such cells are TFH or transitional Th1/TFH $CD4^+$ T cells (*310*). Increased power, specifically a greater number of vaccinated subjects or a larger proportion of unprotected vaccinated subjects, will be necessary in order to support this hypothesis.

Overall, this characterization of the PfSPZ-specific cellular immune response should advance our understanding of the role of $CD4^+$ T cells against human malaria infection as well as delineate the striking heterogeneity of $CD4^+$ T cell responses

following vaccination with a whole parasite. The main future goals will be to substantiate these findings in a larger clinical trial using Fluidigm anlaysis and other assays to assess the molecular phenotype at the protein level.

5. VRC 314- PfSPZ Vaccine Trial #2

5.1 Introduction

The VRC312 study demonstrated that IV administration of the PfSPZ Vaccine was safe, immunogenic and induced high-level protection when volunteers were challenged three weeks following the final immunization. Six out of six subjects who received five doses of $1.35x10^5$ PfSPZ and three out of nine subjects who received four doses were protected (*116*). However, protection was short-lived. Six volunteers (three from each vaccination group) who were protected upon the first CHMI were rechallenged 21 weeks following the final immunization. Only 2/6 were protected, one from each vaccination group (Overall vaccine efficacy (VE) = 33%, p =0.2273). As a result, the PfSPZ Vaccine did not meet the efficacy standards of greater than 80% for a year (*111, 204*).

As no long-term protection was afforded by $1.35x10^5$ PfSPZ, a follow-up study (VRC314) was designed to test if a higher dose ($2.7x10^5$ PfSPZ) administered IV was safe and could confer durable protection (*205*) **(Figure 5.1)**. Additionally, as a deployable malaria vaccine would likely require as few immunizations as possible, the study assessed how the number of doses affected protective efficacy. VRC314 was conducted over two study sites due to the large number of vaccine recipients (Vaccine Research Center, NIAID, NIH and the University of Maryland, Baltimore; both USA).

VRC 314 Groups				Study Week							
Site	**Group**	**Vaccine Dose**	**#Subjects**	**0**	**4**	**8**	**12**	**16**	**20**	**23**	**44**
Site 1	Group 1	2.7 x 10^5 IV	12	V1	V2	-	-	-	V3	*C	**R
	Group 2	2.2 x 10^6 IM (half in each arm)	9	V1	V2	V3	-	-	V4	C	R
	Group 3	1.35 x 10^5 IV; may opt for 4.5 x 10^5 IV for V5	12	V1	V2	V3	V4	-	V5	C	R
Site 2	Group 4	2.7 x 10^5 IV	12	V1	V2	V3	-	-	V4	C	R
	Group 5	2.7 x 10^5 IV	12	V1	V2	V3	-	-	V4		C
Site 1	Group 6	9.0 x 10^5 IV	15	V1	-	V2	-	V3	-		C
Site 1	Group 7	2.7 x 10^5 IV; may opt for 4.5 x 10^5 IV for V3 and V4	12	V1	V2		V3		V4		C
All Sites	Group 8	Controls (no vaccine)	52	*C=CHMI; **R=repeat CHMI There will be 6 to 7 CHMI conducted, depending upon timing of each group enrollment. When a single CHMI is conducted over two days, there will be 8 control subjects and when conducted within one day there will be 6 control subjects. Typically 2 back-up controls per CHMI will also be enrolled.							
	Total		136	Target study week is shown. Allowed windows are specified in the protocol. Cumulative enrollment of up to 150 subjects is permitted to account for extra back-up controls or replacement vaccine subjects who may be enrolled due to subject withdrawals.							

Figure 5.1 VRC314 clinical study

This figure is taken from reference (*205*). The vaccination schedule, PfSPZ dose and route for all subjects immunized under the VRC314 Clinical study. Note that not all subjects included in this table were assessed by Fluidigm analysis.

First, the immunogenecity and protective efficacy of IV administration of PfSPZ given by varying doses and schedules were assessed. Group 3 served as a positive control for protection in the study, by repeating the vaccination regimen assessed in VRC312. Non-human primate (NHP) data acquired after the start of the study suggested that a higher dose would increase protection (data not published). As a result, subjects in Group 3 received four doses of $1.35x10^5$ PfSPZ followed by a fifth dose of $4.5\ x10^5$ PfSPZ.) Subjects in Groups 1 and 4 received three or four doses of $2.7\ x\ 10^5$ PfSPZ, respectively. Cellular immunogenecity was assessed by flow cytometry by *in vitro* stimulation with PfSPZ and PfRBC two weeks following the final immunization in all groups. Immunization induced high-level antibody and $CD4^+$ T cell responses. $CD8^+$ T cell responses to PfSPZ and PfRBC were low to undetectable in all groups.

Groups 1, 3, and 4 were challenged three weeks following the final immunization. In Group 3, 8/12 were protected (VE = 62%, p=0.025). In subjects who received three or four doses of $2.7x10^5$, 3/9 (VE = 24%, p=0.335) and 7/9 (VE = 73%, p=0.035) were protected, respectively. Immune correlates were assessed from samples isolated two weeks following the final immunization. Neither the magnitude nor quality of $CD4^+$ or $CD8^+$ T cells correlated with protection. PfSPZ-specific antibody levels assessed by automated immunofluorescence assays (aIFA) correlated with outcome (p=0.0098), but waned substantially after 59 weeks.

Given the administrative hurdles for the deployment of a malaria vaccine administered IV, this study also assessed the protective efficacy of the PfSPZ Vaccine administered by the IM administration of a much higher dose. Subjects in

Group 2 received four doses of $2.2x10^6$ PfSPZ on the same schedule as Group 4. Two weeks following the final immunization, antibody levels and $CD4^+$ T cell responses in Group 2 were significantly lower compared to Groups 1, 3, and 4 (PfSPZ administered IV). Following CHMI, 3/8 subjects were protected (VE = 29%). These data suggest that PfSPZ administered IM at 8-fold higher dose was less efficient at inducing protective immunity compared to IV.

Finally, the third important aim in this study was to assess durable immunity of the PfSPZ Vaccine administered by the IV route. Subjects in Group 5 received four doses of 2.7×10^5 PfSPZ (the same dose and schedule as Group 4) and were challenged 21-24 weeks following the final immunization. Following CHMI, 6/11 subjects were protected (VE = 55%, p=0.0373).

The increased number of vaccinated subjects in VRC314 provided greater statistical power for in-depth analysis of PfSPZ-specific $CD4^+$ T cells compared to Chapter 4. Furthermore, it also provided an opportunity to test hypotheses generated in the previous chapter concerning possible correlates and/or biomarkers of PfSPZ-induced protection. Thus, the aims of this chapter are: (1) compare molecular signatures of PfSPZ-specific $CD4^+$ T cell responses induced by different vaccination regimens; (2) characterize single-cell transcriptional profile of such responses from protected vs. unprotected vaccinated subjects; (3) test hypothesis that circulating $CD4^+$ TFH cells are associated with protection; and (4) assess multi-order combinations of gene expression in order to explore cell-intrinsic gene networks.

5.2 Results

5.2.1 Isolation of PfSPZ-specific CD4$^+$ T cells from subjects vaccinated with varying doses under clinical study VRC314

The first aim of this chapter was to isolate individual PfSPZ-specific CD4$^+$ T cells from vaccinated subjects who were assessed for short-term protection in VRC314 (*205*) **(Figure 5.1**). Responses were assessed from PBMCs isolated two weeks following the final immunization (one week prior to challenge). Analysis of short-term protection consisted of three cohorts: ten subjects who received four doses of 1.35×10^5 followed by a fifth dose of 4.5×10^5 PfSPZ (VRC314 Group 3), seven subjects who received three doses of 2.7×10^5 PfSPZ (Group 1), and nine subjects who received four doses of 2.7×10^5 PfSPZ (Group 4).

In addition, ten subjects from Group 5 were analyzed in order to explore potential correlates for long-term protection. These subjects received four doses of 2.7×10^5 PfSPZ as in Group 4, but underwent CHMI 21-25 weeks following the final immunization. Responses were assessed from PBMCs isolated two weeks following the final immunization, as above. All other subjects in these four groups (1, 3, 4, and 5) had low to undetectable CD4$^+$ T cell responses as determined by cytokine production of IFN-γ, IL-2 and TNF-α in an independent experiment, and as such were excluded from analysis prior to assessment of CD154 responses. Vaccination groups 2, 6, and 7 were not examined, as either overall T cell responses were too low or samples were not available at the time of analysis.

Overall $CD4^+$ T cell responses defined by coexpression of CD154 and CD69 protein were assessed by flow cytometry for each cohort, in the same manner as described in Chapters 3 and 4 **(Figure 5.2)**. Six subjects across all vaccine groups had responses that were below the threshold for downstream Fluidigm analysis. Following exclusion of these subjects, the total magnitude of $CD69^+CD154^+$ $CD4^+$ T cells was similar across all groups with the exception of Group 3, which had significantly lower responses. This pattern is similar to that seen in independent experiments measuring $CD4^+$ T cell responses as assessed by cytokine production of IFN-γ, IL-2 and TNF-α from the same subjects (*205*). In total, 26 subjects from VRC314 were assessed by Fluidigm **(Table 5.1)**, over twice the number of vaccinated subjects analyzed in the previous chapter.

Quantitative gene expression was acquired as described in the previous chapter, using Fluidigm 96.96 Dynamic Arrays with the same gene panel, plate layout and quality control measures. Expression of 84 genes from 2,128 single cells was retained for downstream analysis. As previously discussed, gene expression was not normalized as part of the multistep data filtering process. Of note, *CD154* mRNA levels were slightly higher in Group 1 compared to other cohorts **(Figure 5.3)**. However, *CD69* and *GAPDH* mRNA levels were similar across all groups, suggesting that there was no overall disparity among internal controls. Overall, the data quality was similar to the previous chapter in terms of the percentage of genes and cells retained downstream of data acquisition (data not shown).

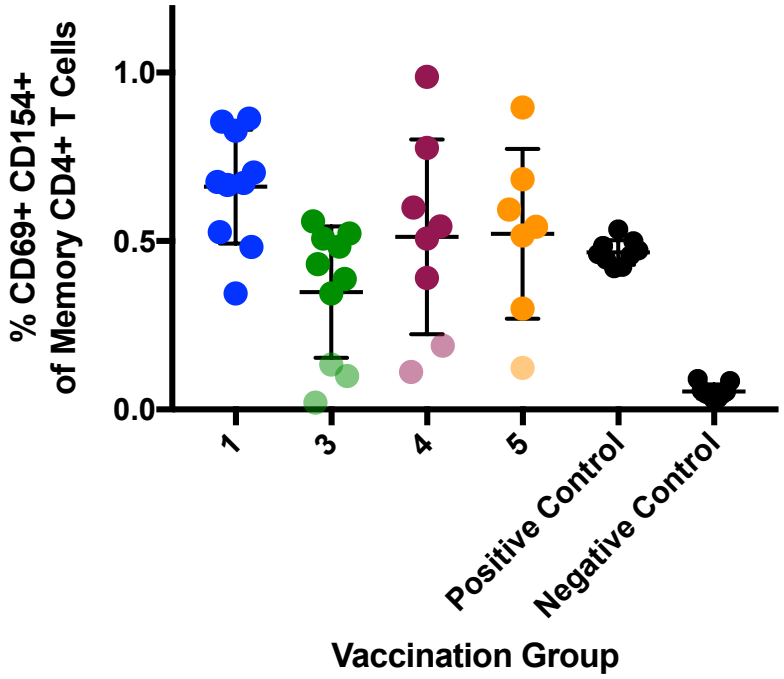

Figure 5.2 PfSPZ-specific CD4$^+$ T cell responses

PBMCs isolated from samples at two weeks following the final vaccination were stimulated *in vitro* with 135,000 PfSPZ for 15 hours. The frequency of CD69$^+$CD154$^+$ cells is represented as a percentage of the memory CD4+ T cell population as assessed by flow cytometry. Subjects with responses below the limit for Fluidigm analysis are shaded. Mean +/ standard error of the mean (SEM).

	Group	Vaccine Regimen	CHMI	Sample Timepoint	Overall VE (Protected/ Total)	Fluidigm Analysis (Protected/ Total)
Vaccinees	1	3 or 4 doses of $2.7x10^5$ PfSPZ Vaccine	3 weeks post final vaccination	2 weeks post final vaccination	3/9	2/7
	4				7/9	5/6
	5		21-25 weeks post final vaccination		6/11	4/6
	3	5 doses of $1.35x10^5$ PfSPZ Vaccine†	3 weeks post final vaccination		8/12	4/7
Total						26

Table 5.1 VRC314 subjects analyzed by Fluidigm

All subjects with $CD4^+$ T cell responses above limit of detection for Fluidigm analysis organized by vaccination group and protection outcome. †Subjects in group 3 received four doses of $1.35x10^5$ PfSPZ followed by a fifth dose of 4.5×10^5 PfSPZ.

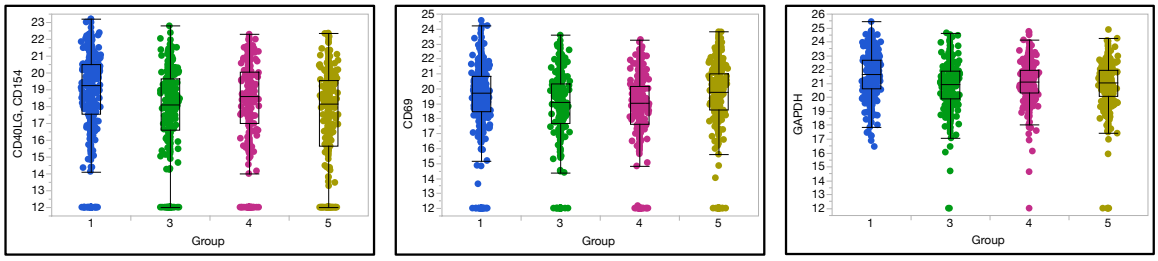

Figure 5.3 Controls for gene expression analysis

Single-cell gene expression from subjects across all four vaccination groups for *CD154*, *CD69*, and *GAPDH*. Et values are shown on the y-axis. Median +/- IQR.

5.2.2 Global transcriptomic profiles of PfSPZ-specific CD4$^+$ T cells from vaccinated subjects across different vaccination regimens

The transcriptomic profile of CD4$^+$ T cells induced by the vaccination regimen similar to that assessed in VRC312 (Group 3) was first compared to the shortened, high-dose regimen first assessed in VRC314 (Groups 4 and 5*).* The goal was to determine if there was any difference in the quality and phenotype of cellular immunity as a function of vaccination dose and schedule. Subjects from Groups 4 and 5 are combined in this analysis, as both cohorts received four doses of 2.7 x 10^5 with the only difference being the time of challenge. All samples were isolated two weeks after the final vaccination, which is reflective of peak immunogenecity. Note that both cohorts (Group 3 vs. 4/5) exhibited similar protective short-term efficacy, but only four doses of 2.7 × 10^5 PfSPZ conferred durable protection. As previously described, differentially expressed genes are defined as those that exhibited a statistically significant effect due to vaccination ($p < 0.01$) based on a likelihood ratio test of the combined discrete and continuous model components, and which exhibited at least a two-fold change in expression.

Thirteen genes were differentially expressed between the two cohorts, of which eleven were enriched in subjects who received the shortened, high-dose vaccination regimen **(Figure 5.4-A)**. *TBET* and *IFNG* were the only two genes that were significantly enriched in Group 3. The top five upregulated genes in the shortened, high-dose vaccination regimen as a factor of fold-change in the median value were *TRAT1/TRIM, DPP4/CD26, CCR7, IL16,* and *RUNX3,* in decreasing order of fold-change.

Linear discriminant analysis (LDA) further suggested that while some set of variables could maximize separation of the two vaccination groups, this was mostly characterized by a small set of genes that were upregulated in the shortened, high dose vaccination group **(Figure 5.4-B)**. Furthermore, misclassification of individual cells into the two vaccination groups was high (38.4%). The gene component that was most associated with LD1 was *TRAT1/TRIM,* which is involved in TCR signaling during the antiviral response in $CD4^+$ T cells (*311*). Of note, *TBET* and *IFNG* were mostly associated with LD2, which as a whole added very little information in maximizing separation within the dataset compared to LD1.

In order to assess cooperation among differentially expressed genes, unsupervised single-cell hierarchal clustering was examined **(Figure 5.4-C)**. This analysis was performed without regard for vaccination group, as LDA previously determined that the misclassification rate was high. In addition, single cell coexpression of all possible two-way combinations was calculated to account for both negative and positive gene associations **(Figure 5.4-D)**. *TRAT1/TRIM*, the gene component that drove the greatest separation between the two groups, clustered positively with *IL16* and *CXCR4*. The two genes enriched in Group 3 (*TBET* and *IFNG*) clustered positively together among all differentially expressed genes, but the association was relatively weak (spearman rank correlation: $\rho = 0.21$ and $p<0.01$). Interestingly, the genes that displayed the most significant cooperation (spearman rank correlation: $|\rho| > 0.25$ and $p<0.001$) were *IL2RB/DPP4, FAS/DPP4,* as well as a negative correlation between *TRAT1/TRIM* and *IFNG.*

A.

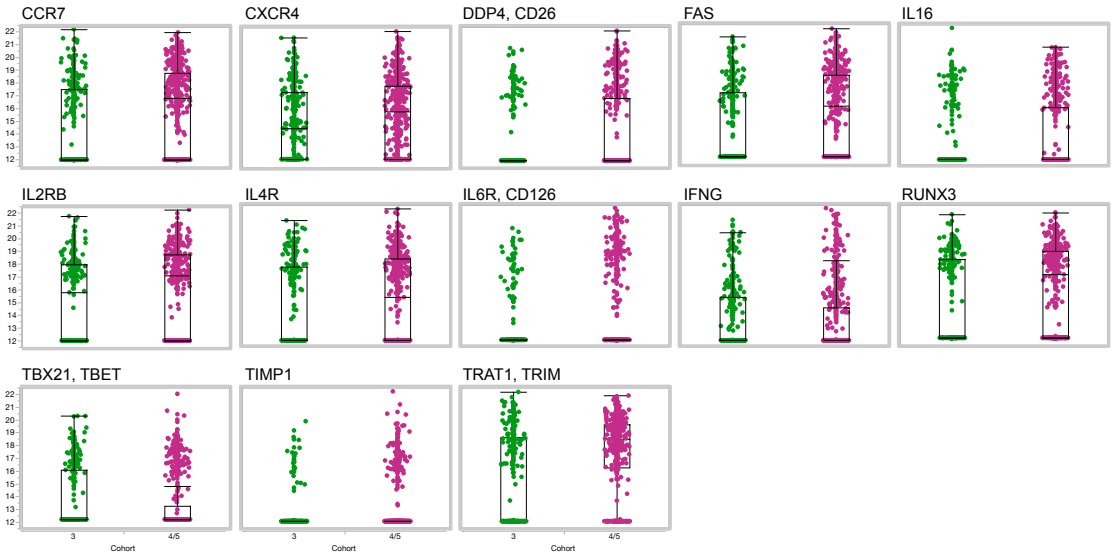
CCR7
CXCR4
DDP4, CD26
FAS
IL16
IL2RB
IL4R
IL6R, CD126
IFNG
RUNX3
TBX21, TBET
TIMP1
TRAT1, TRIM
Cohort
3
4/5

B.

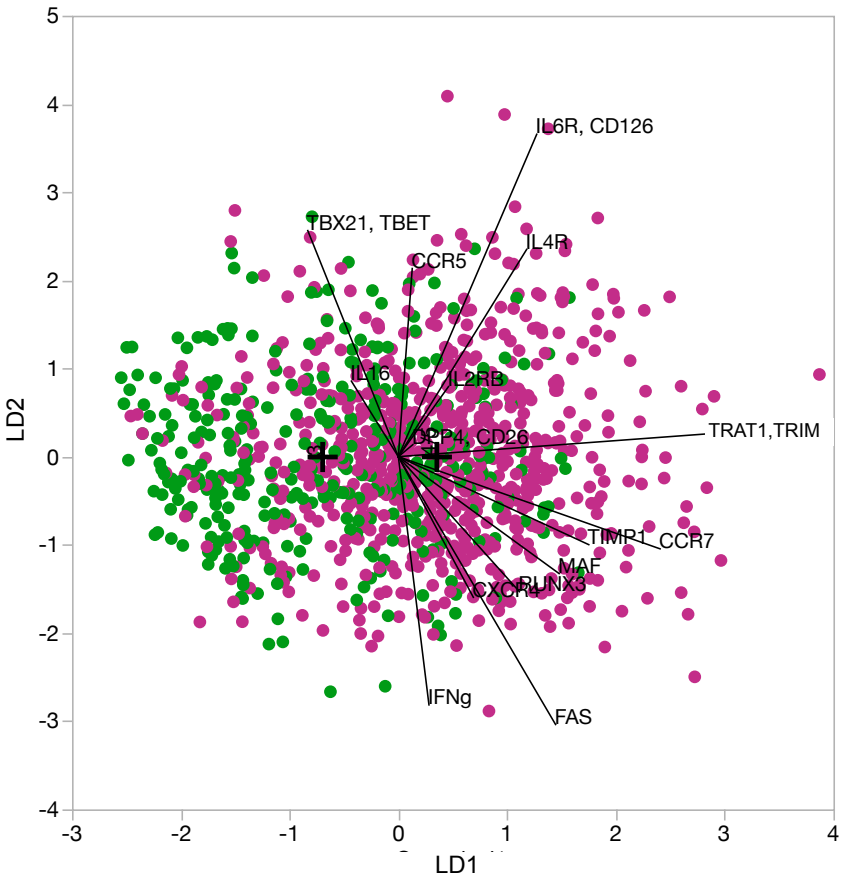
IL6R, CD126
TBX21, TBET
IL4R
CCR5
IL16
IL2RB
TRAT1,TRIM
DDP4, CD26
TIMP1
CCR7
MAF
CXCR4
RUNX3
IFNg
FAS
LD1
LD2

C.

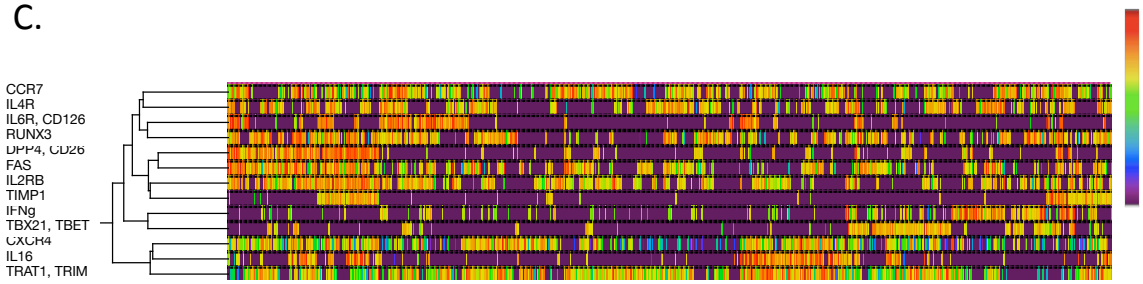

D.

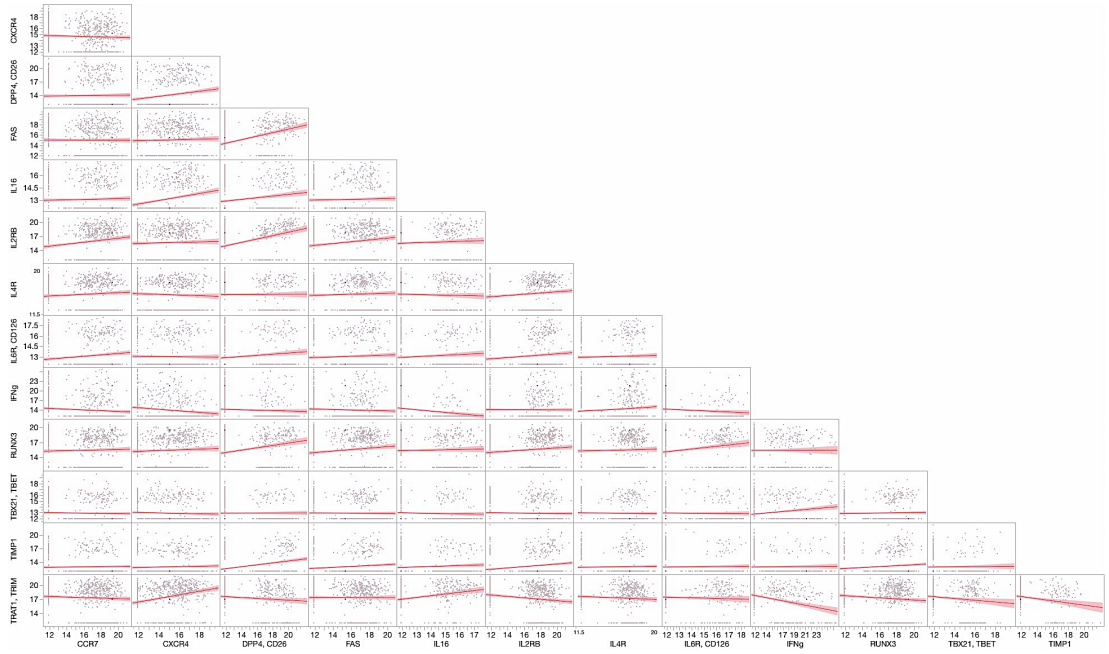

Figure 5.4 Fluidigm analysis of vaccine immunogenecity

Transcriptional signatures of subjects which received either four doses of $2.7x10^5$ PfSPZ (Group 4/5) or four doses of $1.35\ x10^5$ followed by one dose of $4.5x10^5$ PfSPZ (Group 3). **(A)** List of differentially expressed genes ($p< 0.001$ and fold-change >2). **(B)** Linear discriminant analysis and **(C)** unsupervised two-way heirarchical clustering and **(D)** pair-wise correlations of single-cell gene expression restricted to those genes which are differentially expressed.

5.2.3 Gene signatures associated with short-term protection following vaccination

In order to assess if T cell quality prior to challenge was associated with short-term protection, the gene expression profiles of $CD4^+$ T cells were assessed from all vaccinated subjects in Groups 1, 3, and 4. Note that the overall protective efficacy is lower in Group 1 (24% VE) compared to Groups 3 and 4 (62% and 73%, respectively). Group 5 was examined separately, as these subjects were challenged 21-24 weeks following the final immunization. Analysis was first performed by combining all of the vaccination groups (1, 3, and 4) in order to maximize statistical power, and then assessed within each group.

Twenty-five genes were differentially expressed ($p<0.01$ and fold-change >2) between all protected and unprotected vaccinated subjects prior to challenge **(Figure 5.5-A and B)**. 8/25 differentially expressed genes were enriched in the protected cohort, which was broadly composed of cytokines *IFNG*, *IL21*, *IL2*, and *IL13*, as well as chemokine receptors *CCR5*, *IL2RA/CD25*, and *IL6R/CD126*. Of note, the finding of enriched *IL21* gene expression in protected subjects was repeated, but expression was not exclusive as seen in the VRC312 study. The top five enriched genes in the unprotected cohort were *CD27*, *LEF1*, *STAT3*, *FOXP1*, and *TRAT1/TRIM*, in order of decreasing fold-change. Increased expression of *IL4R*, *IL7R*, *IL16* and *RORA* in unprotected subjects was seen in both VRC312 and VRC314 studies **(Chapter 4.3)**.

By contrast, only 6/84 analyzed genes were differentially expressed between protected and unprotected subjects in Group 5, which assessed correlates of long-

term protection **(Figure 5.5-C)**. All of these genes were upregulated in the unprotected cohort. Given the weak evidence suggesting that gene expression profiles of $CD4^+$ T cells isolated at two weeks following the final immunization would lend insight into long-term protection, no further analysis was performed for Group 5. All remaining analysis was restricted to Groups 1, 3 and 4.

Multivariate analysis was performed in order to determine if sets of differentially expressed genes were sufficient to characterize the transcriptional profile of protected vs. unprotected subjects assessed for short-term protection. Single-cell unsupervised hierarchal clustering alone was unable to clearly distinguish between the two cohorts **(Figure 5.5-D)**, suggesting that further analysis would be necessary to dissect a signature associated with protection. However, there was evidence of cell-intrinsic coordination **(Figure 5.5-E** and **F)**. The cytokines that were enriched in protected subjects (*IL13*, *IL2*, *IL21*, *IFNG*) clustered together, and of which coexpression of *IL21* and *IL2* was most significant (spearman rank correlation: $\rho = 0.54$ and $p<0.001$). Among genes enriched in unprotected subjects, coexpression of *CXCR4/IL16* and *CD27/CD84/LEF1* were tightly coordinated based on cluster and correlation analysis ($|\rho| > 0.25$ and $p<0.001$).

The set of differentially expressed genes described above was then assessed in each vaccination group separately. The classification efficiency for each group was then calculated based on the model for protection generated by the set of differentially expressed genes above **(Figure 5.6)**. The Receiver Operating Characteristic (ROC) curves measure the rate of true positives against the false positives at various significance thresholds, reflecting the sensitivity and specificity of the model. The

higher the curve is from the diagonal, the more accurate the model. The area under the ROC curve (AUC) was greatest for Group 4 (AUC = 0.95), where subjects received four doses of 2.7 x 10^5 PfSPZ. Accuracy was significantly lower in Groups 1 (AUC = 0.91) and 3 (AUC = 0.88). With this model, misclassification rates for Group 1, 3, and 4 were 14.9%, 22.1% and 11.6%, respectively.

A.

Groups 1, 3, and 4 (Short-Term)

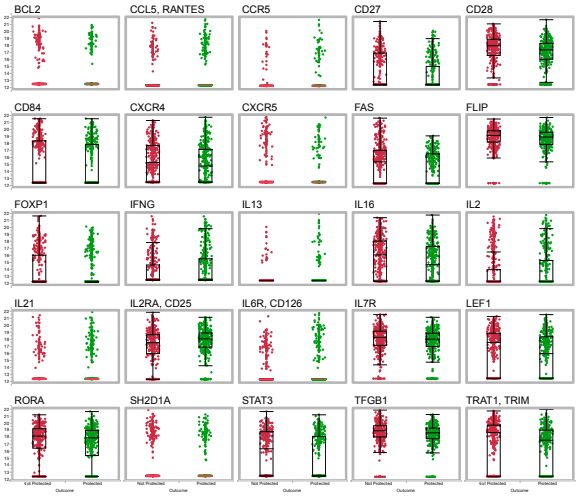

C.

Group 5 (Long-Term)

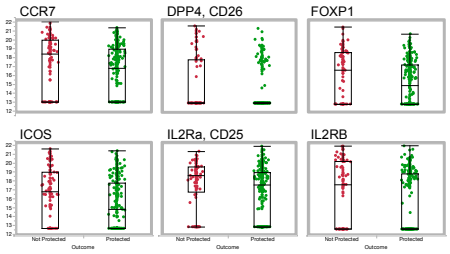

B.

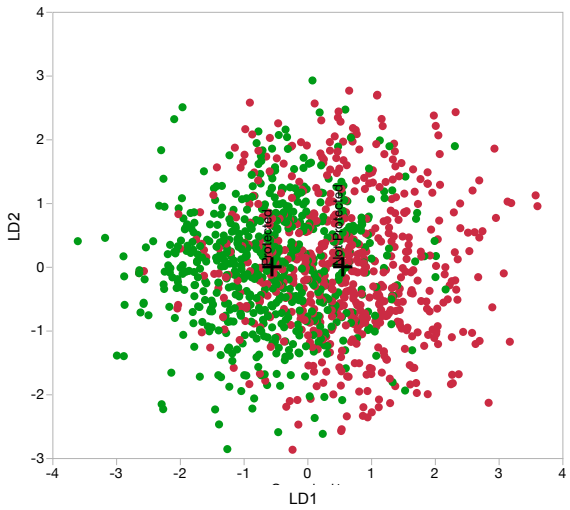

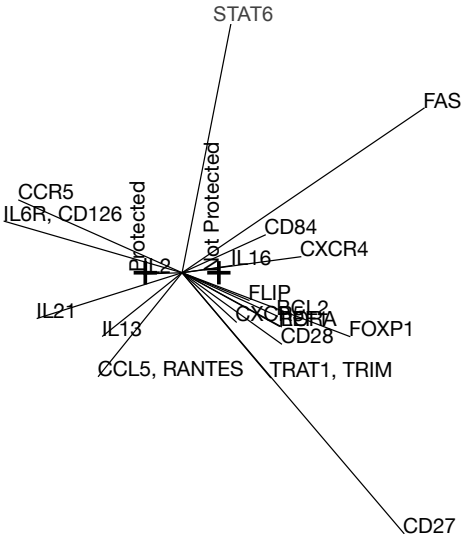

D.

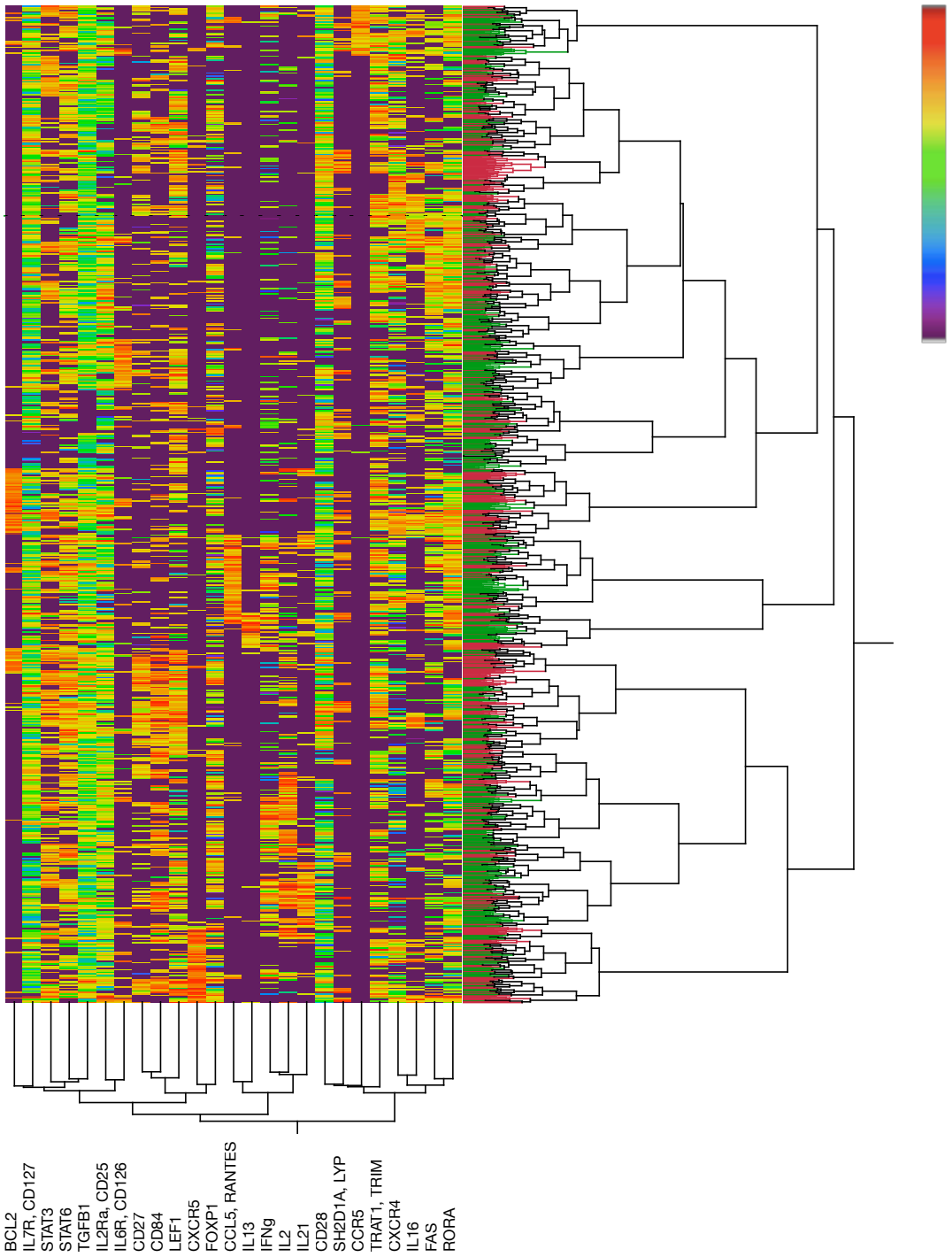
BCL2
IL7R, CD127
STAT3
STAT6
TGFB1
IL2Ra, CD25
IL6R, CD126
CD27
CD84
LEF1
CXCR5
FOXP1
CCL5, RANTES
IL13
IFNg
IL2
IL21
CD28
SH2D1A, LYP
CCR5
TRAT1, TRIM
CXCR4
IL16
FAS
RORA

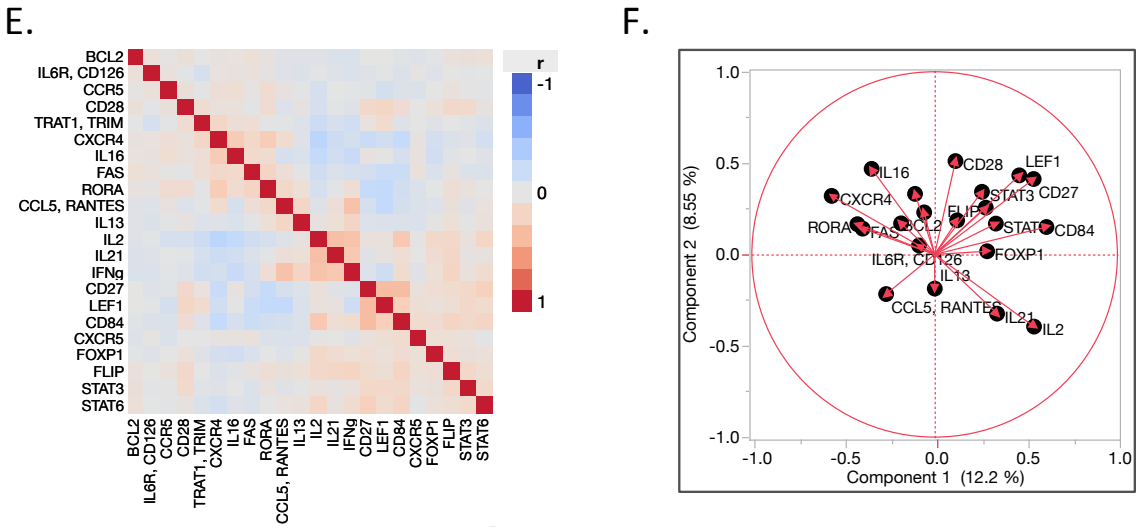

Figure 5.5 Fluidigm analysis of short-term protection

(A) List of differentially expressed genes ($p < 0.001$ and fold-change >2) between protected vs. unprotected subjects for cohorts that were assessed for short-term protection (Group 1,3, and 4) and **(B)** associated linear discriminant plot. **(C)** Differentially expressed genes between protected vs. unprotected subjects assessed for durable protective immunity (Group 5 only). **(D)** Unsupervised two-way clustering, **(E)** pair-wise correlations of single-cell gene expression and **(F)** principal components analysis restricted to those genes which are differentially expressed in subjects assessed for short-term protection.

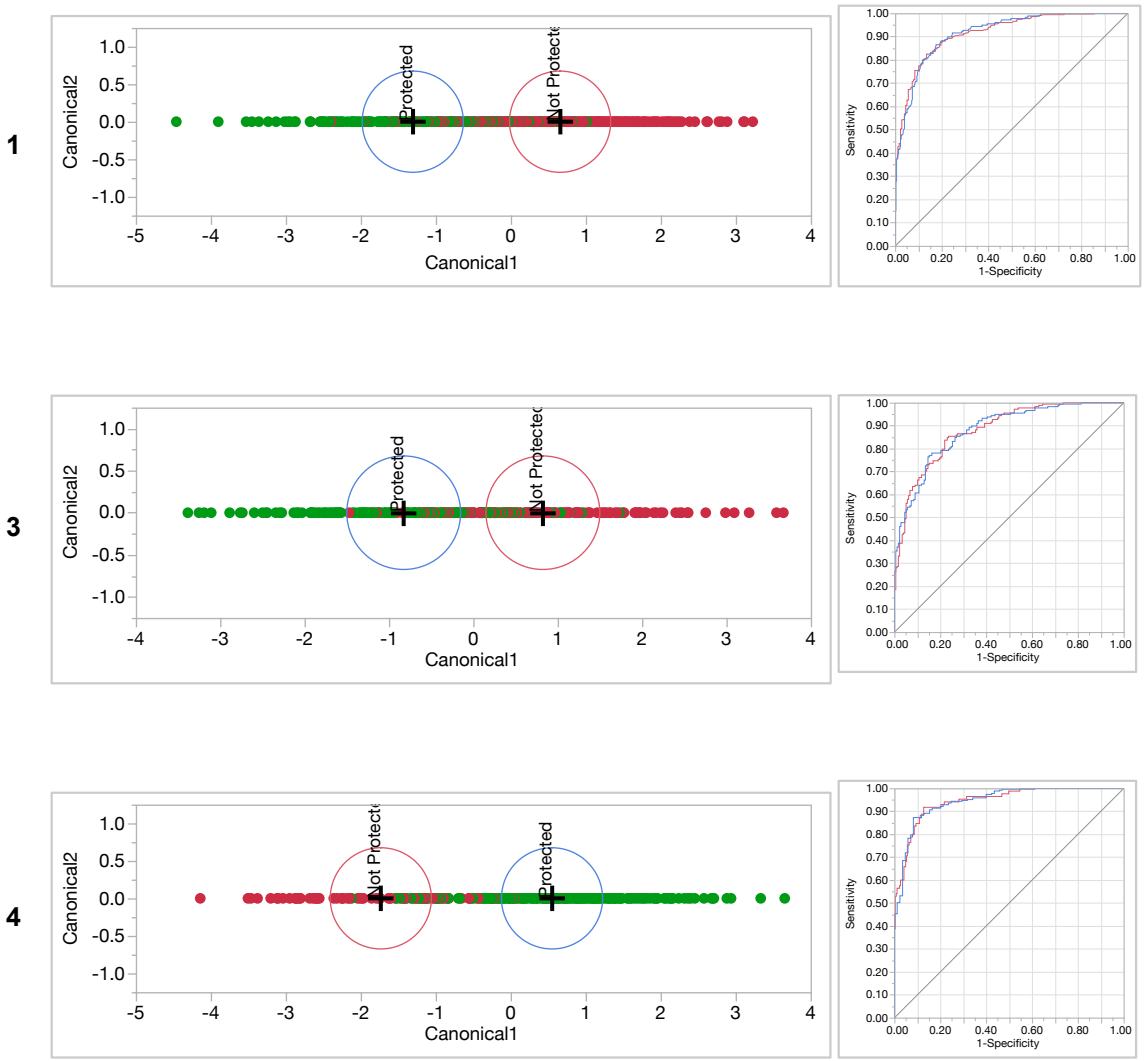

Figure 5.6 Accuracy of protective model by vaccination group

Wide linear discriminant analysis assessing the percentage single cells misclassified into each designated cohort. Circles represent the normal 50% contours. Associated Receiver Operating Characteristic (ROC) curves are shown for each vaccination group and plot the rate of true positives (sensitivity) against the false positives (1-specificity) at various significance thresholds.

5.2.4 Further investigation of IL21-expressing CD4$^+$ T cells

As enriched *IL21* expression in protected vs. unprotected prior to challenge was demonstrated in both VRC312 and VRC314, further analysis of this cohort of cells was performed. The subject-level median gene expression of *IL21* in this study correlated (spearman rank correlation: $\rho = 0.39$, $\beta_{protection} = 1.52$, $p = 0.014$) with antibodies titers against the circumsporozoite protein (CSP), the major surface protein on PfSPZ **(Figure 5.7-A)**. Increased *IL21* expression was most significantly associated with protection in vaccination Group 1 and 4, which received three and four doses of $2.7x10^5$ PfSPZ vaccine, respectively **(Figure 5.7-B)**. Among all genes, *IL21* expression was correlated at a statistically significant level (spearman rank correlation: $\rho > 0.25$ and $p<0.001$) with *ICOS, IFNG,* and *IL2*.

To further understand the function of *IL21*-expressing CD4$^+$ T cells induced by PfSPZ vaccination, the frequency of cells in this subset that expressed different combinations of transcription factors was analyzed at the single cell level. Analysis was restricted to six canonical transcription factors that have been reported to drive differentiation of key CD4 T cell subsets (*85, 87*). As an internal control, coexpression of transcription factors among all cells, not just those that expressed *IL21*, was also examined **(Figure 5.8)**.

IL21-expressing cells predominantly coexpressed *BCL6*, *TBET*, and *GATA3*, alone or in combination **(Table 5.2).** *TBET* and *BCL6* were the most frequently co-expressed 2nd order combination (10.4%), followed by *BCL6* and *GATA* (8.4%), then *GATA3* and *BCL6* (4.8%). The most commonly expressed single transcription

factor was *BCL6* (12%), while 6.0% expressed all three markers. None of the *IL21*-positive cells expressed *FOXP3* or *RORC*, compared to 18.1% total discrete expression in the overall $CD4^+$ T cell population **(Figure 5.8)**. Of note, approximately 20% of all *IL21*-positive T cells did not discretely express any one of the five transcription factors, a similar proportion compared to the total population.

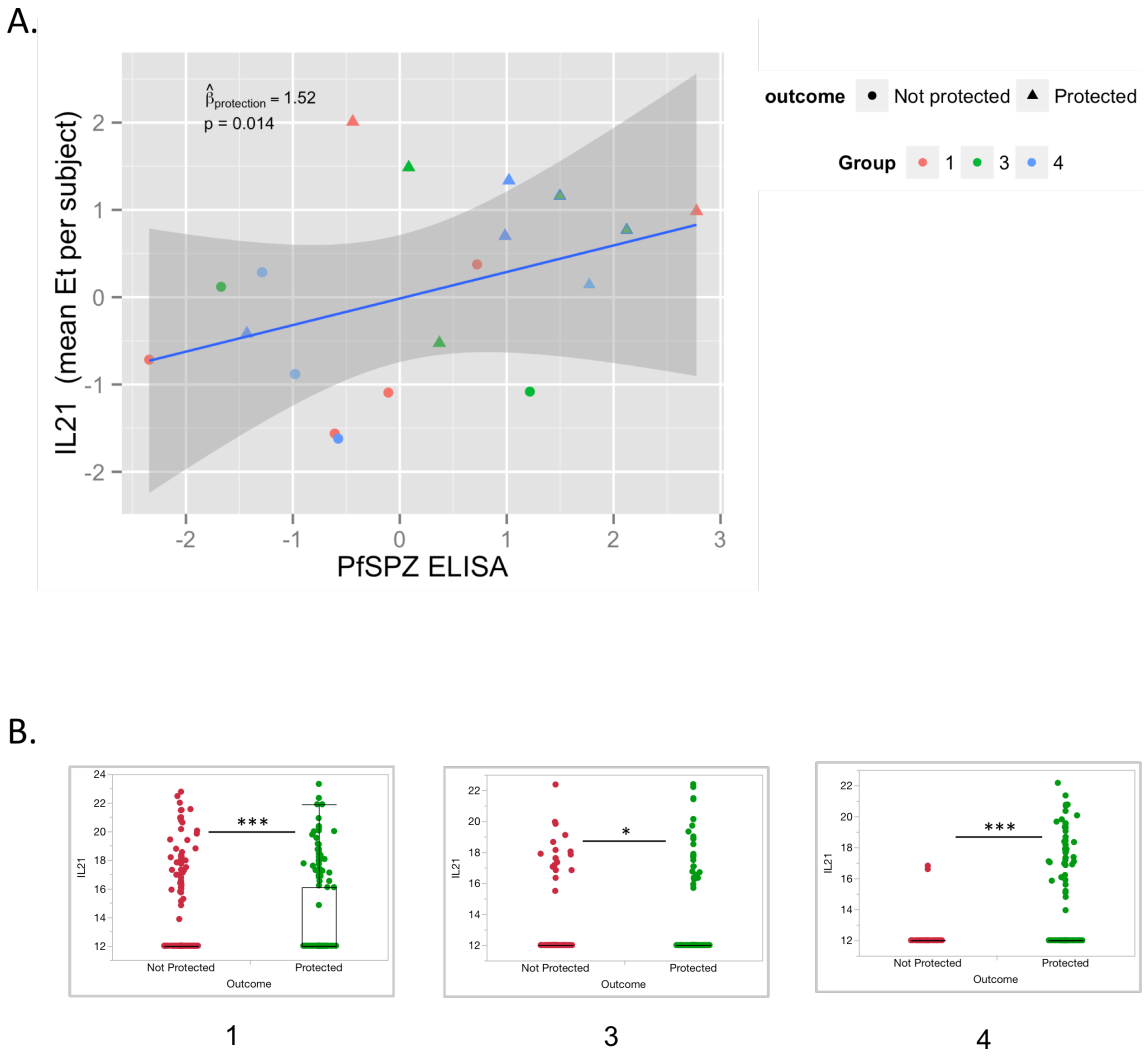

Figure 5.7 *IL21* gene expression and PfCSP antibodies

The mean IL21 gene expression at the subject-level is plotted against the PfSPZ ELISA. **(B)** IL21 gene expression at the single-cell broken by vaccination group. *** p<0.0001, * p <0.01

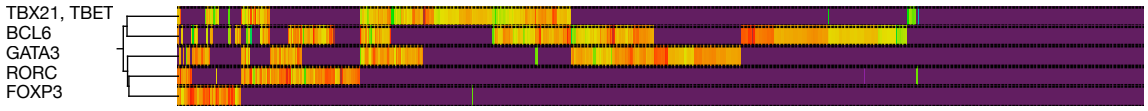

Figure 5.8 Canonical Th transcriptional factors

Single cell hierarchal clustering of five key transcription factors are shown for all single cells isolated from vaccination groups 1,3, and 4.

TBET	BCL6	RORC	GATA3	FOXP3	$\hat{p}$	Lower 95% CI	Upper 95% CI
-	-	-	-	-	0.2329317	0.1804293	0.2854342
-	+	-	-	-	0.1204819	0.0800493	0.1609145
+	+	-	-	-	0.1044177	0.0664348	0.1424006
-	-	-	+	-	0.0843373	0.0498209	0.1188538
-	+	-	+	-	0.0843373	0.0498209	0.1188538
+	-	-	-	-	0.0803213	0.0465629	0.1140797
+	+	-	+	-	0.0602410	0.0306879	0.0897940
+	-	-	+	-	0.0481928	0.0215908	0.0747947
-	-	+	-	-	0.0321285	0.0102256	0.0540315
-	-	-	-	+	0.0240964	0.0050493	0.0431434
-	+	+	-	-	0.0160643	0.0004485	0.0316800
+	-	+	-	-	0.0120482	0.0000000	0.0255994
-	-	+	+	-	0.0120482	0.0000000	0.0255994
+	+	+	+	-	0.0120482	0.0000000	0.0255994
+	+	-	-	+	0.0120482	0.0000000	0.0255994
+	+	+	-	-	0.0080321	0.0000000	0.0191191
+	-	+	+	-	0.0080321	0.0000000	0.0191191
+	-	-	-	+	0.0080321	0.0000000	0.0191191
-	+	-	-	+	0.0080321	0.0000000	0.0191191
-	-	-	+	+	0.0080321	0.0000000	0.0191191
+	+	+	-	+	0.0040161	0.0000000	0.0118716
+	-	-	+	+	0.0040161	0.0000000	0.0118716
-	+	-	+	+	0.0040161	0.0000000	0.0118716
+	+	-	+	+	0.0040161	0.0000000	0.0118716
+	-	+	+	+	0.0040161	0.0000000	0.0118716
+	+	+	+	+	0.0040161	0.0000000	0.0118716

Table 5.2 Analysis of Th transcription factors for *IL21*$^+$ CD4$^+$ T cells

Proportion of all possible combinations of the five transcription factors at the single cell level. Upper and lower 95% Confidence Intervals are given.

5.2.5 Expanded modular analysis of protected vs. unprotected subjects

In order to understand the relevance of key $CD4^+$ T cell differentiation pathways, gene set enrichment analysis (GSEA) was performed **(Figure 5.9)**, using modules previously described in **Table 4.2**. Additional modules were developed based on categories in previously described blood transcriptional modules, such as T cell activation, maturation, apoptosis, and chemokine receptors *(270, 292)*. However, the incorporated genes were curated to better reflect $CD4^+$ T cell-intrinsic mechanisms reported in the literature (*85, 87*). In total, thirteen modules were assessed. Analysis was performed as described in **Section 4.2.4**. Briefly, the average effect of all genes in a set was calculated as a Z-score, taking into account both the discrete and continuous components of mRNA expression. Based on evidence that the accuracy of the protective transcriptional model varied across vaccination groups **(Figure 5.6)**, modular analysis was performed for each group separately.

Overall, the absolute values of Z-scores in Group 3 were much lower compared to those in Groups 1 and 4 **(Figure 5.9)**. In Group 3, only 2/13 modules displayed a significant effect due to protection outcome ($p<0.01$): chemokines and chemokine receptors. Both modules were only slightly enriched in protected subjects ($|Z\text{-score}| <5$).

In contrast, 8/13 and 6/13 modules displayed a significant protective effect in Groups 1 and 4, respectively. Two of these modules displayed a common significant effect in both groups: “Th1” and “Memory.” The remaining modules with a

significant protective effect in one vaccination group were not significant in the other groups.

The "Th1" module was enriched in protected subjects prior to challenge in both Groups 1 (Z-score = 5.62) and 4 (Z-score = 3.23). This effect was predominately driven by increased expression of *IFNG* and *IL2* in the protected cohort. Overall expression of the remaining makers in the "Th1" module was not increased in the protected cohort. However, *IFNG* expression weakly correlated with *TBET* (spearman rank correlation: $\rho = 0.19$ and $p < 0.001$) and *TNF* (spearman rank correlation: $\rho = 0.24$ and $p < 0.001$).

Additionally, the module associated with T cell memory was commonly enriched in the unprotected subjects in both Groups 1 (Z-score = -4.30) and 4 (Z-score = -5.18). This effect was characterized by overall increased expression of *CD27*, *CD28* and *IL7R*, three out of the four markers in this module.

Given the positive correlation of subject-level *IL21* expression and antibody levels demonstrated in both clinical studies VRC312 and VRC314, it was hypothesized that the TFH module would be enriched in protected subjects. However, there was no significant effect due to the protection outcome ($|Z\text{-score}| < 1$ in all vaccination groups). Although overall expression of *IL21* was significantly increased in protected subjects, *CXCR5* was significantly enriched in unprotected subjects with a greater median fold-change **(Figure 5.5-A)**. Of note, *CXCR5* expression appeared discoordinate with *IL21* (spearman rank correlation: $\rho = 0.0045$ and $p=0.89$). There was no difference in expression of the remaining markers in this module.

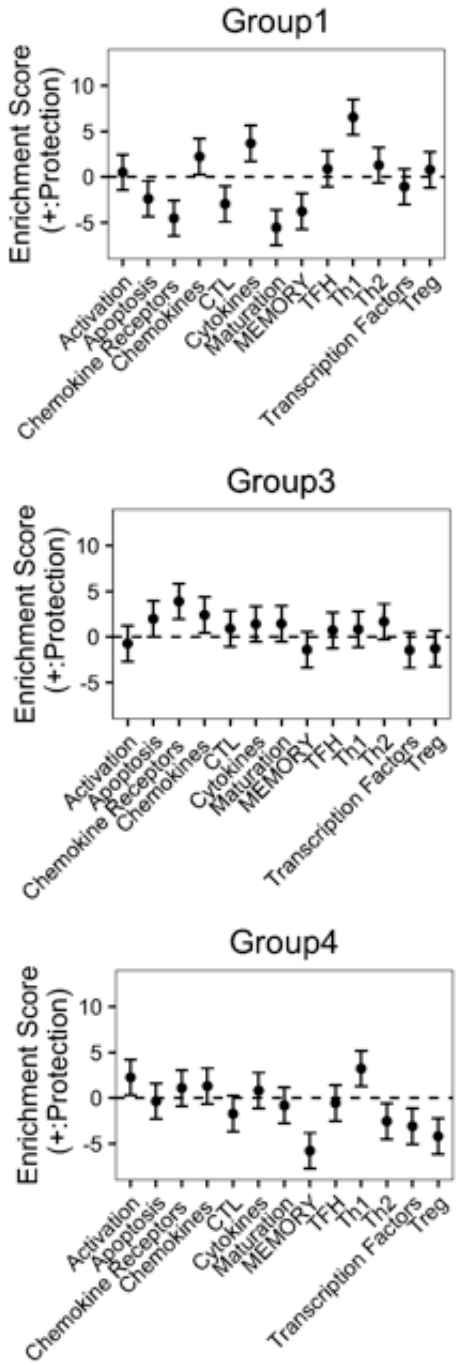

Modules	Gene	
Activation	ICOS HLADRA TNFRSF4/OX40	TNFRSF9/CD137 TNFSF14/LIGHT DPP4/CD26
Apoptosis	BAX TNFSF10, TRAIL MYC	FAS FASLG,CD95LG FLIP
Chemokine Receptors	IL21R IL2RA, CD25 IL2RB IL4R	IL6R, CD126 IL7R, CD127 TGFBR1
Chemokines	CCR3 CCR4 CCR6 CCR7	CCR8 CCL3, MIP1A CCL5, RANTES
Cytokines	IL3 IL4 IL5 IFNG IL10 IL13	IL16 IL17A IL2 IL21 TGFB1
Maturation	BCL2 CD48/BLAST FAS IL7R/CD127	PDRM1/BLIMP1 SLAMF5 SLAMF1/CD150
Memory	CD27 CD28	CCR7 IL7R
Transcription Factors	TBET GATA3 RORA RORC FOXP3	BCL6 EOMES FOXP1 IRF4

Figure 5.9 Modular analysis by vaccination group

Enrichment of curated modules designed for analysis of CD4 T cells. Genes for each of the modules not previously described in **Table 4.2** are listed in associated table. FDR adjusted p-value of less than 1%.

5.2.6 Coexpression analysis of cytokines associated with canonical Th subsets as function of protection outcome

As protein coexpression of multiple cytokines has been shown to be important in a number of settings *(312, 313),* the protective effect of different combinations of cytokines at the transcriptional level was assessed here. Analysis was restricted to cytokines that are reflective of canonical Th subsets: *IFNG, IL2, TNF, IL10, IL21,* and *IL17.* In order to maximize power for calculations of third and fourth-order gene combinations, all vaccination groups challenged three weeks following the final vaccination were combined in this analysis (Groups 1, 3, and 4). Discrete expression of any gene is defined as $E_t > 13$, approximately 1 mRNA molecule.

First, unsupervised hierarchal clustering of all cytokines independent of protection outcome was performed **(Figure 5.10-A)**. Overall expression of cytokines was assessed, in addition to second and third-order combinations. Over 70% of all $CD4^+$ T cells discretely expressed any one of the six cytokines, most commonly *TNF (35.5%), IFNG (34.6%), IL2 (29.8%),* and *IL21 (15.5%).* Expression of these four cytokines was particularly linked among "high producers." Accordingly, among cells that discretely expressed any one cytokine above the median value, 29% discretely expressed all four **(Figure 5.10-A)**. The most common second order combinations were *IL2/TNF, IL2/IFNG,* and *IL21/IFNG,* in decreasing order. Interestingly, *IL13* expression clustered independently of these four cytokines, consistent with the broad Th1 vs. Th2 $CD4^+$ T cell paradigm. Discrete expression of *IL17* or *IL10* was relatively low compared to other cytokines (7.9% total of cells). Of note, 21.4% of cells did not express any one of these seven cytokines.

In order to assess if cooperation among genes was different between the two cohorts, spearman correlations were calculated for every second order combination of the seven cytokines. There was no difference in the cooperation of all pairs of genes with the exception of increased coordination of *IL17* and *IL10* in the unprotected cohort (**Figure 5.10-B**). However, this difference was weakly significant ($p<0.01$), as the overall percentage of cells that discretely express either of these genes is low (**Figure 5.10-A**).

A.

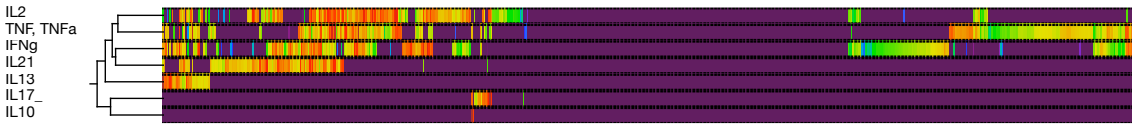

B.

Protected

	IFNg	IL13	IL2	IL21	IL10	IL17_	TNF, TNFa
IFNg	1.0000	0.2068	0.3672	0.2870	0.1011	-0.0354	0.2634
IL13	0.2068	1.0000	0.0432	0.0983	-0.0094	-0.0184	0.0424
IL2	0.3672	0.0432	1.0000	0.3489	-0.0250	0.0869	0.3382
IL21	0.2870	0.0983	0.3489	1.0000	-0.0189	-0.0651	0.0991
IL10	0.1011	-0.0094	-0.0250	-0.0189	1.0000	-0.0055	-0.0287
IL17_	-0.0354	-0.0184	0.0869	-0.0651	-0.0055	1.0000	0.1087
TNF, TNFa	0.2634	0.0424	0.3382	0.0991	-0.0287	0.1087	1.0000

Unprotected

	IFNg	IL13	IL2	IL21	IL10	IL17_	TNF, TNFa
IFNg	1.0000	0.1720	0.2968	0.2644	-0.0218	-0.0583	0.1819
IL13	0.1720	1.0000	0.0117	-0.0099	-0.0118	-0.0218	0.0412
IL2	0.2968	0.0117	1.0000	0.2885	-0.0360	0.0899	0.3520
IL21	0.2644	-0.0099	0.2885	1.0000	0.0461	-0.0288	0.1311
IL10	-0.0218	-0.0118	-0.0360	0.0461	1.0000	0.2258	0.0187
IL17_	-0.0583	-0.0218	0.0899	-0.0288	0.2258	1.0000	0.0424
TNF, TNFa	0.1819	0.0412	0.3520	0.1311	0.0187	0.0424	1.0000

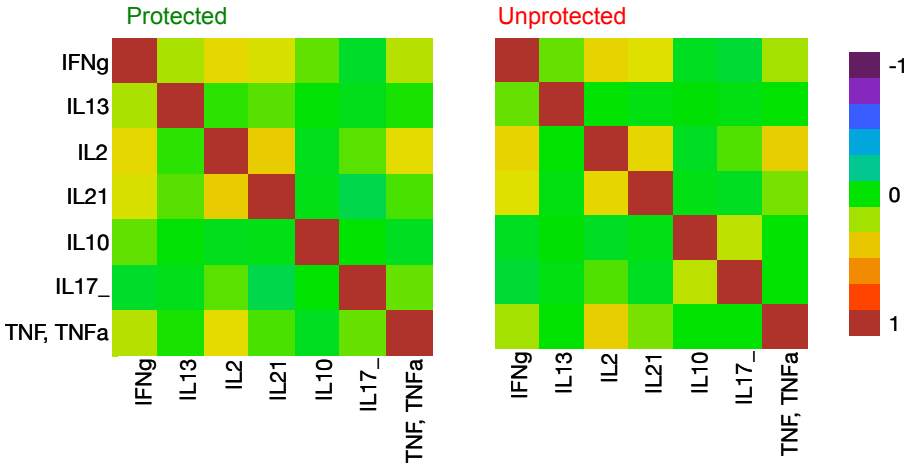

Figure 5.10 Coexpression of canonical Th cytokines

(A) Single cell hierarchal clustering of seven key cytokines are shown for all single cells isolated from vaccination groups 1, 3, and 4. **(B)** Pairwise correlations for all possible combinations broken up by protection outcome.

Finally, the percentage of common combinations of genes was assessed in the protected vs. unprotected cohort **(Figure 5.11-A)**. Note that not all possible combinations of genes are assessed due to statistical power. *IL10* was excluded from this analysis, as expression is detected is less than 2% of all cells. Overall, clusters were formed in an unsupervised fashion. However, the number of clusters was optimized, such that each cluster contained at least 100 single cells. The percentage of protected vs. unprotected cells in each cluster was calculated (**Figure 5.11-B** and **C**).

Among clusters with discrete expression of any one cytokine, cluster 6 was the only one with a significant effect due to protection outcome. This cluster was enriched in the protected cohort ($p<0.001$) and consisted of triple-positive $IL2^+$ $IFNG^+$ $IL21^+$ $CD4^+$ T cells, in the absence of *IL17*, *TNF* and *IL13*. Of interest, this cluster did not consist of the cells that expressed the highest levels of each of these three cytokines. Continuous expression of *IL2*, *IFNG*, and *IL21* was 2-5 logs lower in cluster 6 compared to cluster 5, which consisted of cells that coexpressed all three cytokines in addition to *TNF*. The largest cluster (2) consisted of $CD4^+$ T cells with no expression of any of these genes and was enriched in the unprotected cohort ($p<0.001$).

A.

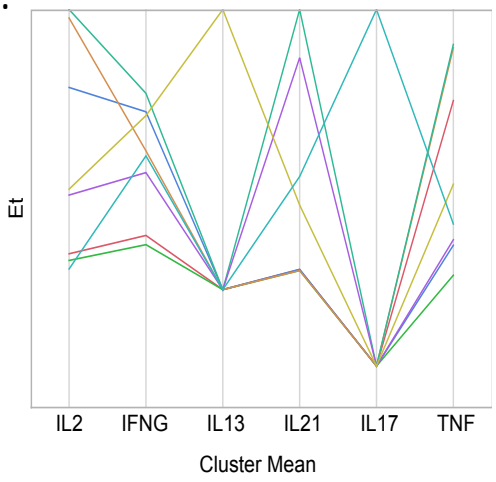

Cluster	IL2	IFNG	IL13	IL21	IL17	TNF
1	12.5572	13.3342	12.0000	12.0293	12.0000	16.3695
2	12.3126	12.9877	12.0000	12.0000	12.0000	12.0092
3	18.6621	17.9853	12.0000	12.0308	12.0000	12.7577
4	21.2100	16.5163	12.0000	12.0000	12.0000	17.6839
5	21.5224	18.6794	12.0000	19.2030	12.0000	17.7708
6	14.7125	15.6980	12.0000	17.8730	12.0000	12.8950
7	14.9292	17.8411	16.6459	13.8066	12.0000	14.2816
8	12.0000	16.3264	12.0000	14.5932	18.3564	13.2898

B.

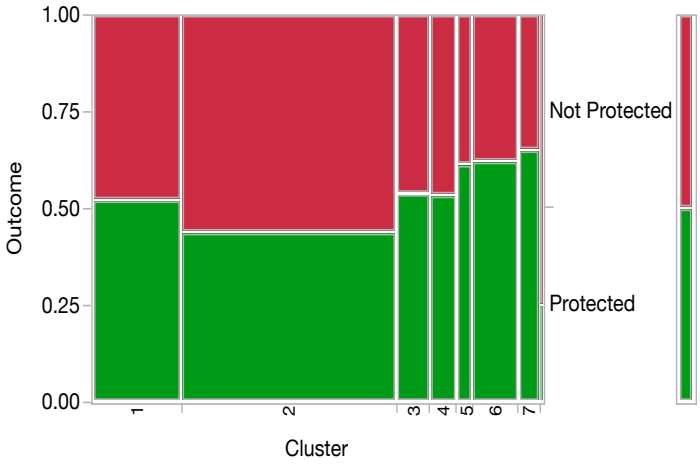

C.

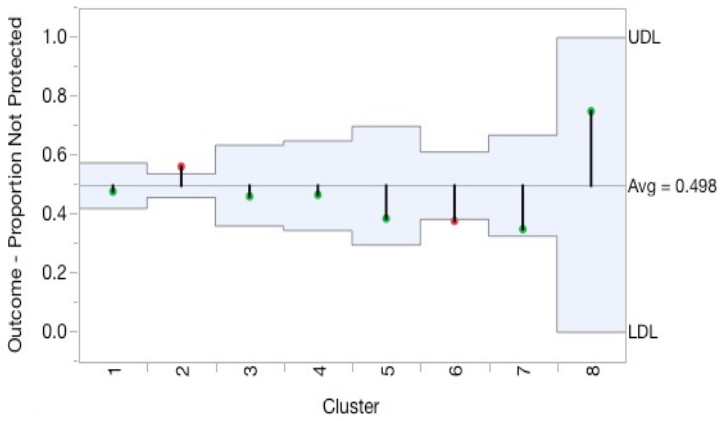

Figure 5.11 Combinations of canonical Th cytokines

(A) Eight combinations of gene with the average Et for each gene for each cluster. Et>13 (~1 mRNA molecule) is consider discrete gene expression. **(B)** Percentage of cells from protected vs. unprotected cells for each of the clusters. Width is proportional to the number of cells in each cohort. Note that cluster 8 is too small to be shown. **(C)** Significance of any of the eight combinations with protection. Comparison of response proportions use a normal approximation to the binomial. Blue box represent the decision limits of significance for each cluster based on number of cells. Red dot indicates that the limit for that cluster is exceeded (α = 0.05).

5.3 Discussion

The main aims of this chapter were to (1) further characterize the overall transcriptional profile of PfSPZ-specific $CD4^+$ T cells of protected vs. unprotected subjects in a larger cohort than previously assessed and (2) test the hypothesis that circulating TFH cells were associated with protection. First, there appeared to be no substantial difference in the quality of $CD4^+$ T cells induced by two vaccination regimens that induced similar levels of protection, as misclassification rate was greater than 30%. Second, *IL21*-expessing cells were enriched in protected vs. unprotected subjects, and predominantly expressed *TBET* and/or *BCL6* among canonical transcription factors. As in the previous chapter, *IL21* expression on a per-subject basis positively correlated with PfCSP-specific antibody levels. Third, modular analysis revealed association of a "Th1" signature with protection. Upon further examination, triple expression of *IFNG*/*IL21*/*IL2* in the absence of *TNF* and *IL17* was significantly increased in protected subjects, among common combinations of canonical cytokines. Overall, these data suggest an important role of Th1/TFH-like cells in PfSPZ-mediated protection.

In-depth transcriptional analysis was predominantly restricted to correlates of short-term protection. Misclassification of individual antigen-specific $CD4^+$ T cells was high (>30%) when comparing the cohorts that received four doses of $2.7x10^5$ PfSPZ vs. four doses of $1.35x10^5$ PfSPZ followed by modified fifth dose. These data are in line with previous experiments, which show no difference in the quality of $CD4^+$ T cell responses from these groups based on protein expression of IFN-γ, IL-2, and

TNF-α (*205*). Additionally, very few genes were differentially expressed at two weeks following the final immunization between protected vs. unprotected in subjects who were challenged 21-24 weeks later vs. one week later (6 vs. 25 differentially expressed genes; **Figures 5.5-A** and **C**). These data suggest that the quality of $CD4^+$ T cells following vaccination assessed by Fluidigm analysis does not necessarily predict durable immunity. Future investigation of correlates for durable protective immunity should assess samples within one week prior to challenge.

It is interesting to note that the accuracy of the protective model for short-term protection was much lower in Group 3 vs. Groups 1 and 4 **(Figure 5.6)**. The level of misclassification for a given group did not appear to be tied to vaccine efficacy (VE = 62% and 73% for Groups 3 and 4, respectively). One possible explanation is that the percentage of non-specific "background" cells was greater in Group 3 compared to Groups 1 and 4 because the overall magnitude of CD154 responses was lower **(Figure 5.2)**. This could decrease the ability to distinguish between PfSPZ-specific cells from protected and unprotected subjects within a given cohort.

The repeated finding of overall enriched *IL21* expression and a positive correlation between per-subject *IL21* expression and PfCSP antibody levels substantiates the hypothesis that either circulating TFH or transitional Th1/TFH cells play an important role in PfSPZ-mediated protection. Modular analysis, as well as coexpression analysis of canonical transcription factors and cytokines provided more nuanced information. Even though *IL21* expression was increased in protected subjects, the TFH module as a whole was not significantly enriched. Notably, IL21

was not associated with other TFH markers, in particularly *CXCR5*, an important chemokine marker of circulating TFH cells that promote antibody responses *(252, 314, 315).* However, there was enrichment of the Th1 module in the protected cohort, as well as triple-positive *IL21*$^{+}$*IFNG*$^{+}$ *IL2*$^{+}$ T cells. Coexpression analysis of transcription factors revealed that *IL21*-expressing cells most commonly expressed *TBET* and/or *BCL6.*

There are three important ways to interpret these data. First, differential gene expression of TFH surface markers in circulating CD4^{+} T cells does not reflect the protein expression, and as such *IL21*-producing cells express *CXCR5* at the protein but not mRNA level. However, studies have demonstrated an association between the transcriptional signatures of circulating TFH cells compared to those in the germinal center *(252, 300).* Second, PfSPZ-specific *IL21*$^{+}$ CD4 T cells are derived from a Th1-lineage that can support antibody maturation. Indeed, in *P. chabaudi* infection, IFN- γ^{+} IL21^{+} cells are critical for the generation of antibodies that control chronic parasitemia, and this cellular subset is predominantly TBET-positive *(316, 317).* Third, it is possible that IL21 acts through some other mechanism such as help for CD8^{+} T cells (*307*). The correlation of *IL21* and PfCSP-specific antibodies simply reflects independent biomarkers of a successful vaccination response. Phenotype characterization of IL21^{+} CD4^{+} T cells is difficult, as the sensitivity for detection of such responses by flow cytometry is low (*318*). Instead, ongoing flow cytometry studies will characterize the phenotype of IL21-producing cells in response to a mitogen stimulation before and after PfSPZ vaccination, particularly assessing the overlap of IL21 protein with chemokine markers associated with Th1 and TFH subsets.

It is unclear if $CD4^+$ T cells contribute as a mediator of protection or if the quality merely reflects a biomarker of a successful vaccine response. Transcriptional analysis in this study was restricted to $CD4^+$ T cells that circulate in the peripheral blood. However, liver-resident $CD8^+$ T cells are hypothesized to be necessary and sufficient for PfSPZ-mediated durable protection (*116, 161*). Cellular immune responses in the liver of non-human primates (NHPs) immunized with PfSPZ do not correlate with those in the peripheral blood (*205*). In particular, the frequency of Pf-specific $CD8^+$ T cells was approximately 100-fold higher in liver than in PBMCs, and the majority of IFN- γ producing lymphocytes in the liver were $CD8^+$ T cells. Future investigation should assess the quality of $CD4^+$ T cells in the livers of PfSPZ-immunized NHPs to order to understand how tissue-resident responses reflect those in the peripheral blood.

Overall, this characterization of PfSPZ-specific $CD4^+$ T cells in larger, independent cohort extends many findings from the previous chapter regarding a gene signature associated with protection following vaccination with a whole parasite and elucidates cooperative gene networks within multifunctional $CD4^+$ T cells. As $CD8^+$ T cells are hypothesized to be critical in protection against liver-stage malaria, an important future goal will be to assess such responses with the same platform in a setting of vaccine-induced protection.

6. ChAd63/MVA ME-TRAP Vaccination

6.1 Introduction

Chapters 4 and 5 in this thesis have investigated the role of malaria-specific $CD4^+$ in protection induced by vaccination with irradiated sporozoites. While $CD4^+$ T cells are thought to play a role in protection against liver-stage malaria, $CD8^+$ T cells are hypothesized to be critical in the clearance of parasitized hepatocytes (*135, 149, 319*). In-depth characterization of such responses induced by vaccination will be critical in elucidation of mechanisms underlying protective immunity. However, $CD8^+$ T cell responses in PfSPZ-vaccinated subjects are low to undetectable (*116, 205*).

Subunit vaccine platforms based on highly potent adenoviruses containing the recombinant insert ME-TRAP elicit $CD8^+$ T cell responses of high magnitude in mice (*159, 320*), NHP (*222*) and humans (*223*). In particular, heterologous prime-boost immunization with ChAd63/MVA ME-TRAP is safe, immunogenic, and elicits protection in malaria naïve-individuals (*153*). This immunization induced a high proportion of cytokine-producing $CD4^+$ and $CD8^+$ T cells, predominantly directed towards TRAP rather than ME. Vaccination induced a total efficacy (sterile protection plus delay in time to patency) of 58% (8/14). Monofunctional $CD8^+$ T cells expressing IFN-γ, but not IL-2 or TNF-α at the time of challenge correlated with protection. Field studies assessing immunogenicity and protective efficacy in adults with chronic exposure have also been very encouraging. Vaccination of

Kenyan male volunteers elicited TRAP-specific $CD8^+$ T cells and reduced the risk of infection by 67% (95% CI 33%-88%) (*321*).

Detection of newly expressed CD107a (LAMP-1) following *in vitro* stimulation of PBMCs enables isolation of live antigen-specific $CD8^+$ T cells (*322*). CD107a resides in membranes of cytotoxic granules and is rapidly expressed on the surface of $CD8^+$ T cells following TCR activation, often concordant with IFN-γ secretion (*322, 323*). Downstream Fluidigm analysis of isolated single cells provides the opportunity to dramatically expand the breadth of phenotypic characterization, revealing more information about the quality of vaccine-induced $CD8^+$ T cells.

The aims of this chapter are the following: (1) isolate TRAP-specific $CD8^+$ T cells following vaccination with ChAd63/MVA ME-TRAP; (2) evaluate the heterogeneity and phenotype of the TRAP-specific $CD8^+$ T cell response at the single cell level and (3) compare the gene expression profiles of such responses from subjects who demonstrated sterile protection, delay to patency or no protection following CHMI in order to identify potential correlates of protection.

6.2 Results

6.2.1 Isolation of live TRAP-specific CD8$^+$ T cells from vaccinated subjects

The first aim of this chapter was to isolate antigen-specific CD8$^+$ T cells from subjects vaccinated with viral vectors containing ME-TRAP. Subjects selected for downstream analysis were pooled from three different clinical trials **(Table 6.1** and **6.2)** (*153, 219, 268*). However, all subjects received one dose of the ChAd63 vector containing the ME-TRAP insert, followed by an MVA boost 56 days later. The protective efficacy of ChAd63/MVA prime-boost vaccination with ME-TRAP was broadly similar across all three trials **(Table 6.2)**.

Overall, fifteen vaccinated subjects who demonstrated sterile protection, a delay to patency or no protection were assessed for downstream analysis (n=5 per group). For each outcome group, subjects across the three different trials with the highest frequencies of IFN-γ^+CD8$^+$ T cells at one day prior to challenge (CH-1) were selected in order to optimize downstream sorting. It is important to note that a delay to patency is defined as a start of treatment greater than 2 times the standard deviation in days after the mean time to treatment of the unvaccinated infection controls for each specific trial. As such, the minimum number of days to patency required for classification of delayed protection may vary slightly across the trials.

Protection Outcome	Patient ID	Clinical Trial	Days to Parasitemia	ELISPOT	IFNγ+/ CD3+CD8+ T cells
Sterilely Protected	009	MAL34	21	858	0.081
	012	MAL34	21	4224	0.226
	049	MAL34	21	5082	0.168
	1324	VAC52	21	1024	0.155
	1378	VAC52	21	2390	0.655
Delay to Parasitemia	1426	VAC45	14	4970	0.534
	1314	VAC52	17	2924	0.421
	1318	VAC52	16	4628	1.7
	1319	VAC52	17	3018	0.195
	1362	VAC52	14.5	2056	0.286
Not Protected	1429	VAC45	12.5	3486	0.468
	1431	VAC45	8.5	3372	0.331
	1312	VAC52	13	5284	2.14
	1321	VAC52	12.5	2088	0.789
	1330	VAC52	12.5	3000	0.869

Table 6.1 ChAd63/MVA ME-TRAP vaccinated subjects assessed by Fluidigm.

Subjects are grouped by protection outcome with relevant cellular immune responses assessed at one day prior to challenge. IFN-γ ELISPOT reponses and the frequency of IFN-γ^+ cells as a total of the $CD3^+CD8^+$ T cell population is measured in response to TRAP (T9/96 strain) stimulation.

Clinical Trial	Vaccination Regimen	Protective Efficacy (sterile, delay)
MAL34	ChAd63 ME-TRAP $5x10^5$ vp IM, followed by MVA ME-TRAP 2 $x10^8$ pfu ID	3/14, 5/14
VAC45	ChAd63 ME-TRAP $5x10^5$ vp IM, followed by MVA ME-TRAP 2 $x10^8$ pfu IM	2/15, 5/15
VAC52	Mixture of ChAd63 ME-TRAP $5x10^5$ vp and ChAd63 CS $5x10^5$ vp IM, followed by mixture of MVA ME-TRAP 2 $x10^8$ pfu and MVA CS 2 $x10^8$ pfu IM	3/13, 4/13

Table 6.2 Vaccination regimen for selected subjects from each trial.

Protective efficacy reflects the number of subjects who demonstrated sterile protection or delay to patency following CHMI. Note that this table does not cover all regimens assessed in each trial: only those which were assessed in this analysis. IM = intramuscular, ID = intradermally, pfu = particle forming units, vp = viral particles. CS = circumsporozoite.

Cellular immune responses were assessed from PBMCs isolated at CH-1 in order to explore transcriptional signatures associated with protection. Live CD107a^{+} memory CD8^{+} T cells were detected following *in vitro* stimulation with TRAP (T9/96) peptide pools **(Figure 6.1)**. Double staining with CD69 did not substantially reduce the frequency of background events compared to the matched control sample, and as such the marker is not included in the flow cytometry panel (data not shown). As previously described, *in vitro* stimulation was performed in the absence of Golgi inhibitors to limit changes in intracellular transport (See **Chapter 3.2.2**).

CD8^{+} T cell responses defined by protein expression of CD107a were assessed by flow cytometry for all fifteen vaccinated subjects **(Figure 6.2)**. During each sort, a positive and negative control for the CD107a assay was included. One vaccinated subject who was sterilely protected (Patient ID 009) had a CD8^{+} T cell response below the threshold required for the Fluidigm assay as defined in Chapter 3, and as such was excluded from downstream analysis. Of note, this subject had the lowest IFN-γ ELISPOT responses and frequency of IFN-γ^{+}CD8^{+} T cells among all fifteen subjects as determined by previous studies (*153*). After exclusion of this subject, the median CD8^{+} T cell responses in the delayed cohort were significantly lower compared to the sterilely protected and nonprotected groups ($p<0.05$).

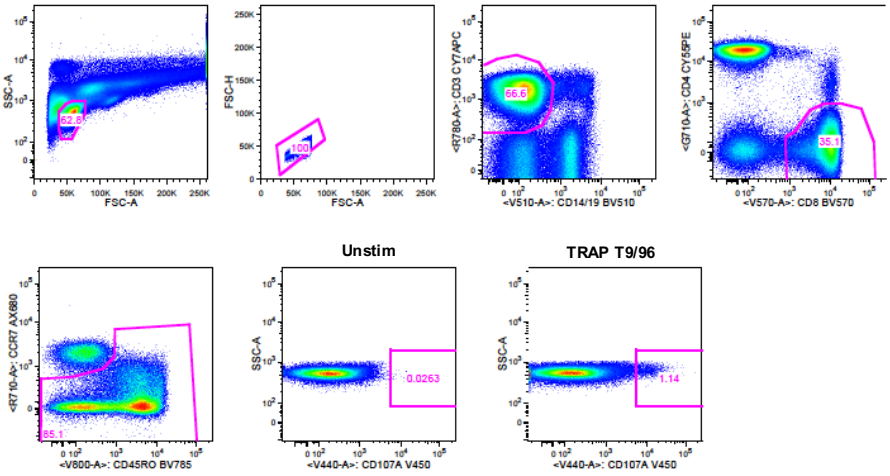

Figure 6.1 Gating strategy for isolation of live TRAP-specific CD8$^+$ T cells.

Surface staining by flow cytometry of PBMCs isolated one day prior to challenge is shown for a representative vaccinated subject. PBMCs are stimulated *in vitro* for 18 hours with TRAP (T9/96 strain) peptide pool in the presence of CD107a antibody without Golgi inhibitors. This timepoint correpsonded to the peak CD107a expression (data not shown). Memory T cells are defined by differential expression of CCR7 and CD45RO.

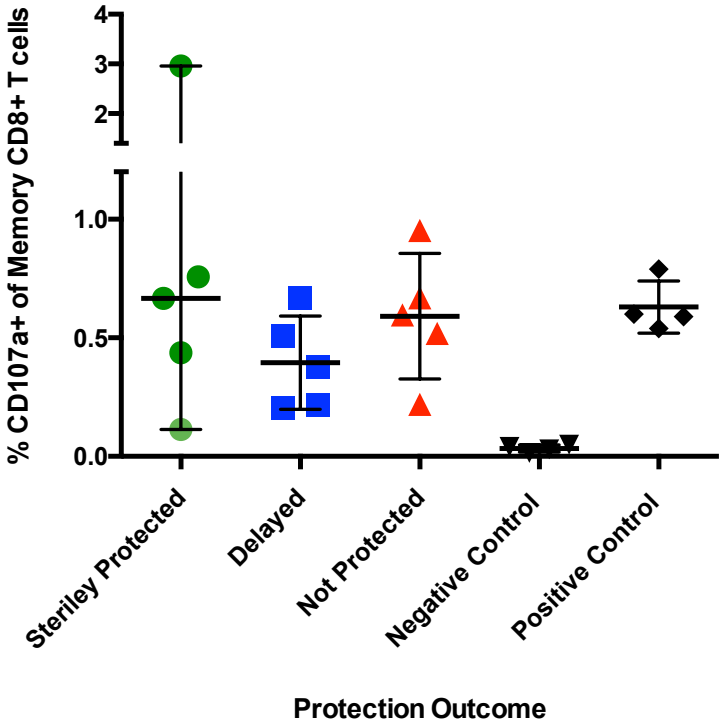

Figure 6.2 CD107$^+$ CD8$^+$ T cell responses.

Magnitude of TRAP-specific CD107a$^+$ memory CD8$^+$ T cells. Background is subtracted. Responses are organized by protection outcome. Subjects with responses below the limit for Fluidigm analysis are shaded. Negative and positive controls to ensure appropriate CD107a staining were included for each sort. For the negative controls, PBMCs from a CMV-seropositive subject were stimulated with CMV peptides. For the positive controls, PBMCs from a malaria-naïve subject were stimulated with the TRAP (T9/96) peptide pool. Median +/ IQR.

Single cell gene expression was acquired using Fluidigm 96.96 Dynamic arrays. Out of 96 genes in the previously described panel, seven were altered in order to assess for expression of markers more relevant for $CD8^+$ vs. $CD4^+$ T cell function (see Chapter 2 for more details). All of the remaining methods for data acquisition and filtering were as previously described in Chapters 3-5. Expression of 86 genes from 1,119 single cells was retained for downstream analysis. Following exclusion of statistical outliers and correction for the cellular detection rate (CDR), there was no significant difference in the median gene expression of *CD8a*, *CD107a*, and *GAPDH* among three cohorts **(Figure 6.3-A)**.

In order to assess the sensitivity of downstream quantitative RT-PCR, mRNA expression of markers previously assessed by flow cytometry in evaluation of ChAd63/MVA ME-TRAP vaccination was examined **(Figure 6.3-B)**. 96.4% of sorted $CD107a^+CD8^+$ T cells expressed *CD107A* by gene expression, serving as an internal positive control. Of interest, 87.8% of isolated cells discretely expressed *IFNG*, *TNF* or *IL2*.

A.

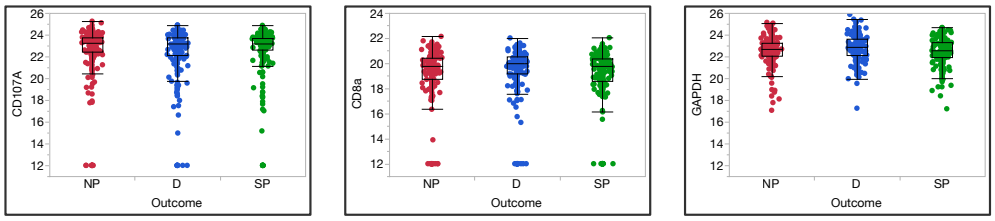

B.

Figure 6.3 Gene expression controls.

(A) Single-cell gene expression of cells from three examined cohorts for *CD107A*, *CD8a* and *GAPDH* following data filtering. **(B)** Hierarchical clustering of cells from all vaccinated subjects for markers previously assessed by flow cytometry.

6.2.2 Global characterization of TRAP-specific CD8$^+$ T cells

The first aim of this study was to characterize the phenotype and heterogeneity of TRAP-specific CD8$^+$ T cells induced by ChAd63/MVA immunization in greater depth. Global expression of single cells from all vaccinated subjects was examined independent of protection outcome.

Principal components analysis (PCA) was used to understand the intrapopulation variation within the TRAP-specific CD8$^+$ T cell response **(Figure 6.4-A)**. PC1 and PC2 accounted for 7.82% and 4.95% of the variance within the data, respectively. Moreover, the first fifteen principal components accounted for 38.9% of the variation. The components that describe greatest variation within the data included genes encoding effector molecules (*IFNG, TNFSF10/TRAIL, GRZMB*) and activation markers (*IL2RA/CD25, IL2RB*), as well as *CD107A*.

In order to investigate the cooperation among groups of genes, pair-wise correlations of all possible combinations of genes were determined **(Figure 6.4-B)**. There was evidence of overall coordination of genes at the single cell level. In particular, three main networks of genes emerged, characterized by different combinations of activation markers, effector molecules, and chemokine receptors (highlighted in black).

As CD8$^+$ T cell-mediated IFN-γ production is hypothesized to be critical in protection against liver-stage malaria (*135, 150, 319*), all genes that significantly correlated with *IFNG* expression were determined (spearman rank correlation: ρ >

0.20 and p<0.001; **Figure 6.4-C**). *IFNG* directly correlated with expression of a number of genes, most notably *CCL5/MIPa, IL2RA/CD25, CSF2/GMCSF,* and *CD107A*, in order of decreasing spearman rank correlation coefficients. Of note, *IFNG* negatively correlated with *CXCR4* and *TRAT1/TRIM* (spearman rank correlation: $\rho = -0.34$ and $\rho = -0.28$, respectively $p<0.001$). This finding is consistent with data in previous chapters **(Figures 4.8-B and 5.5-E**).

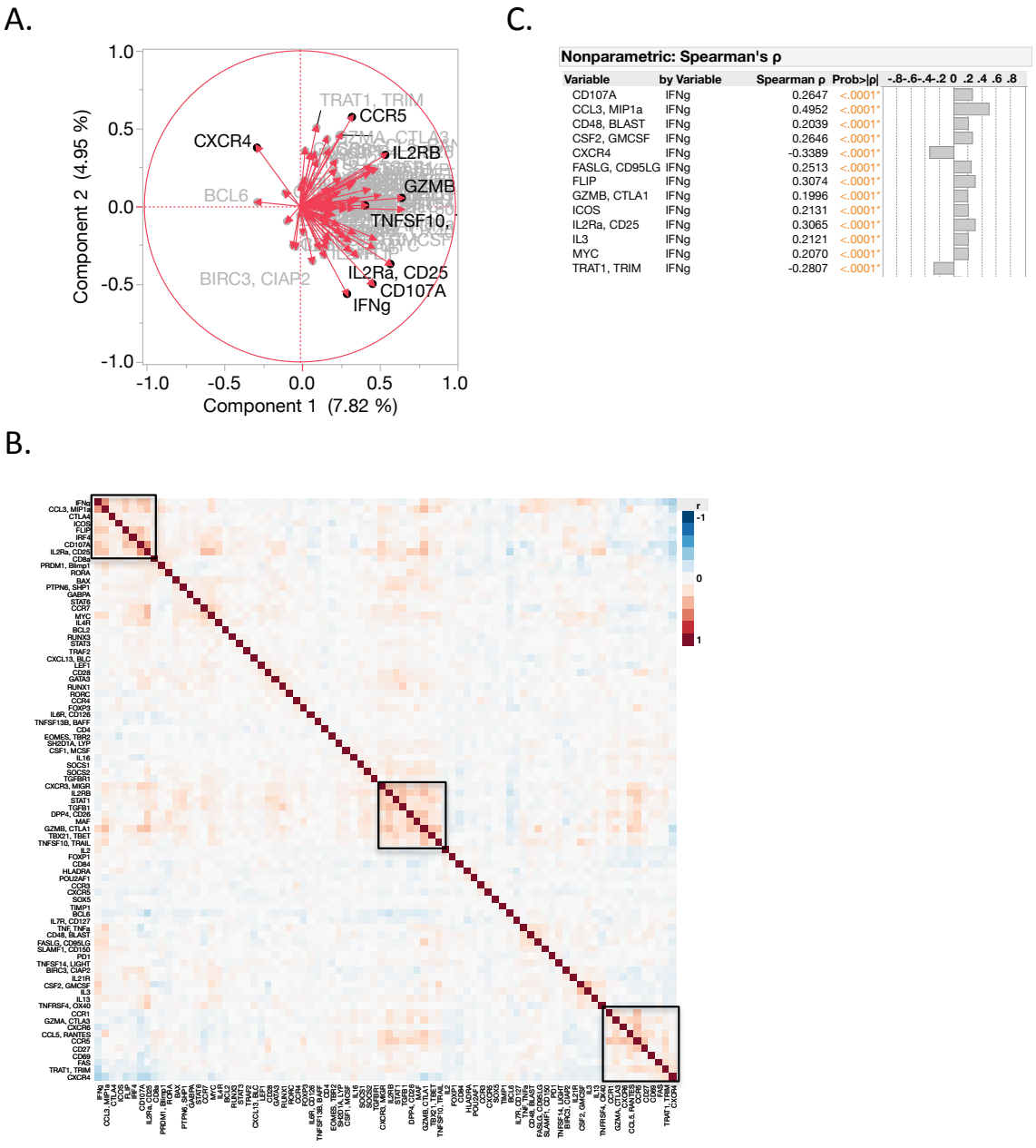

Figure 6.4 Global characterization of all TRAP-specific CD107a^{+} CD8^{+} T cells.

(A) Principal components analysis. Genes which describe the greatest variance are highlighted. **(B)** All possible pairwise pairwise correlations clustered by significance. **(C)** Genes which correlate significantly with *IFNG* ($p<0.0001$, $\rho>0.20$).

6.2.3 Multifunctional use of effector molecules

As TRAP-specific $CD8^+$ T cells are hypothesized to mediate killing of parasitized hepatocytes (*153, 159, 219, 324, 325*), it is important to understand the mechanisms of actions that are induced by vaccination. Accordingly, single-cell coordination among key effectors molecules that are involved in killing target cells was investigated (*73, 326-329*). Analysis was restricted to expression of six genes: cytokines *IFNG* and *TNF*, granzymes *GZMA* and *GZMB*, and apoptosis-inducing ligands *FASLG/CD95LG* and *TNFSF10/TRAIL* **(Figure 6.5-A)**.

The percentage of cells that discretely expressed any of the six markers was variable **(Figure 6.5-B)**. *TNFSF10/TRAIL*, *GZMA*, and *TNF* were each expressed in less 40% of cells. By contrast, *IFNG* and *GZMB*, the most common effector molecules, were expressed in 81% and 88% of TRAP-specific $CD107a^+CD8^+$ T cells, respectively.

In order to investigate second-order combinations, all significant pairwise correlations were calculated (spearman rank correlation: $\rho > 0.20$ and $p<0.001$; **Figure 6.5-C**). Differential expression of *GZMA* and *GZMB* was tightly linked (spearman rank correlation: $\rho = 0.30$ and $p<0.001$), as 98% of *GZMA*-positive cells expressed *GZMB* **(Figure 6.5-A)**. Principal components analysis **(Figure 6.5-D)** and single-cell hierarchal clustering **(Figure 6.5-A)** restricted to these six effector molecules highlighted two broad groups of cooperation: *(1) IFNG, TNF,* and *FASLG* and *(2) TNFS10/TRAIL, GZMA,* and *GZMB*.

Finally, higher order combinations of discrete expression among the six effector molecules were examined **(Figures 6.5-E** and **F)**. Only combinations that were evident in greater than 1% of the population were examined, resulting in 14 different phenotypes. Of interest, all assessed phenotypes were *IFNG*$^{+}$*GZMB*$^{+}$ (highlighted in green for clarity) underscoring the coordinate gene expression of these two molecules. The most frequent combinations of six genes were expression of *IFNG* and *GZMB* alone (*GZMA*$^{-}$*TNFSF10*$^{-}$ *FASLG*$^{-}$; 17% of population) or in combination with *FASLG* (*GZMA*$^{-}$*TNFSF10*$^{-}$; 14% of population).

A.

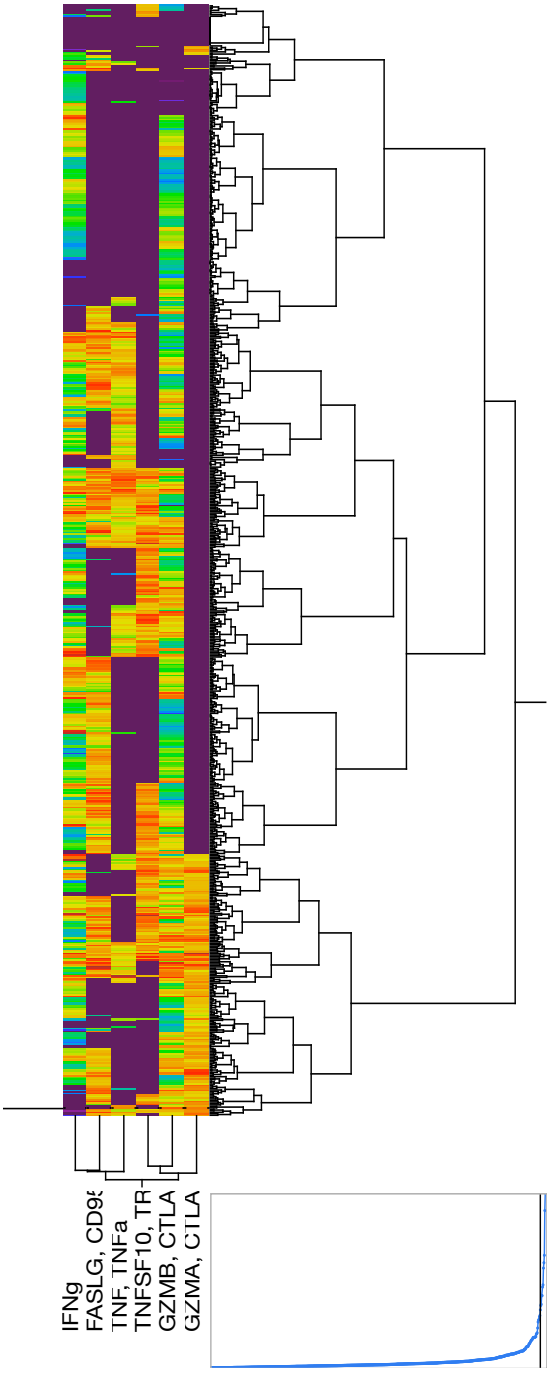

B.

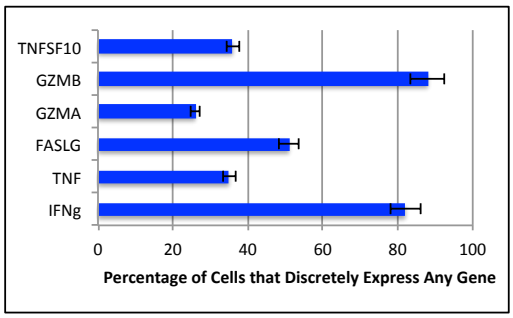

C.

Nonparametric: Spearman's ρ

Variable	by Variable	Spearman ρ	Prob>|ρ|
GZMB, CTLA1	TNFSF10, TRAIL	0.3517	<.0001*
GZMB, CTLA1	GZMA, CTLA3	0.2963	<.0001*
FASLG, CD95LG	IFNg	0.2380	<.0001*
FASLG, CD95LG	GZMB, CTLA1	0.2341	<.0001*
GZMB, CTLA1	TNF, TNFa	0.2111	<.0001*
FASLG, CD95LG	TNF, TNFa	0.2060	<.0001*
TNF, TNFa	IFNg	0.1923	<.0001*
GZMB, CTLA1	IFNg	0.1693	<.0001*
FASLG, CD95LG	TNFSF10, TRAIL	0.1645	<.0001*
TNFSF10, TRAIL	TNF, TNFa	0.1640	<.0001*
TNFSF10, TRAIL	IFNg	0.1446	<.0001*
FASLG, CD95LG	GZMA, CTLA3	0.1142	0.0018*
GZMA, CTLA3	TNFSF10, TRAIL	0.1088	0.0029*
GZMA, CTLA3	TNF, TNFa	-0.0738	0.0435*
GZMA, CTLA3	IFNg	0.0005	0.9899

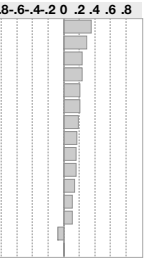

D.

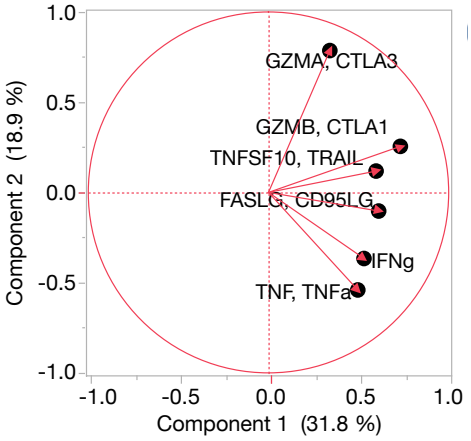

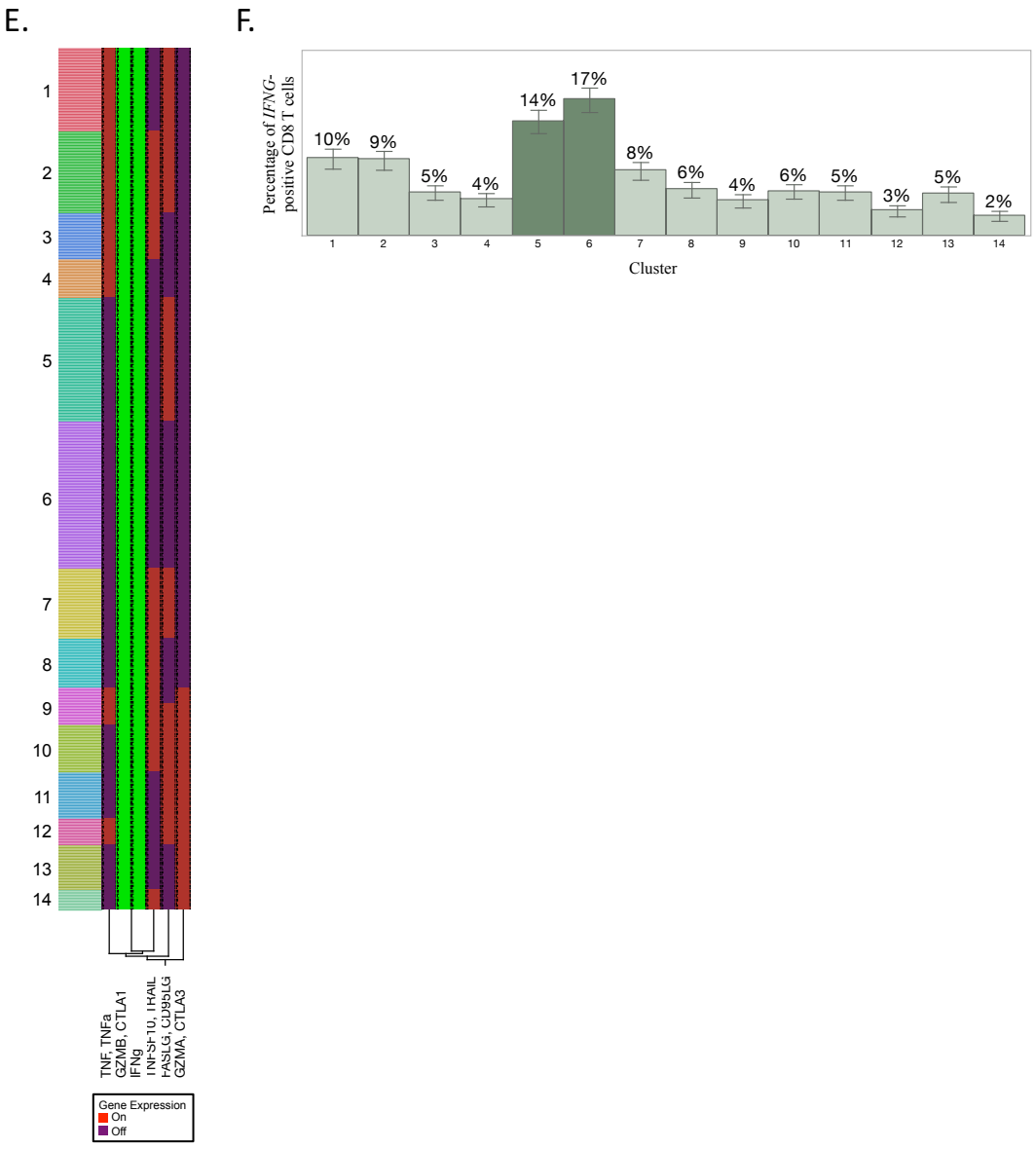

Figure 6.5 Coordinate expression of effector molecules among all TRAP-specific CD107a$^+$ CD8$^+$ T cells.

(A) Single cell hierarchal clustering of individual cells from all vaccinated subjects. **(B)** Discrete expression of any given gene, defined as E_t value > 13, which is equivalent 1 mRNA molecule. **(C)** Pairwise correlations that are statistically significant. **(D)** Principal components analysis of all effector molecules. **(E)** Discrete expression of genes for *IFNG*$^+$ cells only. Clustering of all possible combinations that comprise greater than 1% of population. **(F)** Percentage of common combinations represented as percentage of *IFNG*$^+$ population.

6.2.4 Characterization of monofunctional IFNG$^+$ CD8$^+$ T cells

In order to further characterize TRAP-specific CD8$^+$ T cells, analysis was focused on the transcriptional phenotype of *IFNG$^+$TNF$^-$IL2$^-$* "monofunctional" T cells induced by ChAd63/MVA vaccination. The frequency of monofunctional, but not total, IFN-γ$^+$CD8$^+$ T cells correlate with protection in malaria-naïve volunteers (*153*). As such, it was hypothesized that monofunctional *IFNG*$^+$CD8$^+$ T cells would have a unique transcriptional signature with specialized effector functions compared to the other *IFNG*-expressing CD8$^+$ T cells.

Individual CD8$^+$ T cells from all vaccinated subjects were divided into two cohorts: *IFNG$^+$TNF$^-$IL2$^-$* ("G") and *IFNG$^+$TNF$^+$IL2$^-$* ("GT"), the second common phenotype within the IFNG$^+$ population **(Figure 6.6-A)**. As the frequencies of *IFNG$^+$TNF$^-$IL2$^+$* and triple positive *IFNG$^+$TNF$^+$IL2* were small (<5% of all CD8$^+$ T cells; **Figure 6.3-B)**, these subsets were excluded from the analysis. Of note, median *IFNG* expression was significantly higher in the GT vs. G subsets, but statistical significance was low ($p<0.01$; **Figure 6.6-A**)

Linear discriminant analysis revealed that gene components other than *IFNG* or *TNF* could drive the separation of two cellular subsets, suggesting that a unique global transcriptional signature exists for monofunctional CD8$^+$ T cells **(Figure 6.6-B)**. The top gene components that best distinguished the cohorts consisted of effector molecules, as well as inflammation marker *CCL3/MIP1a* and *CD107A* **(Figure 6.6-C)**. Monofunctional *IFNG*$^+$ CD8$^+$ T cells ("G") were characterized by increased expression of *GZMA* and *CD107A* ($p<0.001$). Double-positive *IFNG$^+$TNF$^+$IL2$^-$*

("GT") were characterized by increased expression of *TNFSF10*, *CCL3/MIPa*, and *GZMB,* in order of decreasing fold-change.

A.

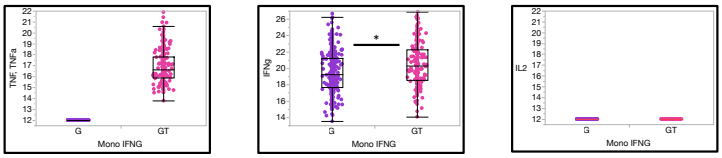

B.

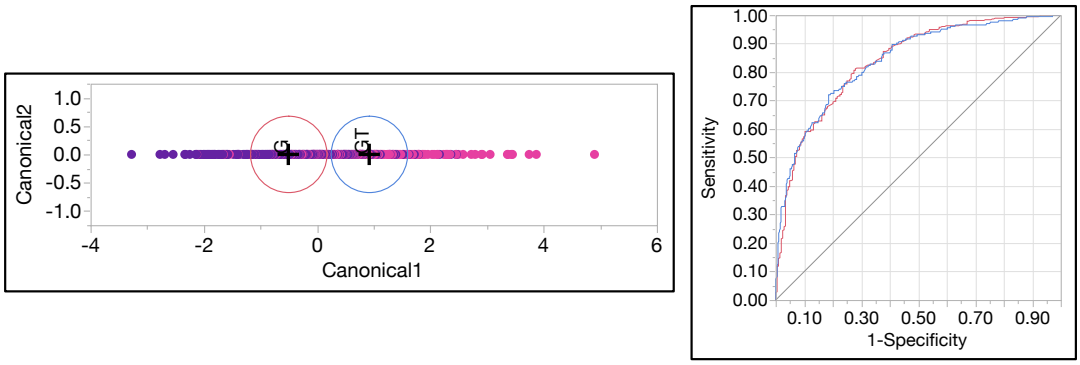

C.

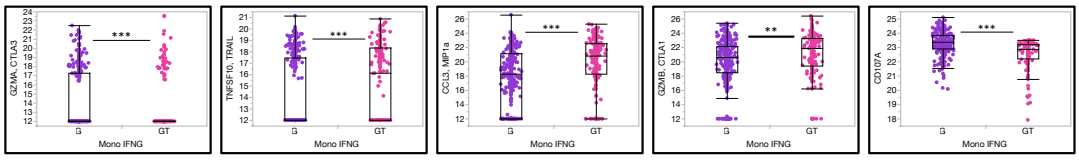

Figure 6.6 Characterization of monofunctional *IFNG*$^{+}$ CD8^{+} T cell subset.

(A) Functional characterization of the two subsets. **(B)** Linear discriminant analysis of the two subsets assessing all genes. **(C)** Differential expression of genes which described the greatest variance between the two groups. ***p<0.0001, **p<0.001, p<0.01.

6.2.5 Global gene signatures from protected vs. unprotected cohorts

The next aim of this chapter was to assess the global transcriptional signatures of $CD107a^+$ $CD8^+$ T cells from protected vs. nonprotected subjects vaccinated with ChAd63/MVA ME-TRAP.

Analysis of immune correlates was first restricted to genes encoding cytokines that have been previously assessed by flow cytometry in these subjects *(153, 219, 268)*. The median expression of *IFNG* in $CD107a^+$ $CD8^+$ T cells was statistically higher in nonprotected compared to protected subjects **(Figure 6.7-A)**. Of note, there was no significant difference within the protected cohort between sterilely protected and delayed subjects. Cluster analysis was then used to assess the frequency of common phenotypic combinations of *IFNG*, *IL2*, and *TNF* in protected vs. nonprotected subjects **(Figure 6.7-B** and **C)**. While there was trend towards a higher frequency of monofunctional $IFNG^+$ $CD8^+$ T cells in the protected cohort (the sum of clusters 3 and 4), it was not statistically significant. However, there was a significant difference in the frequency of low vs. high cytokine producers within the monofunctional $IFNG^+$ $CD8^+$ T cell subsets (clusters 3 vs. 4; $p<0.001$). Protected subjects were enriched in low producers of *IFNG*, while unprotected subjects were enriched in high producers. There was no difference in the frequency of the other phenotypes between the two cohorts.

A.

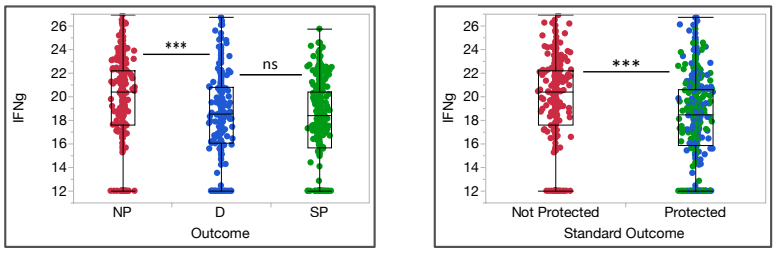
IFNg
***
ns
NP
D
SP
Outcome
IFNg
***
Not Protected
Protected
Standard Outcome

B.

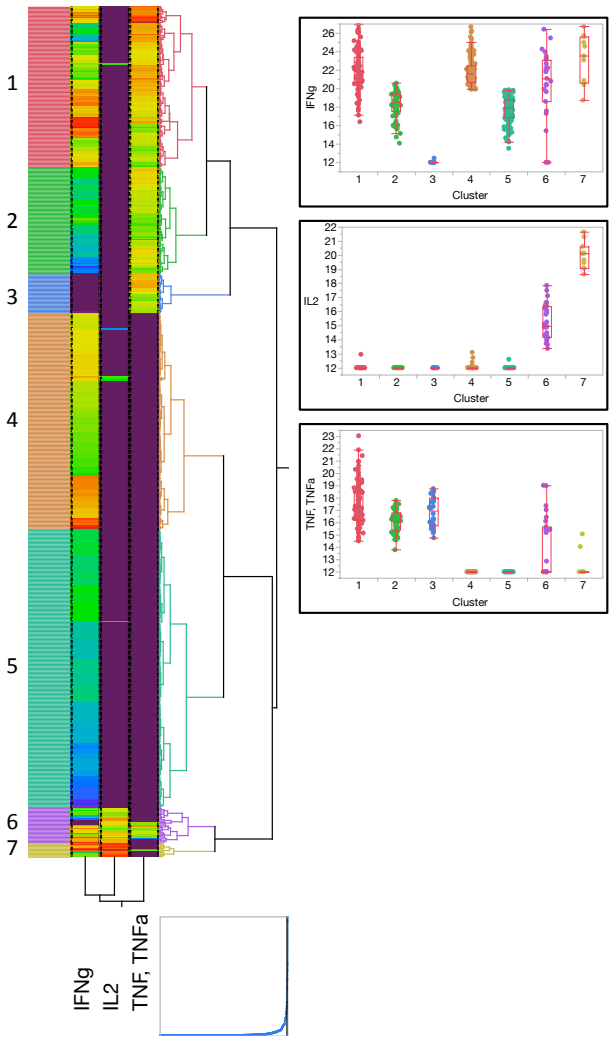
1
2
3
4
5
6
7
IFNg
IL2
TNF, TNFa
Cluster

C.

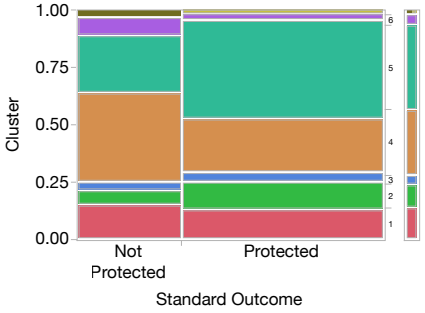
Cluster
1.00
0.75
0.50
0.25
0.00
Not Protected
Protected
Standard Outcome

Figure 6.7 Assessment of $CD8^+$ T cell functionality based on previous studies.

(A) Gene expression of *IFNG* organized by protection outcome. **(B)** Hierarchal clustering of markers typically assessed by flow cytometry. Seven clusters are identified based on prominent patterns of gene combinations. Median expression of each of the genes within the cluster are shown. **(C)** Quality of protected vs. not protected based on percentage of each cluster.

Next, analysis of immune correlates was expanded to include all genes that were assessed by the Fluidigm assay. When all three protection outcome groups were examined simultaneously, misclassification of individual $CD8^+$ T cells into each of the three cohorts was high (>30%; **Figure 6.8-A**). This rate was only slightly lower when delayed and sterilely protected subjects were combined (27.6%; AUC = 80.3) **Figures 6.8- B**). Examination of all possible pairs of the three cohorts yielded more information **(Figure 6.8-C)**. Single-cell misclassification was lowest between the sterilely protected and nonprotected cohorts (19.5%, AUC = 88.6). This was followed by sterilely protected vs. delayed (23.4%, AUC = 84.2) and delayed vs. nonprotected (28.6%, AUC = 80.1).

A.

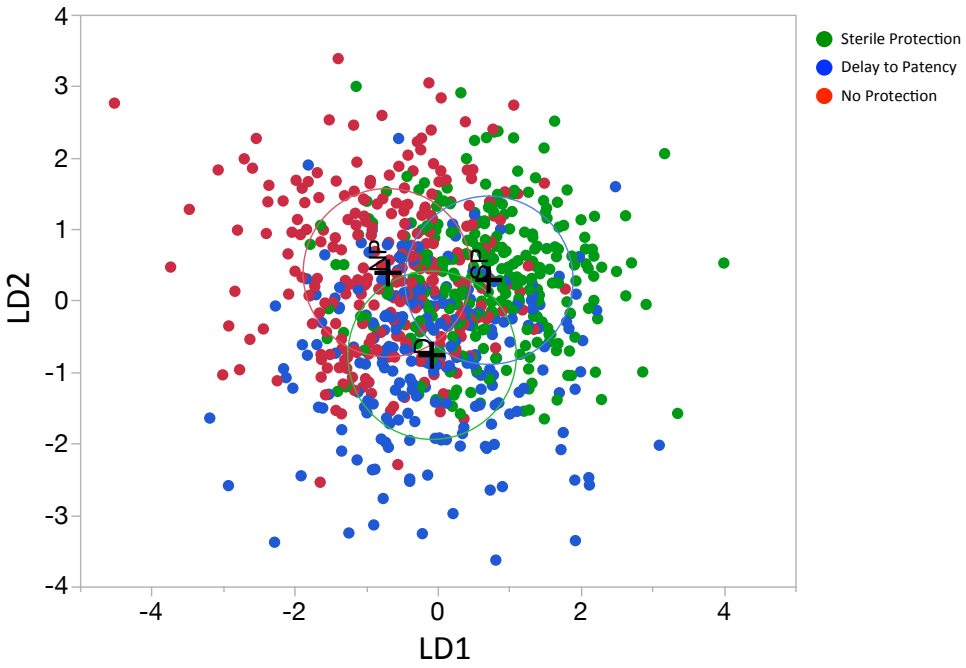
Sterile Protection
Delay to Patency
No Protection
LD2
LD1
4
3
2
1
0
-1
-2
-3
-4

B.

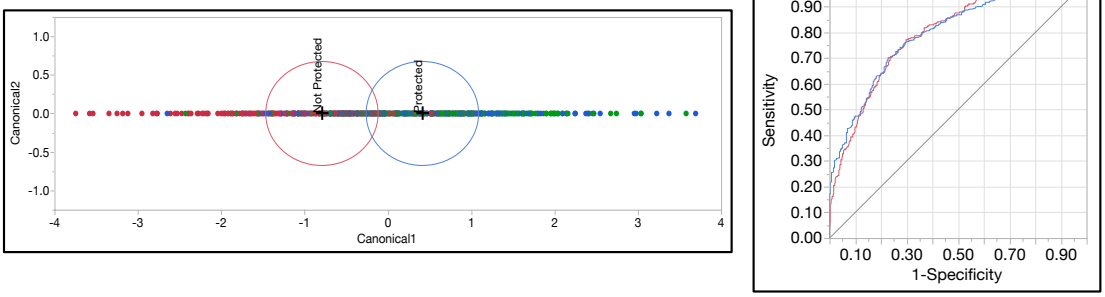
Canonical2
Canonical1
Not Protected
Protected
Sensitivity
1-Specificity

C.

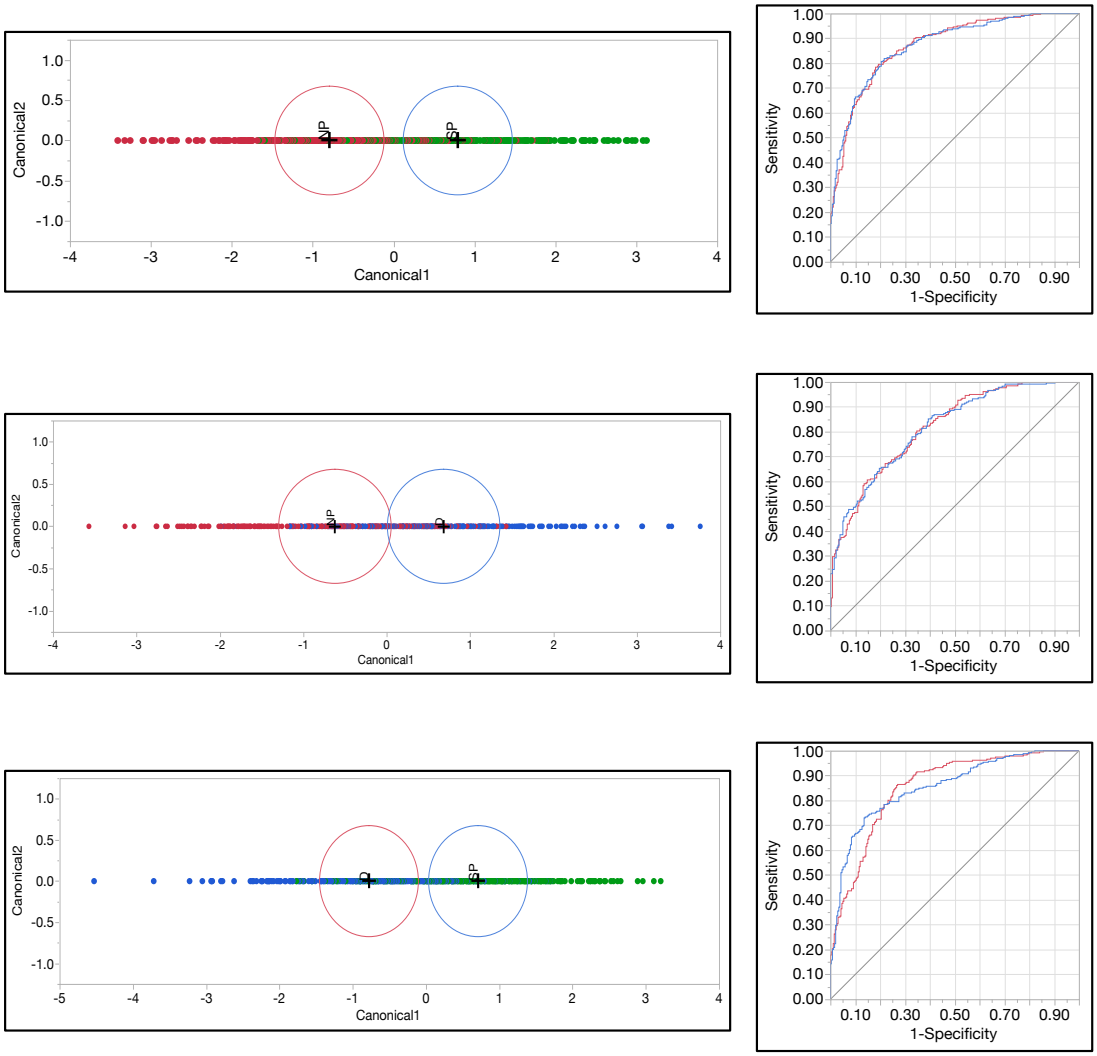

Figure 6.8 Global differences among protected vs. nonprotected cohorts.

(A) Linear discriminant analysis (LDA) assessing all three cohorts. Wide discriminant analysis with corresponding ROC curves assessing **(B)** protected vs. nonprotected subjects and **(C)** all two-way combinations of the three cohorts.

As the global transcriptional signatures of sterilely protected vs. nonprotected subjects appeared the most distinct, the differences in gene expression between these two cohorts were further parsed. Seventeen genes were differentially expressed between the two cohorts, of which 11 were enriched in the protected subjects **(Figure 6.9-A and B)**. Although separation between the two cohorts was not precise, unsupervised single-cell hierarchal clustering helped to further identify combinations of differentially expressed genes. In particular, *IFNG* and *CCL3/MIP1a,* which were individually enriched in unprotected subjects, clustered together. By contrast, *CXCR4, TRAT1, CXCR3/MIGR,* and *STAT1,* which were individually enriched in protected subjects, notably clustered together.

Of interest, although differential expression of granzyme-encoding genes was significant **(Figure 6.5-C)**, *GZMB* was significantly enriched in the protected cohort **(Figure 6.9-A and B)**, while *GZMA* was enriched in the unprotected cohort. Further examination revealed that while almost all *GZMA* cells expressed *GZMB,* the protected cohort was enriched in monoproducers of *GZMB,* which expressed more of the transcript per cell than double-positive $GZMA^{+}GZMB^{+}$ cells **(Figure 6.9-D)**.

A.

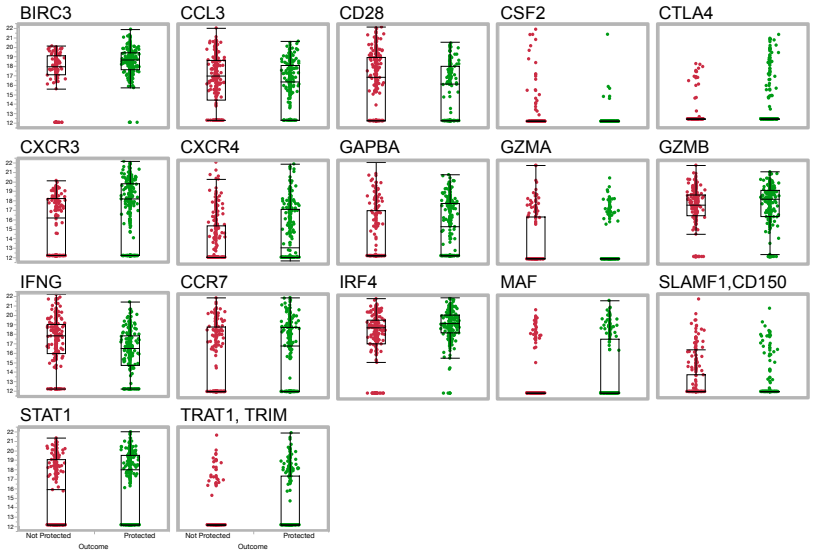
BIRC3
CCL3
CD28
CSF2
CTLA4
CXCR3
CXCR4
GAPBA
GZMA
GZMB
IFNG
CCR7
IRF4
MAF
SLAMF1,CD150
STAT1
TRAT1, TRIM
Not Protected
Protected
Outcome

B.

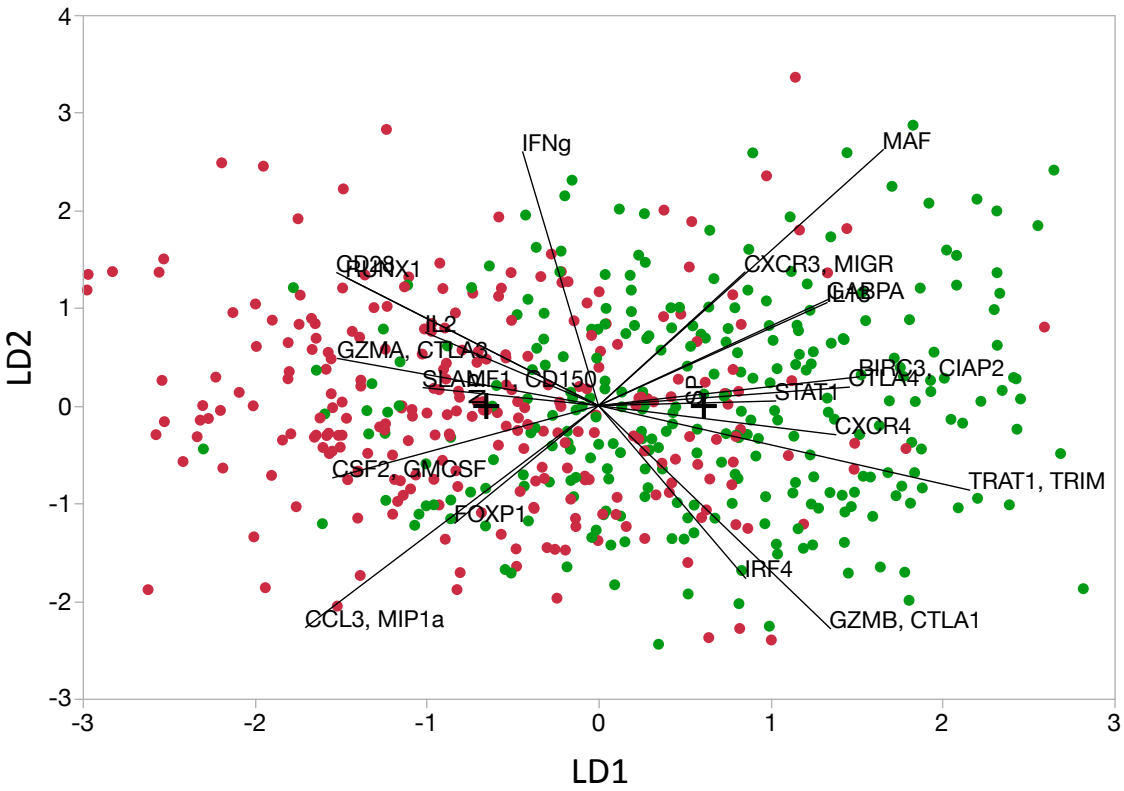
IFNg
MAF
CXCR3, MIGR
CCL3, MIP1a
GZMB, CTLA1
TRAT1, TRIM
CXCR4
BIRC3, CIAP2
CTLA4
STAT1
CSF2, GMCSF
FOXP1
IRF4
LD1
LD2

C.

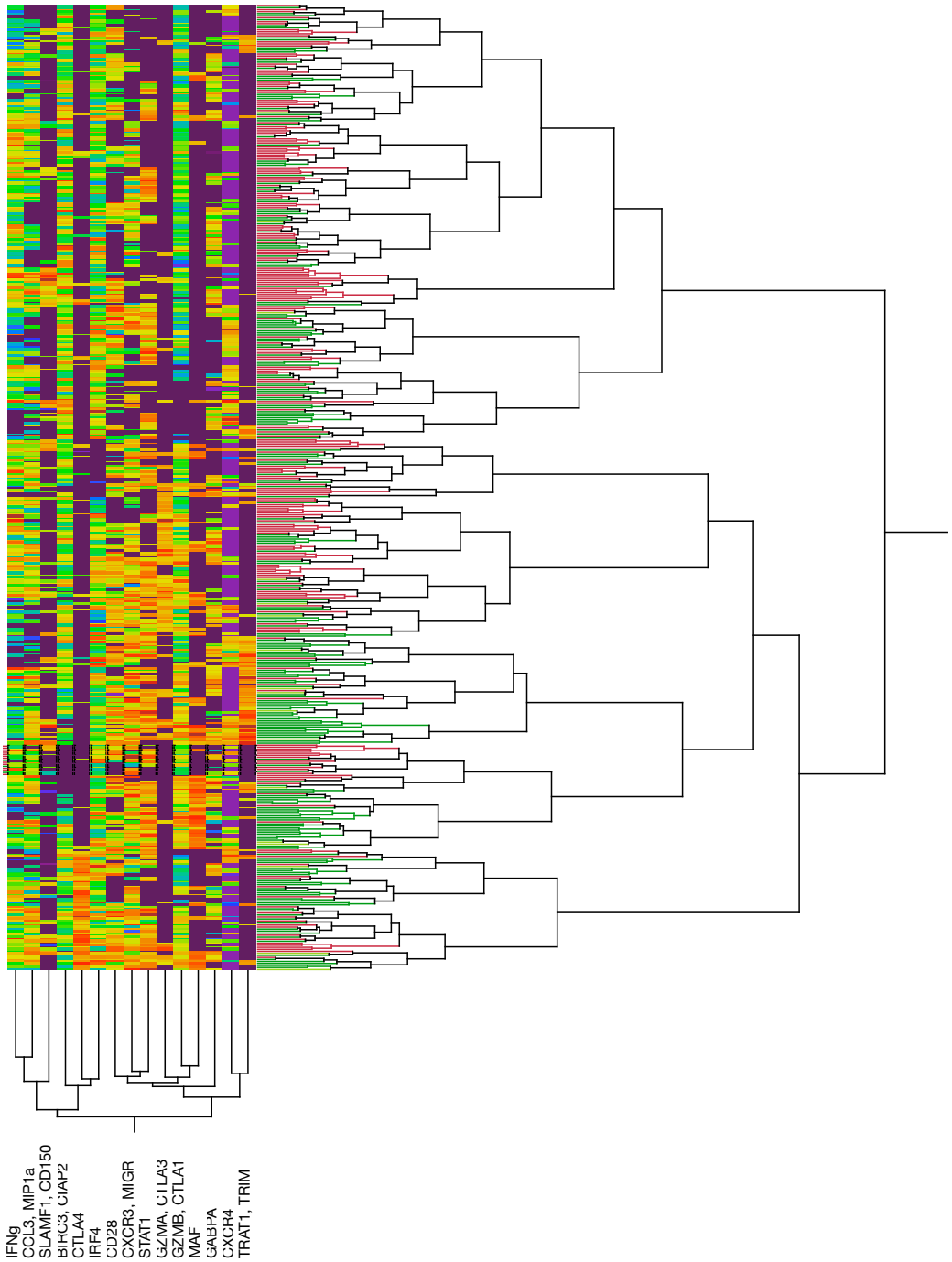
IFNg
CCL3, MIP1a
SLAMF1, CD150
BIRC3, CIAP2
CTLA4
IRF4
CD28
CXCR3, MIGR
STAT1
GZMA, CTLA3
GZMB, CTLA1
MAF
GABPA
CXCR4
TRAT1, TRIM

D.

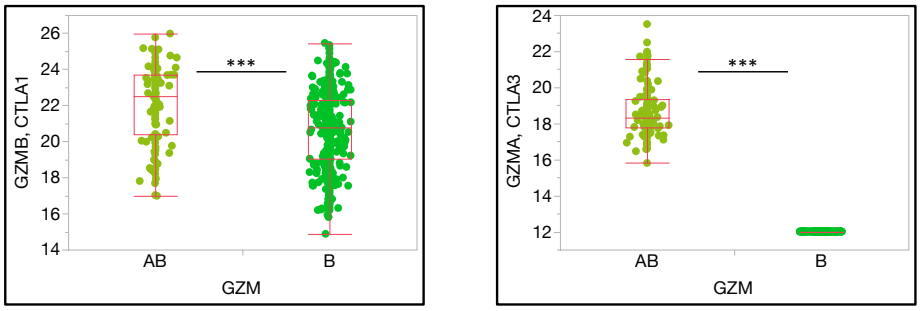

Figure 6.9 Differential gene expression between sterilely protected and nonprotected vaccinated subjects.

(A) List of all differentially expressed genes (DEGs) ($p<0.0001$, median fold-change > 2), **(B)** Linear discriminant analysis with overlaid DEGs. **(C)** single-cell hierarchal clustering restricted to DEGs expressed in greater than 10% of population. **(D)** Level of *GZMB* expression in $GZMA^-$ (B) vs. $GZMA^+$ cells (AB). ***$p<0.0001$

6.2.6 Gene set enrichment analysis of sterilely protected subjects

In order to gain greater insight into the molecular networks involved in sterile protection, gene set enrichment (GSEA) was performed. Blood transcriptional modules previously described in Chapter 4 were used (*291*). Briefly, only modules containing at least four genes that were measured by Fluidigm were included for analysis (n=11). An aggregate Z-score was generated, taking into account both discrete and continuous components of gene expression. Due to the limited number of genes in each of the modules and the potential bias, data interpretation was focused on enriched modules with an enrichment score or aggregate |Z-score| > 5 (see Chapter 4.2.4 for more details).

Modular analysis first assessed sterilely protected vs. nonprotected subjects, as these cohorts were the most distinct **(Figure 6.10-A** and **Table 6.3)**. Of the 11 modules tested, 8 exhibited a significant effect due to protection outcome, all of which were enriched in the sterilely protected cohort ($p<0.01$). The top enriched modules (|Z-score| > 5) were T cell differentiation (Th2)(M19), enriched in NK cells (I)(M7.2), and enriched in T cells (I)(M7.0). Enrichment of these three modules was predominantly characterized by increased expression of *TRAT1/TRIM*, *TBX2/TBET*, *GZMB*, and *DPP4/CD26* **(Table 6.3)**.

In order to explore mechanisms required for complete but not partial protection, modular analysis was then performed comparing the sterilely protected vs. delayed cohort **(Figure 6.10-B** and **Table 6.4)**. Of the 11 modules tested, 6 exhibited a significant effect to protection outcome ($p<0.01$). Of modules with the greatest change (|Z-score| > 5), two were enriched in sterilely protected: signaling in T cells

(I)(M35.0) and (II)(M35.1). Further examination revealed significant overlap in the genes that composed the two modules, such that enrichment of both was characterized by increased expression of *TNFSRF4*, *IL2RA*, and *TNF* **(Table 6.4)**. The module with the greatest fold-change in the delayed cohort was T cell activation (II)(M7.3) (Z-score = -8.2). Enrichment of this module was characterized by increased expression of *GZMA* and *CCL5/RANTES* in delayed vs. sterilely protected subjects **(Table 6.4)**.

Of the top three modules that were enriched in sterilely protected vs. nonprotected subjects, two displayed a similar pattern of enrichment in sterilely protected vs. delayed. Both T cell differentiation (Th2) (M19) and T cell activation (I)(M7.1) were enriched in the sterilely protected cohorts. However, this was characterized by increased expression of only one gene (*TRAT1/TRIM*) in sterilely protected subjects compared to those who showed delay to patency and no protection. As a result, the Z-scores for the modules were much lower.

A.

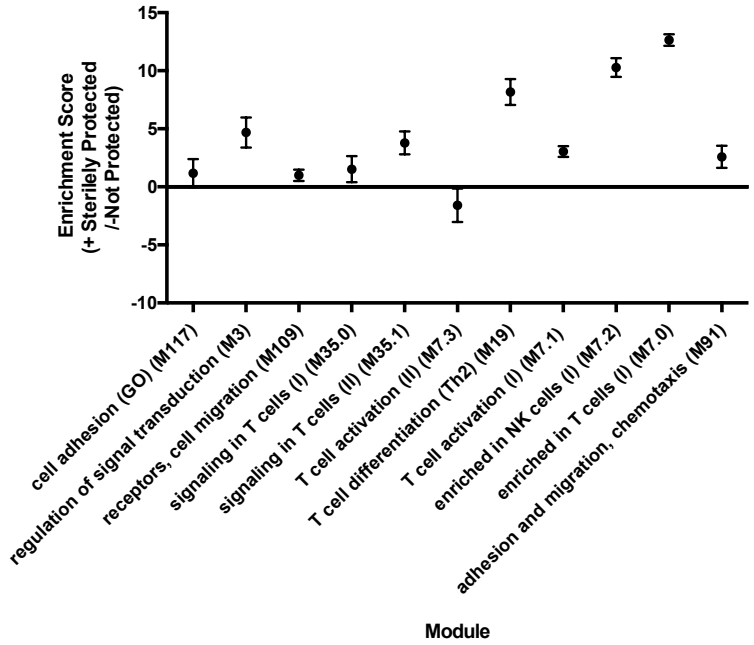

B.

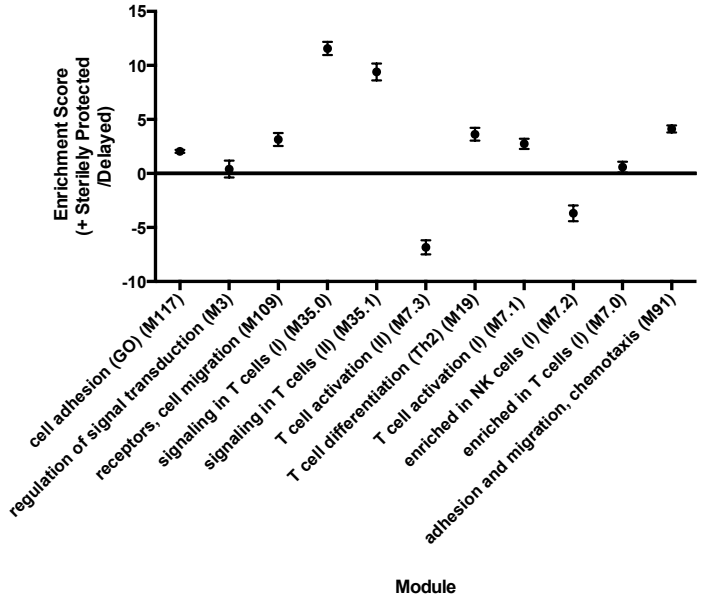

Figure 6.10 Modular analysis of sterilely protected subjects.

Gene set enrichment analysis of sterilely protected subjects vs. (A) nonprotected subjects and (B) subjects who demonstrated delayed to patency. Y-axis shows enrichment score or aggregate Z-score of all genes in the module. Note that in both graphs a positive Z-score indicates enrichment in the sterilely protected cohort.

T cell differentiation (Th2)(M19)		Enriched in NK cells (I) (M7.2)		Enriched in T cells (I) (M7.0)	
TRAT1, TRIM	4.863391	**TBX21, TBET**	4.863391	**TRAT1, TRIM**	4.863391
DPP4, CD26	2.714139	**GZMB, CTLA1**	2.975904	**GZMB,CTLA1**	2.975904
GATA3	0.717576	**GZMA**	-2.69497	**SH2D1A,LYP**	1.599006
CD28	-0.1265	**IL2RB**	2.264661	**CCL5, RANTES**	1.525649
		CCL5, RANTES	1.525649	**RORA**	1.316644
		RORA	1.316644	**IL7R**	-1.14045
		EOMES	0.4612781	**CD27**	0.9342079
		FASLG, CD95LG	-0.43568	**GATA3**	0.717576
				CD28	-0.1265
				LEF1	-0.082687
				ICOS	0.0651693

Table 6.3 Modules enriched in sterilely protected vs. nonprotected subjects.

Individual Z-scores for all of the genes in the modules are listed in descending order.

signaling in T cells (I) (M35.0)		signaling in T cells (II) (M35.1)		T cell activation (II) (M7.3)	
TNFRSF4	3.512717	**TNFRSF4**	3.512717	**GZMA**	-3.63986
IL2RA	3.055554	**IL2RA**	3.055554	**CCL5, RANTES**	-2.71057
TNF	3.054146	**TNF**	3.054146	**ICOS**	-1.71363
FASLG	1.300153	**IL2RB**	-2.16534	**TRAT1, TRIM**	0.699948
GZMB	0.8271	**FASLG**	1.300153	**CXCR3, MIGR**	0.3807357
CD40LG	0.5655252	**GZMB**	0.8271	**SLAMF1, CD150**	0.3303508
LEF1	0.2364555	**BCL6**	0.5397541	**IFNG**	-0.186509
		IFNG	-0.186509		
		CCR5	-0.031528		

Table 6.4 Modules enriched in sterilely protected vs. delayed subjects.

Individual Z-scores for all of the genes in the modules are listed in descending order.

6.3 Discussion

The main aims of this chapter were to (1) characterize the single-cell transcriptomic profiles of TRAP-specific CD107a$^+$ CD8$^+$ T cells following vaccination with ChAd63/MVA ME-TRAP and (2) assess the gene expression signatures of such responses from protected vs. nonprotected subjects prior to challenge. First, TRAP-specific CD107a$^+$ CD8$^+$ T cells from vaccinated subjects predominantly express *IFNG* and *GZMB* alone or in combination with FASLG among six key effector molecules. Second, analysis of monofunctional *IFNG*$^+$*TNF*$^-$*IL2*$^-$ CD8$^+$ T cells, which have been previously correlated with protection, are transcriptionally distinct from the total *IFNG*$^+$CD8$^+$ T cell population with enriched expression of *CD107A* and *GZMA*. Finally, while there was limited power for correlates analysis due to the number of subjects, initial data suggested that global transcriptional signatures between sterilely protected and nonprotected subjects were unique. Sterilely protected subjects were enriched in modules associated with T cell differentiation and overall enrichment in T cells.

Detection of *de novo*-expression on CD107a following *in vitro* restimulation with TRAP peptide pools was successful in isolating live malaria-specific CD8$^+$ T cells that could be assessed for expression of a large number of genes at the single cell level. This experimental approach did not increase the sensitivity of identifying TRAP-specific CD8$^+$ T cells following vaccination compared to previous flow cytometry studies *(153, 268),* as 100% of analyzed cells expressed *CD107A*, *IFNG*, *IL2* or *TNF* at the transcriptomic level **(Figure 6.3-B)**. However, Fluidigm analysis dramatically expanded the breadth of phenotypic characterization of such responses.

It is important to note the study limitations in order to appropriately interpret the results. First, only $CD107a^+$ $CD8^+$ T cells were analyzed. The frequency of $CD107a^+$ $CD8^+$ T cells was shown to be notably lower than the frequency of IFN-γ^+ $CD8^+$ T cells at the time of challenge following ChAd63/MVA ME-TRAP vaccination (*153*). As such, there exists a subset of $CD107a^-$ cytokine-producing cells that is not captured by this experimental approach. Phenotypic and correlates analysis reflects only a subset of the total $CD8^+$ T cell response. Second, Fluidigm analysis was restricted to those subjects with the highest IFN-γ^+ $CD8^+$ T cell responses across the three trials. It is possible that the quality of these responses do not reflect the full spectrum of cellular phenotypes of TRAP-specific $CD8^+$ T cells.

In this study, there was an enrichment of *IFNG*$^+$ $CD107a^+$ $CD8^+$ T cells in nonprotected subjects. By contrast, IFN-γ^+ secretion as assessed from ELISPOT assay of flow cytometry analysis $CD8^+$ T cell responses has been associated with protection induced by viral vector vaccination in multiple studies (*153, 219, 268*). Furthermore, transcriptional analysis of whole PBMCs revealed that genes associated with IFN-γ induction were enriched in sterilely protected vs. nonprotected subjects (*330*) . However, as this study was restricted to $CD107a^+$ cells, a subset of the total $CD8^+$ T cell responses, this finding is not inconsistent with previous data.

The multiple cellular phenotypes based on combinations of key effector molecules is consistent with previous studies that demonstrate the remarkable heterogeneity among antigen-specific $CD8^+$ T cells based on protein expression of granzymes,

perforin, and IFN-γ (*329, 331, 332*). It is interesting to note that almost all CD107a$^+$ CD8$^+$ T cells in this study expressed both *IFNG* and *GZMB*, consistent with previous work showing high expression of these two markers among CD107$^+$ CD8$^+$ T cells (*322*). Most studies that have aimed to dissect the effector function of CD8$^+$ T cells against liver-stage malaria have demonstrated different requirements based on the murine *Plasmodium* strain and vaccination model (*135, 149, 333-335*). However, induction of memory CD8$^+$ T cell responses against *P. berghei* is independent of perforin, TRAIL, or FASLG in RAS (*336*) and DC-LM prime/boost immunization approaches (*337*). Given the expression of markers in TRAP-specific CD8$^+$ T cells, future studies should examine protein expression of these markers by flow cytometry in order to assess whether protective responses are skewed towards a specific "killing" phenotype.

Although monofunctional IFN-γ$^+$ CD8$^+$ T cells have been correlated with protection induced by viral vectors in mice (*320*) and humans (*153*), the effector function of IFN-γ secretion alone or in combination with other cytokines is unknown (*313*). This study provides evidence of a broad transcriptional signature for monofunctional *IFNG*$^+$*TNF*$^-$*IL2*$^-$ CD8$^+$ T cells compared to those cells that also express *TNF*. These data suggest that "monofunctional" IFNG$^+$ CD8$^+$ T cells have other effector functions that may play a role in induction of sterile protection against malaria. Interestingly, monofunctional IFNG$^+$ CD8$^+$ T cell responses were associated with expression of *GZMA* and *CD107A*, while expression of *GZMB* and *TNFSF10/TRAIL* were more associated with double positive *IFNG*$^+$*TNF*$^+$ T cells **(Figure 6.6-C)**. Although viral vector vaccination induces multiple CD8$^+$ T cell effector functions, there may exist an optimal pathway for elimination of infected hepatocytes. Indeed,

granzyme A preferentially induces reactive oxygen species (ROS), while granzyme B is more important for caspase-dependent mechanisms of killing *(338, 339),* suggesting that induction of ROS may best augment IFN-γ-mediated clearance of hepatocytes.

It was not surprising that among the three protection outcome groups, the greatest difference in the transcriptional profiles was between sterilely protected vs. nonprotected subjects. There was wide variation in the time to parasitemia among subjects classified as delayed (14-17 days). As such, the components of cellular and humoral immunity that contribute to partial immunity may have varied. While initial data suggested that sterilely protected subjects were enriched in modules associated with T cell differentiation and overall enrichment of T cells compared to nonprotected subjects, it is important to note that these modules were predominantly characterized by increased expression of *TRAT1/TRIM*. This gene plays a key role in modulation of T cell activation and TCR-mediated signaling via association with CD3-ζ (*340*) and facilitates shuttling of CTLA-4 to the cell surface, thus inhibiting T cell proliferation (*341-343*). Indeed, enriched expression of *TRAT1/TRIM* was associated with low vs. high responders to vaccination with viral vectors containing *M. tuberculosis* antigen 85A (MVA85A) *(344)*. One possibility for enriched expression of *TRAT1/TRIM* in sterilely protected subjects is that the presence of activated $CD8^+$ T cells measured in the peripheral blood could reflect the absence of such responses in the liver, and subsequently poor T-cell mediated clearance of parasitized hepatocytes. On the other hand, it is important to note *TRAT1/TRIM* expression was strongly negatively correlated with *IFNG* expression in this study (Figure 6.4-C). Thus, it is unclear if modular enrichment reflects a true mechanism or merely lower frequencies of $IFNG^+$ $CD107a^+$ $CD8^+$ T cell population in protected

vs. nonprotected subjects. The observation that the top modules that were enriched in sterilely protected vs. nonprotected subjects were not the same as those in sterilely protected vs. delayed subject suggests different components of cellular and/or humoral immunity may be relevant for different levels of protection.

Overall, this characterization of cellular immune response induced by ChAd63/MVA ME-TRAP immunization should advance our understanding of the phenotype of $CD8^+$ T cells in liver-stage protection. In light of encouraging Phase II clinical trials assessing this vaccination platform, future studies should couple transcriptional profiling with flow cytometric analysis in order to elucidate correlates of protection.

7. Concluding Remarks

7.1 Overview

Vaccine approaches that confer durable and high-level protection against malaria infection are urgently needed. While RTS,S/AS01 will likely become the first licensed malaria vaccine, efficacy against clinical malaria is partial and wanes dramatically over time (*117*). Development of next-generation vaccine strategies is partially hindered by a limited understanding of the mechanisms underlying protective immunity. An effective pre-erythrocytic vaccine that induces high-level sterile protection will likely require induction of potent cellular immune responses with a broad range of functions. Indeed, remarkable progress in pre-erythrocytic vaccine development has depended upon strategies that exploit the plasticity of $CD4^+$ T cells and induce potent $CD8^+$ T cells that target liver-stage antigens. In-depth characterization of such responses will be critical in identifying immune correlates and ultimately guiding the development of next-generation vaccine strategies.

The aim of this thesis was to dramatically enhance the breadth and depth of phenotypic analysis from cellular immune responses induced by two malaria vaccine candidates that have demonstrated high-level protection against CHMI: the PfSPZ Vaccine and ChAd63/MVA ME-TRAP. Single cell gene expression analysis of antigen-specific $CD4^+$ and $CD8^+$ T lymphocytes following vaccination and/or CHMI revealed a number of important findings. First, investigation of PfSPZ-specific $CD4^+$ T cells from unvaccinated infection controls revealed enrichment of

modules associated with T cell activation and TFH vs. Th1 differentiation compared to vaccinated and protected subjects. These data likely reflect the increased antigen load seen in the liver following CHMI vs. PfSPZ vaccination and suggest a skewing of $CD4^+$ T cell effector function from $CD8^+$ T cell help to antibody production during CHMI. Second, PfSPZ-specific $CD4^+$ T cells from vaccinated and protected subjects in a small cohort were enriched in *IL21* gene expression compared to unprotected subjects prior to challenge. Median *IL21* expression of this gene on a per-subject level correlated with antibody levels against the immunodominant CS protein. Analysis of a larger independent cohort confirmed both of these findings and provided greater power to dissect this population of $IL21^+$ $CD4^+$ T cells. Interestingly, $IL21^+$ $CD4^+$ T cells displayed increased expression of *IFNG* and *IL2* compared to $IL21^-$ cells and predominantly expressed *BCL6* and/or *TBET*. Furthermore, there was an enrichment of triple positive $IL21^+IFNG^+IL2^+$ $CD4^+$ T cells in protected vs. nonprotected vaccinated subjects prior to challenge. These data provide evidence for a class of Th1/TFH-like cells that could potentially provide help for both $CD8^+$ T cells and humoral responses elicited by PfSPZ vaccination.

Finally, analysis of $CD8^+$ T cells from subjects vaccinated with ChAd63/MVA ME-TRAP provided the opportunity to investigate cellular immune responses that are critical for clearance of infected hepatocytes. There was evidence for multifunctional use of effector molecules in TRAP-specific $CD107a^+$ $CD8^+$ T cells and a broad transcriptional signature of monofunctional $IFNG^+$ $CD8^+$ T cells, which have been previously correlated with protection induced by viral vectors. Furthermore, preliminary data suggested enrichment of genes associated with T cell activation in subjects who demonstrated sterile protection vs. no protection prior to

challenge. Overall, data presented in this thesis demonstrate that Fluidigm analysis is a powerful tool that can be used in conjunction with other immunologic assays in order to expand the phenotypic characterization of cellular immune responses and elucidate potential correlates of protection.

7.2 Conclusion and Future Directions

7.2.1 Single-cell transcriptomics as a powerful technology for analysis of large clinical trials

The initial aim of this thesis was to optimize isolation and downstream single-cell gene expression analysis of malaria-specific T cells. Detection of de novo expression of CD154 and CD107a on the cellular surface following *in vitro* stimulation allowed for the isolation of live PfSPZ-specific $CD4^+$ T cells and TRAP-specific $CD8^+$ T cells, respectively. Both assays allowed for assessment of gene expression from antigen-specific T lymphocytes at single-cell resolution with minimal manipulation, enabling in-depth characterization of T cells that may play a role in protection.

However, it is important to note that findings from the two assays have different interpretations. The CD154 assay increases the sensitivity of detecting antigen-specific $CD4^+$ T cells, thus broadening the characterization of such responses. Indeed, data presented in this thesis demonstrated that approximately 30% of $CD69^+CD154^+$ PfSPZ-specific T cells do not express IFN-γ, IL2 or TNF-α, the most commonly measured cytokines by flow cytometry. By contrast, detection of CD107a identified only a subset of the TRAP-specific $CD8^+$ T cell response, based on previous data demonstrating the presence of cytokine-producing $CD107a^-$ $CD8^+$ T cells. In this light, data from Fluidigm studies are best interpreted in conjunction with flow cytometry analysis of the same immune responses. Given the broad

heterogeneity of $CD4^+$ T cells (*85, 87*), the greater protective relevance of different phenotypes of such responses compared to $CD8^+$ T cells (*313*), and the ability of the CD154 assay to capture a broad set of antigen-specific $CD4^+$ T cells, Fluidigm analysis may best enhance the characterization of $CD4^+$ compared to $CD8^+$ T cells.

Data presented in this thesis also optimized data acquisition and downstream analysis using the Fluidigm platform. It is critical to note that in all of the studies discussed in this thesis, gene expression of the "average" single cell from a subject correlated with the signal in the bulk population, strongly suggesting that the results from this thesis reflect the true biological patterns. One important limitation of the assay that was described in Chapter 3 was the presence of background cells that contaminate analysis of the antigen-specific population. Of interest, in all studies assessing $CD4^+$ and $CD8^+$ T cells (Chapters 4-6), *TRAT/TRIM* and *CXCR4* were among the top five genes that describe the total variation within the T cell population. Furthermore, these genes negatively correlated with *IFNG* expression, an approximate marker of T cell immunogenicity. These data provide greater evidence that the variation between background and antigen-specific T cells is greater than the variation within a population. These two markers could be used with others to identify background cells and remove them from the analysis of the broader antigen-specific population. Indeed, ongoing experiments are combining transcriptional profiles of non-antigen-specific $CD154^+CD4^+$ T cells with computational analysis in order to minimize this biological signal.

This thesis provided the opportunity to look at both malaria-specific $CD4^+$ and $CD8^+$ T cells using largely the same set of markers. It is difficult to make direct

comparisons between the two different studies. Dissimilarities could reflect inherent $CD4^+$ vs. $CD8^+$ T cell heterogeneity, whole parasite vs. viral vector vaccination or the level of sterile protection induced by the two platforms. However, antigen-specific $CD4^+$ T cells largely coexpressed *IL2* with *TNF* and/or *IFNG*, while $CD8^+$ T cells were predominantly $IL2^-$ expressing *IFNG* and/or *TNF,* consistent with previous flow cytometry data *(153, 313).* Furthermore, heterogeneity among PfSPZ-specific $CD4^+$ T cells from vaccinated subjects (as defined by the number of principal components required to account for 50% of the variation within a population) was almost twice that of TRAP-specific $CD8^+$ T cell responses.

Single-cell RNA-Seq (scRNA-Seq) of these same cellular immune responses is an important extension of the findings presented in this thesis (*241, 250, 251, 262*). Indeed, studies are already underway to assess the PfSPZ-specific T cells in the livers of non-human primates (*205*). However, given the greater ease of data acquisition (*241, 244*), the greater maturity of methodologies for analysis (*270, 287*), and the overall cost, the Fluidigm platform may be more useful for rapid monitoring of immune responses to vaccination in a large population.

7.2.2 Role of CD4$^+$ T cells in PfSPZ-mediated protection

Heretofore, analysis of PfSPZ-specific T cell responses has been largely restricted to detection of IFN-γ, IL2 or TNF-α by multiparameter flow cytometry (*116, 167, 205*). The results presented in this thesis provide the broadest characterization of immune responses elicited by the PfSPZ Vaccine with single-cell resolution to date. Given the absence of potent CD8$^+$ T cell responses in the peripheral blood of vaccinated subjects (*205*), in-depth characterization of PfSPZ-specific CD4$^+$ T cell is a critical step in evaluation of this vaccine platform.

First, it is striking that the enriched expression of *IL21* in protected vs. unprotected subjects and the correlation of *IL21*$^+$ CD4$^+$ cells with PfCSP antibodies was found in two independent cohorts of PfSPZ vaccinated subjects. These data highlight the strength and reproducibility of the Fluidigm platform and encourage further investigation of this potential biomarker of protection. Ideally, all studies that use transcriptional analysis to investigate immune correlates should aim to examine at least two identical and independent cohorts of vaccinated subjects: one for generation of hypotheses and another for validation findings. The data presented here are not an exact repeat, as there were no two groups that received the same vaccine dose and schedule; however, immunization regimens were broadly similar and induced high-level sterile protection (*116, 205*).

The biological interpretation of the findings is more difficult. It was hypothesized that *IL21* expression reflected circulating TFH $CD4^+$ T cells. *IL21* cells largely expressed *BCL6*, a canonical transcriptional factor for TFH cells (*301*). However, Th1 but not TFH modules as a whole were enriched in protected vs. unprotected subjects. In light of these results and other studies that provide conflicting results for what markers constitute a sufficient signature of circulating TFH $CD4^+$ T cells (*318, 345-348*), future work will be necessary in order to understand the function of this subset in PfSPZ-elicited protection.

Further characterization of $IL21^+CD4^+$ T cells in PfSPZ vaccinated subjects is not straightforward, as overall $CD4^+$ T cell responses are relatively low and *IL21*-expressing cells constituted a small but significant subset of the total response. However, work is ongoing to optimize detection of such cells by flow cytometry, such that IL21 protein secretion could be readily detected in future studies assessing the PfSPZ Vaccine alongside IFN-γ, IL2 or TNF-α. Moreover, ongoing studies are elucidating how this population could play a role in protection. Future experiments will assess $IL21^+$ $CD4^+$ T cells in the peripheral blood and liver of mice and NHPs administered the PfSPZ Vaccine. In addition, the circulating TFH cell population as defined by protein expression of CXCR5, ICOS, and PD-1 will be assessed in response to mitogen stimulation before and after PfSPZ vaccination in human subjects (*318*). Overall, the data presented in this thesis have provided more evidence for the importance of $CD4^+$ T cells elicited by PfSPZ vaccination. Furthermore, while humoral immunity may not be sufficient for PfSPZ-elicited protection, T cell-mediated maturation of antibodies may be critical in reducing the

parasite burden in the liver and allowing effective clearance of infected hepatocytes by $CD8^+$ T cells.

7.2.3 $CD107a^+$ $CD8^+$ T cells in ChAd63/MVA ME-TRAP induced immunity

Finally, this thesis provided the opportunity to characterize the antigen-specific $CD8^+$ T cell response induced by heterologous prime-boost vaccination with ChAd63/MVA ME-TRAP. As $CD8^+$ T cells are critical in protection against liver-stage malaria, this analysis was an important step forward in elucidation of mechanisms underlying sterile immunity. Furthermore, as monofunctional IFN-γ^+ $CD8^+$ T cells correlate with protection induced by ChAd63/MVA immunization (*153*), this study allowed for an expanded characterization of an important cellular phenotype previously described in humans.

Data presented in thesis highlight the striking heterogeneity of $CD8^+$ T cells and underscore the importance of qualitative analysis of cellular immune responses beyond flow cytometry. TRAP-specific $CD8^+$ T cells induced by vaccination were composed of multiple different effector phenotypes expressing various combinations of *TRAIL, FASLG, GZMA, GZMB, IFNG* and *TNF*. This study could not assess the protective role of each of the different phenotypes, as the CD107 assay captured only a subset of the total $CD8^+$ T cell response. However, "monofunctional" $IFNG^+$ $CD8^+$ T cells, which have been previously correlated with protection, were shown to have a unique transcriptional signature compared to the total $IFNG^+$ population. Of note, $IFNG^+$ TNF^- $CD8^+$ T cells were characterized by enrichment of *GZMA* but not

GZMB, possibly indicating an important role for *GZMA*-induced ROS in augmenting IFN-γ-mediated killing (*331*). Based on the these results and other evidence of overlapping mechanisms of killing (*135, 334, 335, 349*), future work should continue to dissect pathways of killing in mouse models (*333*).

More subjects will likely be required to assess a transcriptional signature of protective $CD8^+$ T cells induced by TRAP. However, it is interesting to note that transcriptional profiles of $CD8^+$ T cells from delayed subjects were more closely related to those from nonprotected subjects compared to those who demonstrated sterile protection. These data suggest that the total magnitude of $CD8^+$ T cell responses or other components of cellular and/or humoral immunity drive partial protection induced by viral vaccination. As such, future gene expression analysis of cellular immune responses should primarily focus on comparing subjects who demonstrated sterile protected vs. no protection. Preliminary data suggests that modules enriched in T cell activation may play a role in sterile protection. However, as these modules were predominantly characterized by *TRAT1/TRIM*, which is strongly negatively correlated with *IFNG* expression, the relevance of this finding is unclear. To circumvent this issue, future transcriptomic studies should investigate the signature of live $CD8^+$ T cells isolated by the IFN-γ secretion assay (*350*), given the importance of this cytokine in pre-erythrocytic immunity and the limited ability of the CD107a assay to capture all IFN-γ-producing cells.

Given the encouraging progress of ChAd63/MVA ME-TRAP in Phase II clinical trials (*219, 321, 351*), the Fluidigm platform could be used to monitor the progress of responses in the field and assess the influence of previous malaria exposure on

the quality of vaccine-elicited $CD8^+$ T cells. Furthermore, given the large genetic diversity of parasites in the field (*202, 352*) and evidence of specific TRAP sequences associated with protection (*321*), single cell gene analysis could be coupled with TCR sequencing in order to link antigen specificity with functionality (*353*).

7.3 Final Remarks

This study describes a powerful technology for single cell transcriptional analysis of antigen-specific immune responses elicited by two clinical advanced malaria vaccine candidates. This strategy could supplement traditional techniques that quantify cellular immune responses against malaria and other diseases where T cell immunity is hypothesized to be critical for vaccine-elicited protection. In addition, elucidation of effector functions could be used to optimize immunization schedules, design novel adjuvants that promote specific immune responses, or predict protection outcome prior to pathogen exposure. Taken together, the results in this thesis delineate the striking heterogeneity of T cells elicited by vaccines and advance our understanding of how multifunctional $CD4^+$ and $CD8^+$ T cells may play a role in protection against human malaria infection. Therefore, future clinical trials should prioritize the use of single-cell transcriptomic technologies to guide the rational design of next-generation vaccines against malaria.

References

1. U. N. G. Assembly. Road map towards to the implementation of the United Nations Declaration Millenium Declaration. (2000).
2. World Health Organization. World Malaria Report: 2015. (2015).
3. P. Maleney *et al*. The Malaria Gap. *The American Journal of Tropical Medicine and Hygiene* **71**, 141-146 (2004).
4. J. Sachs and P. Malaney. The economic and social burden of malaria. *Nature* **415**, 680-685 (2002).
5. Roll Back Malaria Partnership. Roll Back Malaria Annual Report. (2013).
6. S. Okie. A New Attack on Malaria. *New England Journal of Medicine* **358**, 2425-2428 (2008).
7. P. L. Alonso and M. Tanner. Public health challenges and prospects for malaria control and elimination. *Nature Medicine* **19**, 150-155 (2013).
8. S. Bhatt *et al*. The effect of malaria control on Plasmodium falciparum in Africa between 2000 and 2015. *Nature* **526**, 207-211 (2015).
9. M. M. Plucinski *et al.* Effect of the Ebola-virus-disease epidemic on malaria case management in Guinea: a cross-sectional survey of health facilities. *The Lancet Infectious Diseases* **15**, 1017-1023 (2014).
10. L. H. Miller *et al.* Malaria biology and disease pathogenesis: insights for new treatments. *Nature Medicine* **19**, 156-167 (2013).
11. W. E. Collins. Plasmodium knowlesi: A Malaria Parasite of Monkeys and Humans. *Annual Review of Entomology* **57**, 107-121 (2011).
12. B. Singh and C. Daneshvar. Human Infections and Detection of Plasmodium knowlesi. *Clinical Microbiology Reviews* **26**, 165-184 (2013).
13. R. Ramasamy. Zoonotic Malaria – Global Overview and Research and Policy Needs. *Frontiers in Public Health* **2**, (2014).
14. M. E. Sinka *et al.* A global map of dominant malaria vectors. *Parasites & Vectors* **5**, 1-11 (2012).
15. R. Amino *et al.* Quantitative imaging of Plasmodium transmission from mosquito to mammal. *Nature Medicine* **12**, 220-224 (2006).
16. J. Tavares *et al.* Role of host cell traversal by the malaria sporozoite during liver infection. *The Journal of Experimental Medicine* **210**, 905-915 (2013).
17. M. M. Mota *et al.* Migration through host cells activates Plasmodium sporozoites for infection. *Nature Medicine* **8**, 1318-1322 (2002).
18. I. N. Crispe. The Liver as a Lymphoid Organ. *Annual Review of Immunology* **27**, 147-163 (2009).
19. A. Sturm *et al.* Manipulation of Host Hepatocytes by the Malaria Parasite for Delivery into Liver Sinusoids. *Science* **313**, 1287-1290 (2006).
20. R. N. Price *et al.* Vivax Malaria: Neglected and Not Benign. *The American Journal of Tropical Medicine and Hygiene* **77**, 79-87 (2007).
21. J. K. Baird *et al.* Primaquine Therapy for Malaria. *Clinical Infectious Diseases* **39**, 1336-1345 (2004).
22. R. W. Sauerwein *et al.* Experimental human challenge infections can accelerate clinical malaria vaccine development. *Nature Review Immunology* **11**, 57-64 (2011).
23. A. G. Maier *et al.* Malaria parasite proteins that remodel the host erythrocyte. *Nature Review Microbiology* **7**, 341-354 (2009).

24. A. F. Cowman *et al.* Invasion of Red Blood Cells by Malaria Parasites. *Cell* **124**, 755-766 (2006).
25. C. R. S. Garcia *et al.* Tertian and Quartan Fevers: Temporal Regulation in Malarial Infection. *Journal of Biological Rhythms* **16**, 436-443 (2001).
26. Hippocrates. *On Airs, Waters, and Places*. The Genuine Works of Hippocrates (Sydenham Society, London, 400 BCE).
27. D. A. Baker. Malaria gametocytogenesis. *Molecular and Biochemical Parasitology* **172**, 57-65 (2010).
28. N. Regev-Rudzki *et al.* Cell-Cell Communication between Malaria-Infected Red Blood Cells via Exosome-like Vesicles. *Cell* **153**, 1120-1133 (2013).
29. B. F. C. Kafsack *et al.*, A transcriptional switch underlies commitment to sexual development in malaria parasites. *Nature* **507**, 248-252 (2014).
30. A. S. I. Aly *et al.* Malaria Parasite Development in the Mosquito and Infection of the Mammalian Host. *Annual Review of Microbiology* **63**, 195-221 (2009).
31. D. L. Doolan *et al.* Acquired Immunity to Malaria. *Clinical Microbiology Reviews* **22**, 13-36 (2009).
32. M. Desai *et al.*, Epidemiology and burden of malaria in pregnancy. *The Lancet Infectious Diseases* **7**, 93-104.
33. A. J. Cunnington *et al.* Piecing Together the Puzzle of Severe Malaria. *Science Translational Medicine* **5**, 211-218 (2013).
34. B. A. Marchiafava. On summer-autumn malarial fevers. Two monographs on malaria and the parasites of malarial fevers. *London: New Sydenham Society*, 1-232 (1894).
35. A. Scherf *et al.* Antigenic Variation in Plasmodium falciparum. *Annual Review of Microbiology* **62**, 445-470 (2008).
36. X. Z. Su *et al.*, The large diverse gene family var encodes proteins involved in cytoadherence and antigenic variation of plasmodium falciparum-infected erythrocytes. *Cell* **82**, 89-100 (1995).
37. J. D. Smith *et al.*, Switches in expression of plasmodium falciparum var genes correlate with changes in antigenic and cytoadherent phenotypes of infected erythrocytes. *Cell* **82**, 101-110 (1995).
38. L. Turner *et al.*, Severe malaria is associated with parasite binding to endothelial protein C receptor. *Nature* **498**, 502-505 (2013).
39. T. Lavstsen *et al.*, Plasmodium falciparum erythrocyte membrane protein 1 domain cassettes 8 and 13 are associated with severe malaria in children. *Proceedings of the National Academy of Sciences* **109**, E1791–E1800 (2012).
40. A. Salanti *et al.*, Evidence for the Involvement of VAR2CSA in Pregnancy-associated Malaria. *The Journal of Experimental Medicine* **200**, 1197-1203 (2004).
41. L. Jiang *et al.*, PfSETvs methylation of histone H3K36 represses virulence genes in Plasmodium falciparum. *Nature* **499**, 223-227 (2013).
42. W. H. Organization, Management of Severe Malaria: A Practical Handbook. *Global Malaria Programme, World Health Organization, Geneva* (2012).
43. A. J. Cunnington *et al.* Comparison of parasite sequestration in uncomplicated and severe childhood Plasmodium falciparum malaria. *Journal of Infection* **67**, 220-230 (2013).
44. I. C. E. Hendriksen *et al.*, Defining Falciparum-Malaria-Attributable Severe Febrile Illness in Moderate-to-High Transmission Settings on the Basis of

Plasma PfHRP2 Concentration. *Journal of Infectious Diseases* **207**, 351-361 (2013).
45. I. A. Clark *et al.* Human malarial disease: a consequence of inflammatory cytokine release. *Malaria Journal* **5**, 1-32 (2006).
46. B. G. Awandare *et al.* Increased levels of inflammatory mediators in children with severe Plasmodium falciparum malaria with respiratory distress. *Journal of Infectious Diseases* **194**, 1438-1446 (2006).
47. N. J. White *et al.* The murine cerebral malaria phenomenon. *Trends in Parasitology* **26**, 11-15 (2010).
48. E. Hempelmann and K. Krafts. Bad air, amulets and mosquitoes: 2,000 years of changing perspectives on malaria. *Malaria Journal* **12**, 232-232 (2013).
49. Word Health Organization. Global Technical Strategy for Malaria 2016–2030. *World Health Organization* (2015).
50. Herodotus; Strassler, AL. The Landmark Herodotus: The Histories. (2009).
51. W. Gu and R. J. Novak. Predicting the impact of insecticide-treated bed nets on malaria transmission: the devil is in the detail. *Malaria Journal* **8**, 1-10 (2009).
52. P. L. G. Birget and J. C. Koella. An Epidemiological Model of the Effects of Insecticide-Treated Bed Nets on Malaria Transmission. *PLoS ONE* **10**, e0144173 (2015).
53. P. L. Alonso *et al.*, A Malaria Control Trial using Insecticide-Treated Bed Nets and Targeted Chemoprophylaxis in a Rural Area of The Gambia, West AfricaA malaria control trial using insecticide-treated bed nets and targeted chemoprophylaxis in a rural area of The Gambia, West Africa. *Transactions of the Royal Society of Tropical Medicine and Hygiene* **87**, 37-44 (1993).
54. N. Minakawa *et al.* Unforeseen misuses of bed nets in fishing villages along Lake Victoria. *Malaria Journal* **7**, 1-6 (2008).
55. H. Ranson *et al.*, Pyrethroid resistance in African anopheline mosquitoes: what are the implications for malaria control? *Trends in Parasitology* **27**, 91-98.
56. N. Moiroux *et al.*, Changes in Anopheles funestus Biting Behavior Following Universal Coverage of Long-Lasting Insecticidal Nets in Benin. *Journal of Infectious Diseases*, (2012).
57. A. C. Ghani *et al.*, Loss of Population Levels of Immunity to Malaria as a Result of Exposure-Reducing Interventions: Consequences for Interpretation of Disease Trends. *PLoS ONE* **4**, e4383 (2009).
58. R. W. Snow *et al.*, Relation between severe malaria morbidity in children and level of *Plasmodium falciparum* transmission in Africa. *The Lancet* **349**, 1650-1654 (1997).
59. T. F. Pluess *et al.* Indoor residual spraying for preventing malaria. *Cochrane Database of Systematic Reviews* (2010).
60. J. A. Nájera *et al.* Some Lessons for the Future from the Global Malaria Eradication Programme (1955–1969). *PLoS Medicine* **8**, e1000412 (2011).
61. M. Meremiku *et al.* Intermittent preventive treatment for malaria in children living in areas with seasonal transmission. *Cochrane Database of Systematic Reviews* **2** (2012).
62. D. Radeva-Petrova *et al.* Drugs for preventing malaria in pregnant women in endemic areas: any drug regimen versus placebo or no treatment. *Cochrane Database of Systematic Reviews* **10** (2014).

63. A. Kakuru *et al.* Dihydroartemisinin–Piperaquine for the Prevention of Malaria in Pregnancy. *New England Journal of Medicine* **374**, 928-939 (2016).
64. D. O. Freedman. Malaria Prevention in Short-Term Travelers. *New England Journal of Medicine* **359**, 603-612 (2008).
65. D. Payne. Spread of chloroquine resistance in *Plasmodium falciparum*. *Parasitology Today* **3**, 241-246 (1987).
66. A. Dondrop *et al.* Artesunate versus quinine for treatment of severe falciparum malaria: a randomised trial. *The Lancet* **366**, 717-725.
67. P. J. Rosenthal. Artesunate for the Treatment of Severe Falciparum Malaria. *New England Journal of Medicine* **358**, 1829-1836 (2008).
68. P. Ambroise-Thomas. The Tragedy Caused by Fake Antimalarial Drugs. *Mediterranean Journal of Hematology and Infectious Diseases* **4**, e2012027 (2012).
69. N. Mishra *et al.*, Prescription practices and availability of artemisinin monotherapy in India: where do we stand? *Malaria Journal* **10**, 360-360 (2011).
70. A. M. Dondorp *et al.*, Artemisinin Resistance in Plasmodium falciparum Malaria. *New England Journal of Medicine* **361**, 455-467 (2009).
71. R. M. Packard. The Origins of Antimalarial-Drug Resistance. *New England Journal of Medicine* **371**, 397-399 (2014).
72. C. Amaratunga *et al.*, Artemisinin-resistant Plasmodium falciparum in Pursat province, western Cambodia: a parasite clearance rate study. *The Lancet Infectious Diseases* **12**, 851-858 (2012).
73. W. E. Paul. *Fundamental Immunology, 7th Edition*. L. A. J. O'Neill, Ed., (Wolters Kluwer, 2013).
74. A. Iwasaki and R. Medzhitov. Control of adaptive immunity by the innate immune system. *Nature Immunology* **16**, 343-353 (2015).
75. T. Nakatsuji and R. L. Gallo. Antimicrobial Peptides: Old Molecules with New Ideas. *Journal of Investigative Dermatology* **132**, 887-895 (2012).
76. P. N. Nesargikar *et al.* The complement system: history, pathways, cascade and inhibitors. *European Journal of Microbiology & Immunology* **2**, 103-111 (2012).
77. P. J. Murray and T. A. Wynn. Protective and pathogenic functions of macrophage subsets. *Nature Review Immunology* **11**, 723-737 (2011).
78. P. Vantourout and A. Hayday. Six-of-the-best: unique contributions of gamma-delta T cells to immunology. *Nature Review Immunology* **13**, 88-100 (2013).
79. E. Vivier *et al.* Functions of natural killer cells. *Nature Immunology* **9**, 503-510 (2008).
80. D. Voehringer. Protective and pathological roles of mast cells and basophils. *Nat Rev Immunol* **13**, 362-375 (2013).
81. A. Mildner and S. Jung. Development and Function of Dendritic Cell Subsets. *Immunity* **40**, 642-656 (2014).
82. T. Kambayashi and T. M. Laufer. Atypical MHC class II-expressing antigen-presenting cells: can anything replace a dendritic cell? *Nature Review Immunology* **14**, 719-730 (2014).
83. L. Chen and D. B. Flies. Molecular mechanisms of T cell co-stimulation and co-inhibition. *Nature Review Immunology* **13**, 227-242 (2013).

84. J. S. Blum *et al.* Pathways of Antigen Processing. *Annual Review of Immunology* **31**, 443-473 (2013).
85. J. Zhu *et al.* Differentiation of Effector CD4 T Cell Populations. *Annual Review of Immunology* **28**, 445-489 (2010).
86. T. R. Mosmann and R. L. Coffman, TH1 and TH2 Cells: Different Patterns of Lymphokine Secretion Lead to Different Functional Properties. *Annual Review of Immunology* **7**, 145-173 (1989).
87. J. J. O'Shea and W. E. Paul. Mechanisms Underlying Lineage Commitment and Plasticity of Helper CD4+ T Cells. *Science* **327**, 1098-1102 (2010).
88. N. Zhang and M. J. Bevan. CD8+ T Cells: Foot Soldiers of the Immune System. *Immunity* **35**, 161-168 (2011).
89. S. N. Mueller *et al.* Memory T Cell Subsets, Migration Patterns, and Tissue Residence. *Annual Review of Immunology* **31**, 137-161 (2013).
90. G. D. Victora and M. C. Nussenzweig. Germinal Centers. *Annual Review of Immunology* **30**, 429-457 (2012).
91. T. Kurosaki *et al.* Memory B cells. *Nature Review Immunology* **15**, 149-159 (2015).
92. S. L. Nutt *et al.* The generation of antibody-secreting plasma cells. *Nature Review Immunology* **15**, 160-171 (2015).
93. C.A. Siegrist. Mechanisms by which maternal antibodies influence infant vaccine responses: review of hypotheses and definition of main determinants. *Vaccine* **21**, 3406-3412 (2003).
94. O. Kassim *et al.*, Inhibitory factors in breastmilk, maternal and infant sera against in vitro growth of *Plasmodium falciparum* malaria parasite. *Journal of Tropical Pediatrics* **46**, 92-96 (2000).
95. C. Beadle *et al.* Impact of Transmission Intensity and Age on Plasmodium falciparum Density and Associated Fever: Implications for Malaria Vaccine Trial Design. *Journal of Infectious Diseases* **172**, 1047-1054 (1995).
96. D. P. Kwiatkowski. How Malaria Has Affected the Human Genome and What Human Genetics Can Teach Us about Malaria. *American Journal of Human Genetics* **77**, 171-192 (2005).
97. S. Portugal *et al.* Young Lives Lost as B Cells Falter: What We Are Learning About Antibody Responses in Malaria. *The Journal of Immunology* **190**, 3039-3046 (2013).
98. S. Hoffman *et al.* Naturally acquired antibodies to sporozoites do not prevent malaria: vaccine development implications. *Science* **237**, 639-642 (1987).
99. S. L. Hoffman *et al.* Immunity to Malaria and Naturally Acquired Antibodies to the Circumsporozoite Protein of Plasmodium falciparum. *New England Journal of Medicine* **315**, 601-606 (1986).
100. V. Offeddu *et al.* Naturally acquired immune responses against Plasmodium falciparum sporozoites and liver infection. *International Journal for Parasitology* **42**, 535-548 (2012).
101. J. Langhorne *et al.* Immunity to malaria: more questions than answers. *Nature Immunology* **9**, 725-732 (2008).
102. S. Cohen *et al.* Gamma-Globulin and Acquired Immunity to Human Malaria. *Nature* **192**, 733-737 (1961).
103. I. A. McGregor *et al.* Treatment of East African P. falciparum malaria with West African human γ-globulin. *Transactions of The Royal Society of Tropical Medicine and Hygiene* **57**, 170-175 (1963).

104. A. T. R. Jensen *et al.*, Plasmodium falciparum Associated with Severe Childhood Malaria Preferentially Expresses PfEMP1 Encoded by Group A var Genes. *The Journal of Experimental Medicine* **199**, 1179-1190 (2004).
105. K. E. Wright *et al.*, Structure of malaria invasion protein RH5 with erythrocyte basigin and blocking antibodies. *Nature* **515**, 427-430 (2014).
106. A. Scholzen *et al.*, BAFF and BAFF Receptor Levels Correlate with B Cell Subset Activation and Redistribution in Controlled Human Malaria Infection. *The Journal of Immunology* **192**, 3719-3729 (2014).
107. E. Nduati *et al.*, The Plasma Concentration of the B Cell Activating Factor Is Increased in Children With Acute Malaria. *Journal of Infectious Diseases* **204**, 962-970 (2011).
108. P. S. Plotkin SL, in *Vaccines,* O. W. Plotkin SA, Offit PA, Ed. (Elsevier-Saunders, Philadelphia, 2013), pp. 1-13.
109. World Health Organization, World Bank. State of the world's vaccines and immunization. *3rd ed. Geneva, World Health Organization*, (2009).
110. S. Plotkin, History of vaccination. *Proceedings of the National Academy of Sciences* **111**, 12283-12287 (2014).
111. Malaria Vaccine Technology Roadmap. *World Health Organization* (2013).
112. M. A. Thera and C. V. Plowe. Vaccines for Malaria: How Close Are We? *Annual Review of Medicine* **63**, 345-357 (2012).
113. A. V. S. Hill, Pre-erythrocytic malaria vaccines: towards greater efficacy. *Nature Review Immunology* **6**, 21-32 (2006).
114. S. L. Hoffman *et al.* The March Toward Malaria Vaccines. *American Journal of Preventive Medicine* **49**, S319-S333 (2015).
115. C. Ogwang *et al.* Prime Boost Vaccination with Chimpanzee Adenovirus and Modified Vaccinia Ankara Encoding TRAP is effective against P. falciparum Infection in Kenyan Adults. *Science Translational Medicine*, (2015).
116. R. A. Seder *et al.*, Protection Against Malaria by Intravenous Immunization with a Nonreplicating Sporozoite Vaccine. *Science* **341**, 1359-1365 (2013).
117. RTS,S Partnership. Efficacy and safety of RTS,S/AS01 malaria vaccine with or without a booster dose in infants and children in Africa: final results of a phase 3, individually randomised, controlled trial. *The Lancet* (2015).
118. A. L. Goodman and S. J. Draper. Blood-stage malaria vaccines — recent progress and future challenges. *Annals of Tropical Medicine & Parasitology* **104**, 189-211 (2010).
119. M. A. Thera *et al.*, A Field Trial to Assess a Blood-Stage Malaria Vaccine. *New England Journal of Medicine* **365**, 1004-1013 (2011).
120. B. Genton *et al.*, A Recombinant Blood-Stage Malaria Vaccine Reduces Plasmodium falciparum Density and Exerts Selective Pressure on Parasite Populations in a Phase 1-2b Trial in Papua New Guinea. *Journal of Infectious Diseases* **185**, 820-827 (2002).
121. A. D. Douglas *et al.*, The blood-stage malaria antigen PfRH5 is susceptible to vaccine-inducible cross-strain neutralizing antibody. *Nature Communications* **2**, 601 (2011).
122. A. D. Douglas *et al.* A PfRH5-Based Vaccine Is Efficacious against Heterologous Strain Blood-Stage Plasmodium falciparum Infection in Aotus Monkeys. *Cell Host & Microbe* **17**, 130-139 (2015).

123. R. W. Sauerwein and T. Bousema. Transmission blocking malaria vaccines: Assays and candidates in clinical development. *Vaccine* **33**, 7476-7482 (2015).
124. A. N. Vermeulen *et al.* Sequential expression of antigens on sexual stages of Plasmodium falciparum accessible to transmission-blocking antibodies in the mosquito. *The Journal of Experimental Medicine* **162**, 1460-1476 (1985).
125. A. M. Blagborough *et al.* Transmission-blocking interventions eliminate malaria from laboratory populations. *Nature Communications* **4**, 1812 (2013).
126. D. Walliker *et al.* Genetic analysis of the human malaria parasite Plasmodium falciparum. *Science* **236**, 1661-1666 (1987).
127. L. Florens *et al.* A proteomic view of the Plasmodium falciparum life cycle. *Nature* **419**, 520-526 (2002).
128. N. Hall *et al.* A Comprehensive Survey of the Plasmodium Life Cycle by Genomic, Transcriptomic, and Proteomic Analyses. *Science* **307**, 82-86 (2005).
129. R. S. Nussenzweig *et al.* Protective Immunity produced by the Injection of X-irradiated Sporozoites of Plasmodium berghei. *Nature* **216**, 160-162 (1967).
130. D. F. Clyde *et al.* Immunization of man against sporozite-induced falciparum malaria. *The American Journal of the Medical Sciences* **266**, 169-177 (1973).
131. K. H. Rieckmann *et al.* Sporozoite induced immunity in man against an ethiopian strain of Plasmodium falciparum. *Transactions of The Royal Society of Tropical Medicine and Hygiene* **68**, 258-259 (1974).
132. E. M. Riley and V. A. Stewart. Immune mechanisms in malaria: new insights in vaccine development. *Nature Medicine* **19**, 168-178 (2013).
133. N. Yoshida *et al.* Hybridoma produces protective antibodies directed against the sporozoite stage of malaria parasite. *Science* **207**, 71-73 (1980).
134. P. Potocnjak *et al.* Monovalent fragments (Fab) of monoclonal antibodies to a sporozoite surface antigen (Pb44) protect mice against malarial infection. *The Journal of Experimental Medicine* **151**, 1504-1513 (1980).
135. L. Schofield *et al.* Gamma Interferon, CD8+ T cells and antibodies required for immunity to malaria sporozoites. *Nature* **330**, 664-666 (1987).
136. A. Coppi *et al.* The malaria circumsporozoite protein has two functional domains, each with distinct roles as sporozoites journey from mosquito to mammalian host. *The Journal of Experimental Medicine* **208**, 341-356 (2011).
137. D. A. Herrington *et al.* Safety and immunogenicity in man of a synthetic peptide malaria vaccine against Plasmodium falciparum sporozoites. *Nature* **328**, 257-259 (1987).
138. J. P. Vanderberg and U. Frevert. Intravital microscopy demonstrating antibody-mediated immobilisation of Plasmodium berghei sporozoites injected into skin by mosquitoes. *International Journal for Parasitology* **34**, 991-996 (2004).
139. D. A. Espinosa *et al.* Proteolytic Cleavage of the P. falciparum Circumsporozoite Protein is a Target of Protective Antibodies. *Journal of Infectious Diseases*, (2015).

140. H. D. Danforth *et al.* Sporozoites of Mammalian Malaria: Attachment To, Interiorization and Fate Within Macrophages. *The Journal of Protozoology* **27**, 193-202 (1980).
141. M. C. Seguin *et al.* Interactions of Plasmodium berghei sporozoites and murine Kupffer cells in vitro. *The Journal of Immunology* **143**, 1716-1722 (1989).
142. A. Coppi *et al.* Heparan Sulfate Proteoglycans Provide a Signal to *Plasmodium* Sporozoites to Stop Migrating and Productively Invade Host Cells. *Cell Host & Microbe* **2**, 316-327.
143. D. Mazier *et al.* Effect of antibodies to recombinant and synthetic peptides on P. falciparum sporozoites in vitro. *Science* **231**, 156-159 (1986).
144. O. Silvie *et al.* A Role for Apical Membrane Antigen 1 during Invasion of Hepatocytes by Plasmodium falciparum Sporozoites. *Journal of Biological Chemistry* **279**, 9490-9496 (2004).
145. R. Spaccapelo *et al.* Thrombospondin-related adhesive protein (TRAP) of *Plasmodium berghei* and parasite motility. *The Lancet* **350**, 335.
146. Y. Charoenvit *et al.*, Development of two monoclonal antibodies against Plasmodium falciparum sporozoite surface protein 2 and mapping of B-cell epitopes. *Infection and Immunity* **65**, 3430-3437 (1997).
147. K. L. White *et al.* MHC class I-dependent presentation of exoerythrocytic antigens to CD8+ T lymphocytes is required for protective immunity against Plasmodium berghei. *The Journal of Immunology* **156**, 3374-3381 (1996).
148. I. A. Cockburn *et al.* In vivo imaging of CD8(+) T cell-mediated elimination of malaria liver stages. *Proceedings of the National Academy of Sciences of the United States of America* **110**, 9090-9095 (2013).
149. D. L. Doolan and S. L. Hoffman The Complexity of Protective Immunity Against Liver-Stage Malaria. *The Journal of Immunology* **165**, 1453-1462 (2000).
150. W. R. Weiss and C. G. Jiang. Protective CD8+ T lymphocytes in Primates Immunized with Malaria Sporozoites. *PLoS ONE* **7**, e31247 (2012).
151. D. L. Doolan and S. L. Hoffman. IL-12 and NK Cells Are Required for Antigen-Specific Adaptive Immunity Against Malaria Initiated by CD8+ T Cells in the Plasmodium yoelii Model. *The Journal of Immunology* **163**, 884-892 (1999).
152. N. W. Schmidt *et al.* Extreme CD8 T Cell Requirements for Anti-Malarial Liver-Stage Immunity following Immunization with Radiation Attenuated Sporozoites. *PLoS Pathogens* **6**, e1000998 (2010).
153. K. J. Ewer *et al.* Protective CD8+ T-cell immunity to human malaria induced by chimpanzee adenovirus-MVA immunisation. *Nat Commun* **4**, (2013).
154. M. Tsuji *et al.* Gamma delta T cells contribute to immunity against the liver stages of malaria in alpha beta T-cell-deficient mice. *Proceedings of the National Academy of Sciences* **91**, 345-349 (1994).
155. G. A. Oliveira *et al.* Class II-Restricted Protective Immunity Induced by Malaria Sporozoites. *Infection and Immunity* **76**, 1200-1206 (2008).
156. S. Chakravarty *et al.* CD8+ T lymphocytes protective against malaria liver stages are primed in skin-draining lymph nodes. *Nature Medicine* **13**, 1035-1041 (2007).
157. M. Plebanski *et al.* Direct processing and presentation of antigen from malaria sporozoites by professional antigen-presenting cells in the induction of CD8+ T-cell responses. *Immunology Cell Biology* **83**, 307-312 (2005).

158. M. R. Ebrahimkhani *et al.* Cross-presentation of antigen by diverse subsets of murine liver cells. *Hepatology* **54**, 1379-1387 (2011).
159. A. Reyes-Sandoval *et al.* CD8+ T Effector Memory Cells Protect against Liver-Stage Malaria. *The Journal of Immunology* **187**, 1347-1357 (2011).
160. S. W. Tse *et al.* The chemokine receptor CXCR6 is required for the maintenance of liver memory CD8⁺ T cells specific for infectious pathogens. *Journal of Infectious Diseases* **210**, 1508-1516 (2014).
161. S. W. Tse *et al.* Unique transcriptional profile of liver-resident memory CD8+ T cells induced by immunization with malaria sporozoites. *Genes and Immunity* **14**, 302-309 (2013).
162. M. C. Seguin *et al.* Induction of nitric oxide synthase protects against malaria in mice exposed to irradiated Plasmodium berghei infected mosquitoes: involvement of interferon gamma and CD8+ T cells. *The Journal of Experimental Medicine* **180**, 353-358 (1994).
163. S. L. Hoffman and D. L. Doolan. Malaria vaccines-targeting infected hepatocytes. *Nat Med* **6**, 1218-1219 (2000).
164. L. Rénia *et al.* In vitro activity of CD4+ and CD8+ T lymphocytes from mice immunized with a synthetic malaria peptide. *Proceedings of the National Academy of Sciences* **88**, 7963-7967 (1991).
165. I. A. Cockburn *et al.* CD8+ T Cells Eliminate Liver-Stage Plasmodium berghei Parasites without Detectable Bystander Effect. *Infection and Immunity* **82**, 1460-1464 (2014).
166. M. Mauduit *et al.* Minimal Role for the Circumsporozoite Protein in the Induction of Sterile Immunity by Vaccination with Live Rodent Malaria Sporozoites. *Infection and Immunity* **78**, 2182-2188 (2010).
167. J. E. Epstein *et al.* Live Attenuated Malaria Vaccine Designed to Protect Through Hepatic CD8+ T Cell Immunity. *Science* **334**, 475-480 (2011).
168. A. C. Gruner *et al.* Sterile Protection against Malaria Is Independent of Immune Responses to the Circumsporozoite Protein. *PLoS ONE* **2**, e1371 (2007).
169. A. Trieu *et al.* Sterile Protective Immunity to Malaria is Associated with a Panel of Novel P. falciparum Antigens. *Molecular & Cellular Proteomics* **10**, (2011).
170. J. C. Aguiar *et al.* Discovery of Novel *Plasmodium falciparum* Pre-Erythrocytic Antigens for Vaccine Development. *PLoS ONE* **10**, e0136109 (2015).
171. R. J. Longley *et al.* Malaria vaccines: identifying *Plasmodium falciparum* liver-stage targets. *Frontiers in Microbiology* **6**, 965 (2015).
172. S. C. Gilbert *et al.* A protein particle vaccine containing multiple malaria epitopes. *Nature Biotechnology* **15**, 1280-1284 (1997).
173. L. F. Scheller and A. F. Azad. Maintenance of protective immunity against malaria by persistent hepatic parasites derived from irradiated sporozoites. *Proceedings of the National Academy of Sciences* **92**, 4066-4068 (1995).
174. I. A. Cockburn *et al.* Prolonged Antigen Presentation Is Required for Optimal CD8+ T Cell Responses against Malaria Liver Stage Parasites. *PLoS Pathogens* **6**, e1000877 (2010).
175. D. Perez-Mazliah and J. Langhorne. CD4 T-cell subsets in Malaria: TH1/TH2 revisited. *Frontiers in Immunology* **5**, (2015).
176. W. R. Weiss *et al.* The role of CD4+ T cells in immunity to malaria sporozoites. *The Journal of Immunology* **151**, 2690-2698 (1993).

177. L. H. Carvalho *et al.* IL-4-secreting CD4+ T cells are crucial to the development of CD8+ T-cell responses against malaria liver stages. *Nature Medicine* **8**, 166-170 (2002).
178. M. G. Overstreet *et al.* CD4+ T Cells Modulate Expansion and Survival but Not Functional Properties of Effector and Memory CD8+ T Cells Induced by Malaria Sporozoites. *PLoS ONE* **6**, e15948 (2011).
179. E. M. Bijker *et al.* Cytotoxic Markers Associate With Protection Against Malaria in Human Volunteers Immunized With *Plasmodium falciparum* Sporozoites. *Journal of Infectious Diseases* **210**, 1605-1615 (2014).
180. W. H. H. Reece *et al.* A CD4+ T-cell immune response to a conserved epitope in the circumsporozoite protein correlates with protection from natural Plasmodium falciparum infection and disease. *Nature Medicine* **10**, 406-410 (2004).
181. M. Tsuji *et al.* CD4+ cytolytic T cell clone confers protection against murine malaria. *The Journal of Experimental Medicine* **172**, 1353-1357 (1990).
182. L. Rénia *et al.* Effector functions of circumsporozoite peptide-primed CD4+ T cell clones against Plasmodium yoelii liver stages. *The Journal of Immunology* **150**, 1471-1478 (1993).
183. O. C. Finney *et al.* Regulatory T cells in malaria: friend or foe? *Trends in Immunology* **31**, 63-70.
184. M. Espinoza-Mora *et al.*, Depletion of Regulatory T Cells Augments a Vaccine-Induced T Effector Cell Response against the Liver-Stage of Malaria but Fails to Increase Memory. *PLoS ONE* **9**, e104627 (2014).
185. C. Ocaña-Morgner *et al.* Malaria Blood Stage Suppression of Liver Stage Immunity by Dendritic Cells. *The Journal of Experimental Medicine* **197**, 143-151 (2003).
186. M. Walther *et al.* Upregulation of TGF-β, FOXP3, and CD4+CD25+ Regulatory T Cells Correlates with More Rapid Parasite Growth in Human Malaria Infection. *Immunity* **23**, 287-296 (2005).
187. M. Guebre-Xabier *et al.* Memory phenotype CD8+ T cells persist in livers of mice protected against malaria by immunization with attenuated Plasmodium bergheisporozoites. *European Journal of Immunology* **29**, 3978-3986 (1999).
188. M. N. Wykes and M. F. Good. What have we learnt from mouse models for the study of malaria? *European Journal of Immunology* **39**, 2004-2007 (2009).
189. J. Langhorne *et al.* The relevance of non-human primate and rodent malaria models for humans. *Malaria Journal* **10**, 1-4 (2011).
190. A. G. Craig *et al.* The Role of Animal Models for Research on Severe Malaria. *PLoS Pathogens* **8**, e1002401 (2012).
191. M. Spring *et al.* Controlled Human Malaria Infection. *Journal of Infectious Diseases* **209**, S40-S45 (2014).
192. M. B. Laurens *et al.* A consultation on the optimization of controlled human malaria infection by mosquito bite for evaluation of candidate malaria vaccines. *Vaccine* **30**, 5302-5304 (2012).
193. S. H. Hodgson *et al.* Evaluating Controlled Human Malaria Infection in Kenyan Adults with Varying Degrees of Prior Exposure to Plasmodium falciparum using sporozoites administered by intramuscular injection. *Frontiers in Microbiology* **5**, (2014).
194. S. Shekalaghe *et al.* Controlled Human Malaria Infection of Tanzanians by Intradermal Injection of Aseptic, Purified, Cryopreserved *Plasmodium*

falciparum Sporozoites. *The American Journal of Tropical Medicine and Hygiene* **91**, 471-480 (2014).
195. S. H. Hodgson *et al.* Lessons learnt from the first controlled human malaria infection study conducted in Nairobi, Kenya. *Malaria Journal* **14**, 1-12 (2015).
196. RTS,S Partnership. A Phase 3 Trial of RTS,S/AS01 Malaria Vaccine in African Infants. *New England Journal of Medicine* **367**, 2284-2295 (2012).
197. RTS,S Partnership. First Results of Phase 3 Trial of RTS,S/AS01 Malaria Vaccine in African Children. *New England Journal of Medicine* **365**, 1863-1875 (2011).
198. J. A. Stoute *et al.* A Preliminary Evaluation of a Recombinant Circumsporozoite Protein Vaccine against Plasmodium falciparum Malaria. *New England Journal of Medicine* **336**, 86-91 (1997).
199. A. Olotu *et al.* Seven-Year Efficacy of RTS,S/AS01 Malaria Vaccine among Young African Children. *New England Journal of Medicine* **374**, 2519-2529 (2016).
200. RTS,S Partnership. Final results from a pivotal phase 3 malaria vaccine trial. *The Lancet*.
201. J. M. Lumsden *et al.* Protective Immunity Induced with the RTS,S/AS Vaccine Is Associated with IL-2 and TNF-α Producing Effector and Central Memory CD4+ T Cells. *PLoS ONE* **6**, e20775 (2011).
202. D. E. Neafsey *et al.* Genetic Diversity and Protective Efficacy of the RTS,S/AS01 Malaria Vaccine. *New England Journal of Medicine* **373**, 2025-2037 (2015).
203. T. C. Luke and S. L. Hoffman. Rationale and plans for developing a non-replicating, metabolically active, radiation-attenuated Plasmodium falciparum sporozoite vaccine. *Journal of Experimental Biology* **206**, 3803-3808 (2003).
204. T. L. Richie *et al.* Progress with Plasmodium falciparum sporozoite (PfSPZ)-based malaria vaccines. *Vaccine* **33**, 7452-7461 (2015).
205. A. S. Ishizuka *et al.* Protection against malaria at 1 year and immune correlates following PfSPZ vaccination. *Nature Medicine* **22**, 614-623 (2016).
206. A. C. Teirlinck *et al.* Longevity and Composition of Cellular Immune Responses Following Experimental *Plasmodium falciparum* Malaria Infection in Humans. *PLoS Pathogens* **7**, e1002389 (2011).
207. K. Nganou-Makamdop *et al.* Long Term Protection after Immunization with *P. berghei* Sporozoites Correlates with Sustained IFNγ Responses of Hepatic CD8+ Memory T Cells. *PLoS ONE* **7**, e36508 (2012).
208. R. L. Beaudoin *et al.* Plasmodium berghei: Immunization of mice against the ANKA strain using the unaltered sporozoite as an antigen. *Experimental Parasitology* **42**, 1-5 (1977).
209. M. Roestenberg *et al.* Protection against a Malaria Challenge by Sporozoite Inoculation. *New England Journal of Medicine* **361**, 468-477 (2009).
210. A. Yayon *et al.* Stage-Dependent Effects of Chloroquine on Plasmodium falciparum In Vitro1. *The Journal of Protozoology* **30**, 642-647 (1983).
211. G. J. H. Bastiaens *et al.* Safety, Immunogenicity, and Protective Efficacy of Intradermal Immunization with Aseptic, Purified, Cryopreserved Plasmodium falciparum Sporozoites in Volunteers Under Chloroquine

Prophylaxis: A Randomized Controlled Trial. *The American Journal of Tropical Medicine and Hygiene* **94**, 663-673 (2016).
212. J. C. R. Hafalla *et al.* Priming of CD8+ T cell responses following immunization with heat-killed Plasmodium sporozoites. *European Journal of Immunology* **36**, 1179-1186 (2006).
213. C. R. Garcia *et al.* Comparative cost models of a liquid nitrogen vapor phase (LNVP) cold chain-distributed cryopreserved malaria vaccine vs. a conventional vaccine. *Vaccine* **31**, 380-386 (2013).
214. A.-K. Mueller *et al.* Genetically modified Plasmodium parasites as a protective experimental malaria vaccine. *Nature* **433**, 164-167 (2005).
215. A. M. Vaughan *et al.* Genetically engineered, attenuated whole-cell vaccine approaches for malaria. *Human Vaccines* **6**, 107-113 (2010).
216. B. C. L. van Schaijk *et al.* A genetically attenuated malaria vaccine candidate based on P. falciparum b9/slarp gene-deficient sporozoites. *eLife* **3**, e03582 (2014).
217. Noah S. Butler *et al.* Superior Antimalarial Immunity after Vaccination with Late Liver Stage-Arresting Genetically Attenuated Parasites. *Cell Host & Microbe* **9**, 451-462 (2011).
218. S. J. Draper and J. L. Heeney. Viruses as vaccine vectors for infectious diseases and cancer. *Nature Review Microbiology* **8**, 62-73 (2010).
219. K. J. Ewer *et al.* Progress with viral vectored malaria vaccines: A multi-stage approach involving "unnatural immunity". *Vaccine* **33**, 7444-7451 (2015).
220. A. Reyes-Sandoval *et al.* Single-dose immunogenicity and protective efficacy of simian adenoviral vectors against Plasmodium berghei. *European Journal of Immunology* **38**, 732-741 (2008).
221. A. Reyes-Sandoval *et al.* Prime-Boost Immunization with Adenoviral and Modified Vaccinia Virus Ankara Vectors Enhances the Durability and Polyfunctionality of Protective Malaria CD8+ T-Cell Responses. *Infection and Immunity* **78**, 145-153 (2010).
222. S. Capone *et al.* Immune responses against a liver-stage malaria antigen induced by simian adenoviral vector AdCh63 and MVA prime–boost immunisation in non-human primates. *Vaccine* **29**, 256-265 (2010).
223. G. A. O'Hara *et al.* Clinical Assessment of a Recombinant Simian Adenovirus ChAd63: A Potent New Vaccine Vector. *Journal of Infectious Diseases* **205**, 772-781 (2012).
224. S. J. McConkey *et al.* Enhanced T-cell immunogenicity of plasmid DNA vaccines boosted by recombinant modified vaccinia virus Ankara in humans. *Nature Medicine* **9**, 729-735 (2003).
225. D. P. Webster *et al.* Enhanced T cell-mediated protection against malaria in human challenges by using the recombinant poxviruses FP9 and modified vaccinia virus Ankara. *Proceedings of the National Academy of Sciences of the United States of America* **102**, 4836-4841 (2005).
226. I. Chuang *et al.* DNA Prime/Adenovirus Boost Malaria Vaccine Encoding P. falciparum CSP and AMA1 Induces Sterile Protection Associated with Cell-Mediated Immunity. *PLoS ONE* **8**, e55571 (2013).
227. R. J. Longley *et al.* Development of an In Vitro Assay and Demonstration of Plasmodium berghei Liver-Stage Inhibition by TRAP-Specific CD8+ T Cells. *PLoS ONE* **10**, e0119880 (2015).
228. K. M. Quinn *et al.* Comparative Analysis of the Magnitude, Quality, Phenotype, and Protective Capacity of Simian Immunodeficiency Virus Gag-

Specific CD8+ T Cells following Human-, Simian-, and Chimpanzee-Derived Recombinant Adenoviral Vector Immunization. *The Journal of Immunology* **190**, 2720-2735 (2013).
229. K. M. Quinn *et al.* Antigen expression determines adenoviral vaccine potency independent of IFN and STING signaling. *The Journal of Clinical Investigation* **125**, 1129-1146 (2015).
230. P. Bejon *et al.* A Phase 2b Randomised Trial of the Candidate Malaria Vaccines FP9 ME-TRAP and MVA ME-TRAP among Children in Kenya. *PLoS Clinical Trials* **1**, e29 (2006).
231. V. S. Moorthy *et al.* A Randomised, Double-Blind, Controlled Vaccine Efficacy Trial of DNA/MVA ME-TRAP Against Malaria Infection in Gambian Adults. *PLoS Medicine* **1**, e33 (2004).
232. E. B. Imoukhuede *et al.* Low-Level Malaria Infections Detected by a Sensitive Polymerase Chain Reaction Assay and Use of This Technique in the Evaluation of Malaria Vaccines in an Endemic Area. *The American Journal of Tropical Medicine and Hygiene* **76**, 486-493 (2007).
233. D. Kimani *et al.* Translating the Immunogenicity of Prime-boost Immunization With ChAd63 and MVA ME-TRAP From Malaria Naive to Malaria-endemic Populations. *Molecular Therapy* **22**, 1992-2003 (2014).
234. T. Rampling *et al.* Safety and High Level Efficacy of the Combination Malaria Vaccine Regimen of RTS,S/AS01B with ChAd-MVA Vectored Vaccines Expressing ME-TRAP. *Journal of Infectious Diseases* **5**, 772-781 (2016).
235. H. Streeck *et al.* The role of IFN-gamma Elispot assay in HIV vaccine research. *Nature Protocols* **4**, 461-469 (2009).
236. S. A. Calarota and F. Baldanti. Enumeration and Characterization of Human Memory T Cells by Enzyme-Linked Immunospot Assays. *Clinical and Developmental Immunology* **2013**, 8 (2013).
237. S. P. Perfetto *et al.* Seventeen-colour flow cytometry: unravelling the immune system. *Nature Review Immunology* **4**, 648-655 (2004).
238. Y. D. Mahnke andM. Roederer. OMIP-001: Quality and phenotype of Ag-responsive human T-cells. *Cytometry A* **77**, 819-820 (2010).
239. P. K. Chattopadhyay and M. Roederer. Good Cell, Bad Cell: Flow Cytometry Reveals T-cell Subsets Important in HIV Disease. *Cytometry Part A* **77**, 614-622 (2010).
240. S. C. Bendall *et al.* A Deep Profiler's Guide to Cytometry. *Trends in Immunology* **33**, 323-332 (2012).
241. P. K. Chattopadhyay *et al.* Single-cell technologies for monitoring immune systems. *Nature Immunology* **15**, 128-135 (2014).
242. V. Proserpio and B. Mahata. Single-cell technologies to study the immune system. *Immunology* **147**, 133-140 (2016).
243. J. Herderschee *et al.* Emerging single-cell technologies in immunology. *Journal of Leukocyte Biology* **98**, 23-32 (2015).
244. M. H. Dominguez *et al.* Highly multiplexed quantitation of gene expression on single cells. *Journal of Immunological Methods* **391**, 133-145 (2013).
245. P. Dalerba *et al.* Single-cell dissection of transcriptional heterogeneity in human colon tumors. *Nat Biotech* **29**, 1120-1127 (2011).
246. G. Guo *et al.* Resolution of Cell Fate Decisions Revealed by Single-Cell Gene Expression Analysis from Zygote to Blastocyst. *Developmental Cell* **18**, 675-685 (2010).

247. M. Ennen *et al.* Single-cell gene expression signatures reveal melanoma cell heterogeneity. *Oncogene* **34**, 3251-3263 (2015).
248. S. J. A. Buczacki *et al.* Intestinal label-retaining cells are secretory precursors expressing Lgr5. *Nature* **495**, 65-69 (2013).
249. Q. F. Wills *et al.* Single-cell gene expression analysis reveals genetic associations masked in whole-tissue experiments. *Nature Biotechnology* **31**, 748-752 (2013).
250. A. K. Shalek *et al.* Single-cell RNA-seq reveals dynamic paracrine control of cellular variation. *Nature* **510**, 363-369 (2014).
251. A. K. Shalek *et al.* Single-cell transcriptomics reveals bimodality in expression and splicing in immune cells. *Nature* **498**, 236-240 (2013).
252. Bruce T. Schultz *et al.* Circulating HIV-Specific Interleukin-21+ CD4+ T Cells Represent Peripheral Tfh Cells with Antigen-Dependent Helper Functions. *Immunity* **44**, 167-178 (2015).
253. S. Johnson *et al.*, Cooperativity of HIV-specific cytolytic CD4+ T cells and CD8+ T cells in control of HIV viremia. *Journal of Virology* **89**, 7494-7505 (2015).
254. B. Mahata *et al.* Single-Cell RNA Sequencing Reveals T Helper Cells Synthesizing Steroids De Novo to Contribute to Immune Homeostasis. *Cell Reports* **7,** 1130-1142 (2014).
255. J. Arsenio *et al.* Early specification of CD8+ T lymphocyte fates during adaptive immunity revealed by single-cell gene-expression analyses. *Nature Immunology* **15,** 365-372 (2014).
256. L. Flatz *et al.*, Single-cell gene-expression profiling reveals qualitatively distinct CD8 T cells elicited by different gene-based vaccines. *Proceedings of the National Academy of Sciences* **108**, 5724-5729 (2011).
257. M. L. Rojas-Peoa *et al*. Transcription Profiling of Malaria-Naive and Semi-immune Colombian Volunteers in a *Plasmodium vivax* Sporozoite Challenge. *PLoS Neglected Tropical Diseases* **9**, e0003978 (2015).
258. S. Dunachie *et al.* Profiling the host response to malaria vaccination and malaria challenge. *Vaccine* **33**, 5316-5320 (2015).
259. D. Ramskold *et al.* Full-length mRNA-Seq from single-cell levels of RNA and individual circulating tumor cells. *Nat Biotech* **30**, 777-782 (2012).
260. J. J. Trombetta *et al.* in *Current Protocols in Molecular Biology*. (John Wiley & Sons, Inc., 2001).
261. E. Shapiro *et al.* Single-cell sequencing-based technologies will revolutionize whole-organism science. *Nature Review Genetics* **14**, 618-630 (2013).
262. A. P. Patel *et al.* Single-cell RNA-seq highlights intratumoral heterogeneity in primary glioblastoma. *Science* **344**, 1396-1401 (2014).
263. R. M. Kumar *et al.* Deconstructing transcriptional heterogeneity in pluripotent stem cells. *Nature* **516**, 56-61 (2014).
264. P. K. Chattopadhyay and M. Roederer. A Mine Is a Terrible Thing to Waste: High Content, Single Cell Technologies for Comprehensive Immune Analysis. *American Journal of Transplantation* **15**, 1155-1161 (2015).
265. S. C. Bendall *et al.* Single-Cell Mass Cytometry of Differential Immune and Drug Responses Across a Human Hematopoietic Continuum. *Science* **332**, 687-696 (2011).

266. Evan W *et al.* Cytometry by Time-of-Flight Shows Combinatorial Cytokine Expression and Virus-Specific Cell Niches within a Continuum of CD8+ T Cell Phenotypes. *Immunity* **36**, 142-152 (2012).
267. C. Ma *et al.* A clinical microchip for evaluation of single immune cells reveals high functional heterogeneity in phenotypically similar T cells. *Nat Med* **17**, 738-743 (2011).
268. S. H. Hodgson *et al.* Evaluation of the Efficacy of ChAd63-MVA Vectored Vaccines Expressing Circumsporozoite Protein and ME-TRAP Against Controlled Human Malaria Infection in Malaria-Naive Individuals. *Journal of Infectious Diseases*, (2014).
269. M. Roederer *et al.* SPICE: Exploration and analysis of post-cytometric complex multivariate datasets. *Cytometry Part A* **79A**, 167-174 (2011).
270. G. Finak *et al.*, MAST: a flexible statistical framework for assessing transcriptional changes and characterizing heterogeneity in single-cell RNA sequencing data. *Genome Biology* **16**, 278 (2015).
271. P. E. Duffy *et al.* Pre-erythrocytic malaria vaccines: identifying the targets. *Expert Review of Vaccines* **11**, 1261-1280 (2012).
272. E. H. Nardin and R. S. Nussenzweig. T Cell Responses to Pre-Erythrocytic Stages of Malaria: Role in Protection and Vaccine Development Against Pre-Erythrocytic Stages. *Annual Review of Immunology* **11**, 687-727 (1993).
273. P. K. Chattopadhyay *et al.* A live-cell assay to detect antigen-specific CD4+ T cells with diverse cytokine profiles. *Nature Medicine* **11**, 1113-1117 (2005).
274. P. K. Chattopadhyay *et al.* Live-cell assay to detect antigen-specific CD4+ T-cell responses by CD154 expression. *Nature Protocols* **1**, 1-6 (2006).
275. S. P. Schoenberger *et al.* T-cell help for cytotoxic T lymphocytes is mediated by CD40-CD40L interactions. *Nature* **393**, 480-483 (1998).
276. R. Elgueta *et al.* Molecular mechanism and function of CD40/CD40L engagement in the immune system. *Immunological Reviews* **229**, 152-172 (2009).
277. R. Craston *et al.* Temporal dynamics of CD69 expression on lymphoid cells. *Journal of Immunological Methods* **209**, 37-45 (1997).
278. D. Kirchhoff *et al.* Identification and isolation of murine antigen-reactive T cells according to CD154 expression. *European Journal of Immunology* **37**, 2370-2377 (2007).
279. M. H. Dominguez *et al.* Highly multiplexed quantitation of gene expression on single cells. *Journal of Immunological Methods* **391**, 133-145 (2013).
280. J. J. O'Shea and W. E. Paul. Mechanisms underlying lineage commitment and plasticity of helper CD4+ T cells. *Science* **327**, 1098-1102 (2010).
281. J. Zhu *et al.* Differentiation of effector CD4 T cell populations. *Annual Review of Immunology* **28**, 445-489 (2010).
282. D. Z. Soghoian and H. Streeck. Cytolytic CD4(+) T cells in viral immunity. *Expert Review of Vaccines* **9**, 1453-1463 (2010).
283. V. Appay *et al.* Characterization of CD4(+) CTLs ex vivo. *The Journal of Immunology* **168**, 5954-5958 (2002).
284. H. Sahin *et al.* Functional role of chemokines in liver disease models. *Nature Review of Gastroenterology and Hepatology* **7**, 682-690 (2010).
285. T. A. Wynn. IL-13 Effector Functions. *Annual Review of Immunology* **21**, 425-456 (2003).

286. A. S. Ishizuka et al. Protection against malaria at 1 year and immune correlates following PfSPZ vaccination. *Nature Medicine* ***22,*** 614-622 (2016).
287. A. McDavid *et al.* Data exploration, quality control and testing in single-cell qPCR-based gene expression experiments. *Bioinformatics* **29**, 461-467 (2013).
288. G. Finak *et al.* Mixture models for single-cell assays with applications to vaccine studies. *Biostatistics* **15**, 87-101 (2014).
289. A. McDavid *et al.* Modeling bi-modality improves characterization of cell cycle on gene expression in single cells. *PLoS Computational Biology* **10**, e1003696 (2014).
290. T. T. Murooka *et al.* CCL5-mediated T-cell chemotaxis involves the initiation of mRNA translation through mTOR/4E-BP1. *Blood* **111**, 4892-4901 (2008).
291. S. Li *et al.* Molecular signatures of antibody responses derived from a systems biology study of five human vaccines. *Nature Immunology* **15**, 195-204 (2014).
292. T. D. Querec *et al.* Systems biology approach predicts immunogenicity of the yellow fever vaccine in humans. *Nature Immunology* **10**, 116-125 (2009).
293. B. Pulendran and R. Ahmed. Immunological mechanisms of vaccination. *Nature Immunology* **12**, 509-517 (2011).
294. S. P. Kasturi *et al.* Programming the magnitude and persistence of antibody responses with innate immunity. *Nature* **470**, 543-547 (2011).
295. H. I. Nakaya *et al.* Systems biology of immunity to MF59-adjuvanted versus nonadjuvanted trivalent seasonal influenza vaccines in early childhood. *Proceedings of the National Academy of Sciences* **113**, 1853-1858 (2016).
296. X. O. Yang *et al.* T helper 17 lineage differentiation is programmed by orphan nuclear receptors ROR alpha and ROR gamma. *Immunity* **28**, 29-39 (2008).
297. S. L. LaPorte *et al.* Molecular and structural basis of cytokine receptor pleiotropy in the interleukin-4/13 system. *Cell* **132**, 259-272 (2008).
298. K. Nelms *et al.* The IL-4 receptor: signaling mechanisms and biologic functions. *Annual Review of Immunology* **17**, 701-738 (1999).
299. A. T. Bauquet *et al.* The costimulatory molecule ICOS regulates the expression of c-Maf and IL-21 in the development of follicular T helper cells and TH-17 cells. *Nature Immunology* **10**, 167-175 (2009).
300. T. Chtanova *et al.* T follicular helper cells express a distinctive transcriptional profile, reflecting their role as non-Th1/Th2 effector cells that provide help for B cells. *The Journal of Immunology* **173**, 68-78 (2004).
301. D. Yu *et al.* The transcriptional repressor Bcl-6 directs T follicular helper cell lineage commitment. *Immunity* **31**, 457-468 (2009).
302. S. G. Tangye *et al.* The good, the bad and the ugly - TFH cells in human health and disease. *Nature Review Immunology* **13**, 412-426 (2013).
303. K. Ozaki *et al.* A critical role for IL-21 in regulating immunoglobulin production. *Science* **298**, 1630-1634 (2002).
304. S. L. Hoffman *et al.* Development of a metabolically active, non-replicating sporozoite vaccine to prevent Plasmodium falciparum malaria. *Human Vaccines* **6**, 97-106 (2010).

305. J. Illingworth *et al.* Chronic Exposure to Plasmodium falciparum Is Associated with Phenotypic Evidence of B and T Cell Exhaustion. *The Journal of Immunology* **190**, 1038-1047 (2013).
306. A. Morrot and M. M. Rodrigues. Tissue signatures influence the activation of intrahepatic CD8+ T cells against malaria sporozoites. *Frontiers in Microbiology* **5**, (2014).
307. R. Spolski and W. J. Leonard. Interleukin-21: basic biology and implications for cancer and autoimmunity. *Annual Review Immunol* **26**, 57-79 (2008).
308. L. Mewono *et al.* Malaria antigen-mediated enhancement of interleukin-21 responses of peripheral blood mononuclear cells in African adults. *Experimental Parasitology* **122**, 37-40 (2009).
309. R. Spolski and W. J. Leonard. Interleukin-21: a double-edged sword with therapeutic potential. *Nat Rev Drug Discov* **13**, 379-395 (2014).
310. S. Nakayamada *et al.* Early Th1 cell differentiation is marked by a Tfh cell-like transition. *Immunity* **35**, 919-931 (2011).
311. R. Rajsbaum *et al.* Type I interferon-dependent and -independent expression of tripartite motif proteins in immune cells. *European Journal of Immunology* **38**, 619-630 (2008).
312. P. A. Darrah *et al.* Multifunctional TH1 cells define a correlate of vaccine-mediated protection against Leishmania major. *Nature Medicine* **13**, 843-850 (2007).
313. R. A. Seder *et al.* T-cell quality in memory and protection: implications for vaccine design. *Nature Review Immunology* **8**, 247-258 (2008).
314. A. P. Rosário *et al.* IL-27 Promotes IL-10 Production by Effector Th1 CD4+ T Cells: A Critical Mechanism for Protection from Severe Immunopathology during Malaria Infection. *The Journal of Immunology*, (2011).
315. S.E. Bentebibel *et al.* Induction of ICOS+CXCR3+CXCR5+ TH Cells Correlates with Antibody Responses to Influenza Vaccination. *Science Translational Medicine* **5**, 176ra132-176ra132 (2013).
316. V. Carpio *et al.* Protective IL-10-producing Th1 cells also make IL-21, which is regulated by the T-bet/Bcl6 ratio, in a mouse model of chronic malaria. *The Journal of Immunology* **194**, 203.210 (2015).
317. D. N. Perez-Mazliah *et al.* Disruption of IL-21 Signaling Affects T Cell-B Cell Interactions and Abrogates Protective Humoral Immunity to Malaria. *PLoS Pathogens* **11**, e1004715 (2015).
318. J. M. Dan *et al.* A cytokine-independent approach to identify antigen-specific human germinal center Tfh cells and rare antigen-specific CD4+ T cells in blood *Manuscript in preparation.*
319. W. R. Weiss *et al.* CD8+ T cells (cytotoxic/suppressors) are required for protection in mice immunized with malaria sporozoites. *Proceedings of the National Academy of Sciences* **85**, 573-576 (1988).
320. A. Reyes-Sandoval *et al.* Prime-Boost Immunization with Adenoviral and Modified Vaccinia Virus Ankara Vectors Enhances the Durability and Polyfunctionality of Protective Malaria CD8+ T-Cell Responses. *Infection and Immunity* **79**, 2131 (2011).
321. C. Ogwang *et al.* Prime-boost vaccination with chimpanzee adenovirus and modified vaccinia Ankara encoding TRAP provides partial protection against Plasmodium falciparum infection in Kenyan adults. *Science Translational Medicine* **7**, 286re285-286re285 (2015).

322. M. R. Betts *et al.* Sensitive and viable identification of antigen-specific CD8+ T cells by a flow cytometric assay for degranulation. *Journal of Immunological Methods* **281**, 65-78 (2003).
323. K. S. Chan and A. Kaur. Flow cytometric detection of degranulation reveals phenotypic heterogeneity of degranulating CMV-specific CD8+ T lymphocytes in rhesus macaques. *Journal of Immunological Methods* **325**, 20-34 (2007).
324. J. Schneider *et al.* Enhanced immunogenicity for CD8+ T cell induction and complete protective efficacy of malaria DNA vaccination by boosting with modified vaccinia virus Ankara. *Nature Medicine* **4**, 397-402 (1998).
325. R. Wang *et al.* Protection against malaria by Plasmodium yoelii sporozoite surface protein 2 linear peptide induction of CD4+ T cell- and IFN-gamma-dependent elimination of infected hepatocytes. *The Journal of Immunology* **157**, 4061-4067 (1996).
326. E. L. Brincks *et al.* CD8 T cells utilize TNF-related apoptosis-inducing ligand (TRAIL) to control influenza virus infection. *The Journal of Immunology* **181**, 4918-4925 (2008).
327. P. Mirandola *et al.* Activated human NK and CD8+ T cells express both TNF-related apoptosis-inducing ligand (TRAIL) and TRAIL receptors but are resistant to TRAIL-mediated cytotoxicity. *Blood* **104**, 2418-2424 (2004).
328. A. Thorburn. Death receptor-induced cell killing. *Cellular Signalling* **16**, 139-144 (2004).
329. D. Chowdhury and J. Lieberman. Death by a Thousand Cuts: Granzyme Pathways of Programmed Cell Death. *Annual Review of Immunology* **26**, 389-420 (2008).
330. S. Dunachie *et al.* Transcriptional changes induced by candidate malaria vaccines and correlation with protection against malaria in a human challenge model. *Vaccine* **33**, 5321-5331 (2015).
331. W. J. Grossman *et al.* Differential expression of granzymes A and B in human cytotoxic lymphocyte subsets and T regulatory cells. *Blood* **104**, 2840-2848 (2004).
332. M. L. Precopio *et al.* Immunization with vaccinia virus induces polyfunctional and phenotypically distinctive CD8(+) T cell responses. *The Journal of Experimental Medicine* **204**, 1405-1416 (2007).
333. J. Harty and N. Van Braeckel-Budimir. CD8 T cell-mediated protection against liver-stage malaria: Lessons from a mouse model. *Frontiers in Microbiology* **5**, (2014).
334. M. Tsuji *et al.* Development of antimalaria immunity in mice lacking IFN-gamma receptor. *The Journal of Immunology* **154**, 5338-5344 (1995).
335. Rodrigues *et al.* Interferon-γ-independent CD8+ T cell-mediated protective anti-malaria immunity elicited by recombinant adenovirus. *Parasite Immunology* **22**, 157-160 (2000).
336. J. Renggli *et al.* Elimination of P. berghei liver stages is independent of Fas (CD95/Apo-I) or perforin-mediated cytotoxicity. *Parasite Immunology* **19**, 145-148 (1997).
337. N. S. Butler *et al.* Differential Effector Pathways Regulate Memory CD8 T Cell Immunity against *Plasmodium berghei* versus *P. yoelii* Sporozoites. *The Journal of Immunology* **184**, 2528-2538 (2010).
338. M. Bots and J. P. Medema. Granzymes at a glance. *Journal of Cell Science* **119**, 5011-5014 (2006).

339. J. Lieberman. Granzyme A activates another way to die. *Immunological Reviews* **235**, 93-104 (2010).
340. H. Kirchgessner *et al.* The Transmembrane Adaptor Protein Trim Regulates T Cell Receptor (Tcr) Expression and Tcr-Mediated Signaling via an Association with the Tcr ζ Chain. *The Journal of Experimental Medicine* **193**, 1269-1284 (2001).
341. L. B. Jarvis *et al.* Human leukocyte antigen class I-restricted immunosuppression by human CD8+ regulatory T cells requires CTLA-4-mediated interaction with dendritic cells. *Human Immunology* **69**, 687-695 (2008).
342. E. Valk *et al.* T Cell Receptor-Interacting Molecule Acts as a Chaperone to Modulate Surface Expression of the CTLA-4 Coreceptor. *Immunity* **25**, 807-821.
343. M. C. Banton *et al.* Rab8 Binding to Immune Cell-Specific Adaptor LAX Facilitates Formation of trans-Golgi Network-Proximal CTLA-4 Vesicles for Surface Expression. *Molecular and Cellular Biology* **34**, 1486-1499 (2014).
344. M. Matsumiya *et al.* Roles for Treg Expansion and HMGB1 Signaling through the TLR1-2-6 Axis in Determining the Magnitude of the Antigen-Specific Immune Response to MVA85A. *PLoS ONE* **8**, e67922 (2013).
345. Bruce T. Schultz *et al.* Circulating HIV-Specific Interleukin-21+ CD4+ T Cells Represent Peripheral Tfh Cells with Antigen-Dependent Helper Functions. *Immunity* **44**, 167-178.
346. C. S. Ma *et al.* The origins, function, and regulation of T follicular helper cells. *Journal of Experimetnal Medicine* **209**, 1241-1253 (2012).
347. J. S. Hale and R. Ahmed. Memory T follicular helper CD4 T cells. *Frontiers in Immunology* **6** (2015).
348. A. S. Weinmann. Regulatory mechanisms that control T-follicular helper and T-helper 1 cell flexibility. *Immunology Cell Biology* **92**, 34-39 (2014).
349. M. Sedegah *et al.* Cross-protection between attenuated Plasmodium berghei and P. yoelii sporozoites. *Parasite Immunology* **29**, 559-565 (2007).
350. I. Desombere *et al.* The interferon gamma secretion assay: a reliable tool to study interferon gamma production at the single cell level. *Journal of Immunological Methods* **286**, 167-185 (2004).
351. M. O. Afolabi *et al.* Safety and Immunogenicity of ChAd63 and MVA ME-TRAP in West African children and infants. *Molecular Therapy,* ahead of print (2016).
352. A. Ouattara *et al.* Designing malaria vaccines to circumvent antigen variability. *Vaccine* **33**, 7506-7512 (2015).
353. A. Han *et al.* Linking T-cell receptor sequence to functional phenotype at the single-cell level. *Nature Biotechnology* **32**, 684-692 (2014).

Appendix

TRAP peptide pool used for *in vitro* stimulation of PBMCs for flow cytometry

TRAP T9/96 peptide pool	Sequence
1	MNHLGNVKYLVIVFLIFFDL
2	VIVFLIFFDLFLVNGRDVQN
3	FLVNGRDVQNNIVDEIKYSE
4	NIVDEIKYSEEVCNDQVDLY
5	EVCNDQVDLYLLMDCSGSIR
6	LLMDCSGSIRRHNWVNHAVP
7	RHNWVNHAVPLAMKLIQQLN
8	LAMKLIQQLNLNDNAIHLYV
9	LNDNAIHLYVNVFSNNAKEI
10	NVFSNNAKEIIRLHSDASKN
11	IRLHSDASKNKEKALIIIRS
12	KEKALIIIRSLLSTNLPYGR
13	LLSTNLPYGRTNLTDALLQV
14	TNLTDALLQVRKHLNDRINR
15	RKHLNDRINRENANQLVVIL
16	ENANQLVVILTDGIPDSIQD
17	TDGIPDSIQDSLKESRKLSD
18	SLKESRKLSDRGVKIAVFGI
19	RGVKIAVFGIGQGINVAFNR
20	GQGINVAFNRFLVGCHPSDG
21	FLVGCHPSDGKCNLYADSAW
22	KCNLYADSAWENVKNVIGPF
23	ENVKNVIGPFMKAVCVEVEK
24	MKAVCVEVEKTASCGVWDEW
25	TASCGVWDEWSPCSVTCGKG
26	SPCSVTCGKGTRSRKREILH
27	TRSRKREILHEGCTSEIQEQ
28	EGCTSEIQEQCEEERCPPKW
29	CEEERCPPKWEPLDVPDEPE
30	EPLDVPDEPEDDQPRPRGDN
31	DDQPRPRGDNSSVQKPEENI
32	SSVQKPEENIIDNNPQEPSP
33	IDNNPQEPSPNPEEGKDENP
34	NPEEGKDENPNGFDLDENPE
35	NGFDLDENPENPPNPDIPEQ
36	NPPNPDIPEQKPNIPEDSEK
38	DIPEQKPNIPEDSEKEVPSD
39	EDSEKEVPSDVPKNPEDDRE
40	VPKNPEDDREENFDIPKKPE

41	ENFDIPKKPENKHDNQNNLP
42	NKHDNQNNLPNDKSDRNIPY
43	NDKSDRNIPYSPLPPKVLDN
44	SPLPPKVLDNERKQSDPQSQ
45	ERKQSDPQSQDNNGNRHVPN
46	DNNGNRHVPNSEDRETRPHG
47	SEDRETRPHGRNNENRSYNR
48	RNNENRSYNRKYNDTPKHPE
49	KYNDTPKHPEREEHEKPDNN
50	REEHEKPDNNKKKGESDNKY
51	KKKGESDNKYKIAGGIAGGL
52	KIAGGIAGGLALLACAGLAY
53	ALLACAGLAYKFVVPGAATP
54	KFVVPGAATPYAGEPAPFDE
55	YAGEPAPFDETLGEEDKDLD
56	TLGEEDKDLDEPEQFRLPEE
57	EPEQFRLPEENEWN